

ISTANBUL TECHNICAL UNIVERSITY ★ GRADUATE SCHOOL OF SCIENCE
ENGINEERING AND TECHNOLOGY

**A NEW LUMPED PARAMETER (TANK) MODEL FOR RESERVOIRS
CONTAINING CARBON DIOXIDE**



Ph.D. THESIS

Fatma Bahar HOŞGÖR

Department of Petroleum and Natural Gas Engineering

Petroleum and Natural Gas Engineering Programme

JULY 2016

ISTANBUL TECHNICAL UNIVERSITY ★ GRADUATE SCHOOL OF SCIENCE
ENGINEERING AND TECHNOLOGY

**A NEW LUMPED PARAMETER (TANK) MODEL FOR RESERVOIRS
CONTAINING CARBON DIOXIDE**

Ph.D. THESIS

**Fatma Bahar HOŞGÖR
(505062501)**

Department of Petroleum and Natural Gas Engineering

Petroleum and Natural Gas Engineering Programme

Thesis Advisor: Assoc. Prof. Dr. Ömer İnanç TÜREYEN

JULY 2016

İSTANBUL TEKNİK ÜNİVERSİTESİ ★ FEN BİLİMLERİ ENSTİTÜSÜ

**KARBONDİOKSİT İÇEREN REZERVUARLARIN YENİ BİR BOYUTSUZ
PARAMETRE (TANK) MODELİ İLE MODELLENMESİ**

DOKTORA TEZİ

**Fatma Bahar HOŞGÖR
(505062501)**

Petrol ve Doğal Gaz Mühendisliği Anabilim Dalı

Petrol ve Doğal Gaz Mühendisliği Programı

Tez Danışmanı: Doç. Dr. Ömer İnanç TÜREYEN

TEMMUZ 2016

Fatma Bahar Hoşgör, a Ph.D. student of ITU Graduate School of Science, Engineering and Technology student ID 505062501, successfully defended the thesis entitled “A NEW LUMPED PARAMETER (TANK) MODEL FOR RESERVOIRS CONTAINING CARBON DIOXIDE” which she prepared after fulfilling the requirements specified in the associated legislations, before the jury whose signatures are below.

Thesis Advisor : **Assoc. Prof. Dr. Ömer İnanç TÜREYEN**
İstanbul Technical University

Jury Members : **Prof. Dr. Abdurrahman SATMAN**
İstanbul Technical University

Prof. Dr. Altuğ ŞİŞMAN
İstanbul Technical University

Prof. Dr. Mahmut PARLAKTUNA
Middle East Technical University

Prof. Dr. Serhat AKIN
Middle East Technical University

Date of Submission : 30 May 2016

Date of Defense : 1 July 2016





To The Memory of My Loving Grandmother Halime Öztoran,



FOREWORD

First of all, I would like to express my deepest gratitude to my advisor Assoc. Prof. Dr. Ömer İnanç Türeyen for his guidance, advice, insight and patience throughout the study. I would like to thank my jury member Prof. Dr. Abdurrahman Satman for his huge support. I have always made use of their experiences, supports and encouragements during my Ph.D. studies. Secondly, I would like to thank to my other jury member Prof. Dr. Altuğ Şişman for his valuable comments and suggestions that helped to improve the content of my Ph.D. It was a great honor working with them. I would like to thank ITU (Istanbul Technical University) and The Scientific and Technological Research Council of Turkey (TUBITAK Project No:113M425) for their financial supports. Also I would like to express my appreciation to the GÜRİŞ Construction and Engineering Co. Inc. for providing and allowing publication of data presented in this thesis. I like to extend my gratitude to staff of Petroleum and Natural Gas Engineering Department of ITU, especially to my friends Eda Ay Dilsiz, Adalet Yıldız and Melek Deniz for their moral support. Finally, I would like to thank all members of my family, especially my mother Zuhale Öztoran, my father Mehmet Azmi Öztoran, my sister Hatem Ayça Öztoran and my grandmother Halime Öztoran whom I always feel their supports and love during all of my life. At last but not least I would like to say my grateful thanks to my husband Can Hoşgör for his endless support, patience and love. And my dearest son Kaya Bora Hoşgör, I hope this thesis and whole study, endurance and passion behind will inspire you. Thank you for being my son and for your understanding for the times that I spent on this thesis instead of being with you.

July 2016

Fatma Bahar HOŞGÖR
(Petroleum and Natural Gas
Engineer, M.Sc.)

TABLE OF CONTENTS

	<u>Page</u>
FOREWORD	ix
LIST OF TABLES	xiii
LIST OF FIGURES	xv
ABBREVIATIONS	xix
SYMBOLS	xxi
SUMMARY	xxiii
ÖZET	xxv
1. INTRODUCTION	1
1.1 Literature Review	5
1.1.1 Numerical Models	7
1.1.2 Lumped Parameter Models	10
1.1.3 Models for Geothermal Reservoirs Containing CO ₂	13
2. THERMODYNAMIC PACKAGE	19
2.1 Thermophysical properties of H ₂ O	19
2.2 Thermophysical properties of CO ₂	21
2.3 H ₂ O-CO ₂ System.....	25
3. METHODOLOGY	41
3.1 Utilization of Lumped Parameter Models	41
3.2 Description of the Model.....	44
3.3 Mass Balance for Water	48
3.4 Energy Balance on Fluids and Rock	50
3.5 Mass Balance on the Carbon Dioxide Component	53
3.6 Selection of the Primary Variables.....	55
3.7 Change of Phases During Simulation.....	56
3.8 Linearization of Equations	57
3.9 Solution of Finite Difference Equations.....	58
3.10 Verification Studies with Petrasim.....	63
3.10.1 One tank closed system.....	64
3.10.1.1 Production case	64
3.10.1.2 Reinjection case	68
3.10.2 Two tank closed system	72
3.10.2.1 Production case	72
3.10.2.2 Reinjection case	77
3.10.3 One tank open system	81
3.11 Sythetic Applications with Tank Model.....	85
3.11.1 One Tank Closed Model	85
3.11.1.1 The effect of mass fraction of CO ₂ in reservoir water	85
3.11.1.2 The effect of production rate.....	88
3.11.1.3 The effect of reinjection	90
3.11.1.4 The effect of physical parameters to tank model	95

Porosity.....	95
Bulk volume	99
Compressibility of rock	102
3.11.2 One Tank Open Model.....	106
3.11.2.1 The effect of mass fraction of CO ₂	106
3.11.2.2 The effect of recharge constant	110
3.11.2.3 The effect of initial mass fraction of CO ₂ in recharge source	113
4. ANALYTICAL MODEL	117
4.1 Description of the Model.....	117
4.1.1 Constant Carbon Dioxide Mass Fraction	118
4.1.2 Variable Carbon Dioxide Mass Fraction.....	121
4.2 Reduced forms of the equations	122
4.3 Comparison of Analytical Model with Lumped Parameter Model	123
4.4 Applications with Analytical Model	125
4.4.1 Effects of various parameters on the behavior of carbon dioxide content	125
4.4.1.1 The ratio of reinjected to produced carbon dioxide mass fraction...	126
4.4.1.2 The recharge and reinjection mass rates	127
5. APPLICATION TO GERMENCIK FIELD	131
5.1 Germencik Field	131
5.2 Field Development	132
5.3 Modelling Study	134
5.3.1 Case study: one tank open system.....	136
6. CONCLUSIONS AND RECOMMENDATIONS	141
6.1 Conclusions	141
6.2 Recommendations for Future Works.....	143
6.2.1 Effects of brine salinity	143
6.2.2 Gravity effect.....	144
6.2.3 Time stepping.....	144
REFERENCES	145
CURRICULUM VITAE	153

LIST OF TABLES

	<u>Page</u>
Table 1.1 : The installed power plant in Turkey	4
Table 1.2 : The estimated projections of geothermal applications for the year 2018.....	5
Table 2.1 : The critical and triple point parameters for H ₂ O.....	19
Table 2.2 : The critical and triple point parameters for CO ₂	22
Table 2.3 : Data for viscosity of CO ₂ calculation tabulated by Vargaftik et al.....	24
Table 2.4 : Coefficients for equation 2.15.....	30
Table 2.5 : Regression coefficients for equation 2.16.....	31
Table 2.6 : Regression coefficients for equation 2.20.....	36
Table 3.1 : Sample tank connections.....	48
Table 3.2 : Proposed primary variables.....	56
Table 3.3 : Data used in the one tank closed model.....	64
Table 3.4 : Data used in Petrasim for one tank closed model.....	70
Table 3.5 : Data used in one tank closed reinjection model.....	69
Table 3.6 : Data used in Petrasim for one tank closed reinjection model.....	69
Table 3.7 : Data used in the two tanks production model.....	73
Table 3.8 : Data used in Petrasim for two tanks production model.....	74
Table 3.9 : Data used in the two tanks production/injection model.....	77
Table 3.10 : Data used in Petrasim for two tanks production/injection model.....	78
Table 3.11 : Data used in the one tank recharge model.	81
Table 3.12 : Data used in Petrasim for the one tank recharge model.....	82
Table 3.13 : Reservoir properties for one tank closed model.....	85
Table 3.14 : Reservoir properties for one tank open model.....	104
Table 4.1 : Parameters used in the analytical model for the verification example	132
Table 4.2 : Parameters used in the tank model for the verification example	132
Table 4.3 : Model parameters used in the analytical model.....	135
Table 5.1 : Wells drilled in Germencik Omerbeyli geothermal field by MTA.....	132
Table 5.2 : Wells drilled in Germencik Omerbeyli geothermal field by GÜRİŞ.....	132
Table 5.3 : Data used in one tank open model	137



LIST OF FIGURES

	<u>Page</u>
Figure 1.1 : World map of the major tectonic plates and location of the world's geothermal provinces	1
Figure 1.2 : Installed Geothermal Capacity as per countries	2
Figure 1.3 : Geothermal sites in Turkey	3
Figure 2.1 : Pressure–temperature regions of IAPWS-IFT97 for water	20
Figure 2.2 : Viscosity behavior of water.....	21
Figure 2.3 : Pressure-temperature-density graph of gaseous CO ₂	23
Figure 2.4 : Temperature–enthalpy graph of gaseous CO ₂	23
Figure 2.5 : Pressure–temperature–viscosity behavior of gaseous CO ₂	24
Figure 2.6 : Liquid enthalpy versus temperature.	25
Figure 2.7 : Enthalpy of solution versus temperature.....	26
Figure 2.8 : Viscosity of gas phase versus temperature	27
Figure 2.9 : Enthalpy of gas phase versus temperature.....	28
Figure 2.10 : Henry's constant of CO ₂ versus temperature	29
Figure 2.11 : Partial pressure of CO ₂ versus temperature.....	30
Figure 2.12 : Pressure – temperature behavior of water–CO ₂ mixtures for various mass fractions of CO ₂ based on Sutton.....	32
Figure 2.13 : Pressure – temperature behavior of water–CO ₂ mixtures for various mass fractions of CO ₂ based on Santoya	33
Figure 2.14 : Pressure – temperature behavior of water–CO ₂ mixtures for various mass fractions of CO ₂ based on Cramer	33
Figure 2.15 : Comparison of approaches for Henry's constant calculations.	34
Figure 2.16 : Pressure–temperature–enthalpy behavior of water–CO ₂ mixtures for $f_{cl}=0.015$	35
Figure 2.17 : Henry's law constant for CO ₂ in NaCl solutions from 0 to 0.05 mass fraction based on Cramer's approach.....	37
Figure 2.18 : Pressure of pure water and brine with various NaCl concentration based on Cramer's approach.	38
Figure 2.19 : Henry's law constant for CO ₂ in NaCl solutions from 0 to 0.05 mass fraction based on Satman	38
Figure 2.20 : Pressure of pure water and brine with various NaCl concentration based on Satman.....	39
Figure 2.21 : Henry's law constant for CO ₂ in NaCl solutions of 0 to 5000 ppm.....	39
Figure 2.22 : Pressure of pure water and brine containing 5000 ppm NaCl.....	40
Figure 3.1 : Parts of a geothermal system.....	42
Figure 3.2 : Various types of tank models	43
Figure 3.3 : Properties of a representative tank in the model	45
Figure 3.4 : Example for configuration of tanks	48
Figure 3.5 : Example for configuration of geothermal sytem.....	62
Figure 3.6 : Structure of generated Jacobian matrix	62

Figure 3.7 : Flow chart of the developed model	63
Figure 3.8 : Illustration of one tank closed sytem production case.....	64
Figure 3.9 : Th Modelling of one tank closed sytem production case in PETRASIM.....	65
Figure 3.10 : Comparison of pressure behavior of one tank closed sytem production case.....	66
Figure 3.11 : Comparison of temperature behavior of one tank closed sytem production case.....	66
Figure 3.12 : Comparison of gas saturation behavior of one tank closed sytem production case.....	67
Figure 3.13: Comparison of mass fraction of CO ₂ in liquid phase of one tank closed sytem production case.....	67
Figure 3.14: Comparison of mass fraction of CO ₂ in gas phase of one tank closed sytem production case.....	68
Figure 3.15 : Illustration of one tank closed reinjection case.....	68
Figure 3.16 : Comparison of pressure behavior of one tank closed reinjection case	70
Figure 3.17 : Comparison of temperature behavior of one tank closed reinjection case	70
Figure 3.18 : Comparison of gas saturation behavior of one tank closed reinjection case	71
Figure 3.19 : Comparison of mass fraction of CO ₂ in liquid phase in one tank closed reinjection case.....	71
Figure 3.20 : Comparison of mass fraction of CO ₂ in gas phase in one tank closed reinjection case.....	72
Figure 3.21 : Illustration of two tanks production case.....	72
Figure 3.22 : Modelling of two tanks production case with PETRASIM.....	73
Figure 3.23 : Comparison of pressure behavior for two tank production case.	74
Figure 3.24 : Comparison of temperature behavior for two tanks production case	75
Figure 3.25 : Comparison of gas saturation behavior for two tanks production case.....	75
Figure 3.26 : Comparison of mass fraction of CO ₂ in liquid phase for two tanks production case.	76
Figure 3.27 : Comparison of mass fraction of CO ₂ in gas phase for two tanks production case.....	76
Figure 3.28 : Illustration of two tanks production/injection case.....	77
Figure 3.29 : Comparison of pressure behavior for two tank production/injection case.....	78
Figure 3.30: Comparison of temperature behavior for two tanks production/injection case.....	79
Figure 3.31 : Comparison of gas saturation behavior for two tanks production/injection case.....	79
Figure 3.32 : Comparison of mass fraction of CO ₂ in liquid phase for two tanks production/injection case	80
Figure 3.33 : Comparison of mass fraction of CO ₂ in gas phase for two tanks production/injection case	80
Figure 3.34 : Illustration of recharge model.....	81
Figure 3.35 : Comparison of pressure behavior for recharge model.....	82
Figure 3.36: Comparison of temperature behavior for recharge model.....	83

Figure 3.37 : Comparison of gas saturation behavior for recharge model.....	83
Figure 3.38 : Comparison of mass fraction of CO ₂ in water for recharge model.....	84
Figure 3.39 : Comparison of mass fraction of CO ₂ in gas phase for recharge model.....	84
Figure 3.40 : Pressure behavior for various amounts of CO ₂ dissolved in water.....	86
Figure 3.41 : Saturation behavior for various amounts of CO ₂ dissolved in water.....	87
Figure 3.42 : Evolution of the mass fraction of CO ₂ in water for various amounts of CO ₂ dissolved in water.....	87
Figure 3.43 : Evolution of the mass fraction of CO ₂ in the gas phase for various amounts of CO ₂ dissolved in water.....	88
Figure 3.44 : Pressure behavior for various flow rates.....	89
Figure 3.45 : Gas saturation behavior for various flow rates.....	89
Figure 3.46 : Evolution of the mass fraction of CO ₂ in water for various flow rates.....	90
Figure 3.47 : Evolution of the mass fraction of CO ₂ in gas phase for various flow rates.....	91
Figure 3.48 : Pressure behavior for various percentage of reinjection.....	91
Figure 3.49 : Temperature behavior for various percentage of reinjection.....	92
Figure 3.50 : Gas saturation behavior for various percentage of reinjection.....	93
Figure 3.51 : Evolution of the mass fraction of CO ₂ in water for various percentage of reinjection.....	94
Figure 3.52 : Evolution of mass fraction of CO ₂ in gas phase for various percentage of reinjection.....	94
Figure 3.53 : Pressure behavior for various porosity.....	96
Figure 3.54 : Temperature behavior for various porosity.....	96
Figure 3.55 : Gas saturation behavior for various porosity.....	97
Figure 3.56 : Evolution of mass fraction of CO ₂ in water for various porosity.....	98
Figure 3.57 : Evolution of the mass fraction of CO ₂ in gas phase for various porosity.....	98
Figure 3.58 : Pressure behavior for various bulk volumes.....	99
Figure 3.59 : Temperature behavior for various bulk volumes.....	100
Figure 3.60 : Gas saturation behavior for various bulk volumes.....	100
Figure 3.61 : Behaviour of mass fraction of dissolved CO ₂ in water for various bulk volumes.....	101
Figure 3.62 : Behaviour of mass fraction of CO ₂ in gas phase for various bulk volumes.....	102
Figure 3.63 : Pressure behavior for various rock compressibility.....	103
Figure 3.64 : Temperature behavior for various rock compressibility.....	103
Figure 3.65 : Gas saturation behavior for various rock compressibility.....	104
Figure 3.66 : Behaviour of mass fraction of dissolved CO ₂ in water for various rock compressibility.....	105
Figure 3.67 : Behaviour of mass fraction of CO ₂ in gas phase for various rock compressibility.....	105
Figure 3.68 : Illustration of one tank open model.....	106
Figure 3.69 : Pressure behavior for various amounts of CO ₂ dissolved in water for one tank open model.....	107

Figure 3.70 : Temperature behavior for various amounts of CO ₂ dissolved in water for one tank open model.....	108
Figure 3.71 : Gas Saturation behavior for various amounts of CO ₂ dissolved in water for one tank open model.....	108
Figure 3.72 : Evolution of the mass fraction of CO ₂ in water for various amounts of CO ₂ dissolved in water for one tank open model.....	109
Figure 3.73 : Evolution of the mass fraction of CO ₂ in gas phase for various amounts of CO ₂ dissolved in water for one tank open model.....	110
Figure 3.74 : Pressure behavior for different ψ	111
Figure 3.75 : Temperature behavior for different ψ	111
Figure 3.76 : Gas saturation behavior for different ψ	112
Figure 3.77 : Evolution of the mass fraction of CO ₂ in water for different ψ	112
Figure 3.78 : Evolution of the mass fraction of CO ₂ in gas phase for different ψ	113
Figure 3.79 : Pressure behavior as per initial mass fraction of CO ₂ in recharge source.....	114
Figure 3.80 : Temperature behavior as per initial mass fraction of CO ₂ in recharge source.....	114
Figure 3.81 : Gas saturation behavior as per initial mass fraction of CO ₂ in recharge source.....	115
Figure 3.82 : Behavior of mass fraction of CO ₂ in water as per initial mass fraction of CO ₂ in recharge source.....	116
Figure 3.83 : Behavior of mass fraction of CO ₂ in gas phase as per initial mass fraction of CO ₂ in recharge source.....	116
Figure 4.1 : Mass balance on carbon dioxide over any tank volume.....	117
Figure 4.2 : The terms for the rate of water accumulation.....	120
Figure 4.3 : Illustration of the sample scenario.....	123
Figure 4.4 : Comparison of mass fraction of CO ₂ in gas phase from analytical model and tank model.....	125
Figure 4.5 : Analytical model results for various β values.....	126
Figure 4.6 : Comparison of mass fraction of CO ₂ in liquid phase.....	127
Figure 4.7 : Comparison of tank model and analytical model with CO ₂ reinjection.....	128
Figure 4.8 : Comparison of mass fraction of CO ₂ in liquid phase with various CO ₂ reinjection.....	129
Figure 4.9 : Behaviour of mass fraction of CO ₂ in liquid phase at early times.....	129
Figure 5.1 : The locations map of Aydın-Germencik geothermal field.....	131
Figure 5.2 : The locations of the wells drilled in the field.....	133
Figure 5.3 : The Geological map of the Germencik Ömerbeyli geothermal field.....	134
Figure 5.4 : Matching of pressure drop response at Well OB-7.....	135
Figure 5.5 : Measured pressure behavior response at Well OB-77.....	136
Figure 5.6 : Illustration of one tank open system of Germencik field.....	137
Figure 5.7 : Temperature drop projection for Germencik field.....	138
Figure 5.8 : The projection for the mass fraction of CO ₂ in Germencik field.....	139
Figure 5.9 : Projection of mass fraction of CO ₂ in water with and without CO ₂ reinjection.....	140
Figure 5.10 : Projection of mass fraction of CO ₂ in water with constant amount of CO ₂ reinjection.....	140

ABBREVIATIONS

<i>a</i>	: Aquifer
<i>B</i>	: Coefficients of Cramer's Henry's constant
<i>b</i>	: Bulk
<i>br</i>	: Brine
<i>C</i> (subscript)	: Carbon dioxide
<i>CG</i>	: Gaseous carbon dioxide
<i>ci</i>	: Connected tank to tank i
<i>CL</i>	: Carbon dioxide in liquid water
<i>cl_inj</i>	: Carbon dioxide injection
<i>cla</i>	: Carbon dioxide aquifer
<i>d</i>	: Characteristic length, m
<i>D</i>	: Regression Coefficients for salting-out calculation
<i>f</i> (subscript)	: Fluid
<i>f</i>	: Mass fraction of CO ₂ , fraction
<i>G</i>	: Gas
<i>i</i>	: Grid block index
<i>inj</i>	: Injection
<i>j</i>	: Grid block index
<i>L</i>	: Liquid
<i>m</i> (subscript)	: Matrix
<i>N</i>	: Number of tanks
<i>n</i>	: Present time, s
<i>NaCl</i>	: Sodium Chloride
<i>NCG</i>	: Noncondensable gas
<i>net</i>	: Net
<i>ni</i>	: Connections between tank i and other tanks
<i>p</i> (subscript)	: Production
<i>R</i>	: Residual
<i>r</i>	: Rock
<i>re</i>	: Recharge
<i>ref</i>	: Reference
<i>rl</i>	: Relative
<i>s</i>	: Steam
<i>sk</i>	: Salting-out coefficient
<i>sol</i>	: Solution
<i>t</i> (subscript)	: Total
<i>TDS</i>	: Total dissolved solid, ppm
<i>v</i>	: Solution vector
<i>w</i>	: Water
<i>X</i>	: Mass fraction, fraction
<i>y</i>	: Regression coefficients for Upton and Santoya's Henry's constant
<i>z</i>	: Coefficients for viscosity of CO ₂ calculation



SYMBOLS

μ	: Viscosity, Pa-s
0	: Initial
A	: Cross-sectional area, m^2
c	: Compressibility, Pa^{-1}
C	: Specific heat capacity, $J/kg-K$
d	: Characteristic length, m
h	: Specific enthalpy, J/kg
H	: Henry's constant for water
Hbr	: Henry's constant for brine
k	: Permeability, m^2
K	: Henry's constant, Pa^{-1}
M	: Mass, kg
m	: Molality, mol/kg
MW	: Molecular weight, g/mol
p	: Pressure, Pa
Q	: Energy rate, J/s
q	: Volumetric flow rate, m^3/s
S	: Saturation, fraction
T	: Temperature, $^{\circ}C$ or K
t	: Time, s
u	: Specific internal energy, J/kg
V	: Volume, m^3
W	: Mass flow rate, kg/s
X	: Mass fraction, fraction
α	: Recharge index, $kg/bar.s$
β	: Reinjection ratio
γ	: Conduction index, $J/K.s$
Δ	: Difference operator
ε	: Thermal expansion coefficient, $1/^{\circ}C$
κ	: Storage capacity, kg/bar
λ	: Fluid part of the recharge index, $kg/Pa.s.m^3$
ξ	: Direction
ρ	: Density, kg/m^3
σ	: Flow resistor, kg/sPa
ϕ	: Porosity
ψ	: Rock part of the recharge index, m^3



A NEW LUMPED PARAMETER (TANK) MODEL FOR RESERVOIRS CONTAINING CARBON DIOXIDE

SUMMARY

The use of geothermal energy all over the world is increasing every day because of its cleanliness, safeness, renewability and sustainability. Today Turkey's energy demand is mainly compensated by imported fossil fuels. However, with the geothermal energy exploration and development activities, Turkey's vast geothermal resources can be evaluated and the geothermal energy can be one of the domestic energy resources that will contribute considerably to our future energy supply.

In order to evaluate a geothermal field and make future performance predictions, geothermal reservoir simulations must be conducted. Early reservoir simulations considered the geothermal water to be pure water. However, geothermal waters may contain significant amounts of non-condensable gasses such as carbon dioxide. Two of the common characteristics of Turkey's geothermal fields are that they are initially all liquid dominated and almost all contain some amounts of carbon dioxide. Carbon dioxide can have a significant effect on the production performance of geothermal reservoirs. The main impact is on the flashing point of water – carbon dioxide mixtures. Even small amounts of carbon dioxide can significantly increase the flashing point considerably. Hence at relatively high values of pressure, a gas phase could form during production either in the well or sometimes in the reservoir. When modeling geothermal systems with carbon dioxide it becomes crucial to include the effects of carbon dioxide in the model. Therefore it is very important to be able to keep track of the inventory of carbon dioxide. During production/injection operations the amount of carbon dioxide could change. This change in carbon dioxide should be modeled accurately to be able to make accurate future performance predictions. It is very important to account for the change in carbon dioxide due to the fluid behavior in reservoir and wellbore. The changes in carbon dioxide significantly effect the flashing point depth and the wellhead pressure. Some certain minimum wellhead pressure is necessary for keeping power plants operational.

In this study, a new nonisothermal lumped parameter model capable of considering the effects of carbon dioxide is developed. This new approach couples both energy and mass balance equations and moreover carbon dioxide mass fraction and hence it can be used to predict both temperature, pressure and corbondioxide changes in the reservoir. The model is based on three conservation equations; mass balances on water and carbon dioxide and an overall energy balance. By doing so, the behaviour of average reservoir pressure, average reservoir temperature and the amount of carbon dioxide can be modeled. Constant or variable production and reinjection rates are also handled.

Furthermore, a new analytical model that is capable of determining the amount of carbon dioxide as a function of time for liquid dominated reservoirs is developed. The analytical approach presented in this study is an original contribution to the literature.

The developed analytical equations are very easy to use and provide useful insight about how the carbon dioxide changes with time and which parameters affect it most. The tank model is first verified with analytical model and commercial software PetraSim. Then various synthetic cases that demonstrate the effects of parameters such as, production and injection rate, recharge constant, porosity, bulk volume, compressibility of rock, on the performance of reservoir are presented. Moreover, the effect of salinity on the solubility of CO₂ and the value of the Henry's law constant are examined. Finally, one of Turkey's major fields, Germencik field, is studied. The best model that fits the Germencik field is formed and performance of this field is evaluated. The results indicate that the model works well. It can be utilized to better understand the behavior of hot water systems that contain carbon dioxide and to forecast future performance.



KARBONDİOKSİT İÇEREN REZERVUARLARIN YENİ BİR BOYUTSUZ PARAMETRE (TANK) MODELİ İLE MODELLENMESİ

ÖZET

Türkiye'nin enerji ve elektrik ihtiyacı nüfus artışı ve sanayileşme hızıyla orantılı olarak artmaktadır. Enerji ihtiyacının büyük bir kısmı yurtdışından ithal edilen fosil yakıtlardan karşılanmaktadır. Fosil enerji kaynaklarının giderek azalması ve yakıldığında havaya verdiği yüksek orandaki karbondioksit nedeniyle kirlilik yaratması gibi nedenler alternatif enerji kaynakları arayışını arttırmıştır. Jeotermal enerji düşük karbondioksit emisyon oranı ile hava kirliliği yaratmaması, tükenmeyen, yenilenebilir ve ucuz bir enerji kaynağı olması nedeniyle önemli bir alternatif enerji kaynağıdır. Ülkemiz jeotermal kaynak zenginliği açısından dünya çapında en ön sıralarda yer almaktadır. Enerjide genel olarak dışa bağlı olduğumuz için yerli enerji kaynaklarının kullanımı daha büyük önem arz etmektedir. Ülkemizin giderek artan enerji ihtiyacının bir kısmının yerli kaynağımız olan jeotermal enerji ile karşılanması enerji bağımlılığımızı azaltıp ülke ekonomisine önemli bir katkı sağlayacaktır. Bu nedenle jeotermal enerjinin en verimli ve en doğru şekilde kullanılması açısından bu konu ile ilgili çalışmalar hız kazanmalıdır.

Türkiye'de özellikle son on yıl içinde jeotermal enerjinin kullanımında büyük gelişmeler sağlanmıştır. Jeotermal enerji sıcaklığına bağlı olarak başta elektrik üretimi olmak üzere konut ısıtması, sera ısıtması, termal turizm-tedavi ve endüstri gibi birçok alanda kullanılmaktadır. Türkiye'nin mevcut elektrik kurulu kapasitesi Haziran 2016 itibariyle 695 MWe olarak ve doğrudan kullanım kapasitesi ise 3676 MWh olarak verilmektedir. 2005 yılında jeotermal elektrik kurulu kapasitesinin 17.8 MWe olduğu değerlendirilirse ülkemizde jeotermal enerji kullanımının ne derecede geliştiği görülmektedir. 2014 yılında 38 sahayı kapsayarak yapılan bir çalışma sonucunda elektrik potansiyelinin istatistiksel p10 değerinin 1673 MWe, p90 değerinin ise 3140 MWe olduğu görülmüştür. Yine aynı çalışma, ısıl potansiyel için p10 değerini 5600 MWt ve p90 değerini ise 11400 MWt olarak vermektedir. Mevcut kullanım ve potansiyel dikkate alındığında jeotermal enerjinin kullanımının ülkemizde önümüzdeki yıllarda gelişmeye açık olduğu görülmektedir.

Jeotermal enerji kaynağının kullanımının en etkin şekilde yapılabilmesinde rezervuar mühendisliğinin önemi oldukça fazladır. Rezervuar mühendisliği hesaplamalarının gerçekleştirilebilmesi için jeotermal rezervuar modelinin geliştirilebilmesinde yapılan varsayımların gerçeği mümkün mertebe temsil etmesi gerekmektedir. Literatürde ilk jeotermal rezervuar modellerinde rezervuar akışkanı modellenirken saf su varsayımı yapılmıştır. Fakat tüm dünyada birçok jeotermal rezervuarda su içinde çözünmüş olarak CO₂, N₂, NH₃, H₂ ve H₂S gibi yoğunlaşmayan gazlar bulunabilmektedir ve miktarları kütlece %10 mertebelerine varabilmektedirler. Bu gazlardan hem miktar hem de etki olarak en belirgin olan yoğunlaşmayan gaz karbondioksittir. Ülkemizde de hemen hemen tüm jeotermal rezervuarlarda rezervuar suyunun içinde çözünmüş olarak karbondioksit bulunmaktadır. Türkiye'de enerji üretimi bakımından en büyük

kapasiteye sahip olan Kızıldere, Germencik, Salavatlı ve Afyon Ömer-Gecek gibi jeotermal rezervuarları incelendiğinde çoğunun karbondioksit içerdiği gözlemlenmektedir. Örneğin, Kızıldere sahasında rezervuar suyu ortalama kütlece % 1.5 oranında karbondioksit ihtiva etmektedir. Bu oran derinlere inildikçe % 3 mertebelerine varabilmektedir. Ömer-Gecek ve Germencik sahaları da % 0.4 ve % 2.1 oranında çözünmüş karbondioksit içermektedir.

Rezervuar suyunda çözünmüş karbondioksit içeren bu sahaların modellemeleri yapılırken karbondioksit etkisinin gözardı edilmesi hatalı sonuçlara sebep olur. Karbondioksit varlığı rezervuarın termodinamik koşulları ve faz bileşimlerini etkilemektedir. Karbondioksitin su üstündeki en büyük etkisi ayrışma basıncını arttırmasıdır. Bu etki belirli bir sıcaklıkta sıvı fazından gaz fazına geçişin daha yüksek basınçlarda gerçekleşmesini sağlar. Üretimle basınç düşerken daha yüksek basınçta gazlaşma olduğundan ve iki fazlı akışkanın yüksek sıkıştırılabilirlik özelliğinden dolayı, rezervuar basıncı korunmuş olur. Yani, üretim sırasında karbondioksitin kısmi basıncı rezervuar basıncının düşümüne olumlu olarak katkıda bulunarak basınç düşümünü azaltır. Çok küçük karbondioksit miktarları bile rezervuar basınç davranışını önemli ölçüde etkilemekte ve ayrışma basıncını önemli ölçüde değiştirebilmektedir. Karbondioksitin bir diğer etkisi de bir jeotermal sahada üretim başladığında suyun termodinamik davranışını değiştirmesidir. Karbondioksitin akışın taşınım ve termodinamik karakteristiği üzerinde etkisi vardır. Rezervuarda özellikle basınç-sıcaklık dağılımını ve faz kompozisyonunu etkiler ve iki fazlı bölgeyi genişleterek gaz doymuşluğunu arttırır.

Bu çalışmada, karbondioksit içeren jeotermal sahaların akışkan ve ısı üretimi davranışını incelemek ve tahmin etmek amacı ile izotermal olmayan akışı göz önünde bulunduran yeni bir lumped parametre modeli geliştirilmiştir. Literatürde geliştirilmiş izotermal olmayan lumped parametre modelleri genellikle rezervuarların sadece su içerdiğini varsaymaktadır. Ülkemizde bulunan jeotermal sahaların çoğu karbondioksit içerdiği için, bu rezervuarlar değerlendirilirken akışın taşınım ve termodinamik karakteristiği üzerinde etkili olan karbondioksit de modellemede yer almıştır. Modelleme yöntemi olarak, kullanımının basitliği ve büyük bilgisayar kapasitelerine gereksinim duymaması nedeni ile boyutsuz parametre modeli seçilmiştir. Bu yöntem, rezervuara giren ve rezervuardan çıkan kütleler gözetilerek ve akışkan/kayaç özellikleri kullanılarak, zamana veya rezervuardan yapılan üretime göre ortalama rezervuar basıncı ve sıcaklığının davranışını belirlemeyi amaçlayan bir modelleme şeklidir. Bu tür modeller özellikle sayısal model oluşturmaya yetecek verilerin henüz elde edilmediği rezervuarın erken zamanlarında sayısal modellere iyi bir alternatif oluşturmaktadırlar.

Oluşturulan modelde, jeotermal sistemin her bir birleşeni kayaç ve akışkandan oluşan bir tank olarak tanımlanmıştır. Tanklar, bir rezervuarı, akiferi, ısı kaynağını veya doğal boşaltım gerçekleşebilecek bir bloğu temsil etmektedir. Rezervuar veya akiferi temsil etmek için modelleme çalışmasına bağlı olarak bir ya da birden fazla tank kullanılabilir. Burada, herhangi bir tankın başka bir tank ile keyfi sayıda bağlantı yaptığı düşünülmüştür. Tanklar arasındaki sıvı kütlelerinin akış hızı için Schithuis yaklaşımı kullanılmıştır. Buna göre, beslenmenin tanklar ile beslenme kaynağı arasındaki basınç farkı ile orantılı olduğu varsayılmıştır.

İzotermal olmayan ve karbondioksit içeren sistemler incelendiği için kütle korunumu ve enerji korunumu denklemleri buna uygun olarak geliştirilmiştir. Bu şekilde, ortalama rezervuar basıncı ve sıcaklığı ile beraber karbondioksit miktarı da

incelenilmektedir. Modelde kullanılan denklemler, su için kütle korunumu denklemi, tüm sistem için enerji korunumu denklemi ve karbondioksit için kütle korunumu denklemleridir. Elde edilen diferansiyel denklem takımları sayısal yöntemlerle çözülmüştür. Sayısal çözüm sırasında doğrusal olmayan davranışa sahip denklemleri çözebilmek için, Newton-Raphson tekniği kullanılmıştır. Jeotermal sistem tek veya çoklu tanklar olarak ele alınarak iki adet kütle ve bir adet enerji denklemi her bir tank için beraber çözülmüş bu sayede üretim, doğal beslenme ve re-enjeksiyon sebebi ile rezervuarda oluşacak basınç değişimlerinin yanı sıra sıcaklık ve karbondioksit miktarındaki değişimler de incelenmiştir. Model denklemleri ayrıca ısı iletimi etkisini de içerecek şekilde formüle edilerek iletim yolu ile oluşacak ısı akışının rezervuar performansına etkisinin de gözlemlenmesine olanak sağlanmıştır. Bunlara ek olarak, su-karbondioksit sisteminin davranışını modelleyen bir termodinamik paket oluşturularak geliştirilen modele entegre edilmiştir.

Yapılan modelleme ile karbondioksit miktarındaki azalış ve artış takip edilebilmektedir. Model literatürde bulunan diğer boyutsuz (lumped) parametre modellerinden farklı olarak karbondioksitin etkilerini rezervuar performansı üstünde yansıtabilmektedir. Bu yönü ile çalışmada geliştirilen model orijinaldir. Ayrıca model birden fazla tank için geçerli olmakla birlikte her türlü konfigürasyon için kullanılabilir. Oluşturulan tank modelin sonuçları, jeotermal sahaların incelenmesinde yaygın olarak kullanılan sayısal rezervuar simülatörü PETRASİM sonuçları ile karşılaştırılarak doğrulanmıştır. Ayrıca, literatürde verilen bazı önemli jeotermal sahalara ait basınç ve sıcaklık verileri ile kıyaslamalar yapılmıştır. Farklı sentetik senaryolar üzerinde çalışılarak sonuçlar değerlendirilmiş ve geliştirilen model kullanılarak duyarlılık analizleri yapılmıştır. Son olarak geliştirilen model, Türkiye'nin önemli bir jeotermal sahası olan Germencik sahasına uygulanarak bu saha için ileriye yönelik performans tahminleri yapılmıştır.

Buna göre bu çalışmadan aşağıdaki sonuçlar elde edilmiştir:

- Enjeksiyon sebebi ile rezervuarda oluşan basınç ve sıcaklık değişimleri ile karbondioksit miktarındaki değişim gözlemlenmiştir.
- Duyarlılık analizleri yapılarak, çözülmüş karbondioksit oranının, üretim hızının, re-enjeksiyon miktarının jeotermal rezervuarın basınç, sıcaklık ve gaz doymuşluğu üzerindeki etkileri incelenmiştir.
- Bu modelleme çalışması ile, karbondioksit içeren jeotermal sistemlerin davranışı kapsamlı olarak incelenebilir ve jeotermal sistemin gelecekteki performansı sürdürülebilirlik açısından değerlendirilerek en uygun işletme stratejileri belirlenebilir.

Jeotermal rezervuarlarda basıncın düşmesi ile birlikte ayrışma basıncına ulaşıldığında gaz fazı oluşmaktadır. Üretimin sabit kütleli debide devam etmesi durumunda basınç davranışı gaz fazının açığa çıkması ile birlikte değişmektedir. Buna göre gaz fazı açığa çıktığında basıncın üretim ile birlikte azalım davranışı değişmektedir. Gaz fazı açığa çıkmadan önce suyun genleşmesinden ve doğal beslenmeden sağlanan üretim gaz fazının açığa çıkması ile birlikte bu üretim mekanizmalarına gazın genleşmesi de eklenmektedir. Gaz fazının açığa çıkmasından sonra basıncın azalımı azalmaktadır. Bunun nedeni ise gazın sıkıştırılabilirlik değerinin suyun ya da kayacın sıkıştırılabilirlik değerlerine göre çok daha yüksek olmasındandır. Böylece gaz daha fazla genleşmekte ve daha fazla basınç desteği sağlamaktadır.

Jeotermal sahalarda su içinde çözülmüş karbondioksit miktarı üretim ile birlikte düşmektedir. Bu düşüşün birkaç nedeni bulunmaktadır. Bunlardan ilki üretim ile birlikte gerçekleştirilen enjeksiyon işlemidir. Enjeksiyon suyunda karbondioksit bulunmaması durumunda rezervuar içindeki karbondioksiti seyrelterek azalmasına neden olacaktır. Diğer bir azalım nedeni ise beslenme kaynağından kaynaklanabilmektedir. Eğer beslenme kaynağından gelen su içinde karbondioksit bulunmuyorsa o zaman aynı şekilde bu rezervuar içinde bulunan karbondioksiti seyreltecektir. Son olarak rezervuar içinde gaz fazının açığa çıkması durumunda su içindeki karbondioksitin gaz fazına geçmesi ile birlikte su içindeki karbondioksit oranlarında azalmalar meydana gelmektedir.

Rezervuar içinde gaz fazı oluşması durumunda gaz kompozisyonunun iki bileşeni mevcuttur; karbondioksit ve su buharı. Gaz ilk oluştuğunda gaz kompozisyonu ağırlıklı olarak karbondioksitten oluşmaktadır. Başlangıç karbondioksit oranı ne kadar fazla ise gaz fazı içindeki karbondioksit oranı artmaktadır. Üretim ile birlikte basıncın da düşmesiyle gaz doymuşluğu arttıkça gaz kompozisyonunda su buharı miktarı artmaya başlar. Bu üretimin devam etmesi durumunda gaz içindeki karbondioksit oranının çok küçük mertebelere kadar düşmesine neden olabilir.

Jeotermal suyun geri basılması jeotermal sahalar için büyük önem taşımaktadır. Geri basma oranlarına bağlı olarak basınç ayrışma basıncının altına düşebilir veya düşmeyebilir.

Geliştirilen boyutsuz parametre modelinden ayrı olarak, sıvı etken jeotermal sahaların karbondioksit içeriğini tanımlayan yeni bir analitik yaklaşım türetilmiştir. Sadece karbondioksitin kütle denklemine odaklanan ve tanklar arası akışkan geçişi, beslenme, üretim ve reenjeksiyonda karbondioksitin kütle oranındaki değişimini inceleyen bu yaklaşım sabit karbondioksit reenjeksiyonu ve kütle oran olarak değişken karbondioksit reenjeksiyonu durumları için geliştirilmiştir. Değişken re-enjeksiyon durumunda, karbondioksit reenjeksiyonunun rezervuardaki karbondioksit miktarı ile doğrusal olarak değiştiği düşünülmüştür. Değişken miktarlı karbondioksit reenjeksiyonunun tanımlanması, üretilen karbondioksitin olduğu gibi rezervuara geri basılması veya belirli bir oranda azaltılarak geri basılması durumlarının modellenmesine olanak vermektedir.

Türetilen analitik denklemlerin kullanımı kolaydır ve karbondioksit miktarının zamanla nasıl değiştiği ve hangi parametrelerin en çok etkilediği gibi konularda fikir sahibi olunmasını sağlar. Reenjekte edilen suda karbondioksit oranı arttıkça rezervuardaki karbondioksit seviyesinin korunması sağlanır. Reenjeksiyon debisi düşük ise, akiferden beslenmenin rezervuardaki karbondioksit miktarı üzerindeki etkisi daha fazladır.

1. INTRODUCTION

Geothermal energy has been used to produce electricity for over a century, beginning in Lardarello, Italy in 1904. The largest geothermal district heating system in the world started in Iceland in 1930. At first, the development of geothermal energy was slow but the oil crisis in the 1970s and demand for ecofriendly energy resources spurred the rapid development of geothermal energy.

Geothermal energy is a clean, renewable resource that can be tapped by many countries around the world located in geologically favorable places. Figure 1.1. is the world map that shows the major tectonic plates and location of the world's geothermal provinces which are circled in red.

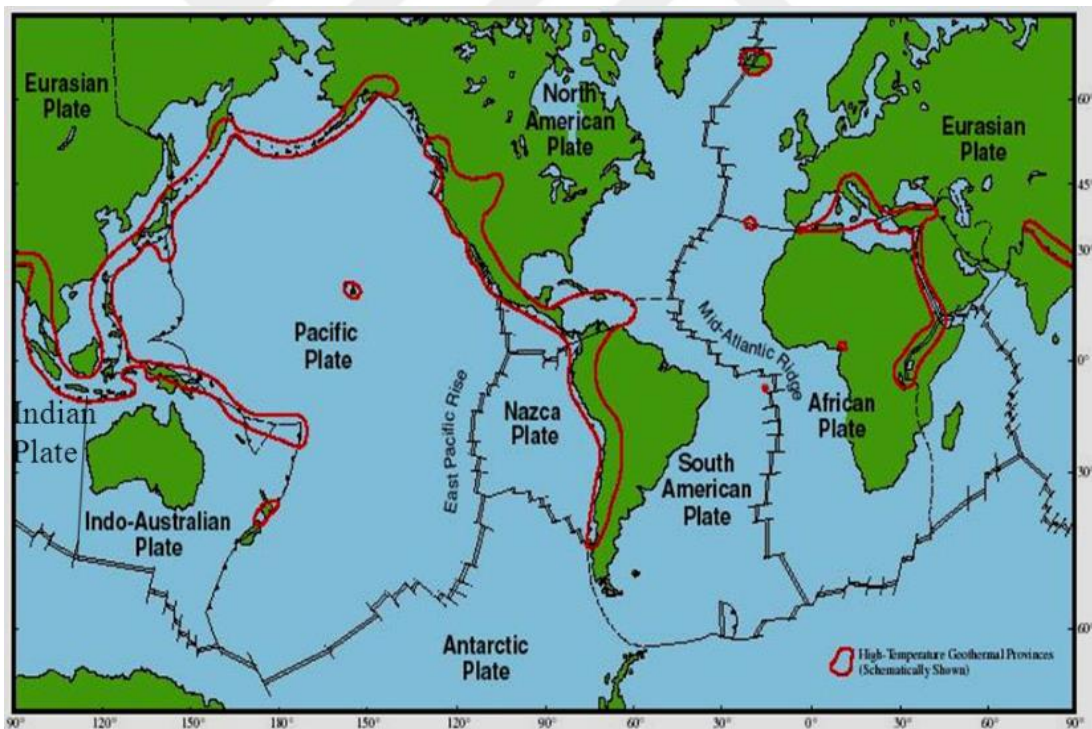


Figure 1.1 : World map of the major tectonic plates and location of the world's geothermal provinces (Smith, 2007).

Geothermal fields are located where the temperature gradient is as high as possible like the places where the earth's crust is thinner, active volcanoes are close by, magma chamber close to the surface and radioactive minerals that give out heat energy present.

Most of the geothermal fields are located at the plate boundaries, because in these places volcanoes are concentrated and hot magma is close to the surface. Geothermal power stations are installed in geothermal fields. Figure 1.2 shows the installed geothermal capacity for various countries all over the world. Turkey became the 7th country that has highest installed geothermal power generation capacity in June 2016. This represents a dramatic growth for geothermal power generation capacity.

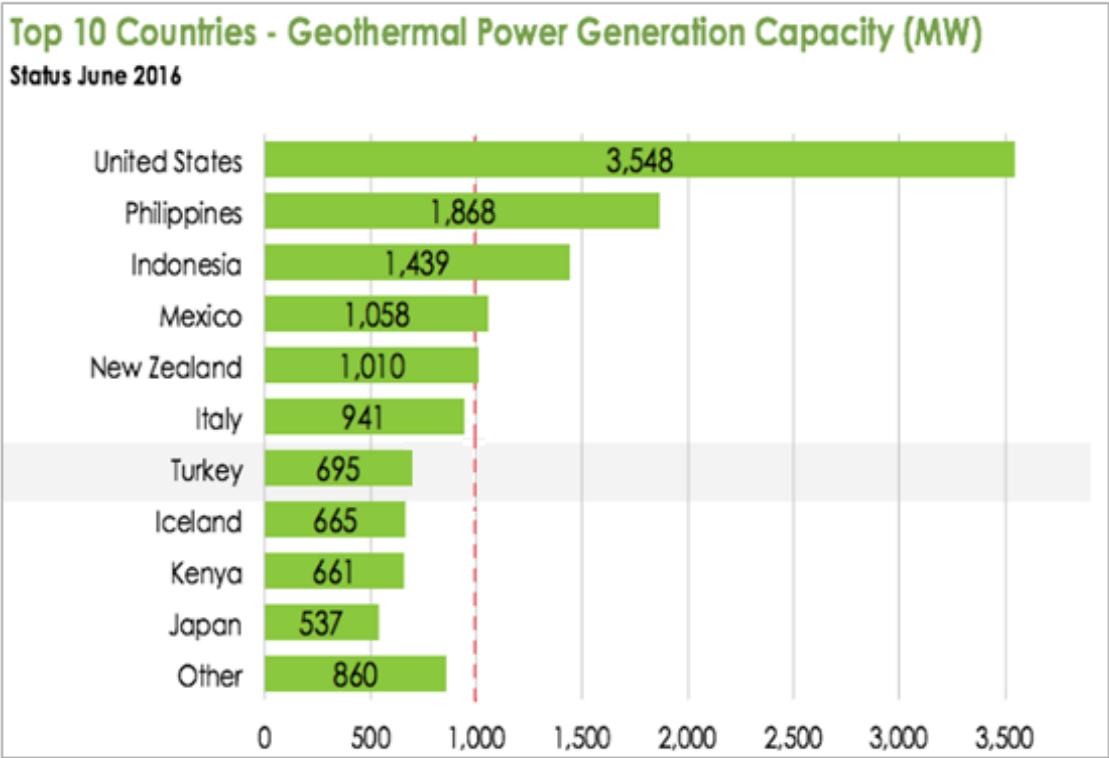


Figure 1.2 : Installed Geothermal Capacity as per countries (Url-1).

Turkey has rich geothermal sources. Tectonic forces, faults and local volcanisms are the main reason for the high heat flow and suitable conditions for hydrodynamics and convective systems in Turkey. The geothermal sites of Turkey are shown in Figure 1.3. According to this, geothermal systems are mainly located in the major grabens of the Menderes Metamorphic Massif, while those that are related with local volcanism are generally in the central and eastern parts of Turkey (Serpen et al., 2010). Figure 1.3 also presents the locations of major geothermal fields, district heating and greenhouse installations and also young volcanoes.

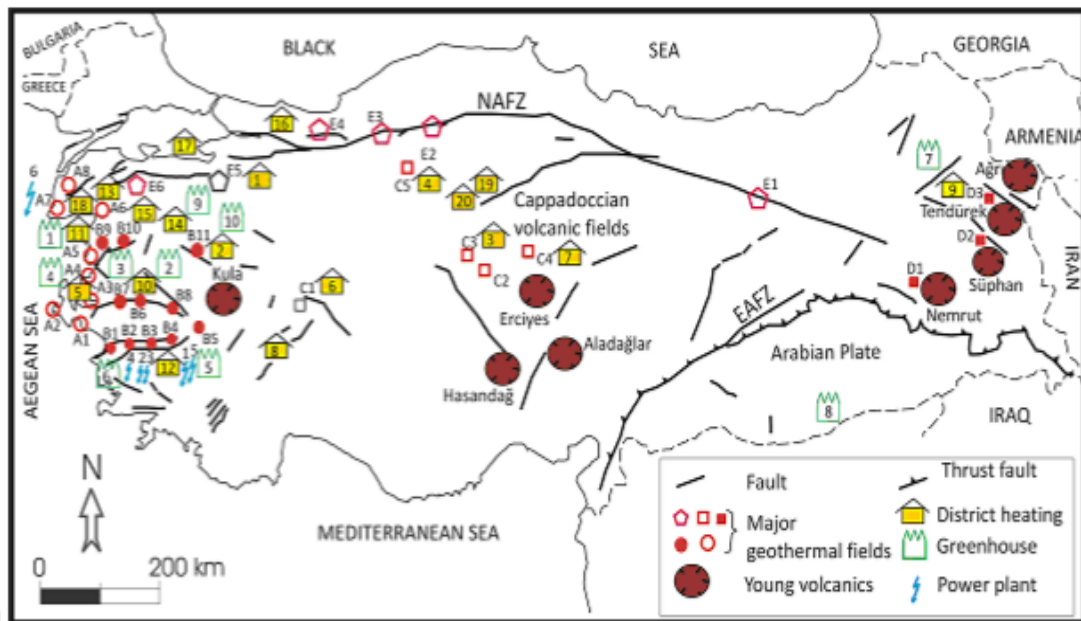


Figure 1.3 : Geothermal sites in Turkey (Serpen et al., 2010, updated from Serpen et al., 2009).

The geothermal research and exploration in Turkey was initiated by MTA (General Directorate of Mineral Research and Exploration) in 1960s. First geothermal exploration well was drilled in İzmir Balcova in 1963 and water at 124 °C temperature was produced. Subsequently, Kızıldere Field in Denizli was discovered. The first, well was drilled in 1968 and a reservoir with a temperature of 198°C was reached. In 1984, the first power plant with a 17.4 MWe capacity was installed. With time, fields such as Seferihisar, Simav, Salavatlı, Tuzla, Dikili, Caferbeyli were discovered and developed for various purposes. Today, the total number of wells drilled is about 1,200 for direct use and power generation. About 300 wells have been drilled in recent years for geothermal power projects (Url-2).

In 2013, the installed geothermal power generation capacity in Turkey was about 162.2 MWe. Currently, installed capacity of Turkey has reached to 695 MWe in June 2016. There are 24 geothermal power plants operating and with an additional 96 MWe in construction and planned projects of 430 MW as reported by Enerji Atlası and Think GeoEnergy (Url-1 and Url-2, 2016). Today, power plants generate a total of 3.676 GWh electricity per year. Table 1.1 lists the installed power plants in Turkey.

Table 1.1 : The installed power plants in Turkey (Url-2).

Geothermal Power Plant	City	In Operation Capacity, MWe
Pamukören	Aydın	22.5
Kerem	Aydın	24
Efeler	Aydın	114.9
Ken Kipaş	Aydın	24
Deniz (Maren 2)	Aydın	24
Çelikler Pamukören	Aydın	67.5
Gümüşköy	Aydın	13.2
Karkey Umurlu	Aydın	12
Dora-3 JES	Aydın	34
Maren	Aydın	44
Dora-2 JES	Aydın	9.5
Galiphoca JES	Aydın	47.4
Dora-1	Aydın	7.95
Babadere	Çanakkale	8
Tuzla	Çanakkale	7.5
Tosunlar-1	Denizli	3.8
Kızıldere-2 Zorlu	Denizli	80
Kızıldere Zorlu	Denizli	15
Kızıldere Bereket Eney	Denizli	6.85
Türkerler Alaşehir	Manisa	24
Alaşehir	Manisa	45
Enerjeo Kemaliye	Manisa	25
Pamukören 3 JES	Aydın	23
Greeneco JES	Denizli	13
	Total	695.1

The energy demand in Turkey is also growing dramatically. The electricity consumption of about 1485 kWh/ capita in 2002 has reached 3429 kWh in 2015 and it is expected to further increase to 6000 kWh in 2023 and 7000 kWh by 2050. High potential of geothermal energy in Turkey can promote to future energy demand. Based on recent projects it is clear that geothermal energy will contribute significantly to Turkey's future energy supply particularly for electricity generation and for space heating. The estimated projections of geothermal applications for the year 2018 reported by Turkish Geothermal Association are given in Table 1.2.

Table 1.2 : The estimated projections of geothermal applications for the year 2018 (TGA, 2013).

Use	Projection
Electricity Production	750 MWe
Heating (residences, hotels, thermal facilities etc.)	4000 MWt
Greenhouse heating	2040 MWt
Drying	500 MWt
Balneology	1100 MWt
Cooling	300 MWt
Aquaculture + others	400 MWt
Total direct use	8340 MWt

In order to evaluate a geothermal field and make future performance predictions, geothermal reservoir simulation studies should take place. Early reservoir simulations considered the geothermal water to be pure water. However, geothermal waters may contain significant amounts of non-condensable gases such as carbon dioxide. Many geothermal reservoirs in Turkey contain some amount of CO₂. For liquid dominated geothermal reservoirs, mass fractions of CO₂ dissolved in liquid water can be as much as 5%. The Kizildere field in Turkey, for example, contains around 1.5% CO₂ dissolved in the liquid water and this value increases up to 3% in the deep zones (Satman et al., 2005).

The Afyon Ömer-Gecek field and Germencik field on the other hand contain 0.4 % and 2.1 % dissolved CO₂ (Satman et al., 2007), respectively. When modelling such geothermal reservoirs (either using numerical models or lumped parameter models) it is crucial to account for the effects of CO₂ in the model in order to utilize geothermal sources in an efficient way. When production starts in a geothermal field, CO₂ dominates the thermodynamic properties of flow. Particularly the flashing point of the water CO₂ mixture changes significantly with changing mass fraction of CO₂ in the mixture. Geothermal systems with CO₂ content have a higher flashing point mixture than systems with pure water. Increasing amounts of CO₂ increase the flashing point pressure. This affect has an important role in reservoir performance.

1.1 Literature Review

The primary objective for geothermal reservoir modeling is to obtain information on the physical conditions in a geothermal system as well as on its nature and properties.

This leads to proper understanding of its characteristics and successful management of the resource. Second objective is to predict the response of a reservoir to future production and estimate the production potential of a system.

Geothermal systems are dynamic systems where continuous transport of fluid, heat and chemical species occur (Donaldson et al., 1983). At first, much of geothermal reservoir development was based on techniques adapted from groundwater and petroleum industries but in time specific models have been evaluated for geothermal systems. The need for reservoir modeling often arises early in the development of a geothermal field. Initially, the volumetric method can be used to predict the potential of the reservoir with the help of data such as area, depth, porosity of the reservoir and fluid properties but calculation of reserves is not meaningful unless the performance of the reservoir can be forecasted. The behavior of geothermal reservoirs can be modeled by three methods. These are decline curve analysis, lumped parameter methods and distributed parameter (numerical) methods.

The decline curve method is the simplest method that involves fitting an equation to observed flow rate decline data from wells but it is not based on any conceptual model of the reservoir. In order to use this approach sufficient production data must be obtained. Another drawback of decline curves is that they cannot take into account changes in field operation (Bodvarsson et al., 1986). The use of logarithmic, harmonic, and exponential functions to curve fit data have been suggested in the literature. Arps (1945) and Chierici (1964) had major effect on development of this method. Successful results have been obtained in Larderello and Geysers Fields (Budd, 1972; Stockton et al., 1984).

In numerical methods, geothermal reservoirs are split into gridblocks and conservation equations are applied on each gridblock. The complex nonlinear partial differential equations are solved numerically with the advancement of the computer. It is the most general technique of modeling because it considers spatial variations in thermodynamic conditions and reservoir properties as well as for different well spacing and locations. Numerical modeling is extremely powerful when based on comprehensive and detailed data. The disadvantages of the numerical models are; they need comprehensive and detailed data that are not available especially at the early time of the field and also the model can be time consuming when it contains very large number of gridblocks. In addition, the long run-times associated with these models

create another disadvantage for history matching where the model needs to be run many times. Lumped parameter (tank) models provide a good alternative to numerical model due to the much fewer parameters requirement and the relatively shorter run times.

Lumped-parameter modeling can be simply described as a highly simplified form of numerical modeling. In numerical models, a geothermal system is represented by many gridblocks while in lumped-parameter models; a single or a few homogeneous tanks form the geothermal system. In lumped parameter models, each component of a geothermal system is represented using a tank that is composed of fluid and rock (Sarak et al, 2005). Volumetric average properties are assigned to these tanks and changes of pressure, temperature and production are monitored. The tanks represent the reservoir, the aquifer, the heating source or the atmospheric block to which natural discharge occurs. Lumped parameter modelling is possible when a minimum knowledge on the system variables is available. The results are comparable with the numerical simulators and they are useful for sensitivity studies to help focus on the more important parameters to be studied by more complex distributed parameter simulators (Castainer et al., 1980).

There are several approaches for the modelling of geothermal systems. However, from the literature survey, it can be observed that numerical and lumped parameter models are generally used to model geothermal system.

1.1.1 Numerical Models

The numerical solution of complex non-linear partial differential equations became possible in the late 1960s with the advent of digital computers. However, the application of these techniques to model the behavior of geothermal reservoirs began to appear in the early 1970s because coupling mass and energy transport in a geothermal reservoir adds considerable complexity to the modeling. In this approach, the governing partial differential equations are replaced by an equivalent set of algebraic equations and the problem is solved numerically.

Mercer (1973) made the first application of a numerical model to a geothermal field problem. He developed a single phase (liquid water) heat transport model and applied to Wairakei geothermal field and simulated until the reservoir became two-phase. Mercer and Faust (1975) formulated the equations of two-phase (steam-water), heat

transport in terms of enthalpy and pressures. Formulation of the basic mass, momentum and energy balances in terms of fluid pressure and enthalpy yields two nonlinear, partial differential equations that are valid for both liquid and vapor dominated hydrothermal reservoirs, as well as for reservoirs that may include both single and two-phase regions. They presented a simulation of a hypothetical hot water reservoir with initial conditions similar to those in the Wairekei reservoir. Faust and Mercer (1976) developed another simulator by using finite difference technique and compared it with the previous one.

Toronyi and Farouq Ali (1975) developed a two-phase, two dimensional reservoir model using finite difference technique which was coupled with a wellbore model. Their model used pressure and water saturation as dependent variables that were simultaneously solved at each block. Their simulator produced stable results under large time step sizes. According to the production results they classified the two phase geothermal reservoir behavior into three depending on the initial liquid saturation. These are vapor dominated system, liquid dominated system and two phase dominated system. Furthermore a two phase two dimensional cross-sectional reservoir model where multiphase equations were formulated in terms of density and internal energy were presented by Lasseter et. al. (1975).

Coats et.al (1974) developed a geothermal model based on methods developed for steamflood analyses in petroleum reservoirs. Coats et al. (1974) formulated the energy balance in terms of internal energies and they overcame the phase transition difficulties by ensuring continuity of thermodynamic formulae across the saturation curve. Coats (1977) approximated density and specific internal energy in superheated region as perturbations from the saturation curves. He also investigated the stability limits for an implicit model formulation and evaluated the model that was stable for time steps corresponding to large saturation changes.

Thomas and Pierson (1978) developed a three-dimensional, finite-difference model for the simulation of geothermal reservoirs that contain water in various regions of a reservoir in any of its vapor or liquid states. The solution technique employed simultaneously solves the mass and energy balances.

Some further modeling studies were published but the effective starting point for the acceptance by the geothermal industry of the usefulness of computer simulation was

the 1980 Code Comparison Study (Stanford Geothermal Program, 1980). Since then, the experiences of developing site-specific models and carrying out generic reservoir modeling studies has led to a steady improvement in the capabilities of the geothermal reservoir simulation codes.

In 1979, the geothermal reservoir modelling group at the University of Auckland and the Earth Sciences Division of Lawrence Berkeley Laboratory collaborated and developed a geothermal simulator called SHAFT78 (Pruess et al., 1979). This simulator is based on mass and energy balance equations for two phase flow in a porous medium. It used an integrated finite difference method to solve finite difference equations that are obtained by formally integrating the basic partial differential equations for mass and energy flow over arbitrary volume elements. In the following years they created MULKOM family of codes for investigations of fundamental reservoir physics and for modelling reservoirs (Pruess; 1983, 1988).

Bodvarsson et al (1982) modelled the fault-charged reservoirs with the consideration of conductive heat transfer. A two-dimensional model of fault-charged hydrothermal systems has been developed that considers the transient development of such systems including the effects of heat losses to the confining layers. The model has been applied to the hydrothermal system at Susanville, California. Additionally, they emphasized that no universal modeling strategy is applicable to all of the geothermal systems since geothermal systems are complex, exhibiting such features as fracture-dominated flow, phase change, chemical reactions and thermal effects. Therefore, in the selection of a proper method, one must consider the amount and quality of the field data available and the objective of the study. (Bodvarsson et al., 1986)

Pruess and Wu (1989) reviewed the methodological aspects of geothermal reservoir modeling with special emphasis on flow in fractured media and pointed out the tangible impacts of reservoir simulation technology on geothermal energy development (Pruess, 1991). Then they released numerical simulator called TOUGH2 which belongs to the MULKOM family of codes for simulating nonisothermal flows of multiphase, multicomponent fluids in permeable (porous or fractured) media. One of the modules included in TOUGH2 models the behaviour of fluids in gas-rich geothermal reservoirs which often contain CO₂ mass fractions according to O'Sullivan et al. (1985) approaches. It accounts for non-ideal behaviour of gaseous CO₂ and dissolution of CO₂ in the aqueous phase according to Henry's law with heat of solution

effect. The thermophysical property correlations are based on the model of Sutton and McNabb (1977) and the viscosity of vapor-CO₂ mixtures is calculated with a formulation given by Pritchett et al. (1981).

1.1.2 Lumped Parameter Models

The first reservoir model for geothermal systems was developed by Whiting and Ramey (1969) with lumped parameter modeling. They proposed a model considering the reservoir as a tank characterized by parameters such as volume, porosity, pressure and temperature. They coupled heat and mass balances and permitted recharge fluid to enter from variety of aquifer geometries. Their study also included a match of the pressure/production performance of the Wairekei geothermal reservoir in New Zealand from 1956 to 1966.

Sanyal et al (1976) presented an analytical modelling of fluid flow and heat transfer in geothermal reservoirs. The model was assumed to be a vertical stack of horizontal layers, permeable and impermeable layers alternating. The heat transfer problem was solved according to the approach proposed by Gringarten and Sauty (1975). In their model, the breakthrough time of injected water in each layer, pressure distribution in space and time and the temperature of the produced water over time can be monitored. The results of this study were compatible with the data coming from Heber geothermal reservoir in the Imperial Valley of California.

Brigham and Morrow (1977) described a block model with both a vapor and liquid zone. They proposed lumped parameter model, taking into account the fact that the distribution of two phases in the reservoir can be homogeneous or separate. However they considered only the case of production of dry steam. These models gave good results in demonstrating the influence of porosity on reservoir behavior.

Castaner (1979) gave a mathematical model for the description of two phase flow. The results of the numerical model describing the total evaluation of the reservoir were verified using laboratory data. An excellent agreement between numerical and experimental results was found. Castanier et al. (1980) included heat transfer in the recharge region to simulate the behavior of the East Mesa reservoir. They developed an analytical model that is suitable for liquid dominated, steam dominated or two phase geothermal system. In this model the reservoir is divided into three different zones. From the center to the periphery, the first zone is the innermost zone which the

reservoir is assumed to be producing from. It is treated as a tank from the viewpoint of mass and energy production, using a lumped-parameter model, but one in which the pressure distribution is calculated by an analytical formulation of pressure behavior of off-centered wells enclosed in a constant pressure boundary circle. The surrounding intermediate zone from which fluids migrate into the production zone is subjected to fluid flow and heat transfer but no production or injection occurs. The outermost, radially infinite (or finite) aquifer zone is subjected to mass transfer. The injection or natural water influx occurs in this zone. Castaner and Brigham (1983) presented the examples of utilization of this lumped parameter model. They made a comparison on the East Mesa reservoir between lumped parameter results and the results obtained by Morris and Campbell (1979) using a complex, fully implicit, three-dimensional finite difference simulator. A reasonable agreement with the Morris and Campbell results was obtained by the lumped parameter technique. This concluded that the small amount of computer time required by the lumped parameter model allows the engineer to perform extensive sensitivity studies on the reservoir parameters and a more complex distributed parameter simulator can then be used efficiently to obtain better accuracy and refine the results. This type of approach would be particularly appropriate and cost effective during field development planning.

Olsen (1984) adopted the methods developed for petroleum reservoirs involving a material balance on the reservoir in geothermal reservoir engineering. He derived depletion models for liquid-dominated geothermal reservoirs. Depletion models with no recharge (or influx), and depletion models including recharge, were used to match field data from the Svartsengi high temperature geothermal field in Iceland. He concluded that lumped parameter models although computationally simple match drawdown-production data. Moreover, the match to production data from Svartsengi was improved when influx obtained using an infinite linear aquifer model with the Hurst simplified method was included.

Axelsson (1985) exhibited a method that could simulate long term production data by simple lumped capacitor/conductor network based on only production/drawdown data and showed that the responses of analytical as well as real systems can be easily simulated by such simple systems. The parameters of simulation also provide information on global hydrological characteristics of hydrothermal systems.

Axelsson (1989) represented an effective method of lumped parameter modeling, which has been used successfully for pressure response data from several Icelandic geothermal reservoirs. In his method, lumped parameter models consisted of series of tanks and resistors that simulate the storage capacity of various parts of a geothermal system. The storage coefficients of the tanks and the conductance coefficients of resistors of the model were estimated by a program. This method tackled the simulation problem as an inverse problem and automatically fits analytical response functions of lumped models to the observed data by using a nonlinear iterative least-squares technique for estimating the model parameters. His work was valid for low temperature liquid reservoirs only and assumed that variations in temperature within the system were neglected. Axelsson and Gunnlaugsson (2000) discussed the usefulness of lumped parameter models in interpreting monitored production data for low temperature geothermal fields. Axelsson et al. (2005) reported that reservoir modeling by using this method is highly cost effective and has been shown to yield quite acceptably accurate results because it tackles the modeling as an inverse problem, which requires much less time and operator intervention than direct or forward modeling. Rezvani-Khalilabad and Axelsson (2008) concluded that lumped parameter modelling was based on the production history of a geothermal system and used to simulate the available pressure decline history, preferably from a centrally located observation well.

Sarak et. al (2005) described a method of lumped parameter modeling for low temperature geothermal reservoirs with the assumption of isothermal behavior. The model considers the effects of fluid production, reinjection and natural recharge, on the pressure (or water level) of low temperature, liquid dominated geothermal systems. The model was similar in concept to the one presented by Axelsson with new variants and revised method of matching and simulating data. In their study, they developed analytical solutions to various combinations of tanks and estimated the characteristics of the reservoir by history matching of observed data.

Onur et al. (2008) proposed a nonisothermal lumped-parameter model which enables one to predict both pressure and temperature behavior of liquid dominated geothermal reservoirs. They showed that the reservoir parameters such as bulk volume and porosity that are not accessible from history matching of pressure alone can be determined by the combination of temperature and pressure data in history matching.

Their model explained the variable rate nonisothermal flow, based on the solution of both mass and energy balance equations considering only convection. Tureyen et al. (2009) developed a generalized lumped parameter model that enables simulation of pressure and temperature of multiple tank and model effect of components such as aquifer and multiple reservoirs that are in hydraulic interaction. Tureyen and Akyapi (2011) extended the Onur et al. (2008) and Tureyen et al. (2009) studies to include the effects of conduction. Also Tureyen et al. (2014a) have studied the the uncertainty in future pressure and/or temperature data simulated by using history-matched lumped-parameter models for single-phase liquid water geothermal systems. With this approach, reservoir management decisions that account for an incomplete knowledge of the actual geothermal system can be made.

1.1.3 Models for Geothermal Reservoirs Containing CO₂

In early geothermal reservoir simulations the reservoir fluids were idealized as pure water but many geothermal reservoirs contain significant amounts of noncondensable gases including H₂S, N₂, NH₃, H₂, CH₄ and CO₂ with the concentration of gas ranges from 0.1 to 10 percent by mass. Subsequent more realistic representations of geothermal fluids must include carbon dioxide, which usually is the most prominent noncondensable gas. CO₂ has large effects on conditions within a reservoir; therefore, it should be examined in detail. H₂O-CO₂ system has not been investigated until 1959. Pollitzer and Strebel (1924) only studied the relations between saturated water vapor and various gases and suggested that the compression of liquid water by CO₂ gas and solution of CO₂ in water causes the partial pressure of water in the vapor phase to increase. Malinin (1959) presented a binary diagram that extended to 600 bars in pressure and to temperatures of 330°C. Ellis and Golding (1963) studied the solubility of CO₂ in water and presented the effects of CO₂. They reported detailed data on solubility of CO₂ in water in the temperature range of 120°C-350°C and at pressures up to 160 atm. They concluded that the higher the sum of partial pressures of gases present, the lower the boiling temperature will be. Takenouchi and Kennedy (1964) studied the water-carbon dioxide system to pressures of 1600 bars and over a temperature range of 110°C to 350°C. They informed that complete miscibility in the H₂O-CO₂ system will not be found at temperatures under 265°C naturally. At higher temperatures a completely mixed supercritical fluid may exist but at lower temperatures this fluid will segregate into two fluid phases. They found that at low

pressures the CO₂ rich phase is the light phase but at higher pressures an inversion in density occurs and the CO₂ rich phase becomes the denser phase.

The effects of CO₂ in modeling geothermal systems have been considered by many authors in the literature. Sutton (1976) showed how to calculate the pressure-temperature curve for a CO₂-H₂O system. He has calculated the boiling curves for a mixture of water and CO₂ under various conditions typical of Broadlands geothermal fields. Sutton and McNabb (1977) investigated the Broadlands fields and showed that pressure-temperature data could be fitted closely by a boiling curve of a CO₂-H₂O mixture of 4.4 percent CO₂ by mass. Grant (1977a) proved this by incorporating CO₂ in a lumped parameter model of Ohaki-Broadlands reservoir and obtaining a reasonable match with field data. Broadlands geothermal field is a hot-water system containing a few per cent of carbon dioxide which makes the field response markedly different from a conventional hot-water system. His block model of Broadlands was the first model to be developed for a two component CO₂-H₂O gas dominated field. He showed that almost all pressure drops during early time was caused by change in partial pressure of CO₂. Thus, a substantial pressure drop may occur without significant boiling since the vapor pressure of water is not greatly affected. Moreover, if the system does not contain CO₂ much larger saturation changes are required to produce similar pressure drop. Atkinson et al. (1980) presented a production history match for the two-component CO₂-H₂O Bagnore geothermal field. They studied the behavior of the vapor dominated geothermal system with a mathematical model that was based on the conservation of mass, energy and CO₂. The relationship between total gas and partial pressure of CO₂ is stated with Gibbs-Dalton laws. The thermodynamics of the model is similar to the one presented by Grant (1977b) and the two-zone block model approach of Brigham and Morrow (1977). The parameters varied for history matching were the sizes of the liquid and vapor regions, porosity and liquid recharge. Reasonable agreement was achieved between the modeled and observed pressure drawdown but there was poor agreement with the observed producing noncondensable gas content.

Zyvolosky and O'Sullivan (1978) presented some of the initial results of a simulation of the behaviour of a multi-dimensional carbon dioxide dominated reservoir. Zyvolosky and O'Sullivan (1980) numerically modeled the transport of CO₂ in a two-phase geothermal system. They gave a very detailed description of the conservation

equations to be used in numerical simulation of geothermal reservoirs. The authors used three conservation equations; a mass balance equation for water, an overall energy balance equation and a mass balance equation for CO₂. In this study the primary variables are taken to be pressure, enthalpy and temperature. Their model showed that CO₂ has significant effect on pressure transients; therefore, monitoring of the gas content is required for correct interpretation of pressure transients in a gassy geothermal field. According to these two studies, they found that, the qualitative behavior of the pressure transients is affected by the saturation and the presence of carbon dioxide. At high liquid saturations, they suggested that discharge is mainly from the liquid phase in which CO₂ content is low. Therefore, the primary effect of the presence of CO₂ on the system is in reducing compressibility of the fluid which leads to faster propagation of pressure transients. They used pressure and temperature curves of Sutton (1976) for a two phase system of water and CO₂ as input. Their study is limited because the thermodynamic package used could only handle two-phase conditions.

Atkinson et. al. (1980) presented a lumped parameter model for vapor dominated reservoirs to be used in modeling the Bagnore geothermal reservoir which contains considerable amounts of CO₂. Since the initial conditions of the Bagnore field was reported to be two phase, the authors have adopted a model that is composed of two tanks; one for modeling the liquid region and the other for modeling the vapor region and mass transfer is allowed between the two tanks.

Pritchett et al (1981) used CO₂ in the analysis of the natural state of Baca reservoir and they formed an equation of state package for water-carbon dioxide mixtures. They concluded that reservoir could be either single phase liquid or two-phase depending on the amount of gas in the reservoir. They studied CO₂ transients in a homogeneous porous medium during a constant rate test. They showed that the CO₂ content could not be properly inferred from pressure-temperature measurements made on flowing wells and the measured CO₂ content may be either higher or lower than that in situ. Moreover, they found that initial fluid enthalpy increases with CO₂ content.

O'Sullivan et. al (1985) used multicomponent two phase reservoir simulator MULKOM (Pruess, 1983, 1988) to describe the effects of CO₂ in geothermal reservoirs in a more complete and detailed way. The H₂O-CO₂ thermodynamic package used in their study was an improved version of the one used by Zyvolosky

and O'Sullivan (1978). They gave a detailed description of how primary variables should be adjusted and updated during the numerical simulation of a geothermal reservoir based on if the fluid is under a compressed liquid state, two phase state or single phase gas state. The results of this investigation showed that in the natural state CO₂ increases the size of the boiling zone considerably and during exploitation the gas escapes rapidly leading to a large early pressure drop. The pressure response is faster at early times because of degassing and slower at later times because of a reduced flowing enthalpy. They also showed that the stable flowing CO₂ content primarily depends on the relative permeability functions, the initial vapor saturation, and the initial partial pressure of CO₂ while smaller effects are due to the flow rate and porosity. The approach presented by the authors are still in use today.

Alkan and Satman (1990) have improved on the lumped parameter model of Whiting and Ramey (1969), originally developed for pure water systems, by introducing a thermodynamic package that describes the behavior of water-CO₂ systems. This thermodynamic package simply replaces the thermodynamic package describing pure water systems. Their model was simple and very general and could be used for a pressurized water-CO₂ system and for a liquid-dominated system. The model of Alkan and Satman (1990) was tested against field data coming from Cerro Prieto, Ohaaki, Bagnore and Kizildere fields.

Moya and Iglesias (1995) also included the effects of CO₂ into reservoir simulators. They developed a new equation of state (EOS) for water-carbon dioxide mixtures. This model considered the non-ideal behavior of both components in the gaseous mixture and included the effect of the compressibility of the liquid phase. They coupled this EOS to the TOUGH numerical simulator to get information about the mass and energy productivities of the geothermal wells. Batistelli et. al (1997) described the correlations employed to calculate the thermophysical properties of multiphase mixtures of water, sodium chloride and carbon dioxide and related EWASG module which is one of the module that belongs to TOUGH2 simulator. Their thermophysical formulation is applicable in temperatures from 100° to 350°C, total pressure up to 80 MPa, partial pressure of CO₂ up to 10 MPa, and salt mass fraction up to halite saturation.

There are some correlations for Henry's constant linking the mass fraction with the partial pressure which can be found in the literature. Cramer (1982) defined Henry's

constant for the dissolution of carbon dioxide in pure water by using polynomial regression of experimental data from 0°C to 300°C. Upton and Santoya (2002) developed a new correlation to estimate the solubility of carbon dioxide in water. This equation was derived from a statistical analysis applied to an updated thermodynamical database containing experimental solubility data reported in the literature.

Satman and Uğur (2002) have modeled the two phase compressibility at the flashing point pressure of water-carbon dioxide systems. Using this definition of compressibility together with a simple mass balance, information could be obtained regarding the overall size of the geothermal reservoir. The developed model is used for modeling the Cerro Prieto, Ohaaki, and Kizildere fields.

Kaya et al. (2005) have used the simulator TOUGH 2 for analyzing the behavior of geothermal reservoirs with carbon dioxide for various different partial pressures of carbon dioxide. The analysis is performed for both single phase and two phase systems. The relationship between the mass fractions of CO₂ in the produced fluid and the mass fraction in the reservoir were studied using various critical gas saturation and irreducible water saturation values.

The study performed by Hosgor et al. (2013) forms the basis of this thesis. But in that study simple models were investigated. Later, Hosgor et al. (2015) have presented a lumped parameter model capable of modeling water-carbon dioxide geothermal systems. They have adopted the approach of O'Sullivan et al. (1985) on a tank in lumped parameter modeling. They have analyzed various effects of parameters such as the initial amount of carbon dioxide, production rate, and reinjection rate on the performance of pressure, temperature, saturation and carbon dioxide amount both in the liquid and gas phases.

1.2 Purpose of Thesis

The purpose of this thesis is to develop a new nonisothermal lumped parameter model (tank model) to examine and predict the behavior of mass and heat production of geothermal fluids with the consideration of the effects of carbon dioxide. The change of pressure and temperature that occurs from production, reinjection and natural recharge, the change of CO₂ saturation with the production and also variation of gas

saturation in the geothermal reservoir can be examined with this model. In addition to this, each component of a geothermal system is represented using a tank that is composed of fluid and rock so the pressure and temperature behavior of any component (reservoir or aquifer) that forms the geothermal reservoir can be modelled. This thesis is organized as follows. In Chapter 2, the thermodynamic package used in the model is given. The thermodynamic properties of H₂O, CO₂ and H₂O-CO₂ system are described in detailed. In Chapter 3, the methodology of the modelling study is given. The general aspects of lumped parameter modelling are discussed, new lumped parameter model developed for geothermal system that contains CO₂ is explained and detailed formulation is given. The verification study of the tank model with PETRASIM TOUGH2 are given. Moreover, some synthetic application studies are performed. The various synthetic cases that demonstrate especially the effects of various parameters on the change of carbon dioxide in the reservoir are examined. In Chapter 4, a new analytical model that give the amount of carbon dioxide as a function of time and amounts of production, reinjection and recharge for liquid dominated reservoirs is presented. The verification study of the tank model with analytical model is given and some synthetic applications with analytical model are represented. In Chapter 5, field application (Germencik geothermal field) is performed and results are discussed in detailed. Finally, the major conclusions obtained from this study and recommendations for future works are presented in Chapter 6.

2. THERMODYNAMIC PACKAGE

PVT behavior of geothermal fluid systems plays a very important role in reservoir performance and energy production studies. Thermophysical properties needed to model the flow of fluid in geothermal reservoir include density, viscosity and specific enthalpy (or internal energy) of the fluid phases as functions of temperature, pressure, and composition. The following subsections focus on the thermophysical properties and related equations used for pure water and CO₂, H₂O-CO₂ systems and additionally H₂O-CO₂-NaCl systems. Basically, the behavior of H₂O-CO₂ systems and the most profound effect of CO₂ on H₂O-CO₂ mixtures are defined. The review of the equations that represent the thermodynamic package of H₂O-CO₂ systems used in this study is given. The main purpose of the thermodynamic package is to provide simple, but accurate representations and models for predicting the overall thermophysical behavior of the H₂O-CO₂ in a geothermal system.

2.1 Thermophysical properties of H₂O

The density, enthalpy and internal energy of water in liquid and gas phase are calculated according to the IAPWS (The International Association for the Properties of Water and Steam) (2007). IAPWS has divided pressure-temperature diagram of water into five regions as given in Figure 2.1 and equations are derived for each regions. Critical and triple points data for H₂O are presented in Table 2.1.

Table 2.1 : The critical and triple point parameters for H₂O (Wagner and Pruess, 2002).

	Temperature (K)	Pressure (MPa)	Vapor Density (kg/m ³)	Liquid Density (kg/m ³)
Critical Point	647.096	22.0640	322	322
Triple Point	273.150	0.00618	0.00485	999.8

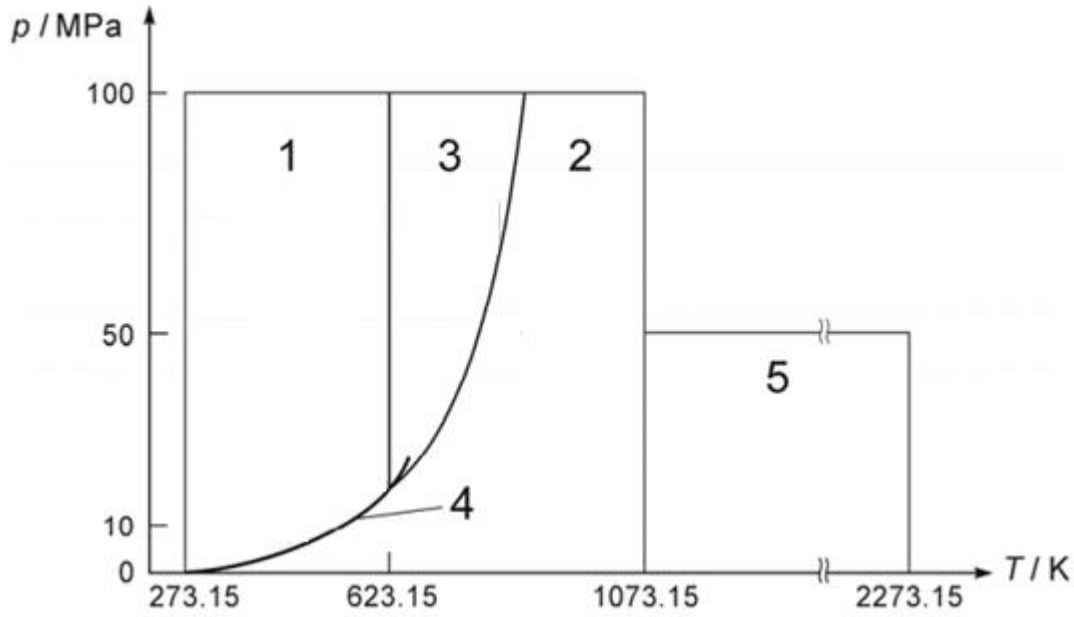


Figure 2.1 : Pressure–temperature regions of IAPWS-IFT97 for water (adapted from IAPWS, 2007).

Viscosity of saturated water is calculated according to Meyer et al. (1977) formula given in equation 2.1;

$$\mu_w = 0.2414 \times 10^{247.8/(T+133.15)} \times 10^{-4} \quad (2.1)$$

Here, T is in $^{\circ}\text{C}$, and μ_w is in Pa.s. The saturated water viscosity can be modified for compressed water as following equation 2.2:

$$\mu_w = 0.2414 \times 10^{247.8/(T+133.15)} \left\{ 1 + \frac{[p - p_s(T)]}{10^{11}} 1.0467(T - 31.85) \right\} \times 10^{-4} \quad (2.2)$$

where p and $p_s(T)$ in Pa is the pressure and saturation pressure, respectively. But above modification can be neglected because of its minor effect. Water viscosity slightly changes with pressure at constant temperature but significantly changes with temperature at constant pressure. Thus, the viscosity of compressed water is approximated by the saturated water relation as given in equation 2.1. Then it can be treated that viscosity of water is independent of pressure as given in Figure 2.2.

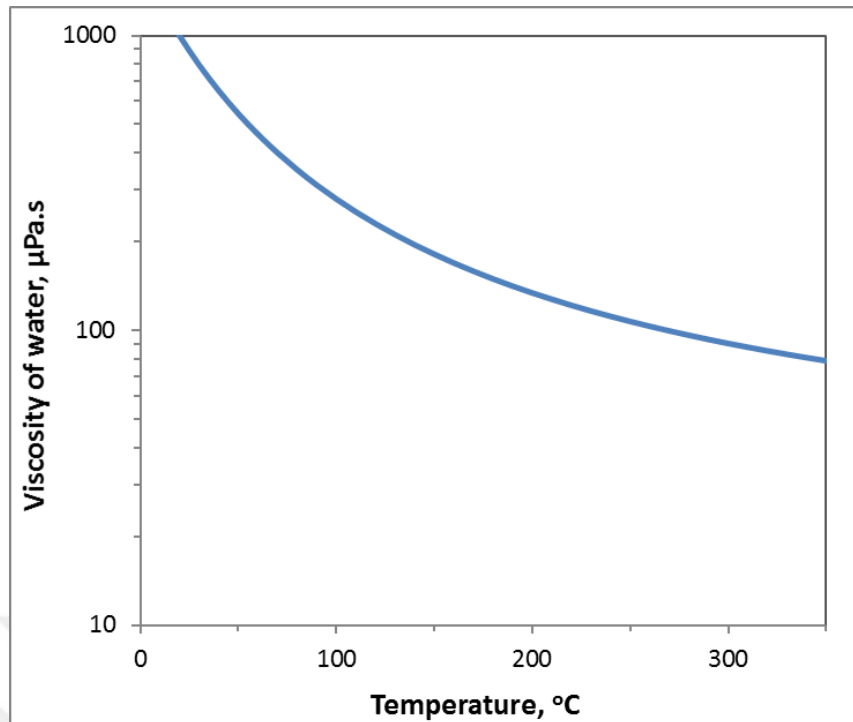


Figure 2.2 : Viscosity behavior of water.

2.2 Thermophysical properties of CO₂

Many geothermal reservoir fluid contain significant amounts of dissolved gases with the concentration of gas ranging from 0.1 to 10 percent by mass. The most prominent noncondensable gas in geothermal fluids is carbon dioxide. CO₂ is typically close to 90% by volume of the total noncondensable geothermal gases. For this reason CO₂ is generally chosen to describe the overall effects of noncondensable gases in geothermal reservoir simulation. The presence of CO₂ considerably influences the behavior of a geothermal reservoir and utilization process.

The origin of gaseous CO₂ in reservoirs is usually organic or magmatic. The four most common mechanisms for the formation of CO₂ gas in the reservoir are described by Michels (1979). The first is a phase change of CO₂ due to change in pressure conditions when the fluid emerges at the surface, the second one is the dissociation of bicarbonate, the third is the result of calcite precipitation and the fourth one is associated with proton consumption. The relative effect of these processes to geothermal fields is different due to the different characteristics of the reservoirs.

Table 2.2 provides the critical and triple points of CO₂. At atmospheric pressure CO₂ changes directly from a solid phase to a gaseous phase through sublimation, or from

gaseous to solid through deposition. Liquid CO₂ forms only at pressures above 0.516 MPa. At lower (subcritical) temperatures and/or pressures, CO₂ can exist in two different states, a liquid and gaseous, as well as two-phase mixture of these states.

Table 2.2 : The critical and triple point parameters for CO₂ (Span and Wagner, 1996).

	Temperature (K)	Pressure (MPa)	Vapor Density (kg/m ³)	Liquid Density (kg/m ³)
Critical Points	304.13	7.3773	467.6	467.6
Triple Points	216.59	0.516	13.8	1179.25

In geothermal applications, the amount of CO₂ in liquid phase is small. For simplicity and dominant effect of water in all liquid phase, the liquid phase density and the liquid phase viscosity of a CO₂ are neglected and density and viscosity of liquid mixture are taken equal to that of the density and viscosity of pure liquid water. For the gas phase, the density of gaseous CO₂ (kg/m³) is determined from correlation in equation 2.3 given by Sutton (1976) as follows;

$$\rho_c = \frac{44 p_c}{8.31 T \times 1000} \quad (2.3)$$

where, p_c is the partial pressure of CO₂ in Pa and T is in K. Density of gaseous CO₂ versus pressure for various temperature is plotted in Figure 2.3. Based on this figure, CO₂ density linearly increases with pressure but decreases with temperature.

The specific enthalpy of the gaseous CO₂ (J/kg) is calculated based on equation 2.4 given by Sutton (1976);

$$h_c = -2.18 \times 10^5 + 732T + 0.252T^2 - 2.63 \times 10^{-5}T^3 \quad (2.4)$$

Change of enthalpy for gaseous CO₂ with respect to temperature is given in Figure 2.4. Enthalpy changes slowly with temperature, because of its relatively low specific heat capacity in gas state. Pressure has minor effect on enthalpy of CO₂.

For the gaseous viscosity of pure CO₂ calculation, curve fitting approach to the data tabulated by Vargaftik et al. (1996) is used. Based on this approach, viscosity of CO₂ is calculated with equation 2.5.

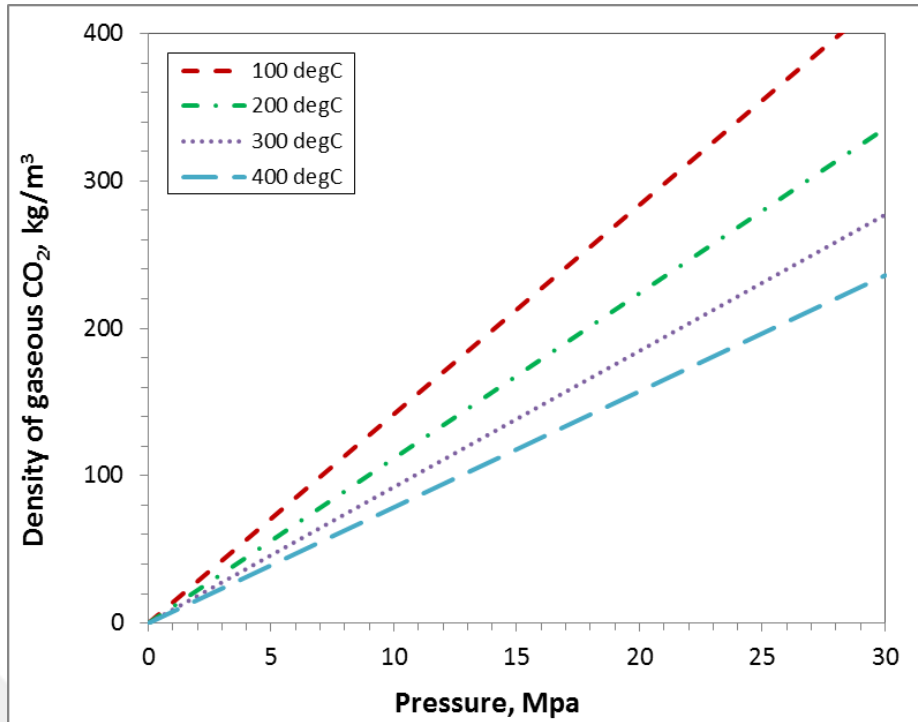


Figure 2.3 : Pressure-temperature-density graph of gaseous CO₂.

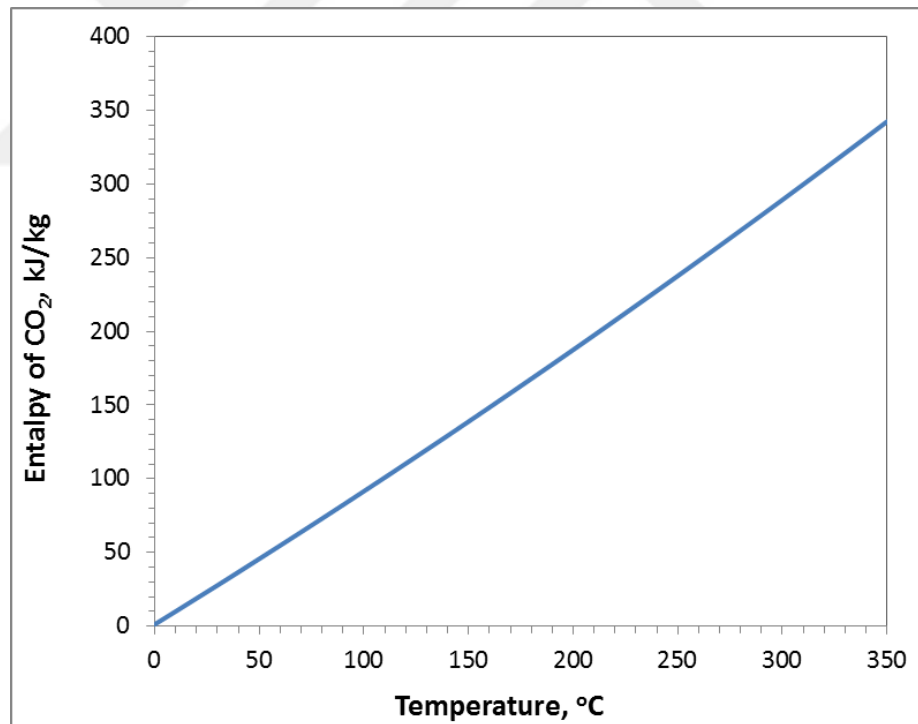


Figure 2.4 : Temperature-enthalpy graph of gaseous CO₂.

$$\mu_C = 10^{-8} (z_1(p) + z_2(p)T + z_3(p)T^2 + z_4(p)T^3 + z_5(p)T^4) \quad (2.5)$$

where T is in °C and μ_c is the viscosity of gaseous CO₂ (Pa.s). The pressure dependent coefficients are found from linear interpolation between the following values tabulated in Table 2.3.

Table 2.3 : Coefficients for viscosity of CO₂ calculation tabulated by Vargaftik et al. (1996).

P (bar)	z_1	z_2	z_3	z_4	z_5
0	1357.8	4.9227	-0.0029661	2.852×10^{-6}	-2.18×10^{-9}
100	3918.9	-35.984	0.25825	-7.11×10^{-4}	6.957×10^{-7}
150	9660.7	-135.479	0.90087	-0.0024727	2.415×10^{-6}
200	13156.6	-179.352	1.12474	-0.0029886	2.859×10^{-6}
300	14769.8	160.731	0.850257	-0.0019907	1.734×10^{-6}
400	15758.3	-144.887	0.673731	-0.0014199	1.135×10^{-6}
500	16171.6	-125.341	0.50075	-7.11×10^{-4}	6.190×10^{-7}
600	16839.4	-115.7	0.40892	-6.35×10^{-4}	3.539×10^{-7}

The viscosity behaviour of pure carbon dioxide based on the data given in Table 2.3 for pressure range from 0 bar to 100 bar is shown in Figure 2.5. As it can be seen from figure, pressure has minor effect on gaseous CO₂ viscosity.

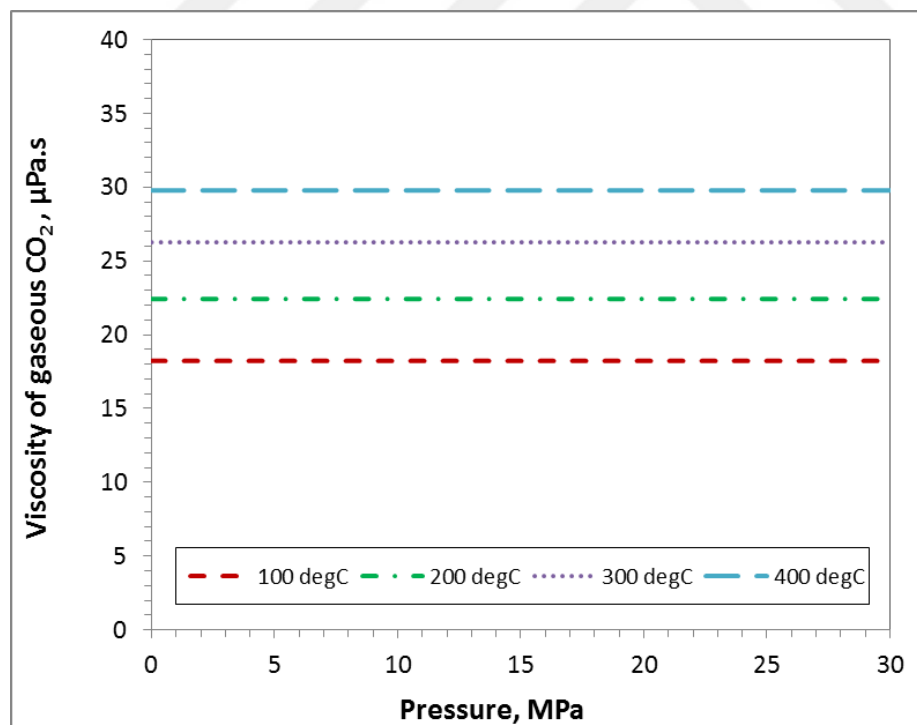


Figure 2.5 : Pressure-temperature-viscosity behavior of gaseous CO₂.

2.3 H₂O-CO₂ System

The thermodynamic package described in this section is actually a collection of correlations and relationships that have been given in the literature previously. Depending upon the input values for the temperature, pressure and mass fraction of CO₂, the thermodynamic package output state may be liquid solution of CO₂ in water, a mixture of liquid solution and vapor and a vapor solution of CO₂ in steam.

For simplicity the liquid phase density and the liquid phase viscosity of a water-CO₂ mixture are taken equal to that of the density and viscosity of liquid water. For the enthalpy of a liquid phase of a water-CO₂ system the relationship given by O'Sullivan et. al. (1985) shown in equation 2.6 is used.

$$h_L = h_w(1 - f_{CL}) + (h_C + h_{sol})f_{CL} \quad (2.6)$$

Here h_L is the enthalpy of the liquid phase (J/kg), h_w is the enthalpy of liquid water (J/kg), f_{CL} is the mass fraction of CO₂ in liquid water, h_C is the enthalpy of the gaseous CO₂ (J/kg) and h_{sol} is the enthalpy of solution. h_C is calculated based on equation 2.4 given in previous subsection. Liquid enthalpy changes for various mass fraction of dissolved CO₂ in liquid with temperature are given in the Figure 2.6.

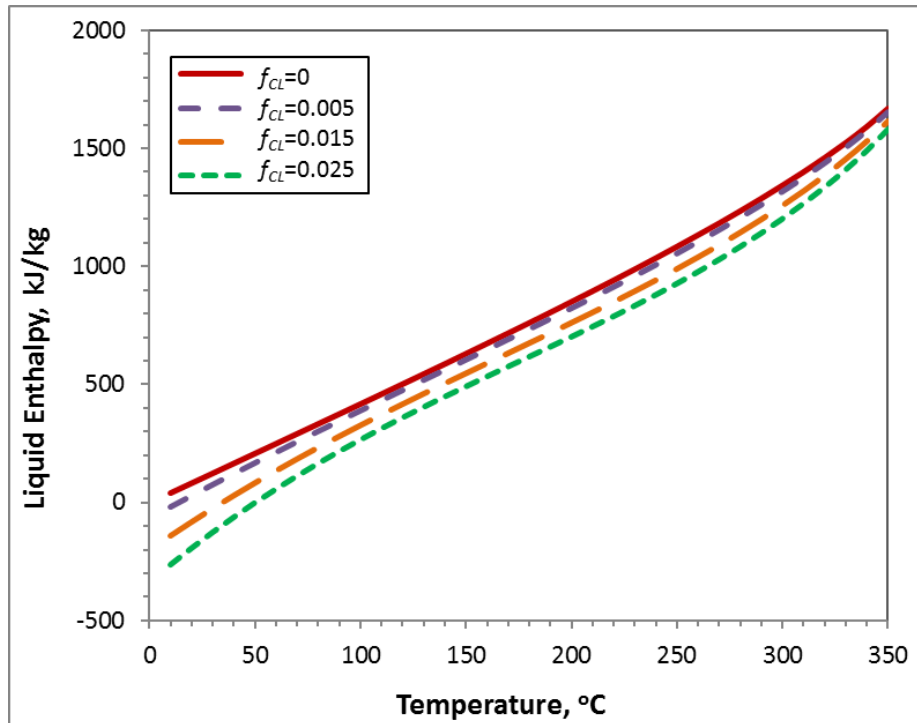


Figure 2.6 : Liquid enthalpy versus temperature.

The solution enthalpy can be determined using equation 2.7 given by Ellis and Golding (1963). Based on their equation, for temperature less than 80°C, negative enthalpy values are calculated. The change of enthalpy of solution with temperature is plotted in Figure 2.7.

$$h_{sol} = \left[\begin{array}{l} -1.351 + 0.01692(T - 273.15) - 7.5524 \times 10^{-5} (T - 273.15)^2 \\ + 1.318 \times 10^{-7} (T - 273.15)^3 \end{array} \right] \times 10^6 \quad (2.7)$$

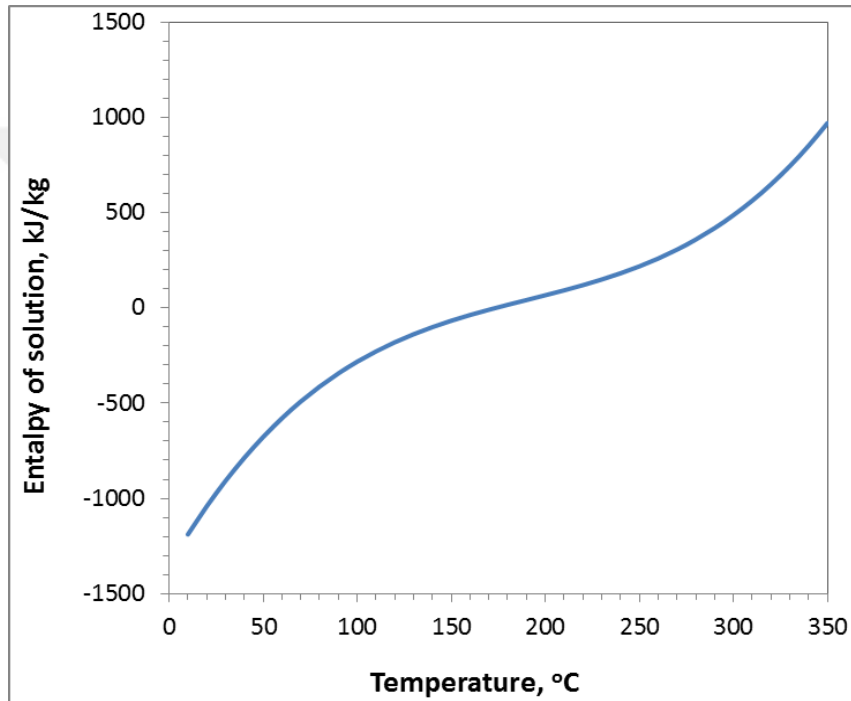


Figure 2.7 : Enthalpy of solution versus temperature.

The pressure of the gas phase can be computed by simply adding up the partial pressure of steam and the partial pressure of CO₂ as given in equation 2.8.

$$p = p_s + p_C \quad (2.8)$$

Here p is the pressure of the gas (Pa), p_s is the partial pressure of steam (Pa) and p_C is the partial pressure of CO₂ (Pa). p_s , in this study is determined from IAPWS (2007).

The gas phase density in the system can be computed using equation 2.9.

$$\rho_G = \rho_s + \rho_C \quad (2.9)$$

where ρ_G is the gas phase density (kg/m^3), ρ_s is the steam density (kg/m^3) and ρ_C (kg/m^3) is the density of gaseous CO_2 which can be calculated from equation 2.3 as stated previous subsection. The gas phase viscosity can be computed using equation 2.10.

$$\mu_G = \mu_s(1 - f_{CG}) + \mu_C f_{CG} \quad (2.10)$$

Where μ_G is the viscosity of the gas phase (Pa.s), μ_s is the viscosity of steam (Pa.s), f_{CG} is the mass fraction of CO_2 in the gas phase, μ_C is the viscosity of gaseous CO_2 that is calculated from equation 2.5. Viscosity of gas phase changes with temperature is given in Figure 2.8.

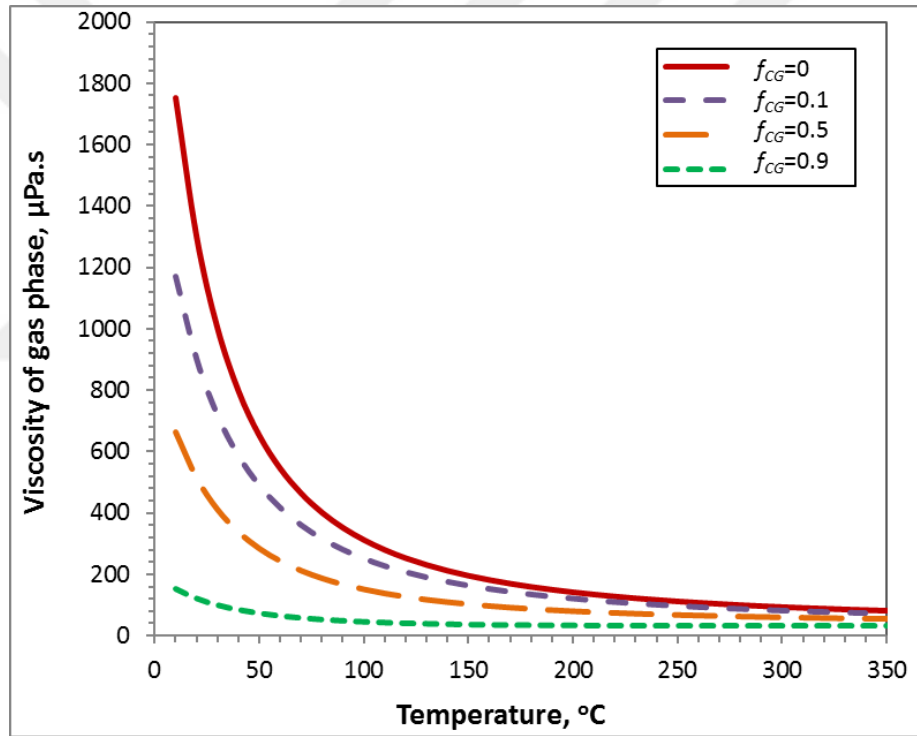


Figure 2.8 : Viscosity of gas phase versus temperature.

The enthalpy of the gas phase can be determined using equation 2.11.

$$h_G = h_s(1 - f_{CG}) + h_C f_{CG} \quad (2.11)$$

where h_G is the enthalpy of the gas phase (J/kg), h_s is the enthalpy of steam (J/kg) and h_C is the enthalpy of gaseous CO_2 . The behaviour of enthalpy of gas phase is shown in Figure 2.9.

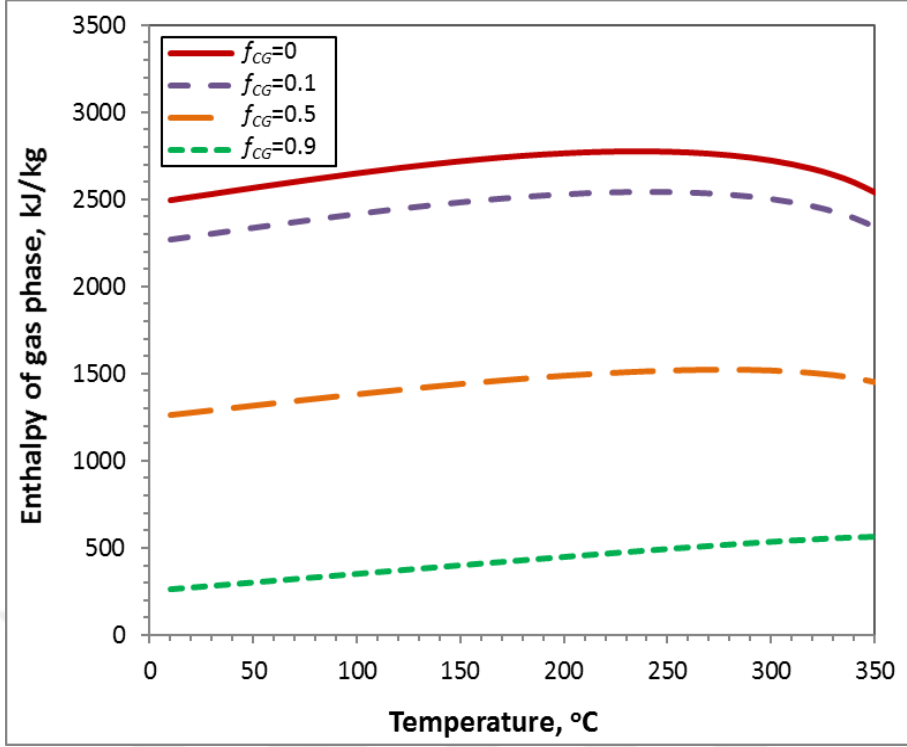


Figure 2.9 : Enthalpy of gas phase versus temperature.

Finally at a given pressure and temperature, the mass fraction of CO₂ in the gas phase can be determined using equation 2.12.

$$f_{CG} = \frac{\rho_C}{\rho_G} \quad (2.12)$$

equations 2.8-2.12 have been taken from O'Sullivan et al. (1985). According to Henry's law, the partial pressure of a noncondensable gas in the gas phase is proportional to the mol fraction of dissolved *NCG* in the aqueous phase. The partial pressure of CO₂ is linked with the mass fraction of CO₂ in the liquid water through Henry's law given in equation 2.13.

$$f_{CL} = p_C K_H \quad (2.13)$$

Here p_C is the partial pressure of CO₂ (Pa), f_{CL} is the mass fraction of CO₂ in liquid water, K_H is Henry's constant (Pa⁻¹). Henry's constant is a function of temperature. And an explicit relation for Henry's constant is given by Sutton (1976).

$$K_H = \left[5.4 - 3.5 \left(\frac{T - 273.15}{100} \right) + 1.2 \left(\frac{T - 273.15}{100} \right)^2 \right] 10^{-9} \quad (2.14)$$

According to equation 2.14, Henry's constant versus temperature can be plotted as in Figure 2.10.

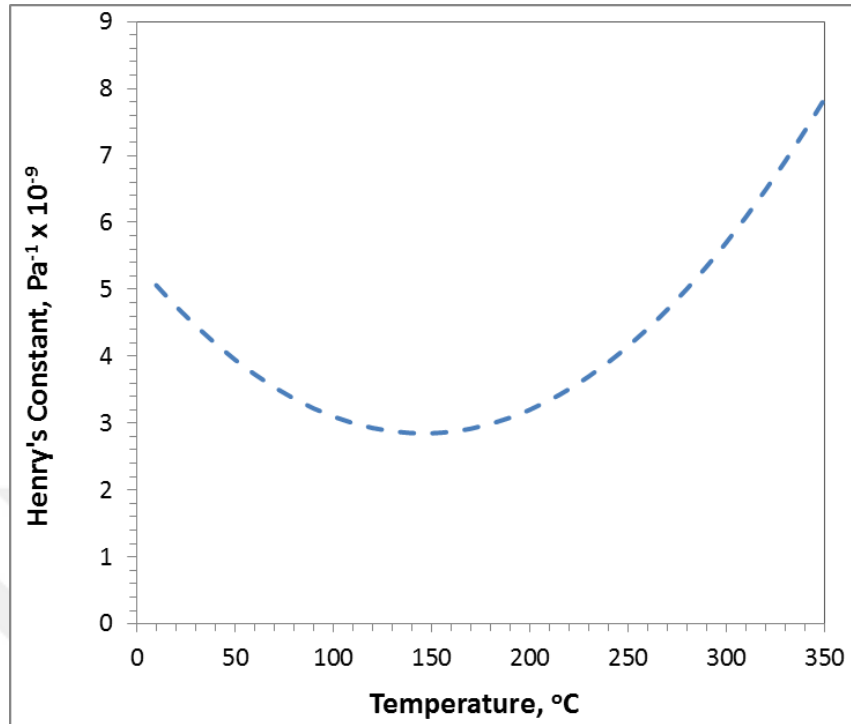


Figure 2.10 : Henry's constant of CO₂ versus temperature.

The dissolution of carbon dioxide in pure water is described with Henry's constant. According to Figure 2.10, At low temperatures Henry's constant decreases with temperature but after a specific turning point temperature Henry's constant increases with temperature. Figure 2.11 illustrates the partial pressure of carbon dioxide as a function of temperature and mass fraction of dissolved carbon dioxide in water. As the mass fraction of CO₂ increases, the partial pressure of CO₂ also increases. Furthermore, because Henry's constant and partial pressure of CO₂ are inversely proportional, at low temperatures partial pressure of CO₂ increases with temperature and after a turning point temperature is reached, partial pressure of CO₂ decreases with temperature.

In this study, Henry's constant for the dissolution of carbon dioxide in pure water is calculated using polynomial regression of data from 0 °C to 300°C published by Cramer (1982) with equation 2.15.

$$K_H = \sum_{i=0}^5 B(i)T^i \quad (2.15)$$

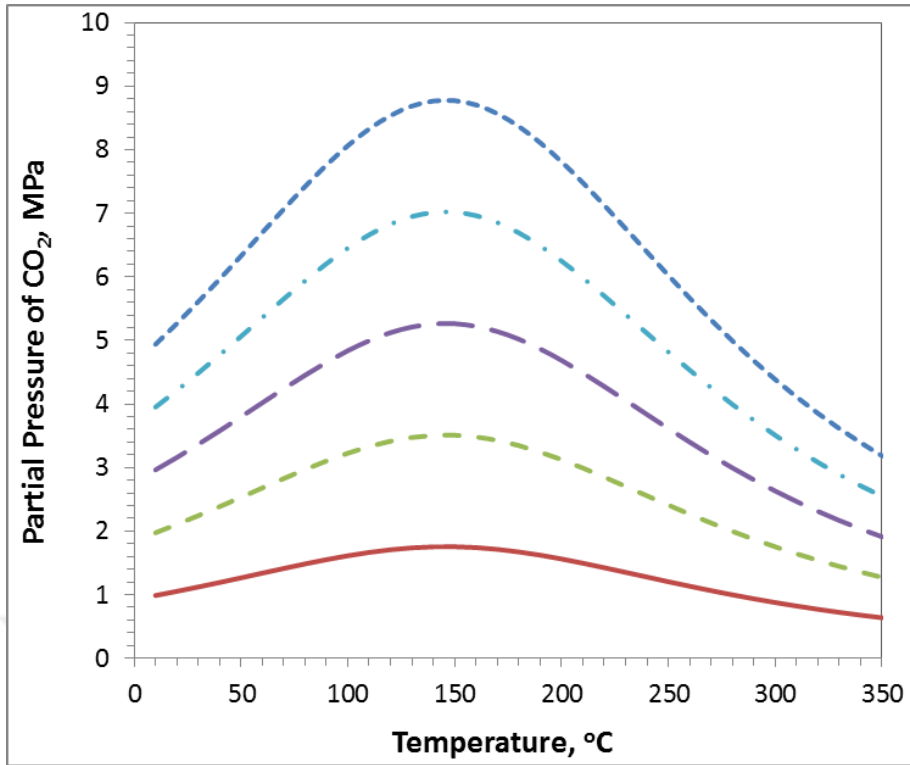


Figure 2.11 : Partial pressure of CO₂ versus temperature.

The values of coefficients $B(i)$ are tabulated in Table 2.4.

Table 2.4 : Coefficients for equation 2.15.

$B(0)$	7.83666×10^7
$B(1)$	1.96025×10^6
$B(2)$	8.20574×10^4
$B(3)$	-7.40674×10^2
$B(4)$	2.18380
$B(5)$	-2.20999×10^{-3}

Another correlation which is provided by Upton and Santoyo (2002) is given as an option for providing the link between the carbon dioxide content and the partial pressure of carbon dioxide. The correlation is given in equation 2.16. y 's are the regression constant and temperature T is given in K. The constants $y(1)$, $y(2)$, $y(3)$ and $y(4)$ of this equations are listed in Table 2.5.

$$\ln K_H = y(1) + y(2)(T + 273.15) + y(3)(T + 273.15)^2 + y(4)(T + 273.15)^3 \quad (2.16)$$

Table 2.5 : Regression coefficients for equation 2.16.

$y(1)$	4.517428673
$y(2)$	2.5554535×10^{-2}
$y(3)$	-1.02213×10^{-4}
$y(4)$	9.30689×10^{-8}

Then the relation between the K_H constant and the partial pressure of CO_2 can be specified as in equation 2.17.

$$p_c = \frac{18}{44} K_H f_{CL} \quad (2.17)$$

where K_H is the Henry's constant and f_{CL} is the mass fraction of CO_2 in water. The effect of dissolved CO_2 on the phase behavior of water can be illustrated through a pressure temperature diagram for various mass fractions of dissolved CO_2 . The flashing point pressures of the water- CO_2 mixture is obtained using equation 2.8 for various temperatures. The partial pressure of steam is obtained using IAPWS (2007). The partial pressure of CO_2 is obtained from Henry's law using equation 2.17. Figure 2.12 illustrates the results according to Henry's constant found from Sutton correlation.

The most profound effect of CO_2 on the behavior of water – CO_2 mixtures is the shift it causes on the flashing point pressures. For example, at around 200°C pure water starts to boil at around 1.5×10^6 Pa. If dissolved CO_2 exists in the water phase with a mass fraction of 0.5% then the mixture would boil at around 3.1×10^6 Pa. At a 2.5% mass fraction, the mixture boils at around 8.9×10^6 Pa. Small amounts of CO_2 dissolved in water considerably changes the flashing point pressure of water. If not accounted for, during production, flashing point depths within wells could be associated with high errors where shallower flashing point depths would be anticipated when actual flashing point depths would be located much deeper. During depletion, if the flashing point is to move into the reservoir, then a gas phase will start to form. This would have the effect such that, the decline rate in pressures due to production would be decreased significantly. This is because below the flashing point pressure a gas phase starts to evolve. Since gas has much higher compressibility when compared with liquids, they can compensate for production simply by expanding more than liquids hence causing a decrease in the pressure decline rate.

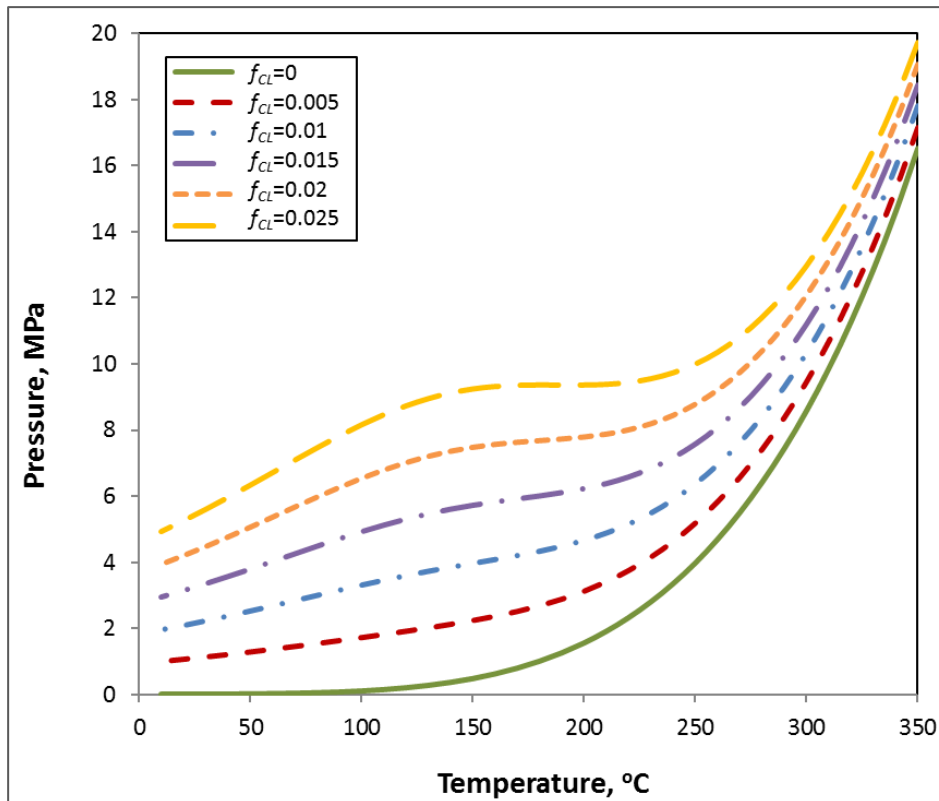


Figure 2.12 : Pressure – temperature behavior of water–CO₂ mixtures for various mass fractions of CO₂ based on Sutton (1976).

p - T diagrams can be changed according to the correlations that is used for Henry’s constant that links the mass fraction with the partial pressure of CO₂. If Upton and Santoyo’s (2002) statistical analysis method is used for Henry’s constant, Figure 2.13 is achieved.

In this study, Cramer’s method is found to be the best approach for Henry’s constant calculations after some verification tests. Henry’s law constant for the dissolution of carbon dioxide in pure water are calculated using polynomial regressions of data from 0 to 300°C published by Cramer (1982) and plotted in Figure 2.14. According to Battistelli et al. (1997), the maximum error for Henry’s constant of pure water is 2.8% based on experimental data by Cramer (1982). The comparison of these three Henry’s constant calculation approach are illustrated in Figure 2.15. As it can be seen, as the mass fraction of CO₂ is increased, the variation of methods is increased. Especially Sutton’s correlation at $f_{CL}=0.025$ shows higher variation. In addition, there is a differentiation at lower temperature values.

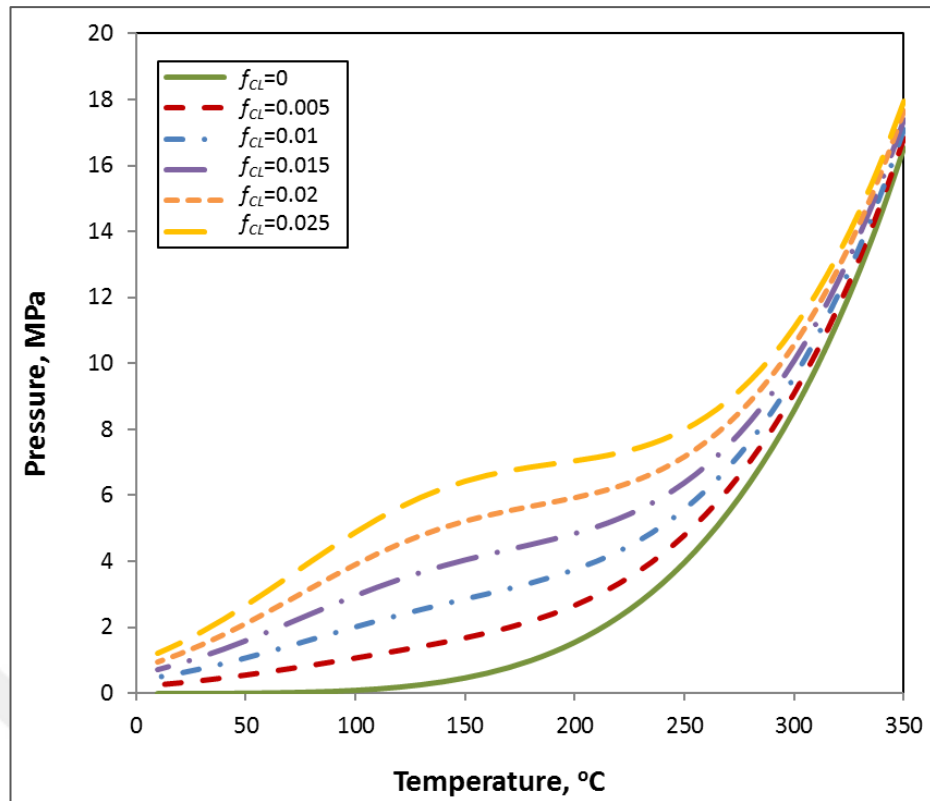


Figure 2.13 : Pressure – temperature behavior of water–CO₂ mixtures for various mass fractions of CO₂ based on Upton and Santoya (2002).

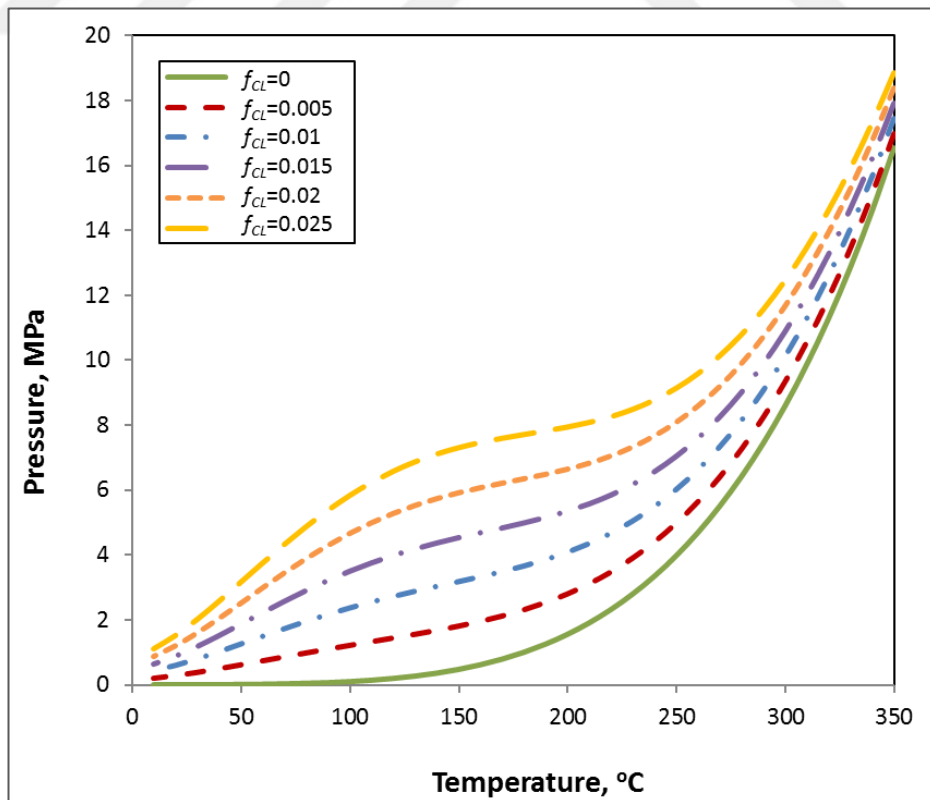


Figure 2.14 : Pressure – temperature behavior of water–CO₂ mixtures for various mass fractions of CO₂ based on Cramer (1982).

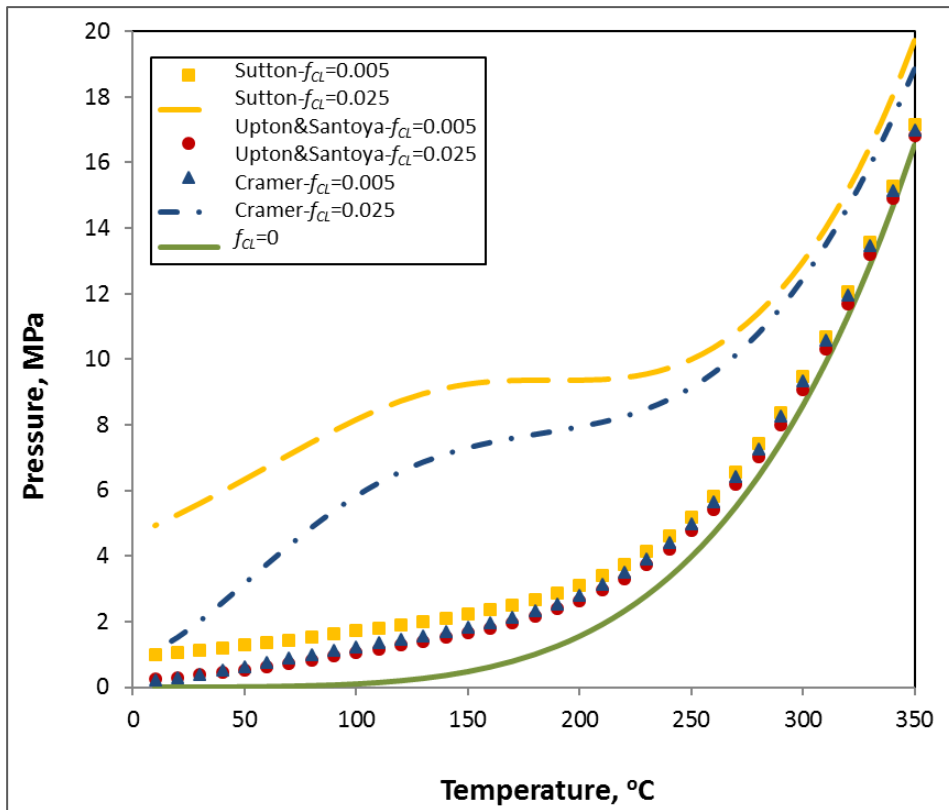


Figure 2.15 : Comparison of approaches for Henry's constant calculations.

Figure 2.16 shows the pressure-temperature-enthalpy behavior of the water-CO₂ mixtures having 0.015 mass fraction of CO₂ dissolved in the liquid phase. The shift caused by the existence of carbon dioxide on the flashing point pressure of the mixture is also visible in the pressure – enthalpy diagram. As the pressure is decreased, once the flashing point pressure is reached then gas starts to form and pressure starts to follow the iso-thermal lines in the two phase region. It is important to note that the gas is initially composed of carbon dioxide. During this time where carbon dioxide dominates the gas phase, the pressure declines rapidly. As pressure is further decreased due to production, steam content starts dominating the gas phase and pressure starts becoming constant (Alkan and Satman 1990). After this point the behavior of the fluids are more or less like that of pure water. For pure water, a fixed temperature enthalpy is not changing much with pressure decrease in single phase liquid region. In two phase region enthalpy changes but pressure stays same and in gas phase region enthalpy changes little bit with pressure.

Large pressure drops occur due to flashing of CO₂ as the enthalpy of the two phase system increases slightly. After most of the CO₂ is in the gas phase, steam quality

becomes the dominant factor determining the enthalpy and pressure becomes nearly constant until the dew point curve is reached.

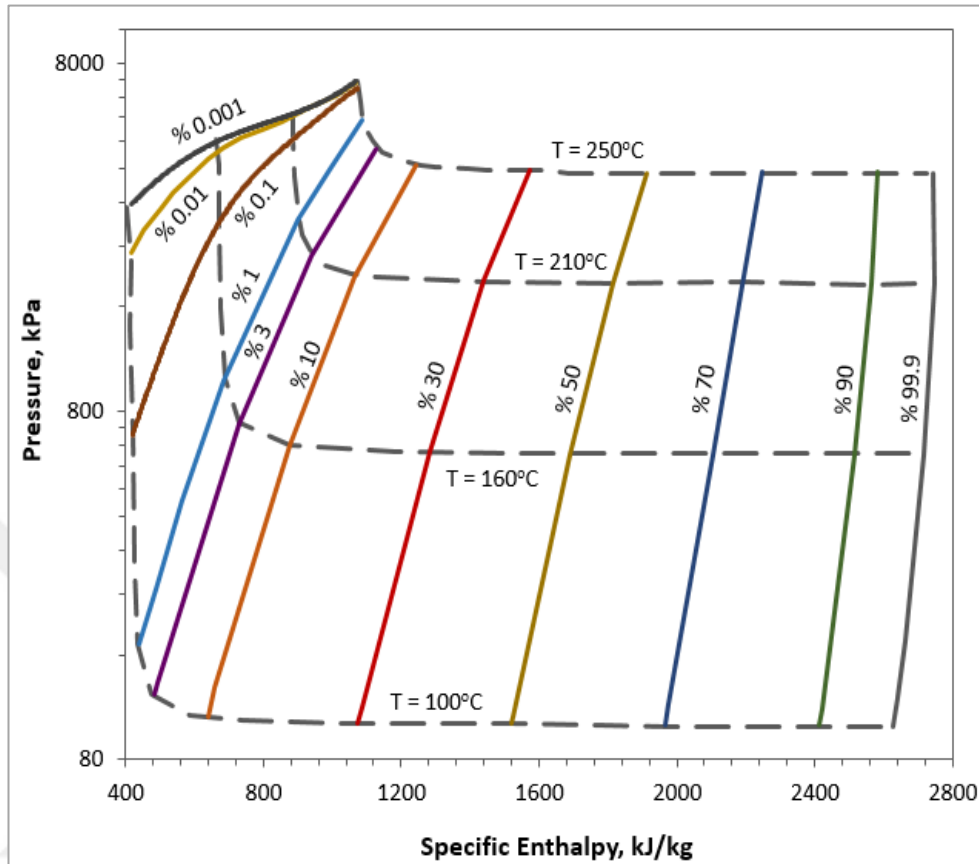


Figure 2.16 : Pressure–temperature–enthalpy behavior of water–CO₂ mixtures for $f_{CL}=0.015$ (Adapted from Alkan and Satman, 1990).

2.4 H₂O - CO₂ - NaCl System

The importance of salt content has received less attention in modelling because there are only a few high salinity reservoirs appeared in the world and effects of salt is significant at high salinity. The total dissolved solids (TDS) content in geothermal reservoir fluids ranges from a few thousand ppm (wt.) up to 280000 ppm (Battistelli et.al, 1997). For strongly salty waters (>100000 ppm) pure water assumption can cause errors as high as 10 % but the average value of the world's geothermal fluids is around 10000 ppm and salt effect can be relatively ignored. In Turkey’s geothermal reservoirs, TDS values are even smaller. Two of the important fields, Kizildere and Germencik have approximately 4000 and 5000 ppm dissolved solid, respectively. Sodium chloride (NaCl) is the predominant solid so the thermodynamic properties of NaCl solutions

are generally used in the simulation of geothermal reservoirs to represent the effect of total dissolved solids.

Adding salt (NaCl) to pure water alters the critical point and two phase region. The main effects of solids dissolved in the liquid phase are the decrease of vapor pressure and enthalpy, and the increase of density and viscosity in the liquid phase. Moreover, CO₂ solubility in liquid phase of brine decreases.

The solubility of CO₂ in the water phase is dependent on temperature and pressure as well as on salt concentration. The presence of salt reduces the CO₂ solubility in the water phase, which is called salting-out. The mass fraction of CO₂ in the water phase is calculated using Henry's law, however, because the salt reduces the solubility of CO₂, the value of the Henry's law constant depends on the salt content of the brine (Battistelli et al., 1997). The Henry's constant can be calculated with equation 2.18;

$$K_{Hbr} = K_H 10^{(m sk_{br})} \quad (2.18)$$

where sk_{br} is the salting-out coefficient, K_H is the Henry's law constant for pure water, K_{Hbr} is the Henry's law constant for brine in Pa and m is the salt molality in mol/kg. Here, molality is calculated with equation 2.19;

$$m = \frac{1000 X_{br}^{NaCl}}{MW(1 - X_{br}^{NaCl})} \quad (2.19)$$

Where MW is the molecular mass of the CO₂ in g/mol and X_{br}^{NaCl} is the mass fraction of NaCl in brine. The salting-out coefficient are calculated using polynomial regressions of data from 0°C to 300°C published by Cramer (1982). The equation for the salting-out coefficient is given by equation 2.20;

$$sk_{br}(T) = \sum_{i=0}^4 [D(i)T^i] \quad (2.20)$$

The coefficients $D(i)$ have values listed in Table 2.6.

Table 2.6 : Regression coefficients for equation 2.20.

$D(0)$	1.19784×10^{-1}
$D(1)$	-7.17823×10^{-4}
$D(2)$	4.93854×10^{-6}
$D(3)$	-1.03826×10^{-8}
$D(4)$	1.08233×10^{-11}

Salt reduces the CO₂ solubility in the water phase. Henry's law constant for the dissolution of CO₂ in pure water and salt mass fractions of 0.01 and 0.05 are given Figure 2.17 (Cramer 1982, Batistelli et al.1997).

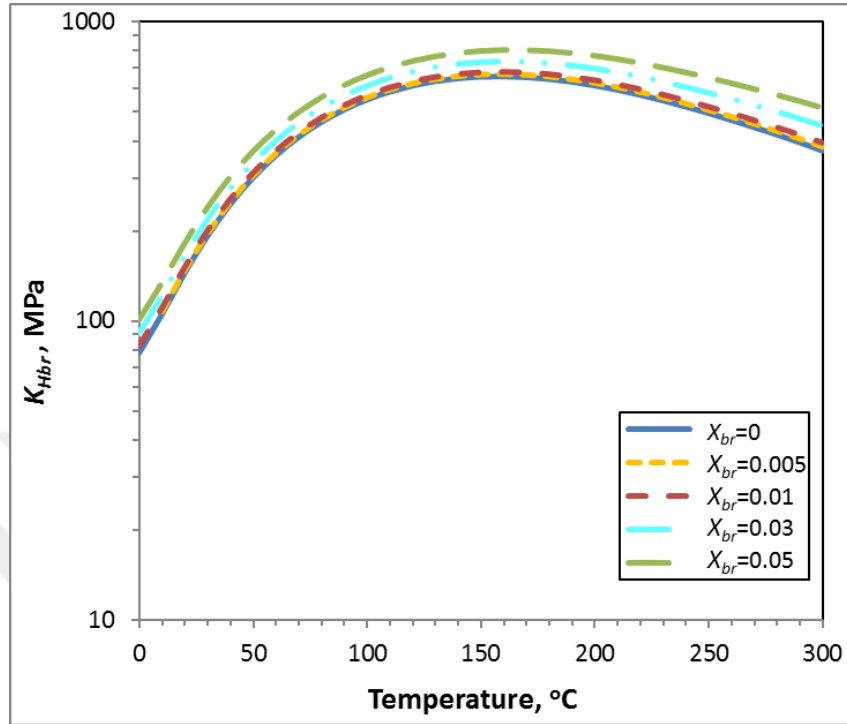


Figure 2.17 : Henry's law constant for CO₂ in NaCl solutions from 0 to 0.05 mass fraction based on Cramer's approach.

The vapor saturated brine pressure versus temperature at different NaCl mass fractions for $f_{CL} = 0.01$ are given in Figure 2.18. It can be seen that dissolved solids generally reduce the vapor pressure.

Another approach for the calculation of Henry's law constant for brine is given in the literature (Satman, 2006). Based on this approach, the Henry's constant can be calculated with equation 2.21;

$$K_{Hbr} = K_H + (0.790613 \times m + 0.003T \times m)101.4 \quad (2.21)$$

Henry's law constant for the dissolution of CO₂ in pure water and salt mass fractions of 0.01 and 0.05 are given Figure in 2.19 and the vapor saturated brine pressure versus temperature at different NaCl mass fractions for $f_{CL} = 0.01$ are given in Figure 2.20. It can be seen that two approaches are compatible with each other.

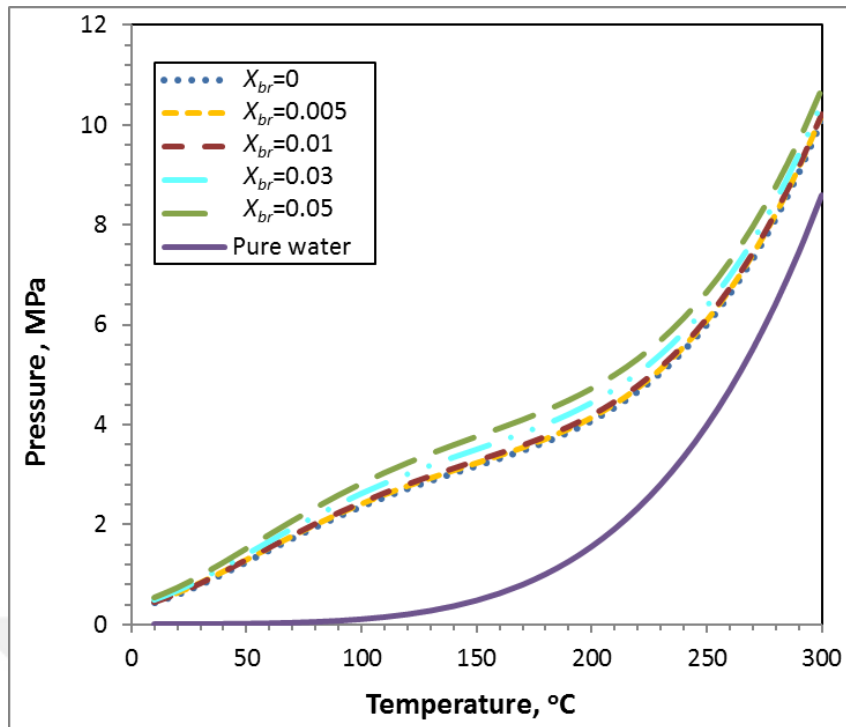


Figure 2.18 : Pressure of pure water and brine with various NaCl concentration based on Cramer's approach.

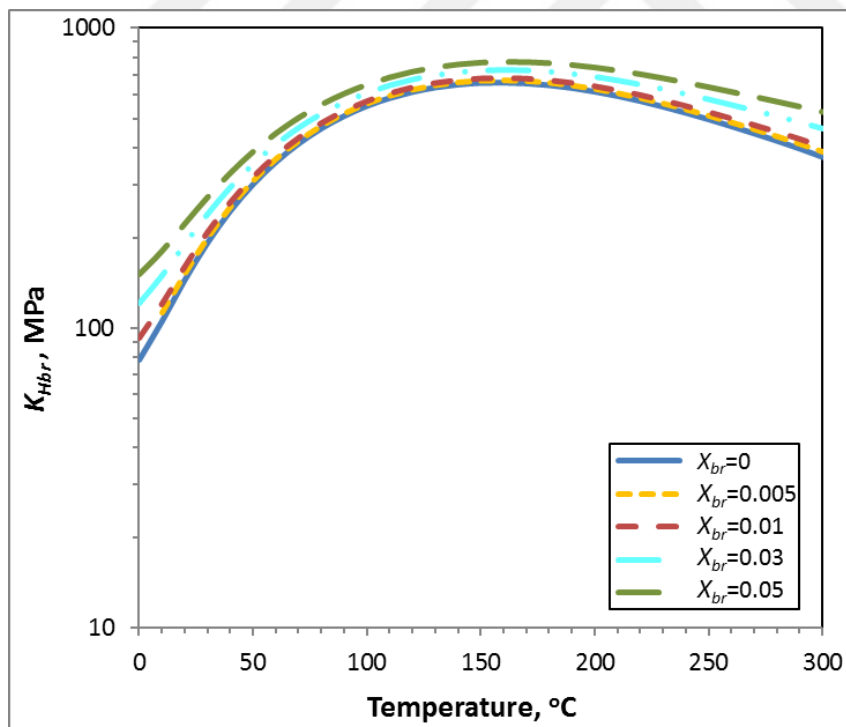


Figure 2.19 : Henry's law constant for CO₂ in NaCl solutions from 0 to 0.05 mass fraction based on Satman (2006).

It is important to emphasize again the average value of the world's geothermal fluids is around 10000 ppm so effect of salt can be relatively ignored. For example,

Germencik field reservoir liquid contains approximately 5000 ppm (0.5 %) dissolved solid. The comparison of Henry's constant and pressure of a reservoir fluid containing $X_{br}=0$ and $X_{br}=0.05$ are illustrated in Figures 2.21 and 2.22.

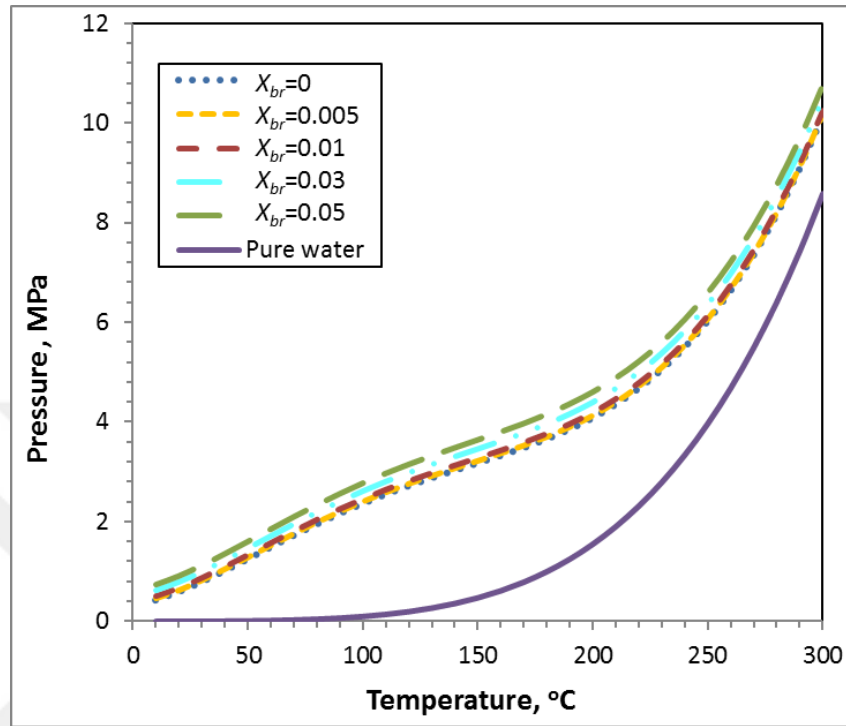


Figure 2.20 : Pressure of pure water and brine with various NaCl concentration based on Satman (2006).

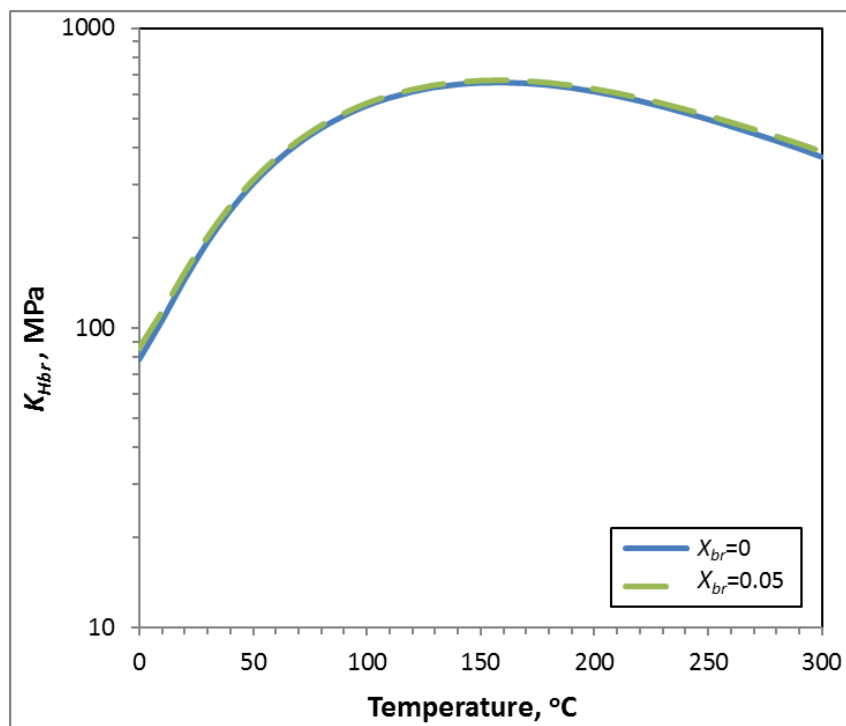


Figure 2.21 : Henry's law constant for CO₂ in NaCl solutions of 0 to 5000 ppm.

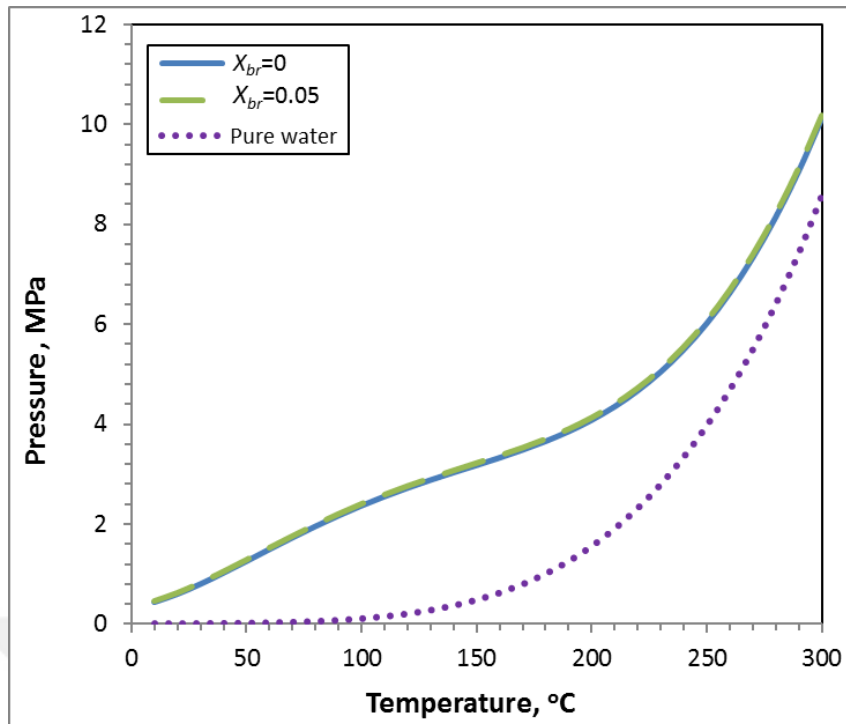


Figure 2.22 : Pressure of pure water and water containing 0-5000 ppm NaCl and 1 % CO₂.

Henry's law constant for CO₂ in NaCl solutions of 0 to 5000 ppm are nearly same. And pressure difference between pure water and brine is caused by the mass fraction of CO₂ in liquid phase.

3. METHODOLOGY

In geothermal system modelling, dominant physical relationships of the geothermal system is formulated in terms of mathematical model. This formulation results in a set of nonlinear partial differential equations which are too complex to be solved by analytical methods. For this reason, numerical model which enables a numerical solution of the equations is developed and computer program is coded for the calculation of these numerical models. The model is capable of representing the wide range of geothermal system types, compressed water, two phase and super heated steam and also changes between these states. The governing equations represent the mass, momentum and energy balance for the geothermal system. This set of equations is completed by adding appropriate physical and thermodynamic relations.

3.1 Utilization of Lumped Parameter Models

Badvorrsson (1966) and Axelsson (1985) have introduced the lumped element models consisting of networks of liquid capacitors and conductors for geothermal reservoir simulation. Every tank has a storage capacity κ , which determines how the reservoir responds to a load of liquid mass with a pressure increase depending on the size of the system and the storage mechanism. The corresponding flow resistor σ controls the property relationship between liquid mass and pressure, and is controlled by the permeability of the reservoir. According to Axelsson (1989) geothermal system consists mainly of three parts: (1) the central part of the reservoir; (2) outer parts of the reservoir, and (3) the recharge source (Figure 3.1). The central and outer parts of the reservoir can be considered as series of homogeneous tanks with average properties. The recharge source is the outermost part of the geothermal system. It can be connected to the outer parts of the reservoir or the central part of the reservoir where production and injection activities take place. If there is no connection to the recharge source, the model is defined as closed system. If there is a connection between recharge source and reservoir, the system is defined as open system.

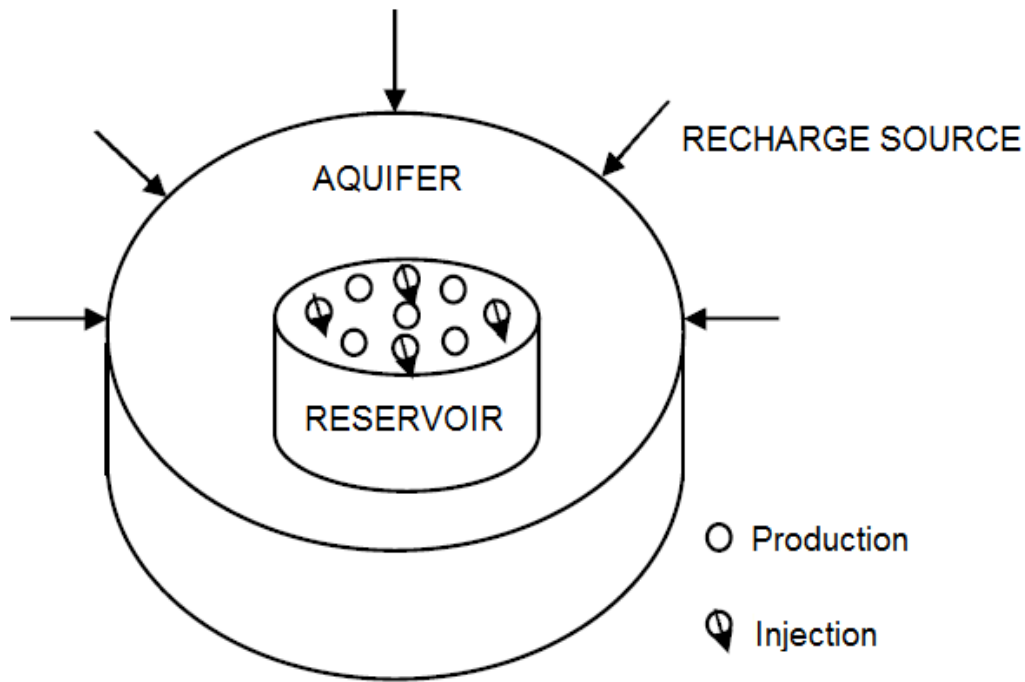
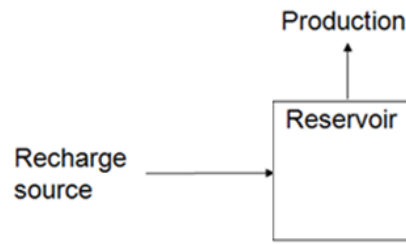


Figure 3.1 : Parts of a geothermal system (Sarak et al., 2005).

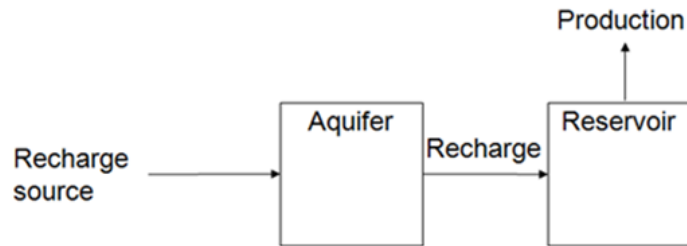
In lumped parameter modelling, each component of a geothermal system is represented by a tank that is composed of fluid and rock. Average properties are assigned to these tanks and changes of pressure, temperature and production are monitored. The tanks represent the reservoir, the aquifer, the heating source or the atmospheric block to which natural discharge occurs. The pressure and temperature changes in the reservoir are modelled by using mass and energy balances so the field potential can be predicted under various production and injection scenarios. Analytical equations for various tank configurations have been developed by Sarak et al. (2005).

Configuration and the number of the tanks can be changed due to the structure of the geothermal system. Geothermal system is named based on the connections that it makes. Different combinations for specific cases are illustrated in Figure 3.2. There is a single tank model in Figure 3.2.a. If the geothermal system is open, which means that is connected to at least one recharge source, pressure and temperature behavior of the geothermal reservoir can be easily simulated with this tank model.

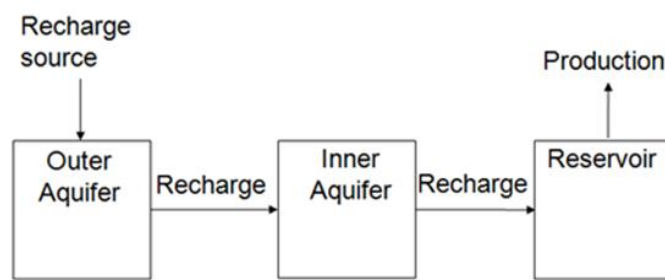
Two tank open model is illustrated in Figure 3.2.b. As it is mention before, if one of the tank is connected to the recharge source the system becomes open system. One of the tank represents the reservoir and the other one represents aquifer. While aquifer is represented with a separate tank, the transient flow regime can be captured in detail.



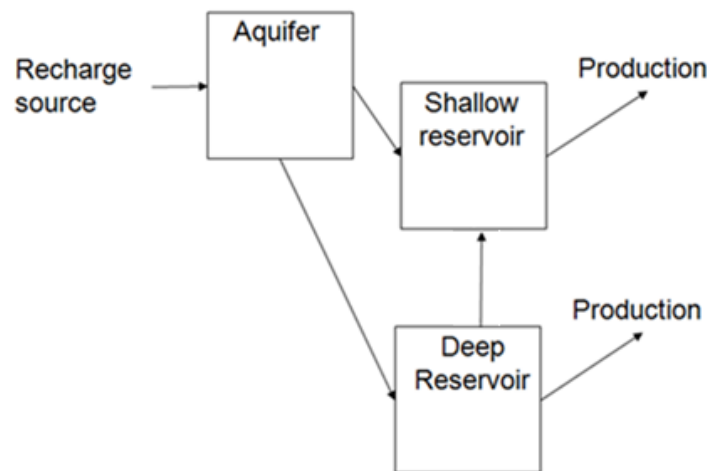
a. One reservoir with recharge source



b. One reservoir – one aquifer with recharge source



c. One reservoir – two aquifers with recharge source



d. Two reservoirs – one aquifer with recharge source

Figure 3.2 : Various types of tank models.

Aquifer is connected to a recharge source so it can be represented with a huge volume of tank which its pressure and temperature is kept constant during production. Production/injection activities occur only in reservoir tank. Two or more tanks can be used to represent aquifer to catch transient flow period as shown in Figure 3.2.c. These aquifer can have same or different recharge constant. In some cases, reservoir can be represented with more than one tank according to the properties and location of the reservoir. For example, shallow and deep reservoirs can be found together in geothermal system. Hydraulic conductivity may or may not be formed between these tanks. They can be connected to same or different aquifers. This case is illustrated in Figure 3.2.d. Production/injection can take place in both tanks.

3.2 Description of the Model

The basic equations represent the mass, momentum and energy balance for the geothermal system containing some amount of CO₂. This set of equations is completed by including an appropriate thermodynamic package described in Section 2. The major assumptions used in the derivations are that the momentum balance is described by Darcy's law and that the geothermal system is in thermal equilibrium which means at each point, the temperature of the rock and matrix and the fluid mixture are the same (Nayfeh et. al, 1975).

The model is based on three conservation equations; mass balance on water, mass balance on carbon dioxide and an overall energy balance. In the model presented here, each component of a geothermal system is represented using a tank that is composed of fluid and rock. Figure 3.3 illustrates any tank i and the connections to neighboring tanks.

The tanks represent either the reservoir, the aquifer, the heating source or the atmospheric block to which natural discharge occurs. In some cases more than one tank can be used to represent the reservoir or the aquifer. Here we will consider that any tank can make an arbitrary number of connections with any other tank. This generalized approach had previously been taken by Tureyen and Akyapi (2011) and Hosgor et al. (2013).

The overall model will be assumed to be composed of a total of N_t number of tanks. Tank i in the system is assumed to make an N_{ni} number of connections to other tanks.

Note that N_{ni} can vary from tank to tank because each tank in the model can make a different number of connections. Liquid water may be injected into the tank at a specified temperature T_{inj} . Production is specified at a total production rate which is the sum of gas and liquid rates. The individual amounts are determined based on their mobility. The fluid is produced at the tank temperature T_i .

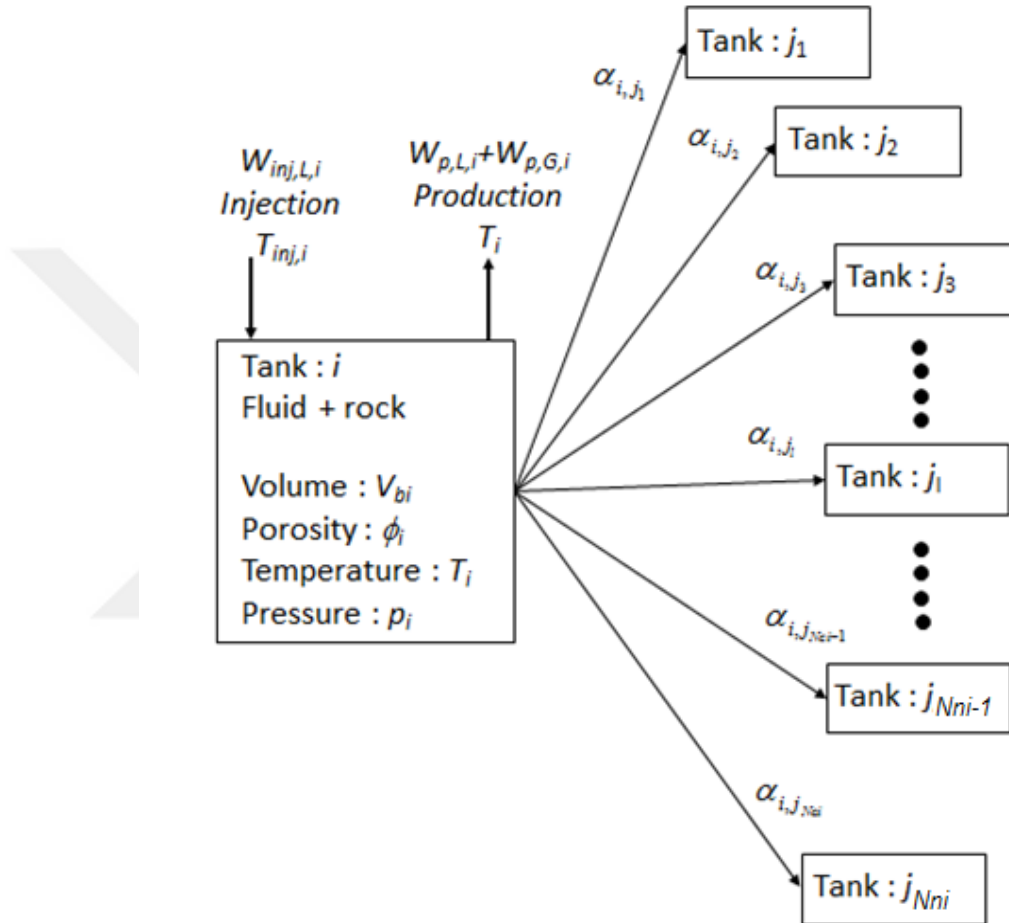


Figure 3.3 : Properties of a representative tank in the model.

The liquid mass flow rate between any tank j_i and tank i is determined using the steady-state Schilthuis (1936) water-influx approach which is used to describe the recharge rate between the tanks, and from the recharge source to the connecting tank. This method assumes that the recharge is proportional to the pressure difference between the reservoir tank and the recharge source, and is given by equation 3.1;

$$W_{i,j_i} = \alpha_{i,j_i} (p_{j_i} - p_i) \quad (3.1)$$

Here W_{i,j_i} is the mass flow rate of the fluid phase transferred between tank i and tank

j_i (kg/s), p_{j_i} is the pressure of tank j_i (Pa), p_i is the pressure of tank i (Pa) and α_{L,i,j_i} is the recharge index (kg/(bar.s)) which represents the mass flow rate for a given unit pressure drop between the tanks. At this point it is important to note that the recharge index is composed of two parts; a rock part (which assumed to independent of pressure and temperature) and a fluid part (which is assumed to be a strong function of pressure and temperature). Hence the recharge index can be written as follows (equation 3.2):

$$\alpha_{i,j_i} = \psi_{i,j_i} \lambda_{j_i} \quad (3.2)$$

Where ψ_{i,j_i} is the rock part of the recharge index (m^3) and λ_i is the fluid part of the recharge index ($\text{kg}/(\text{Pa}\cdot\text{s}\cdot\text{m}^3)$). The fluid part is given by equation 3.3.

$$\lambda_{i,j_i} = \left(\frac{k_{r,l} \rho}{\mu} \right)_{i,j_i} \quad (3.3)$$

where $k_{r,l}$ is the relative permeability of the fluid in m^2 . The rock part of the recharge index is given by equation 3.4.

$$\psi_{i,j_i} \propto \left(\frac{kA}{d} \right)_{i,j_i} \quad (3.4)$$

Here k represents the permeability of the medium of the tanks assumed to be composed of (m^2), A is the cross-sectional area that the fluid passes through when being transferred between the tanks (m^2) and d is some characteristic length which is a measure of the distance the fluid takes when it is being transferred from one tank to the other (m). It is important to note that the individual values of k , A and d need not be known. They are all lumped in ψ_{i,j_i} which is treated as an input parameter or can be treated as a parameter to be adjusted during history matching. The fluid part of the recharge index on the other hand is computed for a given pressure, temperature and saturation. It is important to define recharge index correctly for each phases. If the recharge index is written for liquid phase subscript of L will be used and if it is written for gas phase subscript of G will be used.

In the model, saturation weighted flow rate is assumed and X type relative permeability curves is used. That means relative permeability of gas is directly proportional to saturation of gas.

The model also considers the heat conduction. Based on the law of heat conduction, also known as Fourier's law the energy flux due to conduction between any tank j_i and tank i is given by equation 3.5.

$$Q_{i,j_i} = \gamma_{i,j_i} (T_{j_i} - T_i) \quad (3.5)$$

where Q is the energy rate (J/s) and γ_{i,j_i} is the conduction index (J/(K.s)). As it is seen from this equation, energy flux between tanks are directly proportional to temperature difference and the proportion gives the conduction index which is the property of a material to conduct heat. Conduction index can also be written due to some petrophysical properties;

$$\gamma_{i,j_i} \propto \left(\frac{kA}{d} \right)_{i,j_i} \quad (3.6)$$

Equation 3.6 represents the thermal conductivity of porous media that is formed from rock and fluid. Thermal conductivity can be also given as an input parameter or can be treated as a parameter to be adjusted during history matching.

The geothermal system is considered to be composed of a total of N_t number of tanks. Tank i in the system is assumed to make N_{ni} number of connections to other tanks. All the mass and energy balance equations are solved for each tanks simultaneously. Figure 3.4 illustrates an example of tank configuration. This system contains 6 tanks, this means N_t equals to 6. But N_{ni} values are changing from tank to tank because each tank has different number of connections. For example, tank 1 only connects to tank 2, thus N_{n1} equals to 1 and $j_1=2$. On the other hand, tank 2 has connections with tanks 1, 3 and 5 so N_{n2} equals to 3. In this case, $j_1=1$, $j_2=3$ and $j_3=5$ for tank 2. Table 3.1 lists the number of the tanks and their connections with the other tanks.

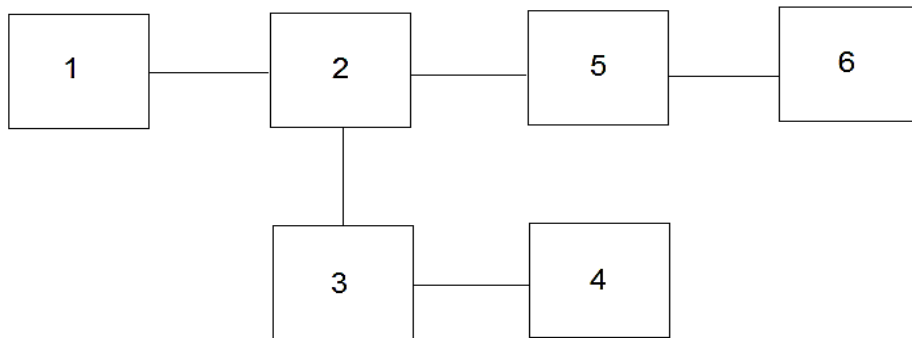


Figure 3.4 : Example for configuration of tanks.

Table 3.1 : Sample tank connections.

Tank Number (<i>i</i>)	Number of Connections (<i>N_{ni}</i>)	Connecting Tanks (<i>j_i</i>)
1	1	<i>j₁</i> = 2
2	3	<i>j₁</i> = 1, <i>j₂</i> = 3, <i>j₃</i> = 5
3	2	<i>j₁</i> = 2, <i>j₂</i> = 4
4	1	<i>j₁</i> = 3
5	2	<i>j₁</i> = 2, <i>j₂</i> = 6
6	1	<i>j₁</i> = 5

The model is based on three conservation equations that have to be solved for each tank. These equations can be listed as below and details for them are given in the following subsection.

- Mass Balance for Water
- Energy Balance on Fluids and Rock
- Mass Balance on Carbon dioxide

3.3 Mass Balance for Water

The mass balance equation for water for any tank is given in equation 3.7;

$$\begin{aligned} & [\text{Accumulation rate of water}] - [\text{Contribution of liquid water from other tanks}] \\ & - [\text{Contribution of vapor from other tanks}] - [\text{Liquid production}] \\ & - [\text{Liquid injection}] - [\text{Vapor production}] - [\text{Vapor injection}] = 0 \end{aligned} \quad (3.7)$$

For the accumulation term, the accumulation of both liquid and vapor is considered and bulk volume of tank *i* is assumed to be constant.

$$\text{Accumulation rate of water} = V_{b,i} \frac{d}{dt} (\rho_L S_L \phi + \rho_G S_G \phi)_i \quad (3.8)$$

In equation 3.8, V_i is the volume of the tank (m^3), ϕ is porosity (fraction), ρ_L and ρ_G are densities of liquid water and gas (kg/m^3) and S_L and S_G are saturations (fraction) of liquid and gas, respectively.

It is important to note that, porosity is a function of pressure and temperature so it should be modelled by using the following equation 3.9 (Onur et.al, 2008) ;

$$\phi(p, T) = \phi_0 [1 + c_r (p(t) - p_0) - \varepsilon (T(t) - T_0)] \quad (3.9)$$

ϕ_i is the initial porosity of the reservoir (fraction), c_r (bar^{-1}) is the rock compressibility, p_0 and T_0 are the initial pressure and temperature respectively. ε is the thermal expansion coefficient of porosity ($1/^\circ\text{C}$).

The liquid mass flow rate between any tank j_l and tank i (contribution from other tanks) is determined using an approach similar to that of Schilthuis (1936) and is given equation 3.10;

$$\text{Contribution of liquid from other tanks} = W_{L,i,j_l} = \alpha_{L,i,j_l} (p_{j_l} - p_i) \quad (3.10)$$

Here W_{L,i,j_l} is the mass flow rate of the liquid phase transferred between tank i and tank j_l (kg/s), p_{j_l} is the pressure of tank j_l (Pa), p_i is the pressure of tank i (Pa) and α_{L,i,j_l} is the recharge index (kg/(bar.s)) of liquid which represents the mass flow rate for a given unit pressure drop between the tanks.

The gas mass flow rate is determined in the same fashion using equation 3.11, except with the subscript L replaced with G .

$$\text{Contribution of vapor from other tanks} = W_{G,i,j_l} = \sum_{l=1}^{N_{ci}} \alpha_{G,i,j_l} (p_{j_l} - p_i) \quad (3.11)$$

For the liquid and gas production we simply use; $W_{p,L,i}$ and $W_{p,G,i}$. To examine the cases with injection of water, an injection term can be added to the mass balance equation, $W_{inj,L,i}$.

Then the mass balance of water for tank i can be written as shown in equation 3.12.

$$\begin{aligned} V_{b,i} \frac{d}{dt} (\rho_L S_L \phi + \rho_G S_G \phi)_i - \sum_{l=1}^{N_{ci}} \alpha_{L,i,j_l} (p_{j_l} - p_i) - \sum_{l=1}^{N_{ci}} \alpha_{G,i,j_l} (p_{j_l} - p_i) \\ + W_{p,L,i} + W_{p,G,i} + W_{inj,L,i} = 0 \end{aligned} \quad (3.12)$$

The first term on the accumulation of mass in the tank, the second term represents the liquid mass contribution from other tanks and the third term represents the gas mass contribution from other tanks. The derivative of time appears in the accumulation term. Numerical approach is applied to take the derivative of time. The most commonly used approach is to apply finite difference technique expressing the partial derivatives in the equations in terms of algebraic approximations obtained by Taylor expansions near the point of interests and solving the resulting set of simplified equations. The details of this technique and solution method is given in section 3.8. When finite difference method is applied to the mass balance, equation 3.13 is obtained;

$$V_{b,i} \frac{(\rho_L S_L \phi + \rho_G S_G \phi)^{n+1} - (\rho_L S_L \phi + \rho_G S_G \phi)^n}{\Delta t} - \sum_{l=1}^{N_{ci}} \alpha_{L,i,j_l} (p_{j_l} - p_i) - \sum_{l=1}^{N_{ci}} \alpha_{G,i,j_l} (p_{j_l} - p_i) + W_{p,L,i} + W_{p,G,i} + W_{inj,L,i} = 0 \quad (3.13)$$

Where the superscript n refers to the present time and $n+1$ refers to the time at which the solutions will be determined. Δt represents the time from n to $n+1$. The subscript i represents the reservoir block index. As it is seen from the equation, this approach requires time step selection. Production and injection terms are handled in updated, $n+1$, timestep. The explicit approach is easier to solve but stability problems arises. To overcome the instability problem, implicit approach is preferred. Using the implicit finite difference method on equation 3.14, the following equation is obtained:

$$V_{b,i} \frac{(\rho_L S_L \phi + \rho_G S_G \phi)^{n+1} - (\rho_L S_L \phi + \rho_G S_G \phi)^n}{\Delta t} - \sum_{l=1}^{N_{ci}} \alpha_{L,i,j_l}^{n+1} (p_{j_l}^{n+1} - p_i^{n+1}) - \sum_{l=1}^{N_{ci}} \alpha_{G,i,j_l}^{n+1} (p_{j_l}^{n+1} - p_i^{n+1}) + W_{p,L,i}^{n+1} + W_{p,G,i}^{n+1} + W_{inj,L,i}^{n+1} = 0 \quad (3.14)$$

3.4 Energy Balance on Fluids and Rock

Temperature of the geothermal reservoir will change due to production, cold water recharge or cold water reinjection. Even for the closed system, as the mass is being removed with the production, pressure will decrease causing reduction in the internal

energy. Thus, temperature of the reservoir will also decrease with the decreased internal energy.

In modelling the non isothermal behavior of a geothermal reservoir, conservation of energy also needs to be solved. Energy balance equation for any tank is given by equation 3.15;

$$\begin{aligned}
 & [\text{Accumulation rate of energy}] \\
 & + [\text{Contribution of energy from other tank by movement of liquid}] \\
 & + [\text{Contribution of energy from other tank by movement of vapor}] \\
 & - [\text{Contribution of energy due to liquid production}] \\
 & - [\text{Contribution of energy due to liquid injection}] \\
 & - [\text{Contribution of energy due to vapor production}] \\
 & - [\text{Contribution of energy due to vapor injection}] \\
 & + [\text{Overall energy contribution from heat transfer by conduction}] = 0
 \end{aligned} \tag{3.15}$$

Here, the accumulation term is defined as given by equation 3.16;

$$\begin{aligned}
 & \text{Accumulation rate of energy} \\
 & = \frac{d}{dt} [V_b (1-\phi) \rho_m C_m T + V_b \phi (\rho_L u_L S_L + \rho_G u_G S_G)]
 \end{aligned} \tag{3.16}$$

The liquid and gas energy flow between any tank j_i and tank i can be given as equation 3.17 and 3.18;

$$\begin{aligned}
 & \text{Contribution of energy from other tank by movement of liquid} \\
 & = \sum_{l=1}^{N_{ci}} \alpha_{L,i,j_i} (p_{j_i} - p_i) h_{L,\xi}
 \end{aligned} \tag{3.17}$$

Contribution of energy from other tank by movement of gas

$$= \sum_{l=1}^{N_{ci}} \alpha_{G,i,j_l} (p_{j_l} - p_i) h_{G,\xi} \quad (3.18)$$

Energy contributions from liquid production, liquid injection and gas production are given as follows; $W_{p,L,i} h_{L,i}$, $W_{p,G,i} h_{G,i}$, $W_{inj,L,i} h_{L,inj,i}$.

We assume that local thermal equilibrium exists in tank i between the gas phase, the liquid phase and the rock. Under this assumption the energy balance can be given as equation 3.19;

$$\begin{aligned} & \frac{d}{dt} \left[(1-\phi) V \rho_m C_m T + V \phi (\rho_L u_L S_L + \rho_G u_G S_G) \right] + W_{p,L,i} h_{L,i} \\ & + W_{p,G,i} h_{G,i} - W_{inj,L,i} h_{L,inj,i} - \sum_{l=1}^{N_{ci}} \alpha_{L,i,j_l} (p_{j_l} - p_i) h_{L,\xi} \\ & - \sum_{l=1}^{N_{ci}} \alpha_{G,i,j_l} (p_{j_l} - p_i) h_{G,\xi} - \sum_{l=1}^{N_{ci}} \gamma_{i,j_l} (T_{j_l} - T_i) = 0 \end{aligned} \quad (3.19)$$

where ρ_m represents the rock matrix density (kg/m³), C_m represents the specific heat capacity of the rock (J/(kg.K)), u represents the internal energy (J/kg) and h represents the enthalpy (J/kg).

When considering the energy contribution from other tanks, we perform an upwinding scheme on the enthalpy as given by equation 3.20. In other words, the flow direction is checked to figure out which block pressure and temperature should be used to determine the internal energy.

$$h_{\xi} = \begin{cases} h_i & \text{if } p_i > p_{j_l} \\ h_{j_l} & \text{if } p_i < p_{j_l} \end{cases} \quad (3.20)$$

For the terms with time derivatives forward finite difference discretization and for the variables implicit approach is applied and equation 3.21 is formed.

$$\begin{aligned}
& V_{b,i} \frac{\left[(1-\phi) \rho_m C_m T + \phi (\rho_L u_L S_L + \rho_G u_G S_G) \right]_i^{n+1}}{\Delta t} \\
& V_{b,i} \frac{\left[(1-\phi) \rho_m C_m T + \phi (\rho_L u_L S_L + \rho_G u_G S_G) \right]_i^n}{\Delta t} \\
& + W_{p,L,i}^{n+1} h_{L,i}^{n+1} + W_{p,G,i}^{n+1} h_{G,i}^{n+1} + W_{inj,L,i}^{n+1} h_{L,inj,i}^{n+1} - \sum_{l=1}^{N_{ci}} \alpha_{L,i,j_l}^{n+1} (p_{j_l}^{n+1} - p_i^{n+1}) h_{L,\xi}^{n+1} \\
& - \sum_{l=1}^{N_{ci}} \alpha_{G,i,j_l}^{n+1} (p_{j_l}^{n+1} - p_i^{n+1}) h_{G,\xi}^{n+1} - \sum_{l=1}^{N_{ci}} \gamma_{i,j_l}^{n+1} (T_{j_l}^{n+1} - T_i^{n+1}) = 0
\end{aligned} \tag{3.21}$$

3.5 Mass Balance on the Carbon Dioxide Component

Finally, the mass balance equation of CO₂ for any tank is given by equation 3.22.

$$\begin{aligned}
& [Accumulation\ rate\ of\ CO_2] \\
& - [Contribution\ of\ dissolved\ in\ water\ CO_2\ from\ other\ tanks] \\
& - [Contribution\ of\ CO_2\ in\ gas\ phase\ from\ other\ tanks] \\
& - [Liquid\ CO_2\ production] - [Gas\ CO_2\ production] + [CO_2\ injection] = 0
\end{aligned} \tag{3.22}$$

Accumulation of carbon dioxide in the tank i is given by equation 3.23;

$$Accumulation\ rate\ of\ CO_2 = V_{b,i} \frac{d}{dt} (\rho_L S_L \phi f_{CL} + \rho_G S_G \phi f_{CG})_i \tag{3.23}$$

The liquid and gas CO₂ mass flow rate between any tank j_l and tank i are given by equation 3.24 and equation 3.25, respectively.

$$Contribution\ of\ liquid\ CO_2\ from\ other\ tanks = \sum_{l=1}^{N_{ci}} \alpha_{L,i,j_l} (p_{j_l} - p_i) f_{CL,\xi} \tag{3.24}$$

$$Contribution\ of\ gas\ CO_2\ from\ other\ tanks = \sum_{l=1}^{N_{ci}} \alpha_{G,i,j_l} (p_{j_l} - p_i) f_{CG,\xi} \tag{3.25}$$

Finally, if the liquid and gas CO₂ production and CO₂ injections (if any) terms are added, the mass balance on the CO₂ component is given by equation 3.26;

$$V_{b,i} \frac{d}{dt} (\rho_L S_L \phi f_{CL} + \rho_G S_G \phi f_{CG})_i - \sum_{l=1}^{N_{ci}} \alpha_{L,i,j_l} (p_{j_l} - p_i) f_{CL,\xi} \quad (3.26)$$

$$- \sum_{l=1}^{N_{ci}} \alpha_{G,i,j_l} (p_{j_l} - p_i) f_{CG,\xi} + W_{p,L,i} f_{CL,i} + W_{p,G,i} f_{CG,i} - W_{inj,L,i} f_{CL,i} = 0$$

Here f represents the mass fraction of CO₂ either in the liquid or the gas phase and W_p represents the production and W_{inj} represents the injection rates in kg/s.

In many cases, the produced CO₂ can be reinjected to the reservoir and re-injected CO₂ mass fraction can be a function of the CO₂ mass fraction that is produced. In that case, mass fraction of CO₂ can be modelled with reinjection ratio, β , given in equation 3.27;

$$f_{inj} = \beta f(t) \quad (3.27)$$

In variable CO₂ mass fraction cases equation 3.27 becomes;

$$V_{b,i} \frac{d}{dt} (\rho_L S_L \phi f_{CL} + \rho_G S_G \phi f_{CG})_i - \sum_{l=1}^{N_{ci}} \alpha_{L,i,j_l} (p_{j_l} - p_i) f_{CL,\xi} \quad (3.28)$$

$$- \sum_{l=1}^{N_{ci}} \alpha_{G,i,j_l} (p_{j_l} - p_i) f_{CG,\xi} + W_{p,L,i} f_{CL,i} + W_{p,G,i} f_{CG,i} - W_{inj,L,i} f_{CL,i} \beta_i = 0$$

In equation 3.28, β is a number that varies between 0 and 1. If β is zero, there is no CO₂ injection and if β equals to 1, then the injected CO₂ mass fraction becomes equal to the CO₂ mass fraction in the tank at any particular time.

The upwinding approach is applied similar to that enthalpy case. The approach is given in equation 3.29;

$$f_{\xi} = \begin{cases} f_i & \text{if } p_i > p_{j_l} \\ f_{j_l} & \text{if } p_i < p_{j_l} \end{cases} \quad (3.29)$$

For the terms with time derivatives forward finite difference discretization and for the variables implicit approach is applied, the generalized mass balance equation for CO₂, equation 3.30, is formed.

$$\begin{aligned}
& V_{b,i} \frac{(\rho_L S_L \phi f_{CL} + \rho_G S_G \phi f_{CG})_i^{n+1} - (\rho_L S_L \phi f_{CL} + \rho_G S_G \phi f_{CG})_i^n}{\Delta t} \\
& - \sum_{l=1}^{N_{ci}} \alpha_{L,i,j_l}^{n+1} (p_{j_l}^{n+1} - p_i^{n+1}) f_{CL,\xi}^{n+1} - \sum_{l=1}^{N_{ci}} \alpha_{G,i,j_l}^{n+1} (p_{j_l}^{n+1} - p_i^{n+1}) f_{CG,\xi}^{n+1} \\
& + W_{p,L,i}^{n+1} f_{CL,i}^{n+1} + W_{p,G,i}^{n+1} f_{CG,i}^{n+1} - W_{inj,L,i}^{n+1} f_{CL,i}^{n+1} \beta_i^{n+1} = 0
\end{aligned} \tag{3.30}$$

3.6 Selection of the Primary Variables

Primary variables are the parameters needed to describe the properties of a system. The thermodynamic conditions at any point in a reservoir are described in terms of a small set of primary variables. The thermodynamic formulation is used to calculate all other fluid properties from these primary variables. The non-isothermal two-phase two-component model consists of three equations with three unknowns or primary variables. For pure water, these can be pressure p , temperature T and saturation S . However, with the consideration of carbon dioxide, the selection of primary variables can be more complex. One of the important points in this model is the changing of primary variables during phase transition. The same approach with O'Sullivan et al. (1985) is used in this study however; selected primary variables are different in two phase region. For the selection of primary variables O'Sullivan et al. (1985) proposed an approach that can be summarized as follows; if the tank contains a single phase fluid, then the primary variables are chosen as pressure, temperature and partial pressure of CO₂, whereas if the tank contains gas and liquid phases at the same time, the gas saturation is used as a primary variable instead of temperature.

In this model after some verification studies, it is decided to use pressure, temperature and partial pressure of CO₂ as primary variables in the single phase region and saturation of gas, temperature and partial pressures of CO₂ as primary variables in the two phase region. By choosing these primary variables, the fluctuations during phase transition are overcome in our tank model. Table 3.2 lists the proposed primary variables for each approach.

Table 3.2 : Proposed primary variables.

	Liquid Phase	Two Phase	Gas Phase
O'Sullivan et al. (1985)	p, T, p_C	p, S_G, p_C	p, T, p_C
Hosgor et al. (2015)	p, T, p_C	S_G, T, p_C	p, T, p_C

3.7 Change of Phases During Simulation

Compressed water may boil to establish a two-phase region or two phase geothermal reservoir may form a superheated steam region with production. Finite difference solution algorithm must be able to handle these transitions. In the single phase liquid region, primary variables are selected as p , and T . First partial pressure of steam, P_s , is calculated from IAPWS then a test for phase transitions is made by checking the inequality $p < p_s +$ in every iteration. If pressure is smaller than sum of the partial pressure of steam and carbon dioxide, a change to the two phase region is made. During phase transition, primary variable becomes the saturation of gas, S_g , and S_g is initialized as a very small value such as 10^{-6} . In two phase region, gas saturation value is checked in every iteration this time. If $S_g < 0$ or $S_g > 1$, the transition to single phase liquid or gas, respectively, is occurred. When the gas saturation equals to 1, a change to single phase gas region is made. In this region, P , and T are the primary variables again. A test for phase transitions is made by checking the inequality $p < p_s +$ in every iteration. If the calculated pressure is equal or greater than the sum of the partial pressure of steam and carbon dioxide, then a transition to two-phase conditions is occurred.

Length of the time steps is also crucial in phase transition period because fluctuations occur during phase transition as it is mentioned before. With the relatively small time steps, fluctuation problem can be overcome. Particular attention is paid to this behaviour in general.

As the primary variables change during the iteration process, the thermodynamic package must be capable of recognizing the appearance and disappearance of phases and providing all needed thermophysical parameters appropriate for the latest iterated values of the primary variables (O'Sullivan et al. 1985).

3.8 Linearization of Equations

Equations 3.14, 3.22 and 3.30 are non-linear equations. This set of non linear partial differential equations with the associated thermodynamic relations is too complex to be solved by analytical methods. Therefore these equations are solved by numerical approach. Derivative of time appears in the all accumulation terms. To take the derivative of time, numerical approach can be utilized.

Overall mass balance, energy balance and carbon dioxide mass balance equations are discretized by using finite difference method as shown by equation 3.31, equation 3.32 and equation 3.33. These three equations have to be solved simulatenously by using an iterative approach given in the literature. The details of solution approach is given in the next subsection.

$$\begin{aligned}
 R_{w,i} = & V_{b,i} \frac{(\rho_L S_L \phi + \rho_G S_G \phi)_i^{n+1} - (\rho_L S_L \phi + \rho_G S_G \phi)_i^n}{\Delta t} \\
 & - \sum_{l=1}^{N_{ci}} \alpha_{L,i,j_l}^{n+1} (p_{j_l}^{n+1} - p_i^{n+1}) - \sum_{l=1}^{N_{ci}} \alpha_{G,j_l}^{n+1} (p_{j_l}^{n+1} - p_i^{n+1}) \\
 & + W_{p,L,i}^{n+1} + W_{p,G,i}^{n+1} + W_{inj,L,i}^{n+1} = 0
 \end{aligned} \tag{3.31}$$

$$\begin{aligned}
 R_{e,i} = & V_{b,i} \frac{\left[(1-\phi) \rho_m C_m T + \phi (\rho_L u_L S_L + \rho_G u_G S_G) \right]_i^{n+1}}{\Delta t} \\
 & - V_{b,i} \frac{\left[(1-\phi) \rho_m C_m T + \phi (\rho_L u_L S_L + \rho_G u_G S_G) \right]_i^n}{\Delta t} \\
 & + W_{p,L,i}^{n+1} h_{L,i}^{n+1} + W_{p,G,i}^{n+1} h_{G,i}^{n+1} + W_{inj,L,i}^{n+1} h_{L,inj,i}^{n+1} - \sum_{l=1}^{N_{ci}} \alpha_{L,i,j_l}^{n+1} (p_{j_l}^{n+1} - p_i^{n+1}) h_{L,\xi}^{n+1} \\
 & - \sum_{l=1}^{N_{ci}} \alpha_{G,i,j_l}^{n+1} (p_{j_l}^{n+1} - p_i^{n+1}) h_{G,\xi}^{n+1} - \sum_{l=1}^{N_{ci}} \gamma_{i,j_l}^{n+1} (T_{j_l}^{n+1} - T_i^{n+1}) = 0
 \end{aligned} \tag{3.32}$$

$$\begin{aligned}
R_{C,i} = & V_{b,i} \frac{(\rho_L S_L \phi f_{CL} + \rho_G S_G \phi f_{CG})_i^{n+1} - (\rho_L S_L \phi f_{CL} + \rho_G S_G \phi f_{CG})_i^n}{\Delta t} \\
& - \sum_{l=1}^{N_{ci}} \alpha_{L,i,j_l}^{n+1} (p_{j_l}^{n+1} - p_i^{n+1}) f_{CL,\xi}^{n+1} - \sum_{l=1}^{N_{ci}} \alpha_{G,i,j_l}^{n+1} (p_{j_l}^{n+1} - p_i^{n+1}) f_{CG,\xi}^{n+1} \\
& + W_{p,L,i}^{n+1} f_{CL,i}^{n+1} + W_{p,G,i}^{n+1} f_{CG,i}^{n+1} - W_{inj,L,i}^{n+1} f_{CL,i}^{n+1} \beta_i^{n+1} = 0
\end{aligned} \tag{3.33}$$

Here \mathbf{R} is the residual vector and can be written as;

$$\mathbf{R} = \begin{bmatrix} R_{w,I} \\ R_{e,I} \\ R_{c,I} \\ \cdot \\ \cdot \\ R_{w,N} \\ R_{e,N} \\ R_{c,N} \end{bmatrix} \tag{3.35}$$

3.9 Solution of Finite Difference Equations

Equations 3.32, 3.33 and 3.34 are solved in a fully implicit manner using the Newton-Raphson technique. Newton raphson method is one of the powerful techniques for solving equations numerically. Like so much of the differential calculus, it is based on the simple idea of linear approximation. There are $3N_t$ equations with $3N_t$ unknowns. These unknowns are pressure, temperature and partial pressure of CO₂ vectors for single phase regions and saturation of gas, temperature and partial pressure of CO₂ vectors for two phase region. The solution vector, \mathbf{v} , and the vector notation forms of these variables are given in equations 3.36, 3.37, 3.38, 3.39 and 3.40.

$$\mathbf{v} = [\mathbf{p} \text{ or } \mathbf{S}_G, \mathbf{T}, \mathbf{p}_C]^T \tag{3.36}$$

$$\mathbf{p}^{n+1,k+1} = \begin{bmatrix} p_1^{n+1,k+1} \\ p_2^{n+1,k+1} \\ \cdot \\ \cdot \\ p_{N_t}^{n+1,k+1} \end{bmatrix} \quad (3.37)$$

$$\mathbf{T}^{n+1,k+1} = \begin{bmatrix} T_1^{n+1,k+1} \\ T_2^{n+1,k+1} \\ \cdot \\ \cdot \\ T_{N_t}^{n+1,k+1} \end{bmatrix} \quad (3.38)$$

$$\mathbf{p}_C^{n+1,k+1} = \begin{bmatrix} p_{C1}^{n+1,k+1} \\ p_{C2}^{n+1,k+1} \\ \cdot \\ \cdot \\ p_{CN_t}^{n+1,k+1} \end{bmatrix} \quad (3.39)$$

Pressure is switched to gas saturation vector for two phase region.

$$\mathbf{S}_G^{n+1,k+1} = \begin{bmatrix} S_{G1}^{n+1,k+1} \\ S_{G2}^{n+1,k+1} \\ \cdot \\ \cdot \\ S_{GN_t}^{n+1,k+1} \end{bmatrix} \quad (3.40)$$

Newton Raphson method can be summarized with below equation 3.41;

$$\mathbf{J}^{n+1,k}(\mathbf{v}^{n+1,k}) \delta \mathbf{v}^{n+1,k+1} = -\mathbf{R}(\mathbf{v}^{n+1,k}) \quad (3.41)$$

The above set of equations has to be written in matrix form and it is solved for each time step until the desired end time. Vector \mathbf{R} is the right hand side vector (residual vector) and it has the form given in equation 3.35;

$\mathbf{v}^{n+1,k+1}$ is the solution vector that represents the primary variables (unknown variable vector) which have to be calculated during simulation. It has the form given in equation 3.41.

$$\mathbf{v}^{n+1,k+1} = \begin{bmatrix} p_1^{n+1} \text{ or } S_{g,1}^{n+1} \\ p_{C,1}^{n+1} \\ T_1^{n+1} \\ p_2^{n+1} \text{ or } S_{g,2}^{n+1} \\ p_{C,2}^{n+1} \\ T_2^{n+1} \\ \cdot \\ \cdot \\ \cdot \\ p_{N_t}^{n+1} \text{ or } S_{g,N_t}^{n+1} \\ p_{C,N_t}^{n+1} \\ T_{N_t}^{n+1} \end{bmatrix} \quad (3.42)$$

Here, primary variables depends on the phase regions (single phase liquid or gas region or two phase region) pressure or gas saturation, partial pressure of carbon dioxide and temperature.

\mathbf{J} is the Jacobian matrix and it has the form given by equation 3.42. \mathbf{J} represents the $3N_t \times 3N_t$ jacobian matrix and k represents the number of the iteration. In this equation, subscripts w , e and c represents the conservation equations for water mass, overall energy and carbon dioxide mass, respectively. In the model, these three conservation equations are solved in a fully implicit manner using the Newton-Raphson technique which is based on the simple idea of linear approximation. After equation 3.42 is solved, $\mathbf{v}^{n+1,k+1}$, the solution vector for the new step ($n+1$) can be calculated.

$$\mathbf{J}^{n+1,k}(\mathbf{v}^{n+1,k}) = \begin{bmatrix} \frac{\partial \mathbf{R}_{w,1}(\mathbf{v}^{n+1,k})}{\hat{\partial \mathbf{v}}_1} & \frac{\partial \mathbf{R}_{w,1}(\mathbf{v}^{n+1,k})}{\hat{\partial \mathbf{v}}_2} & \frac{\partial \mathbf{R}_{w,1}(\mathbf{v}^{n+1,k})}{\hat{\partial \mathbf{v}}_3} & \dots & \frac{\partial \mathbf{R}_{w,1}(\mathbf{v}^{n+1,k})}{\hat{\partial \mathbf{v}}_{3N_i}} \\ \frac{\partial \mathbf{R}_{e,1}(\mathbf{v}^{n+1,k})}{\hat{\partial \mathbf{v}}_1} & \frac{\partial \mathbf{R}_{e,1}(\mathbf{v}^{n+1,k})}{\hat{\partial \mathbf{v}}_2} & \frac{\partial \mathbf{R}_{e,1}(\mathbf{v}^{n+1,k})}{\hat{\partial \mathbf{v}}_3} & \dots & \frac{\partial \mathbf{R}_{e,1}(\mathbf{v}^{n+1,k})}{\hat{\partial \mathbf{v}}_{3N_i}} \\ \frac{\partial \mathbf{R}_{c,1}(\mathbf{v}^{n+1,k})}{\hat{\partial \mathbf{v}}_1} & \frac{\partial \mathbf{R}_{c,1}(\mathbf{v}^{n+1,k})}{\hat{\partial \mathbf{v}}_2} & \frac{\partial \mathbf{R}_{c,1}(\mathbf{v}^{n+1,k})}{\hat{\partial \mathbf{v}}_3} & \dots & \frac{\partial \mathbf{R}_{c,1}(\mathbf{v}^{n+1,k})}{\hat{\partial \mathbf{v}}_{3N_i}} \\ \cdot & \cdot & \cdot & \cdot & \cdot \\ \cdot & \cdot & \cdot & \cdot & \cdot \\ \cdot & \cdot & \cdot & \cdot & \cdot \\ \frac{\partial \mathbf{R}_{w,3N_i}(\mathbf{v}^{n+1,k})}{\hat{\partial \mathbf{v}}_1} & \frac{\partial \mathbf{R}_{w,3N_i}(\mathbf{v}^{n+1,k})}{\hat{\partial \mathbf{v}}_2} & \frac{\partial \mathbf{R}_{w,3N_i}(\mathbf{v}^{n+1,k})}{\hat{\partial \mathbf{v}}_3} & \dots & \frac{\partial \mathbf{R}_{w,3N_i}(\mathbf{v}^{n+1,k})}{\hat{\partial \mathbf{v}}_{3N_i}} \\ \frac{\partial \mathbf{R}_{e,3N_i}(\mathbf{v}^{n+1,k})}{\hat{\partial \mathbf{v}}_1} & \frac{\partial \mathbf{R}_{e,3N_i}(\mathbf{v}^{n+1,k})}{\hat{\partial \mathbf{v}}_2} & \frac{\partial \mathbf{R}_{e,3N_i}(\mathbf{v}^{n+1,k})}{\hat{\partial \mathbf{v}}_3} & \dots & \frac{\partial \mathbf{R}_{e,3N_i}(\mathbf{v}^{n+1,k})}{\hat{\partial \mathbf{v}}_{3N_i}} \\ \frac{\partial \mathbf{R}_{c,3N_i}(\mathbf{v}^{n+1,k})}{\hat{\partial \mathbf{v}}_1} & \frac{\partial \mathbf{R}_{c,3N_i}(\mathbf{v}^{n+1,k})}{\hat{\partial \mathbf{v}}_2} & \frac{\partial \mathbf{R}_{c,3N_i}(\mathbf{v}^{n+1,k})}{\hat{\partial \mathbf{v}}_3} & \dots & \frac{\partial \mathbf{R}_{c,3N_i}(\mathbf{v}^{n+1,k})}{\hat{\partial \mathbf{v}}_{3N_i}} \end{bmatrix} \quad (3.42)$$

The formula for the solution vector calculation is given in equation 3.43:

$$\mathbf{v}^{n+1,k+1} = \delta \mathbf{v}^{n+1,k+1} + \mathbf{v}^{n+1,k} \quad (3.43)$$

$\delta \mathbf{v}^{n+1,k+1}$ is the difference in the solution vector that is obtained by Newton-Raphson method and iteratively adjust primary variables. This process is started with the initial estimates and terminated when convergence to a sufficient level of accuracy is obtained. In this model, the convergence criteria is $\delta \mathbf{v}^{n+1,k+1} \leq 10^{-8}$. For the matrix calculation, Gauss-Jordan elimination method given in the Numerical Recipes (Press et al. 2007) is used.

If a geothermal system that contains 5 tanks as shown in Figure 3.5 is considered, there will be 15 primary variables and the Jacobian matrix will be 15x15. The structure of Jacobian matrix in single phase region where primary variables are p , T , p_{co_2} is given in the Figure 3.6. Here, p , T and p_{co_2} denote the non zero entries. If two phase

region appears the primary variables will be converted to S_g , T and p_{co_2} . The direct method like Gauss Jordan elimination can be used to solve the Jacobian matrix which is non-symmetric and sparse.

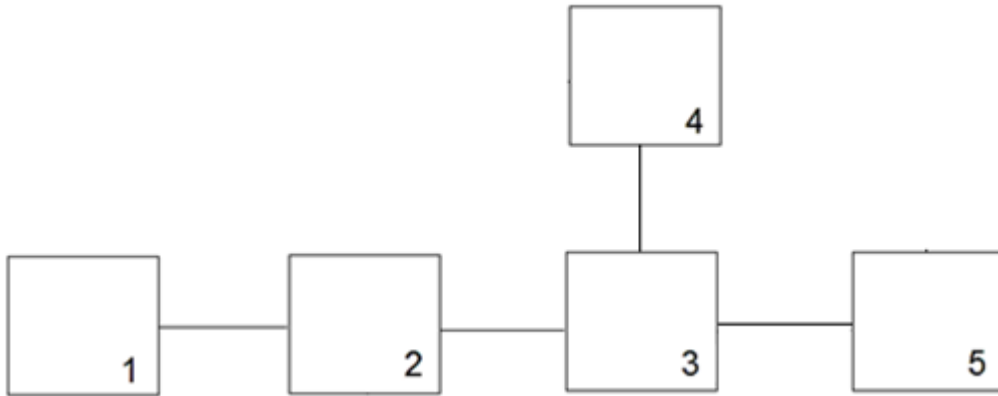


Figure 3.5 : Example for configuration of geothermal system.

$$\mathbf{J} = \begin{bmatrix}
 p & p & p & p & p & 0 & 0 & 0 & 0 & 0 & 0 & 0 & 0 & 0 & 0 \\
 T & T & T & T & T & 0 & 0 & 0 & 0 & 0 & 0 & 0 & 0 & 0 & 0 \\
 p_c & p_c & p_c & p_c & p_c & 0 & 0 & 0 & 0 & 0 & 0 & 0 & 0 & 0 & 0 \\
 p & p & p & p & p & p & p & p & 0 & 0 & 0 & 0 & 0 & 0 & 0 \\
 T & T & T & T & T & T & T & T & 0 & 0 & 0 & 0 & 0 & 0 & 0 \\
 p_c & p_c & p_c & p_c & p_c & p_c & p_c & p_c & 0 & 0 & 0 & 0 & 0 & 0 & 0 \\
 0 & 0 & 0 & p & p & p & p & p & p & p & p & p & p & p & p \\
 0 & 0 & 0 & T & T & T & T & T & T & T & T & T & T & T & T \\
 0 & 0 & 0 & p_c & p_c & p_c & p_c & p_c & p_c & p_c & p_c & p_c & p_c & p_c & p_c \\
 0 & 0 & 0 & 0 & 0 & 0 & p & p & p & p & p & p & 0 & 0 & 0 \\
 0 & 0 & 0 & 0 & 0 & 0 & T & T & T & T & T & T & 0 & 0 & 0 \\
 0 & 0 & 0 & 0 & 0 & 0 & p_c & p_c & p_c & p_c & p_c & p_c & 0 & 0 & 0 \\
 0 & 0 & 0 & 0 & 0 & 0 & p & p & p & 0 & 0 & 0 & p & p & p \\
 0 & 0 & 0 & 0 & 0 & 0 & T & T & T & 0 & 0 & 0 & T & T & T \\
 0 & 0 & 0 & 0 & 0 & 0 & p_c & p_c & p_c & 0 & 0 & 0 & p_c & p_c & p_c
 \end{bmatrix}$$

Figure 3.6 : Structure of generated Jacobian matrix.

The flow chart of the model is illustrated in Figure 3.7. According to model, first input parameters such as initial pressure, temperature, bulk volume, porosity, rock compressibility, rock density, specific heat capacity of the rock matrix, gas saturation, mass fraction of carbon dioxide, rock part of the recharge index (ψ), production rate/injection rate, duration etc. are read from the parameter file. Time step is generated and calculation steps are solved in the loop until the end time is reached. In the loop, residuals are generated and Jacobian matrix is formed and solved. When the difference in the solution vector is smaller than or equal to specified convergence criteria which is decided as 10^{-8} in this calculation, the solution vector at $n+1$ is calculated. The loop is terminated when the end time is reached.

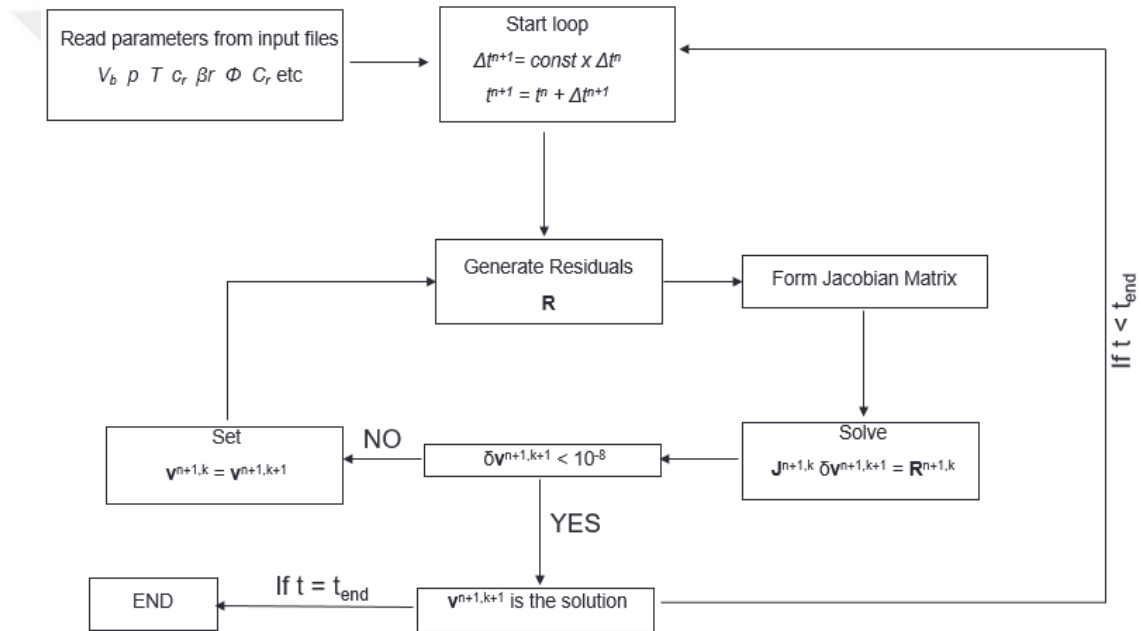


Figure 3.7 : Flow chart of the developed model.

3.10 Verification Studies with Petrasim

The verification of the tank model is carried out with the commercial simulator Petrasim which uses the codes of TOUGH family generated mainly by Pruess et al. (1998). This software can develop numerical models for non-isothermal flow of multicomponent and multiphase fluids in porous media. One tank closed, two tank closed and one tank open cases are given for comparison.

3.10.1 One tank closed system

Two cases are examined for one tank closed system. First case includes only production and the second case includes both production and reinjection.

3.10.1.1 Production case

The illustration of one tank open case that considers only production is given in Figure 3.8 and illustration of same case in PETRASIM is given in Figure 3.9. In this case, a reservoir with a volume of 10^9 m³ and porosity of 20 % is considered. The reservoir's initial pressure and temperature are assumed as 5 MPa and 450 K. It produces with 20 kg/s and there is no recharge or reinjection activity. The initial mass fraction of CO₂ is assumed as 0.01.

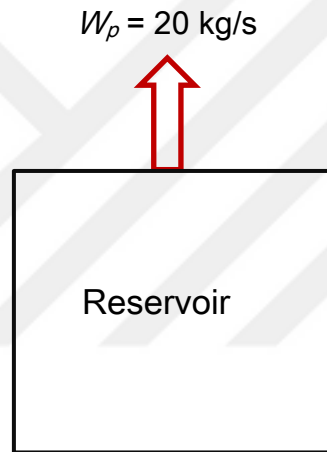


Figure 3.8 : Illustration of one tank closed system production case.

The data used in tank model is summarized in Tables 3.3.

Table 3.3 : Data used in the one tank closed model.

Bulk volume, m ³	1×10^9
Porosity, fraction	0.2
Initial pressure, MPa	5
Initial temperature, K	450
Rock compressibility, Pa ⁻¹	5×10^{-10}
Rock thermal expansion coefficient, K ⁻¹	0
Density of rock, kg/m ³	2600
Heat capacity of rock, J/(kg.K)	1000
Flow rate, kg/s	20
Initial mass of CO ₂ , MPa	0.01

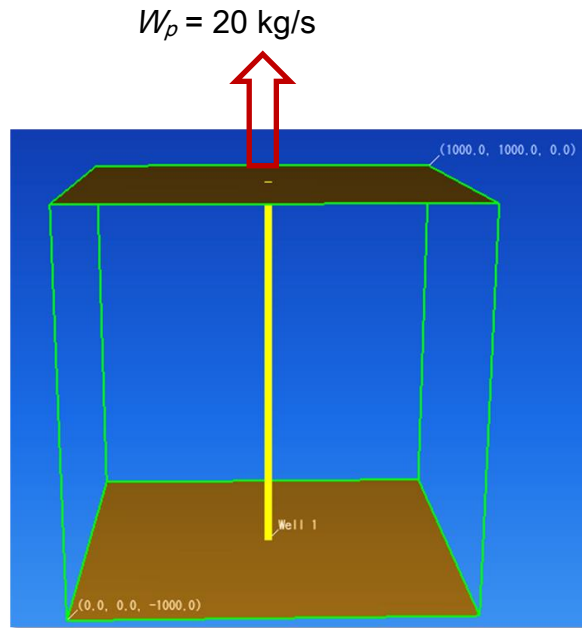


Figure 3.9 : Modelling of one tank closed system production case in PETRASIM.

The data used in the Petrasim software are summarized in Table 3.4. Here all the important parameters used in both cases are same except, tank model uses initial mass fraction of CO₂, whereas Petrasim requests partial pressure of CO₂.

Table 3.4 : Data used in Petrasim for one tank closed model.

Bulk volume, m ³	1×10 ⁹
Porosity, fraction	0.2
Initial pressure, MPa	5
Initial temperature, K	450
Rock compressibility, Pa ⁻¹	5×10 ⁻¹⁰
Rock thermal expansion coefficient, K ⁻¹	0
Density of rock, kg/m ³	2600
Heat capacity of rock, J/(kg.K)	1000
Permeability, m ²	1×10 ⁻¹³
Flow rate, kg/s	20
Partial pressure of CO ₂ , MPa	2.67

Figures 3.10-3.14 illustrate the changes in pressure, temperature, gas saturation, mass fraction of CO₂ in liquid and gas phase. As can be seen from the figures the results of the tank model are compatible with the simulator Petrasim. There is a small variation in the temperature behavior of the system. The same temperature trend is seen in the single phase region but the temperature of the tank model tends to decrease with higher a rate. The temperature drops to 449.83 K in Petrasim, on the other hand temperature

reduces to 449.78 K in tank model at the end of 10000 days. The difference is too small and it can be considered as acceptable.

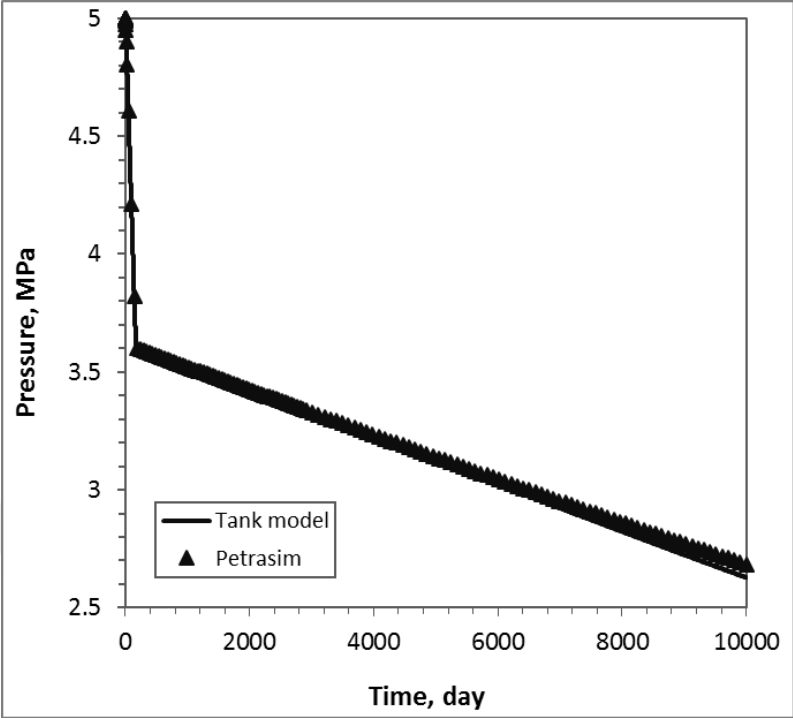


Figure 3.10 : Comparison of pressure behavior of one tank closed system production case.

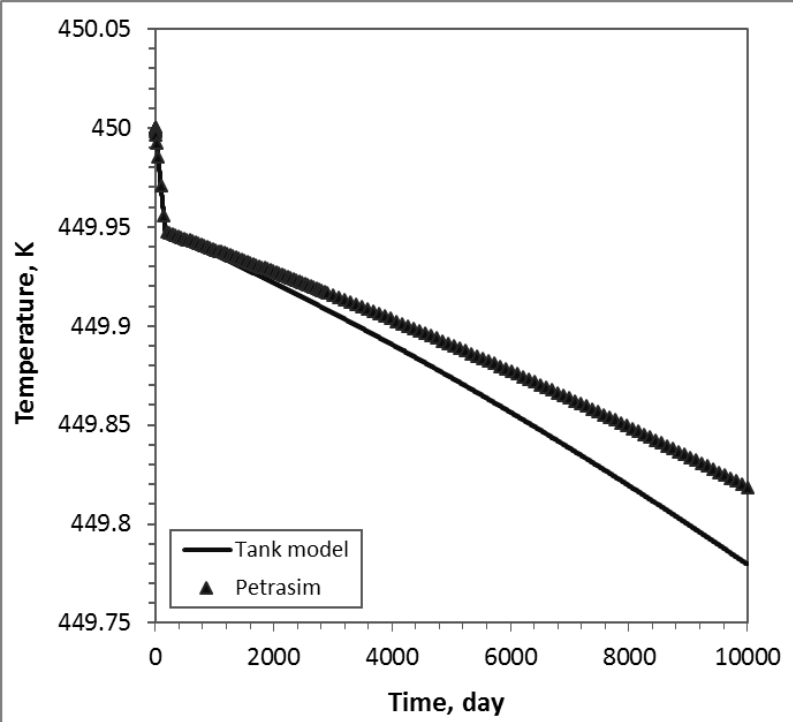


Figure 3.11 : Comparison of temperature behavior of one tank closed system production case.

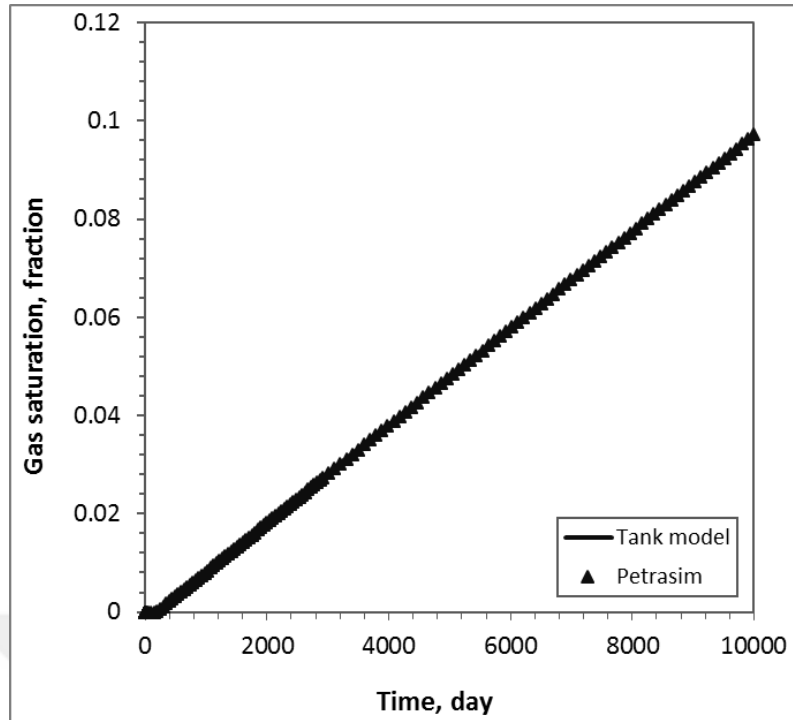


Figure 3.12 : Comparison of gas saturation behavior of one tank closed system production case.

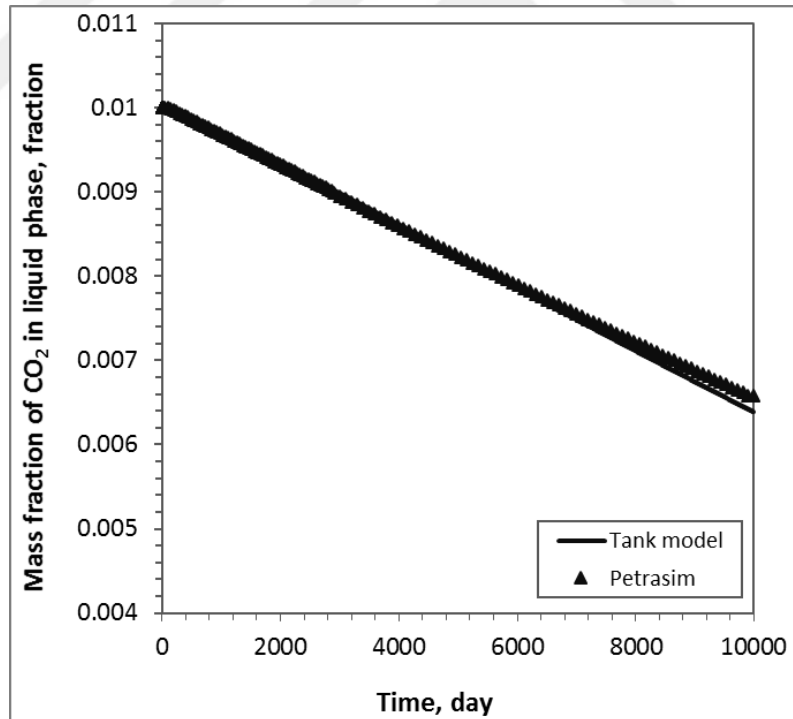


Figure 3.13 : Comparison of mass fraction of CO₂ in liquid phase of one tank closed system production case.

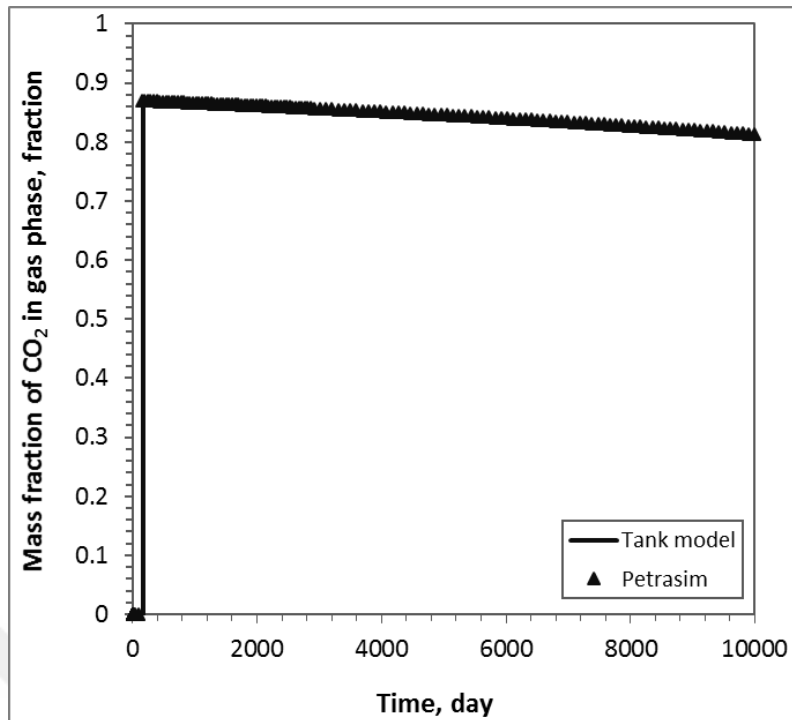


Figure 3.14 : Comparison of mass fraction of CO₂ in gas phase phase of one tank closed system production case.

3.10.1.2 Reinjection case

The illustration of the case is given in Figure 3.15 and properties of reservoir, production and reinjection rates, temperature and enthalpy are summarized in Table 3.5 and 3.6.

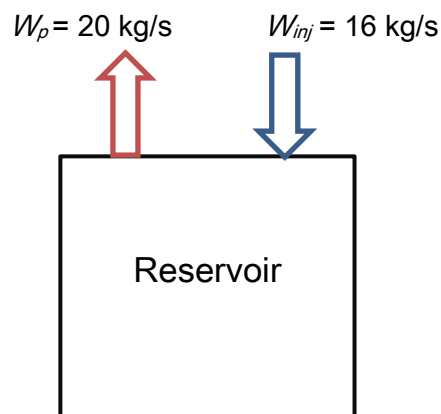


Figure 3.15 : Illustration of one tank closed reinjection case.

In production with reinjection case, it is assumed that reinjection begins with production and reinjection rate equals to 80 % of production rate. Here, initial reservoir temperature is 450 K but colder fluid is reinjected to the reservoir of temperature 333.15 K.

Table 3.5 : Data used in the one tank closed reinjection model.

Bulk volume, m ³	1×10 ⁹
Porosity, fraction	0.2
Initial pressure, MPa	5
Initial temperature, K	450
Rock compressibility, Pa ⁻¹	5×10 ⁻¹⁰
Rock thermal expansion coefficient, K ⁻¹	0
Density of rock, kg/m ³	2600
Heat capacity of rock, J/(kg.K)	1000
Flow rate, kg/s	20
Initial mass fraction of CO ₂ , fraction	0.01
Reinjection rate, kg/s	16
Reinjection temperature, K	333.15
β	0

Table 3.6 : Data used in Petrasim for one tank closed reinjection model.

Bulk volume, m ³	1×10 ⁹
Porosity, fraction	0.2
Initial pressure, MPa	5
Initial temperature, K	450
Rock compressibility, Pa ⁻¹	5×10 ⁻¹⁰
Rock thermal expansion coefficient, K ⁻¹	0
Density of rock, kg/m ³	2600
Heat capacity of rock, J/(kg.K)	1000
Permeability, m ²	1×10 ⁻¹³
Flow rate, kg/s	20
Partial pressure of CO ₂ , MPa	2.67
Reinjection rate, kg/s	16
Reinjection enthalpy, J/kg	2.475×10 ⁵

Figures 3.16-3.20 illustrate the results of pressure, temperature, gas saturation, mass fraction of CO₂ in liquid and mass fraction of CO₂ in gas phase. As can be seen from the figures the results of the tank model are nearly same with the results from simulator Petrasim.

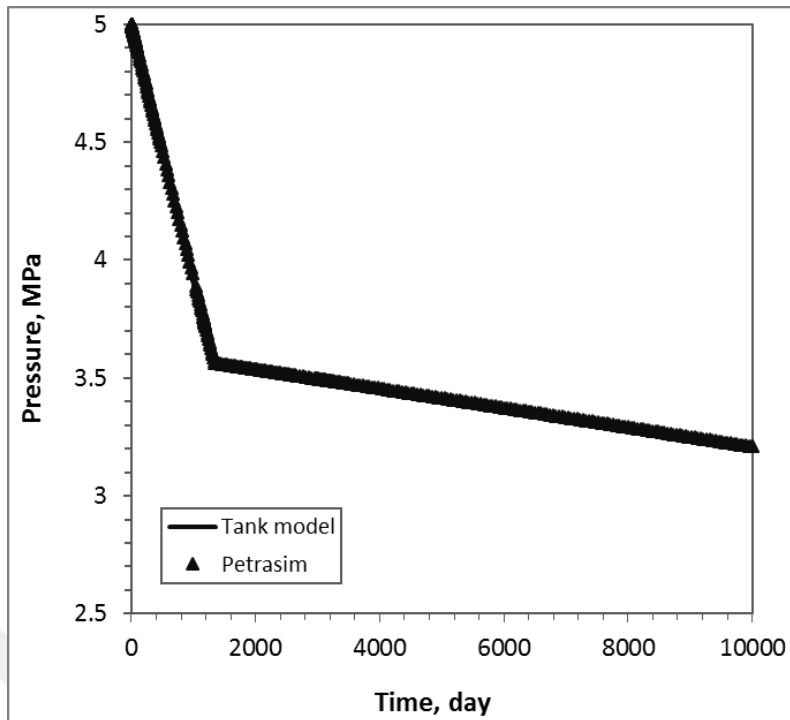


Figure 3.16 : Comparison of pressure behavior of one tank closed reinjection case.

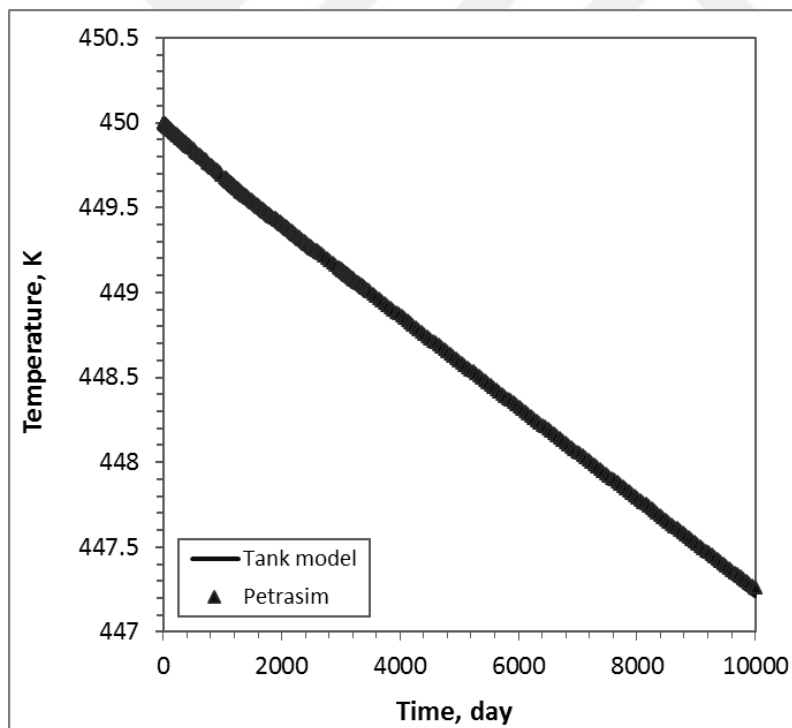


Figure 3.17 : Comparison of temperature behavior of one tank closed reinjection case.

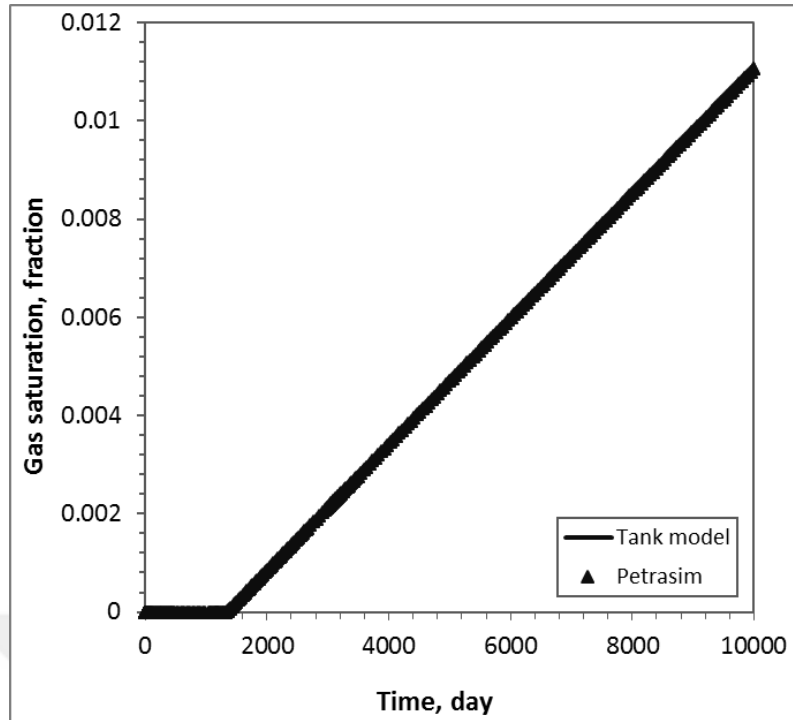


Figure 3.18 : Comparison of gas saturation behavior of one tank closed reinjection case.

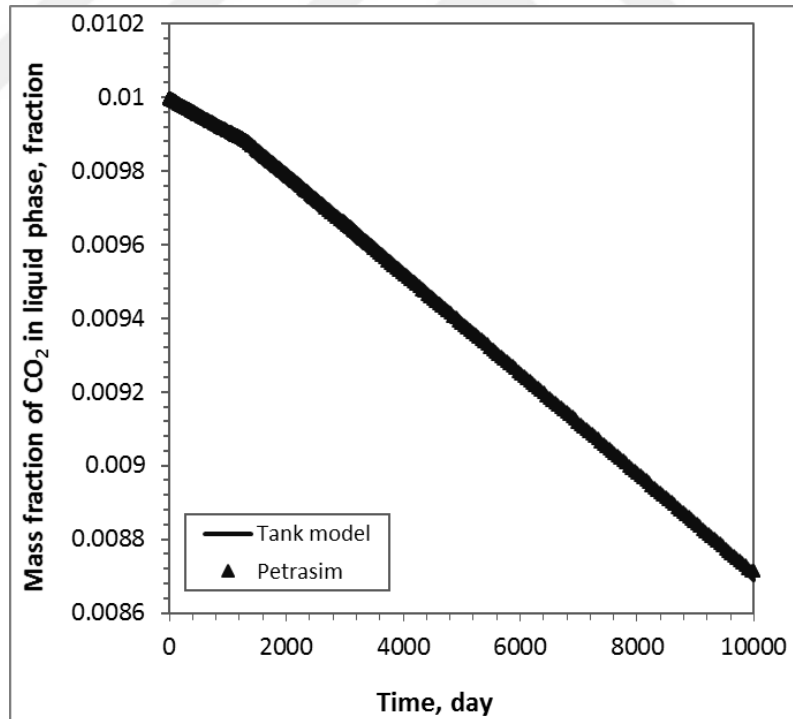


Figure 3.19 : Comparison of mass fraction of CO₂ in liquid phase in one tank closed reinjection case.

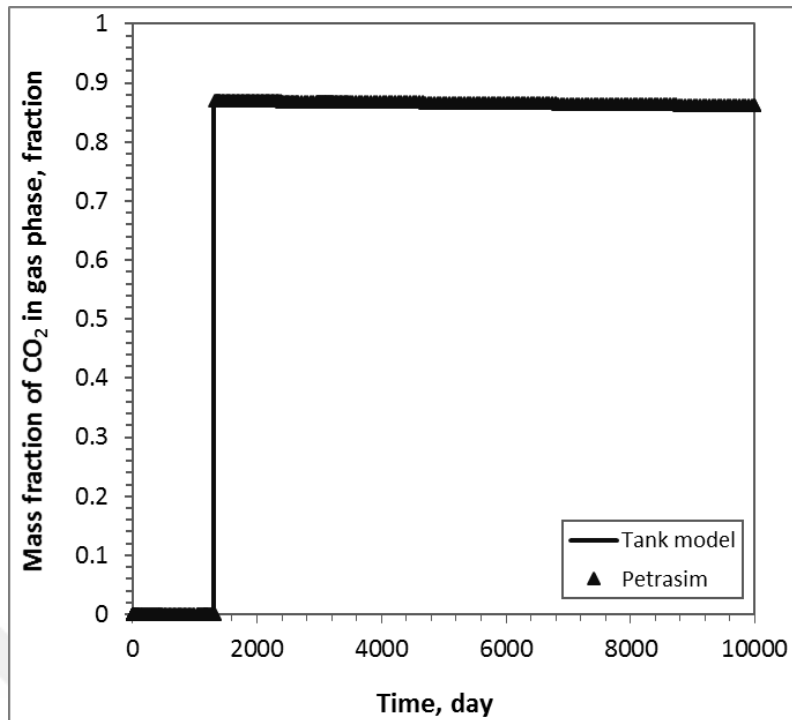


Figure 3.20 : Comparison of mass fraction of CO₂ in gas phase in one tank closed reinjection case.

3.10.2 Two tank closed system

3.10.2.1 Production case

In this scenario, the closed reservoir system is modelled with two tanks. Mass rate between tanks is defined by recharge index that is calculated in each time step. The production rate of 50 kg/s takes place in Tank 2. The illustration of the case is given in Figure 3.21 and the data used in the tank model are given in Table 3.7.

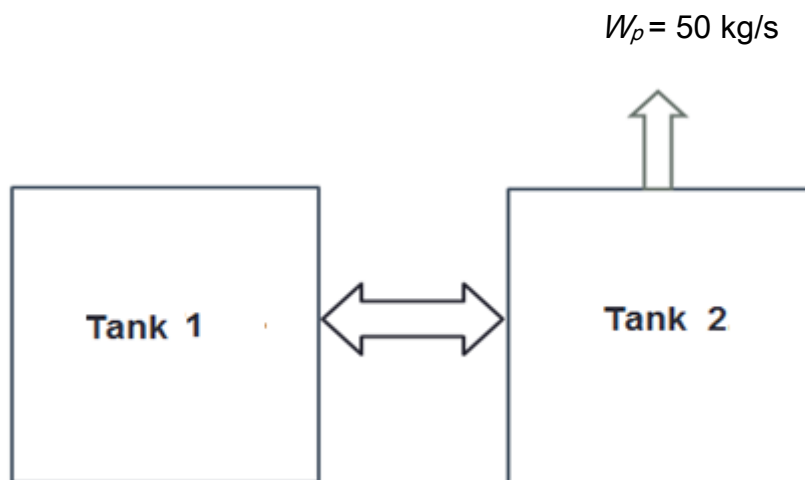


Figure 3.21 : Illustration of two tanks production case.

Table 3.7 : Data used in the two tanks production model.

Bulk volume of Tank 1, m ³	1×10 ⁹
Bulk volume of Tank 2, m ³	1×10 ⁹
Porosity, fraction	0.2
Initial pressure, MPa	5
Initial temperature, K	450
Rock compressibility, Pa ⁻¹	5×10 ⁻¹⁰
Rock thermal expansion coefficient, K ⁻¹	0
Density of rock, kg/m ³	2600
Heat capacity of rock, J/(kg.K)	1000
Initial mass fraction of CO ₂ , fraction	0.01
Production from Tank 2, kg/s	50
Rock part of the recharge index, m ³	1×10 ⁻¹⁰

The modelling approach in PETRASIM simulator is given in Figure 3.22. There are two adjacent tanks that have permeability of $1 \times 10^{-13} \text{ m}^2$ in x direction. The production is occurred in Tank 2 as it is in the tank model. The data used in Petrasim are summarized in Table 3.8.



Figure 3.22 : Modelling of two tanks production case with PETRASIM.

Table 3.8 : Data used in Petrasim for two tanks production model.

Bulk volume of Tank 1, m ³	1×10 ⁹
Bulk volume of Tank 2, m ³	1×10 ⁹
Porosity, fraction	0.2
Initial pressure, MPa	5
Initial temperature, K	450
Rock compressibility, Pa ⁻¹	5×10 ⁻¹⁰
Rock thermal expansion coefficient, K ⁻¹	0
Density of rock, kg/m ³	2600
Heat capacity of rock, J/(kg.K)	1000
Permeability, m ²	1×10 ⁻¹³
Production from Tank 2, kg/s	50
Partial pressure of CO ₂ , MPa	2.67

Figures 3.23-3.27 illustrate the results of pressure, temperature, gas saturation, mass fraction of dissolved CO₂ in water and mass fraction of CO₂ in gas phase. As can be seen from the figures the results of the tank model are compatible with the result of Petrasim software.

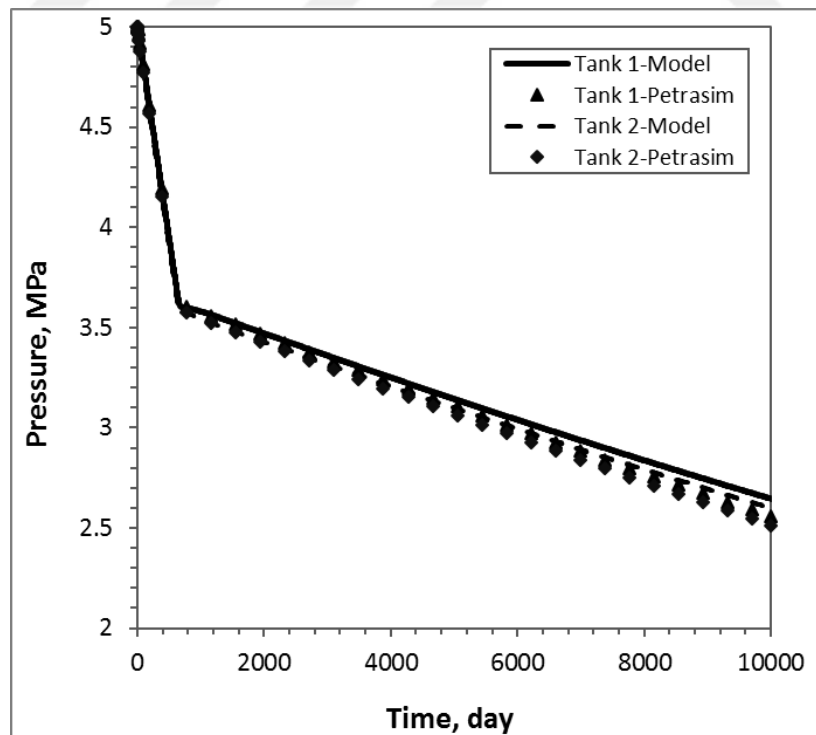


Figure 3.23 : Comparison of pressure behavior for two tanks production case.

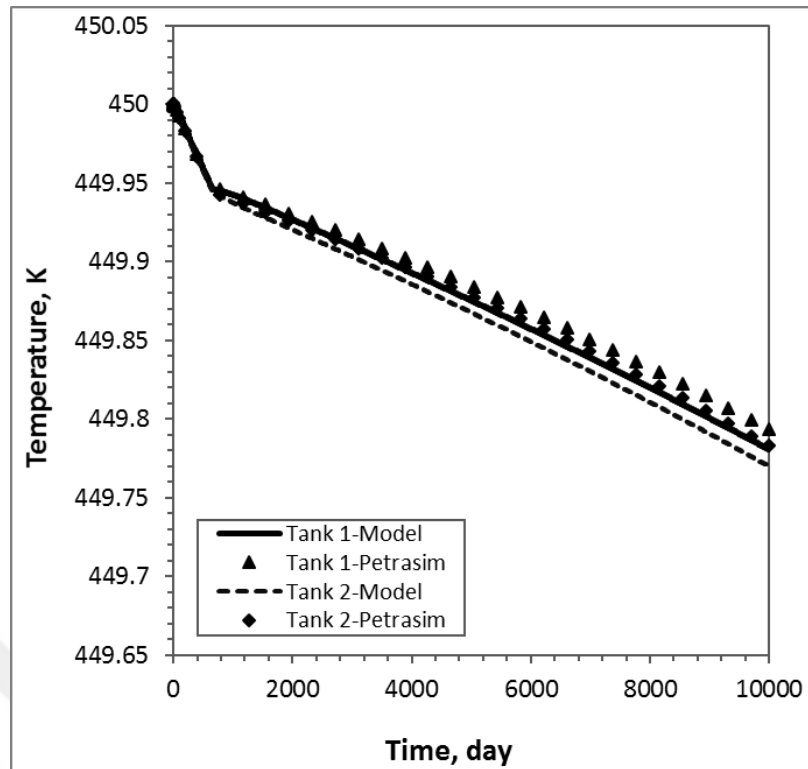


Figure 3.24 : Comparison of temperature behavior for two tanks production case.

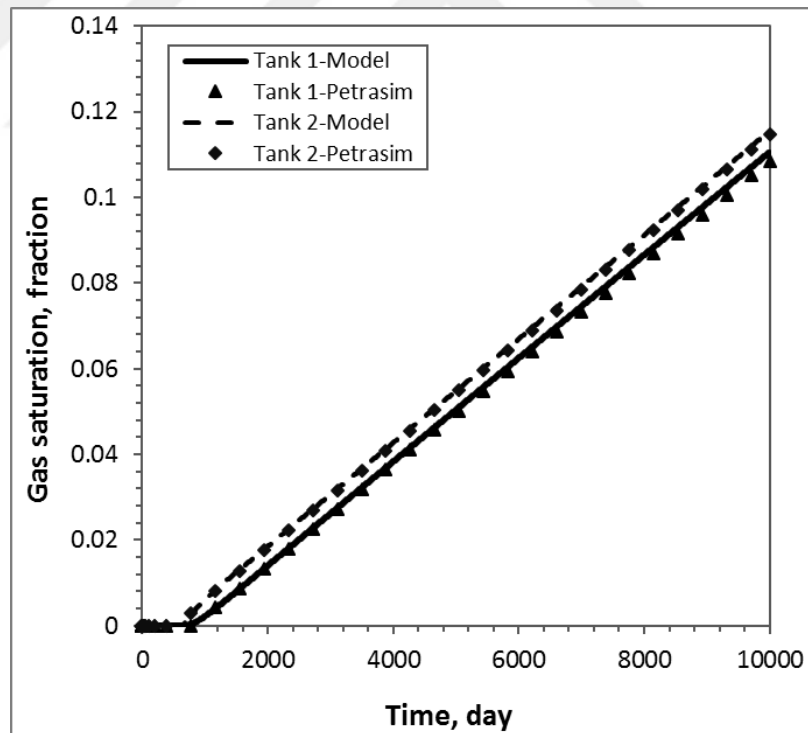


Figure 3.25 : Comparison of gas saturation behavior for two tanks production case.

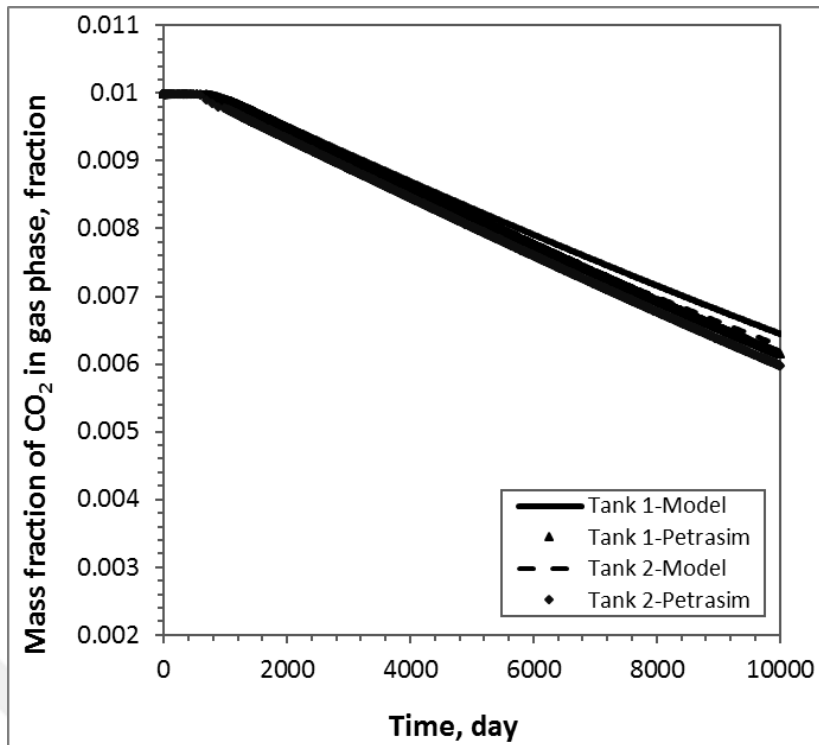


Figure 3.26 : Comparison of mass fraction of CO₂ in liquid phase for two tanks production case.

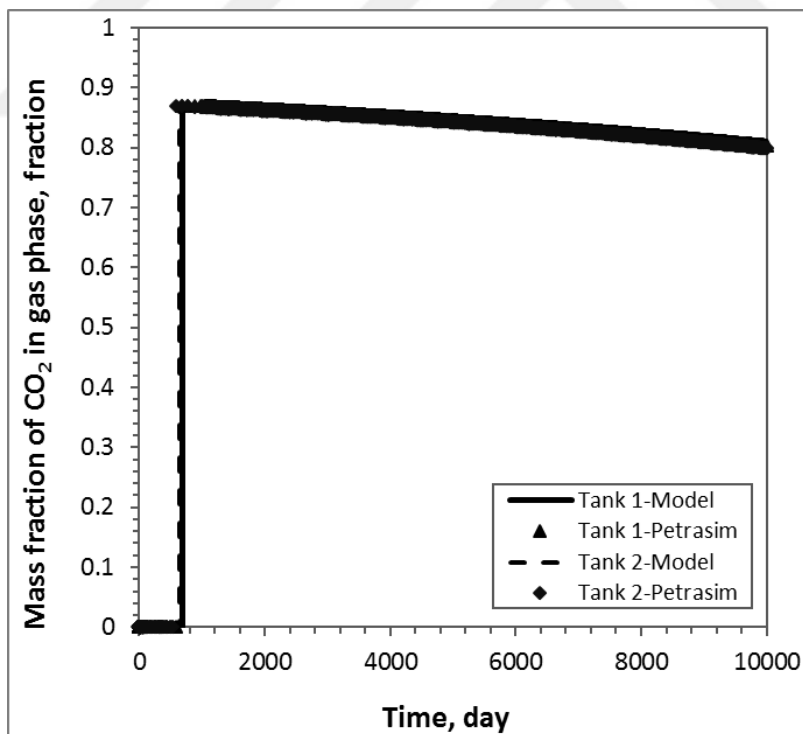


Figure 3.27: Comparison of mass fraction of CO₂ in gas phase for two tanks production case.

3.10.2.2 ReInjection case

In this case, reservoir is modelled with two tanks but it is a closed system and there is no recharge source. Production and injection activities take place in Tank 1. The illustration of the case is given in Figure 3.28 and data used in the tank model and Petrasim are given in Tables 3.9 and 3.10.

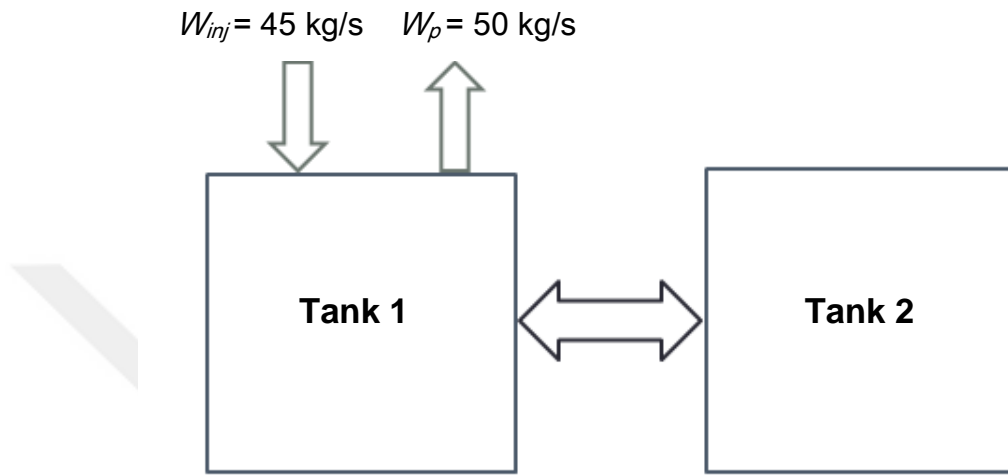


Figure 3.28 : Illustration of two tanks production/injection case.

Table 3.9 : Data used in two tanks production/injection model.

Bulk volume of Tank 1, m ³	1×10^9
Bulk volume of Tank 2, m ³	1×10^9
Porosity, fraction	0.2
Initial pressure, MPa	5
Initial temperature, K	450
Rock compressibility, Pa ⁻¹	1×10^{-9}
Rock thermal expansion coefficient, K ⁻¹	0
Density of rock, kg/m ³	2600
Heat capacity of rock, J/(kg.K)	1000
Initial mass fraction of CO ₂ , fraction	0.01
Production from Tank 1, kg/s	50
Reinjection into Tank 1, kg/s	45
Reinjection temperature, K	373.15
Rock part of the recharge index, m ³	1×10^{-10}
β	0

Figures 3.29-3.33 illustrate the results of pressure, temperature, gas saturation and mass fraction of CO₂ in gas phase. As can be seen from the figures the results of the two tank model are compatible with the results determined from simulator Petrasim.

Table 3.10 : Data used in Petrasim for two tanks production/injection model.

Bulk volume of Tank 1, m ³	1×10 ⁹
Bulk volume of Tank 2, m ³	1×10 ⁹
Porosity, fraction	0.2
Initial pressure, MPa	5
Initial temperature, K	450
Rock compressibility, Pa ⁻¹	1×10 ⁻⁹
Rock thermal expansion coefficient, K ⁻¹	0
Density of rock, kg/m ³	2600
Heat capacity of rock, J/(kg.K)	1000
Permeability, m ²	1×10 ⁻¹³
Production from Tank 1, kg/s	50
Partial pressure of CO ₂ , MPa	2.67
Reinjection into Tank 1, kg/s	45
Reinjection enthalpy, J/kg	4.227×10 ⁵

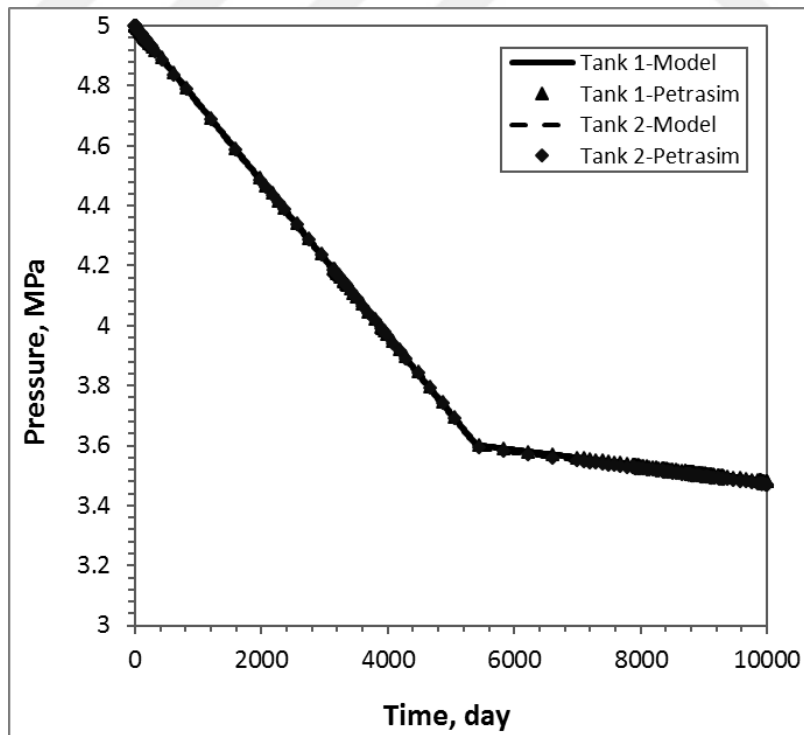


Figure 3.29: Comparison of pressure behavior for two tanks production/injection case.

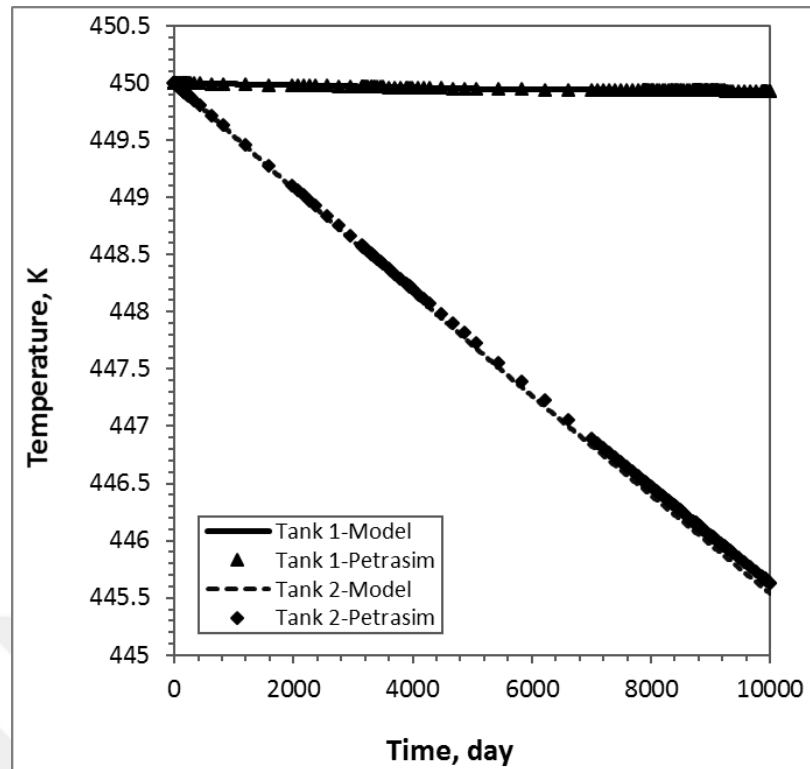


Figure 3.30 : Comparison of temperature behavior for two tanks production/injection case.

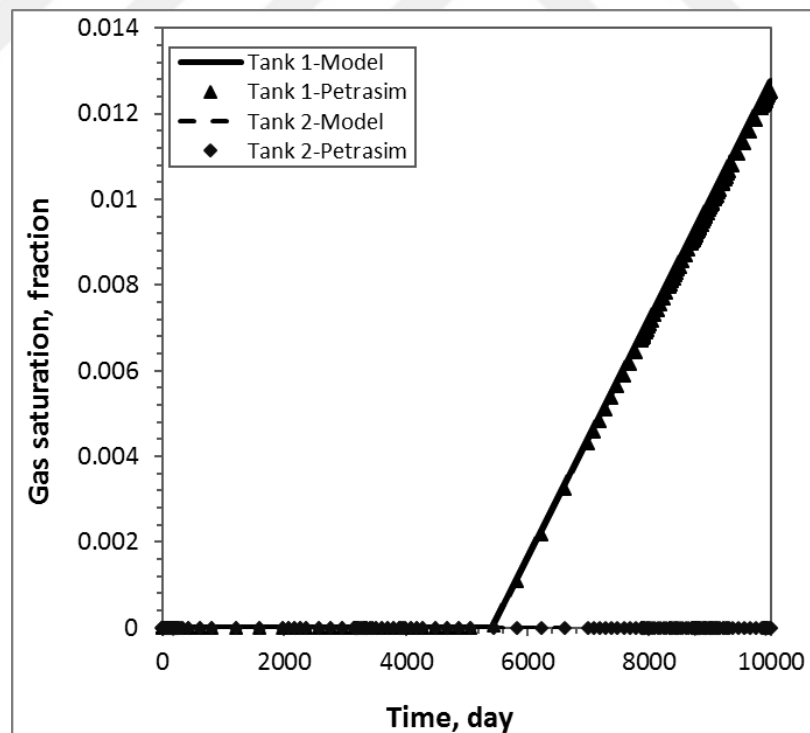


Figure 3.31 : Comparison of gas saturation behavior for two tanks production/injection case.

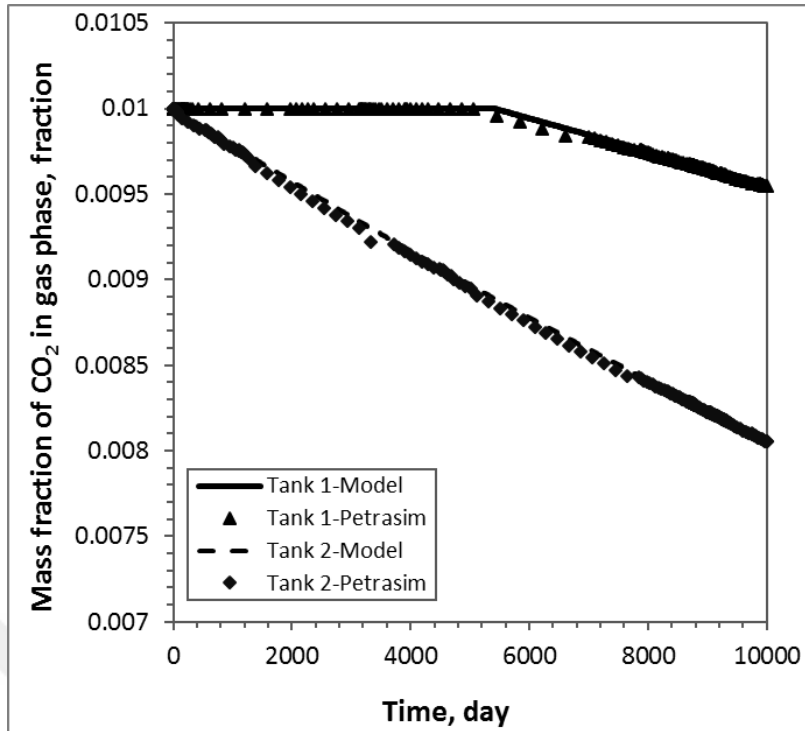


Figure 3.32 : Comparison of mass fraction of CO₂ in liquid phase for two tanks production/injection case.

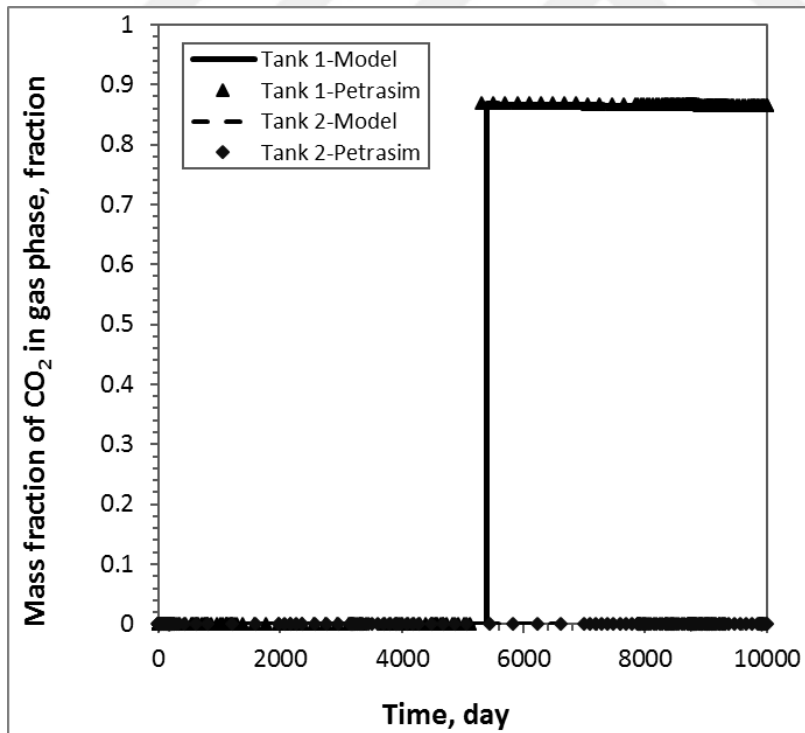


Figure 3.33 : Comparison of mass fraction of CO₂ in gas phase for two tanks production/injection case.

3.10.3 One tank open system

This case, one tank open system as illustrated in Figure 3.34 is chosen for the verification. Reservoir produces with 300 kg/s and there is feeding from recharge source.

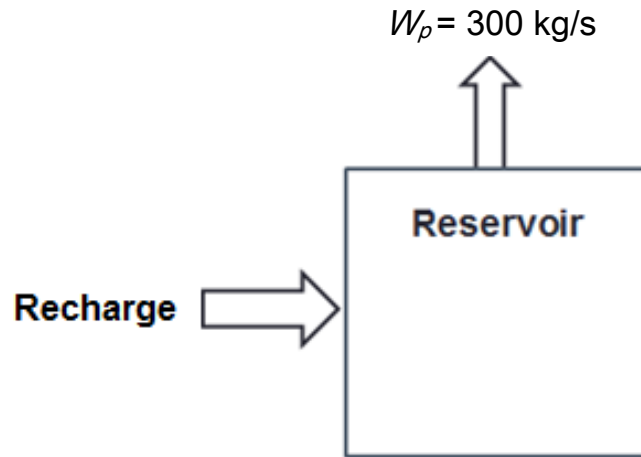


Figure 3.34 : Illustration of recharge model.

The data used in Petrasim and the tank model are given in Tables 3.11 and 3.12, respectively.

Table 3.11 : Data used in the one tank recharge model.

Bulk volume, m^3	1×10^9
Porosity, fraction	0.2
Initial pressure, MPa	5
Initial temperature, K	450
Rock compressibility, Pa^{-1}	5×10^{-10}
Rock thermal expansion coefficient, K^{-1}	0
Density of rock, kg/m^3	2600
Heat capacity of rock, $\text{J}/(\text{kg.K})$	1000
Production, kg/s	300
Initial mass fraction of CO_2 , fraction	0.01
Rock part of the recharge index, m^3	1×10^{-11}

Table 3.12 : Data used in Petrasim for one tank recharge model.

Bulk volume, m ³	1×10 ⁹
Porosity, fraction	0.2
Initial pressure, MPa	5
Initial temperature, K	450
Rock compressibility, Pa ⁻¹	5×10 ⁻¹⁰
Rock thermal expansion coefficient, K ⁻¹	0
Density of rock, kg/m ³	2600
Heat capacity of rock, J/(kg.K)	1000
Permeability, m ²	1×10 ⁻¹⁴
Production, kg/s	300
Partial pressure of CO ₂ , MPa	2.67051

Figures 3.35-3.39 illustrate the results of pressure, temperature, gas saturation, mass fraction of CO₂ in water and mass fraction of CO₂ in gas phase. As can be seen from the figures the results of the one tank open model are compatible with the results determined from simulator Petrasim.

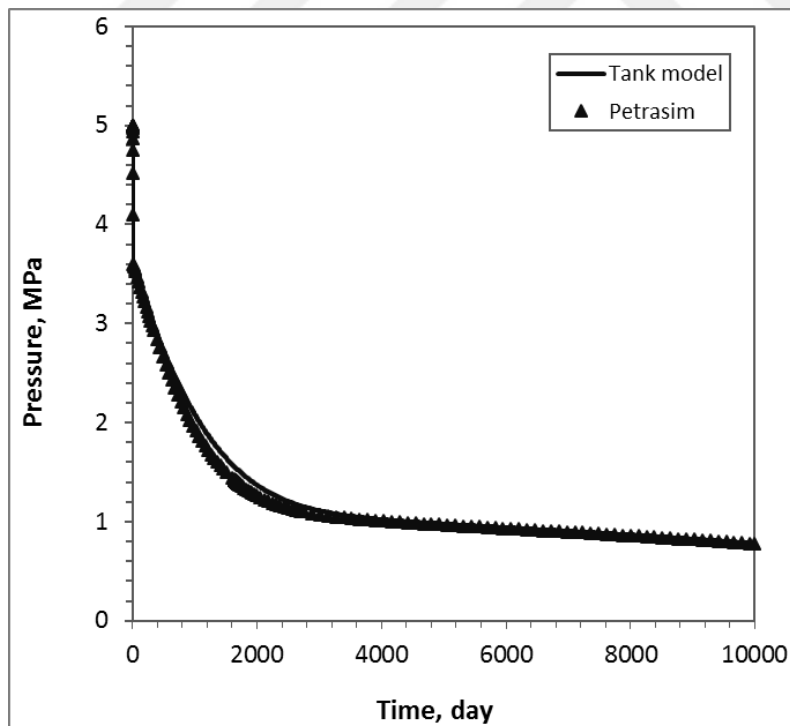


Figure 3.35 : Comparison of pressure behavior for recharge model.

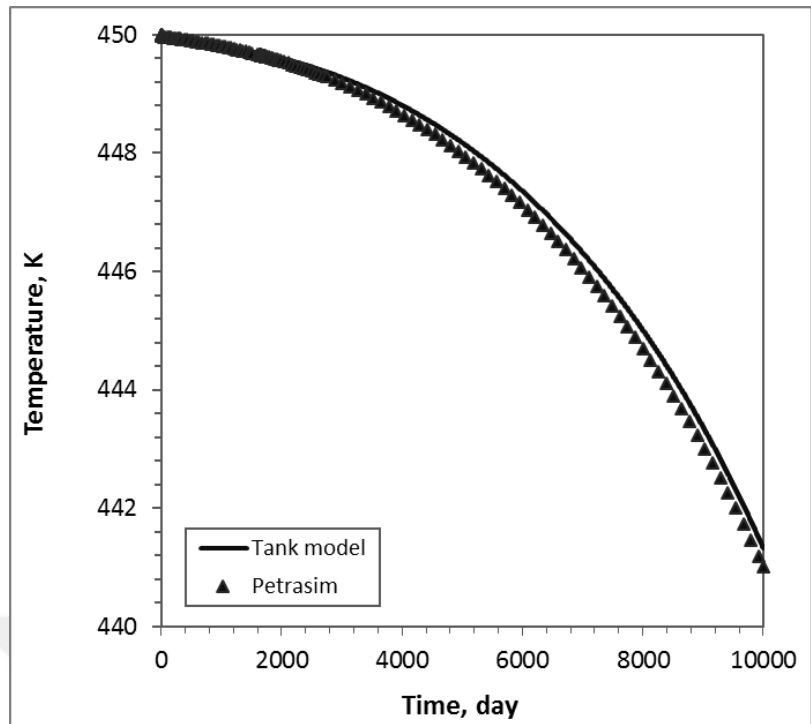


Figure 3.36 : Comparison of temperature behavior for recharge model.

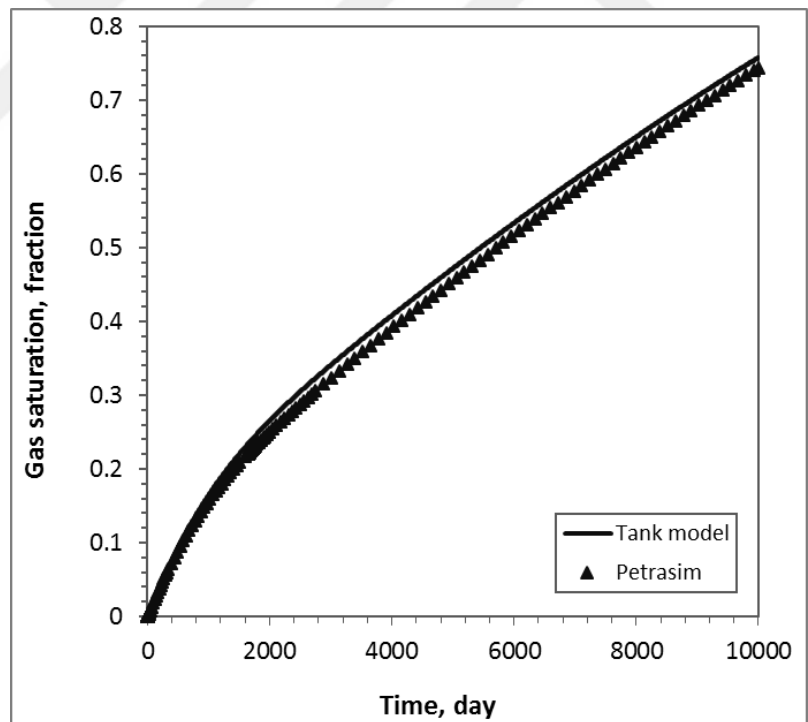


Figure 3.37 : Comparison of saturation behavior for recharge model.

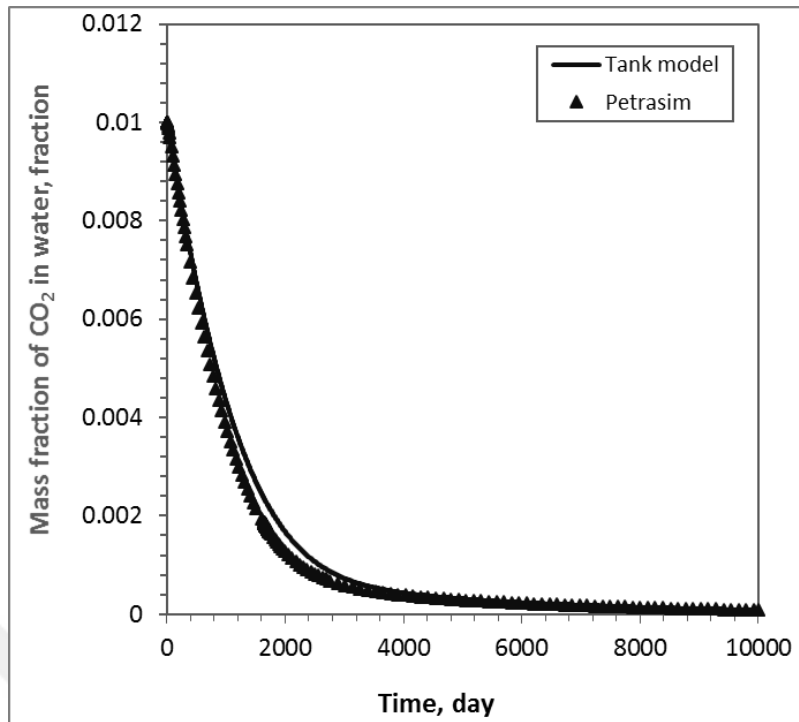


Figure 3.38 : Comparison of mass fraction of CO₂ in water for recharge model.

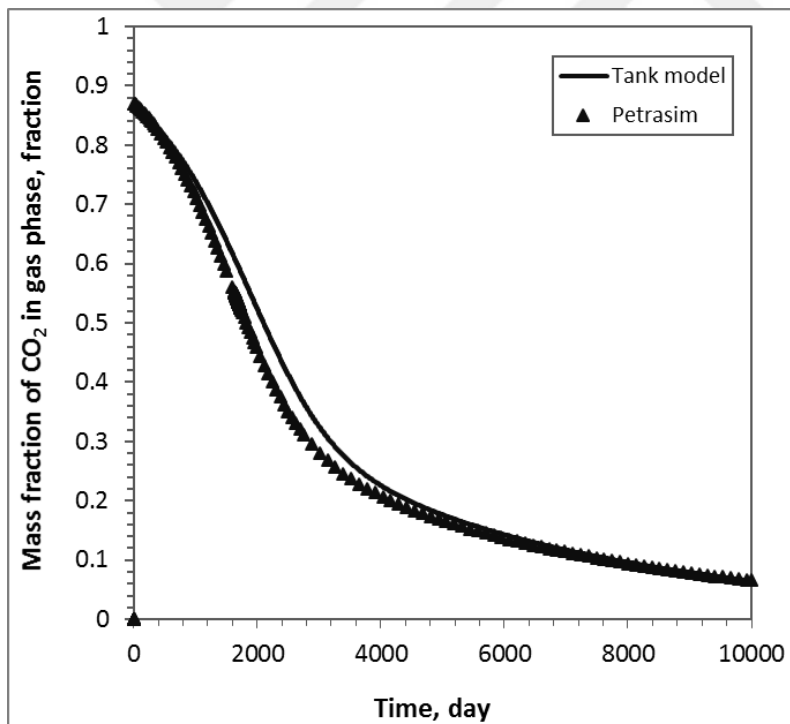


Figure 3.39 : Comparison of mass fraction of CO₂ in gas phase for recharge model.

3.11 Sythetic Applications with Tank Model

3.11.1 One Tank Closed Model

In this section, three different cases including the effects of mass fraction of CO₂ in reservoir water, production rate and reinjection are provided to illustrate the effects of CO₂ on the performance of geothermal reservoirs and the effect of physical parameters such as porosity, bulk volume, rock compressibility and density of rock are examined. For simplicity a single tank model is chosen. The main properties of the reservoir that are used in the models are given in Table 3.13, other circumstances are explained for each case.

Table 3.13 : Reservoir properties for one tank closed model.

Bulk volume, m ³	1×10 ⁹
Porosity, fraction	0.2
Initial pressure, Pa	50×10 ⁵
Initial Temperature, K	450
Rock compressibility, Pa ⁻¹	5×10 ⁻¹⁰
Rock thermal expansion coefficient, K ⁻¹	0
Density of rock, kg/m ³	2600
Heat capacity of rock, J/(kg.K)	1000
Rock part of the recharge index, m ³	1×10 ⁻¹⁰

3.11.1.1 The effect of mass fraction of CO₂ in reservoir water

In this case, the effect of mass fractions of CO₂ on the behavior of the reservoir is examined for four different mass fractions of CO₂ (0%, 0.5%, 1% and 1.5%). Constant production at 2 kg/s is assumed for a duration of 10000 days.

The pressure behavior of such a system is given in Figure 3.40 If no CO₂ were present in the water, then production is maintained in a compressed liquid state until 5000 days. After 5000 days, steam and water co-exist in the reservoir. However, it is important to note that once the reservoir fluid becomes two-phase, the decline rate of pressure is decreased. This is due to the much higher compressibility (when compared with liquid compressibility) of the gas phase that co-exists with the liquid (Satman and Ugur, 2002). When 0.5% CO₂ is dissolved in water, then two-phase conditions are reached earlier (at around 2500 days). The pressure for the remaining 7500 days

remains fairly constant maintained by gas compressibility. As expected, even further increasing the CO₂ content results in pressure maintenance at even earlier times.

Figure 3.41 illustrates how the gas saturation changes with time for the same amounts of dissolved CO₂. As expected, the gas saturation starts increasing as soon as the flashing point pressure is reached in the reservoir. The increases associated with the saturations are linear. At this point it is important to note that, the computed pressures and saturations of the model reflect the average pressure and saturations of the reservoir. During production, gas saturations would be varying with position and would be at a maximum around the well in a case where the bottomhole pressures of wells have dropped below the flashing point pressure.

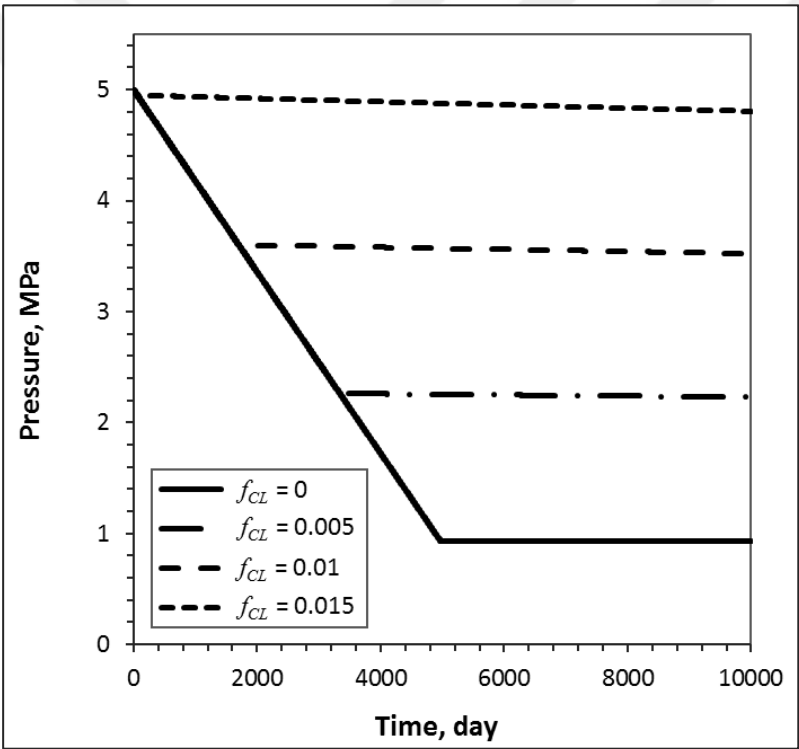


Figure 3.40 : Pressure behavior for various amounts of CO₂ dissolved in water.

Figure 3.42 gives the evolution of the mass fraction of the CO₂ dissolved in the water. For each initial mass fraction, the mass fractions of dissolved CO₂ tend to decrease. However as expected this decrease is very small. This decrease is associated with the transfer of carbon dioxide into the gas phase.

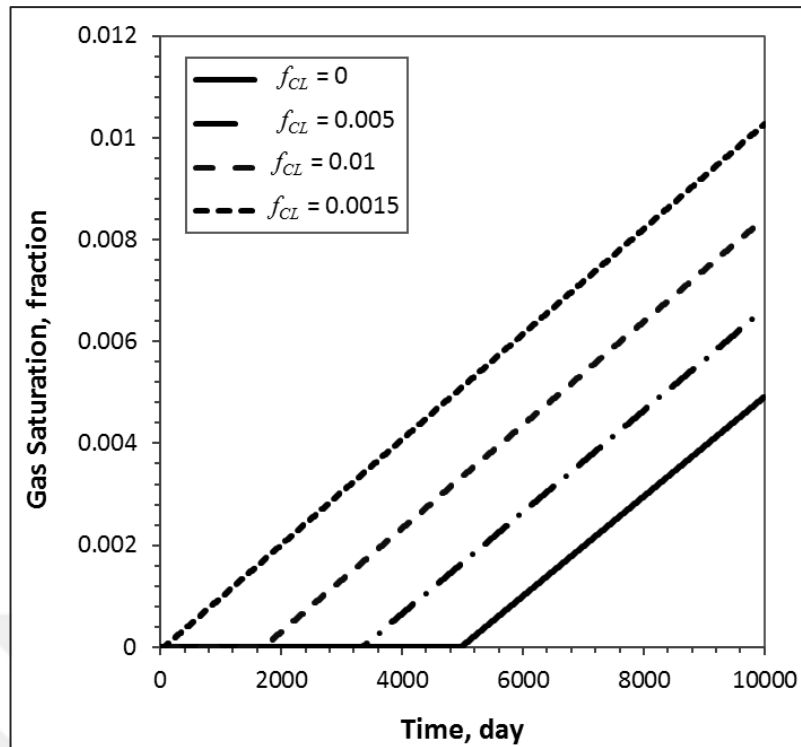


Figure 3.41 : Saturation behavior for various amounts of CO₂ dissolved in water.

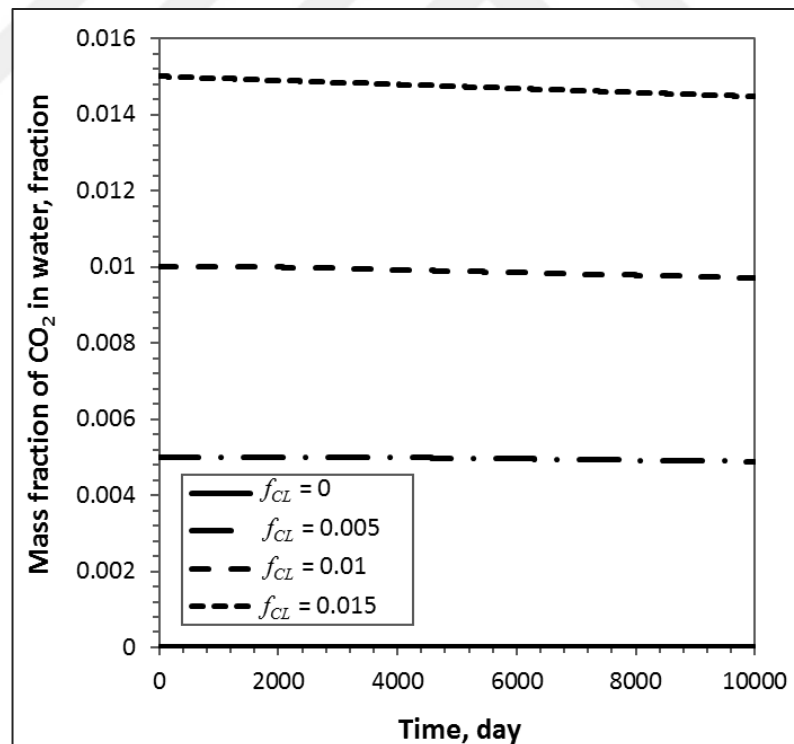


Figure 3.42 : Evolution of the mass fraction of CO₂ in water.

Finally, Figure 3.43 gives the evolution of the mass fraction of CO₂ in the gas phase. At first the mass fractions are zero since no gas phase is present. Then when the

flashing point pressure is reached and gas phase starts to form, we observe that the gas phase is made up of mostly CO₂. For a mass fraction of 1.5% CO₂ dissolved in water, the gas phase is composed of 90% CO₂ whereas for a mass fraction of 0.5% CO₂ dissolved in water, the gas phase is composed of 78% of CO₂.

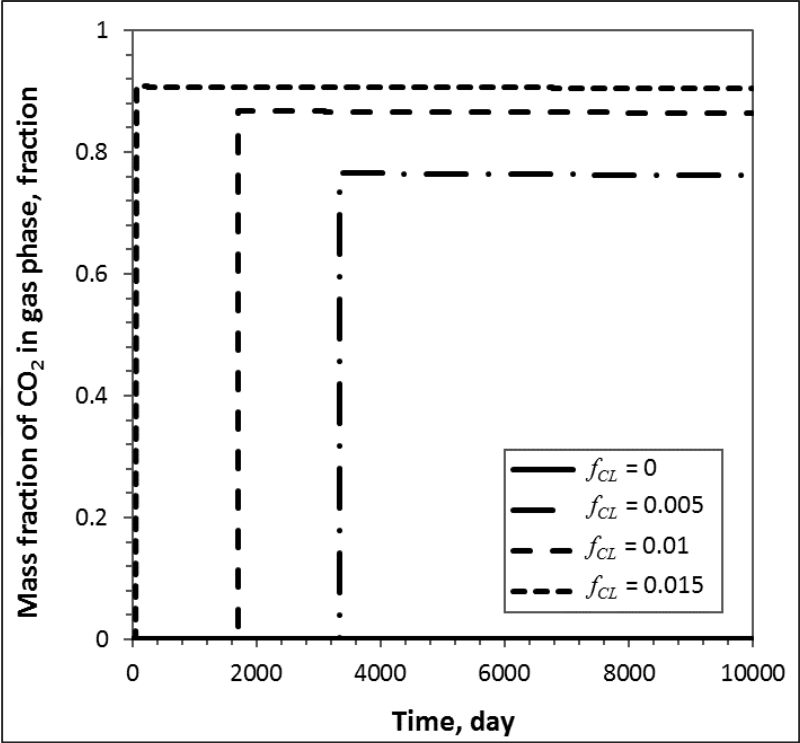


Figure 3.43 : Evolution of the mass fraction of CO₂ in the gas phase.

3.11.1.2 The effect of production rate

In this case, the effect of production rate on the behavior of the reservoir is examined for four different flow rates (2 kg/s, 5 kg/s, 10 kg/s and 20 kg/s) for a duration of 10000 days. Initial mass fraction of CO₂ is taken as 1%. The production rate is the most important parameter. It depends on the physical properties of the reservoir and external parameter such as power plant that is planned to be installed.

The pressure behavior of the system is given in Figure 3.44. As it is seen from the figure, as the flow rate increases pressure decreases rapidly in the liquid phase region and two-phase forms. After the fluid becomes two phase, the pressure decline rate decreases. In Figure 3.45, the gas saturation behavior of the system is given. When the flow rate increases the gas phase is formed earlier. The gas saturation starts increasing as soon as the flashing point pressures are reached in the reservoir. The higher gas saturation is reached with the higher production.

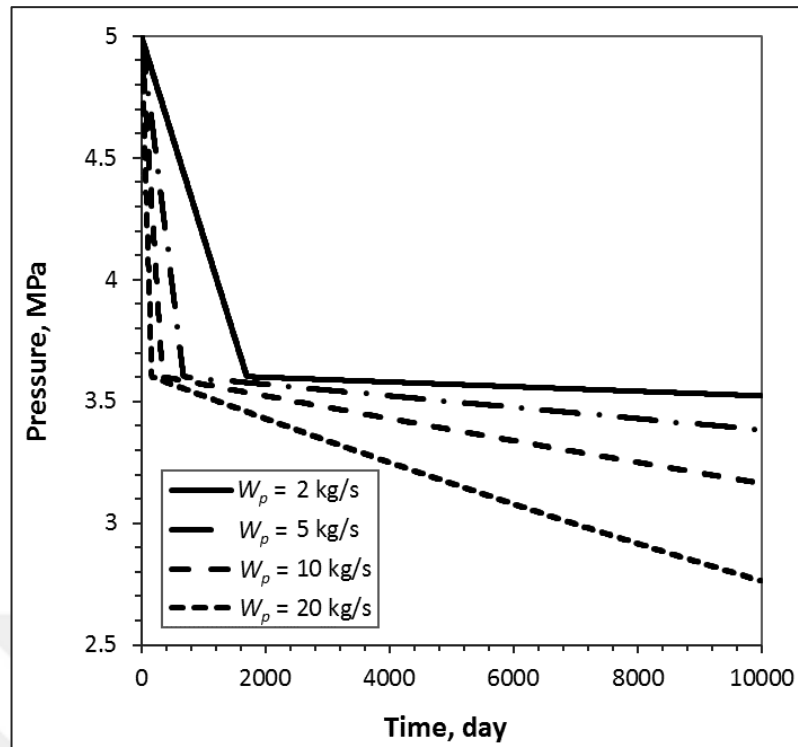


Figure 3.44 : Pressure behavior for various flow rates.

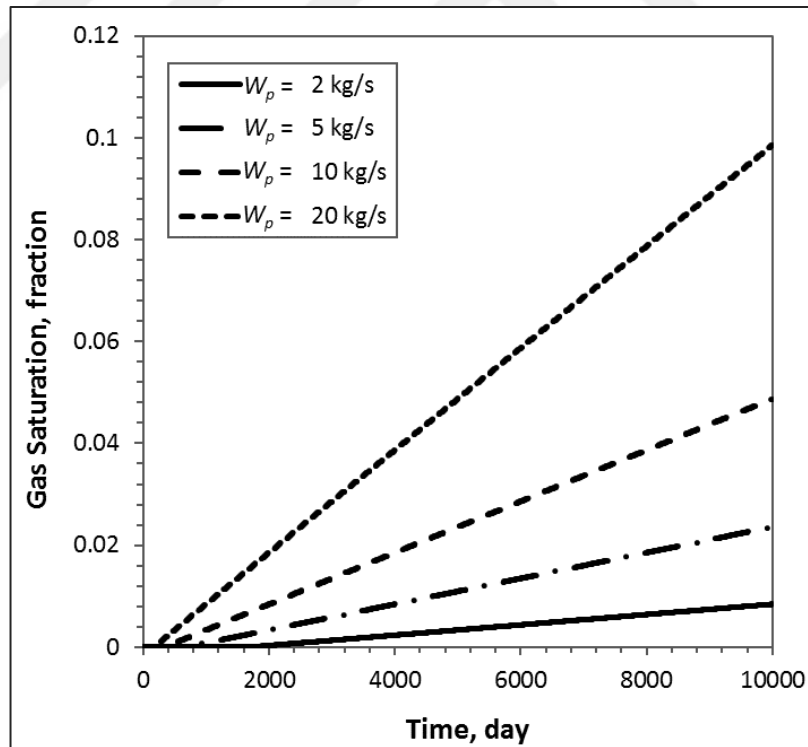


Figure 3.45 : Gas saturation behavior for various flow rates.

Figure 3.46 gives the evolution of the mass fraction of the CO₂ dissolved in the water for various flow rates. In the compressed liquid region there is no change in the mass

fraction of CO₂ as it is still dissolved in the water, after the flashing point is reached the mass fraction starts to decrease and as expected the mass fractions of dissolved CO₂ tend to decrease more as the flow rate is increased. Figure 3.47 gives the evolution of the mass fraction of CO₂ in the gas phase for various flow rates. At the beginning the mass fractions are zero since no gas phase is present. With the increase in the flow rate the flashing point pressure is reached earlier and gas phase that is made up of mostly CO₂ starts to form. Transition of liquid CO₂ to gaseous CO₂ occurs very quickly and tends to stabilize. At late times, the decrease of mass fraction of CO₂ in gas phase with the production is observed clearly at higher flow rates.

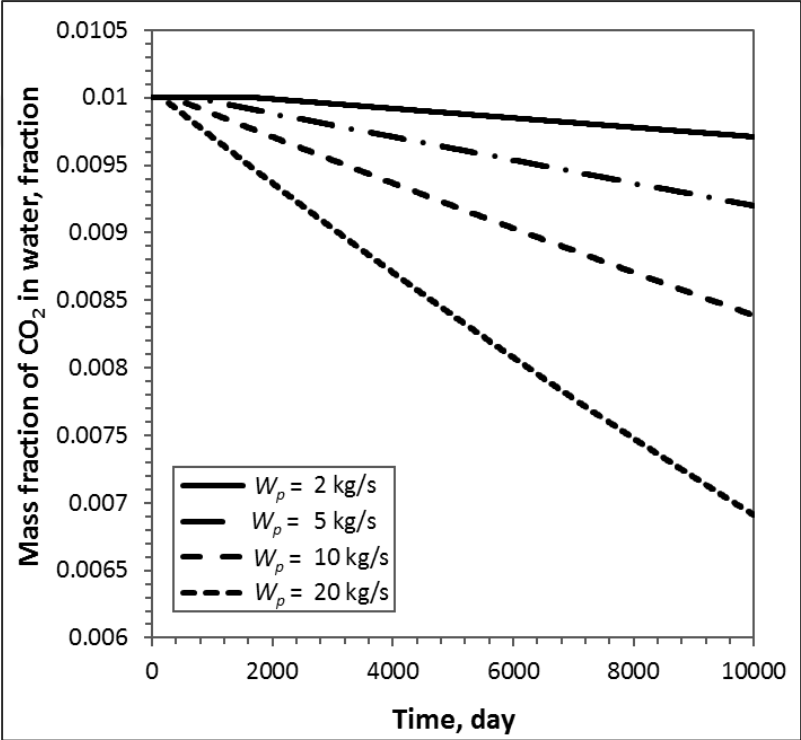


Figure 3.46 : Evolution of the mass fraction of CO₂ in water.

3.11.1.3 The effect of reinjection

In this case, the effect of reinjection on the performance of the geothermal system is examined. No reinjection, 50% reinjection, 80% reinjection and 100% reinjection scenarios are studied. Constant production at 10 kg/s is assumed for a duration of 10000 days and the initial mass fraction of CO₂ is taken as 1%. In Figure 3.48, the pressure behavior of the system is given. If there is no reinjection a rapid pressure drop occurs and after around 250 days gas phase forms. After the reservoir fluid becomes

two-phase, the decline rate of pressure is decreased. With the reinjection the pressure decline is diminished and thus the formation of gas is begun at later times.

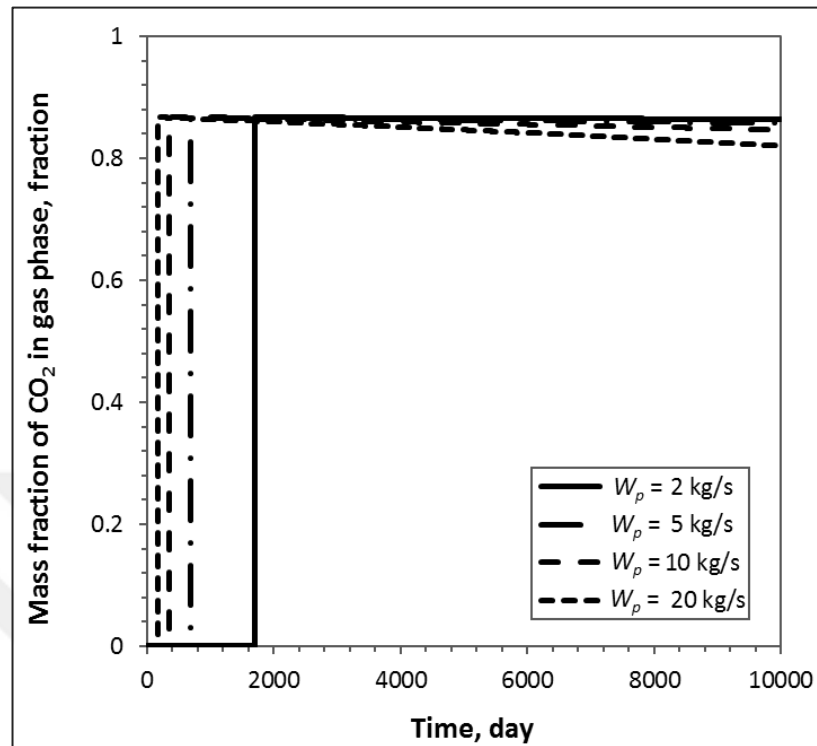


Figure 3.47 : Evolution of the mass fraction of CO₂ in the gas phase.

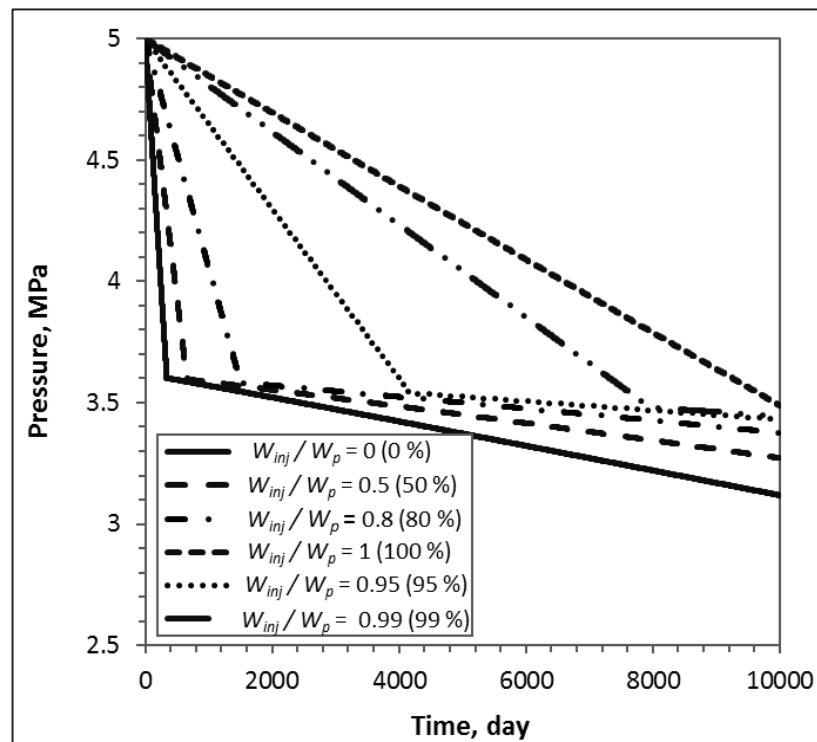


Figure 3.48 : Pressure behavior for various percentage of reinjection.

For example, for 50 % reinjection scenario flashing point pressure is reached around 500 days which is twice as that of the case without reinjection. In 80 % reinjection scenerio the transition time is much more longer. Here, 95 % and 99 % reinjection scenerios are given to emphasize the importance of reinjection rate. In 99 % reinjection still two phase region is formed but when the reinjection rate is increased one percent more to 100 % reinjection no gas is formed and production is maintained in a compressed liquid state for 10000 days. Thus, no rapid pressure reduction occurs and pressure decreases linearly with time. Because reinjection temperature is important parameter in the reinjection cases temperature behaviour graph is also provided. Figure 3.49 illustrates the temperature behavior of the system with initial temperature of 450 K with and without reinjection case. If no reinjection is applied, a faster decrease in temperature occurs in compressed liquid region and after the flashing point is reached a less temperature decrease occurs. The temperature of the system decreases more with the increase in the amount of reinjection of water with a temperature of 333.15 K.

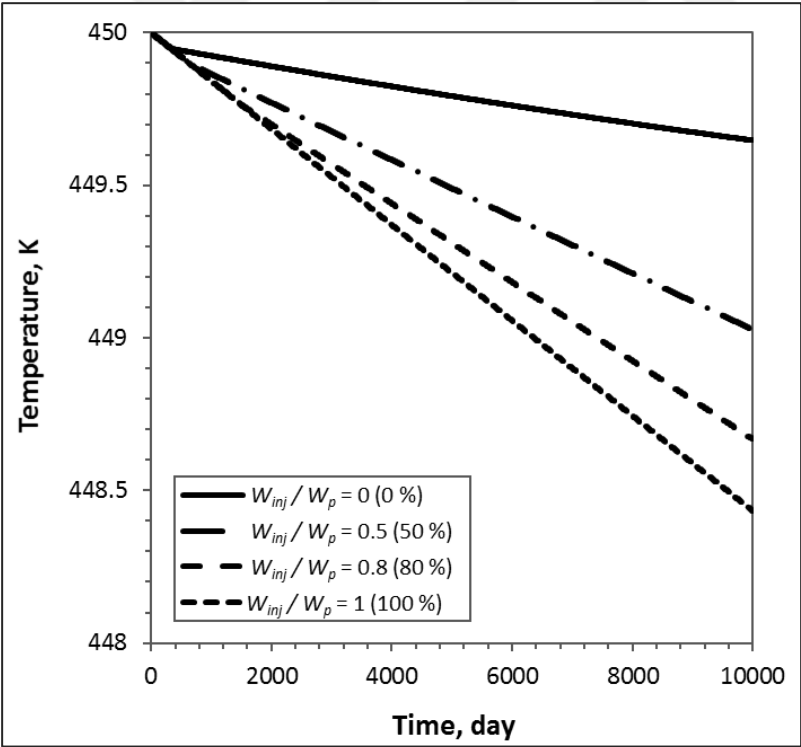


Figure 3.49 : Temperature behavior for various percentage of reinjection.

In Figure 3.50, gas saturation behavior of the system is given. After the flashing point pressure is reached the gas phase begins to form. The time of the occurrence of the first flashing is extended with the increase in the amount of reinjection. If there is no

reinjection, gas saturation increases with the decrease in the total pressure of the system. When the pressure decline is decreased with reinjection, gas saturation decreases. For the 100 % reinjection scenario because the system is maintained in compressed liquid phase, no gas saturation is observed.

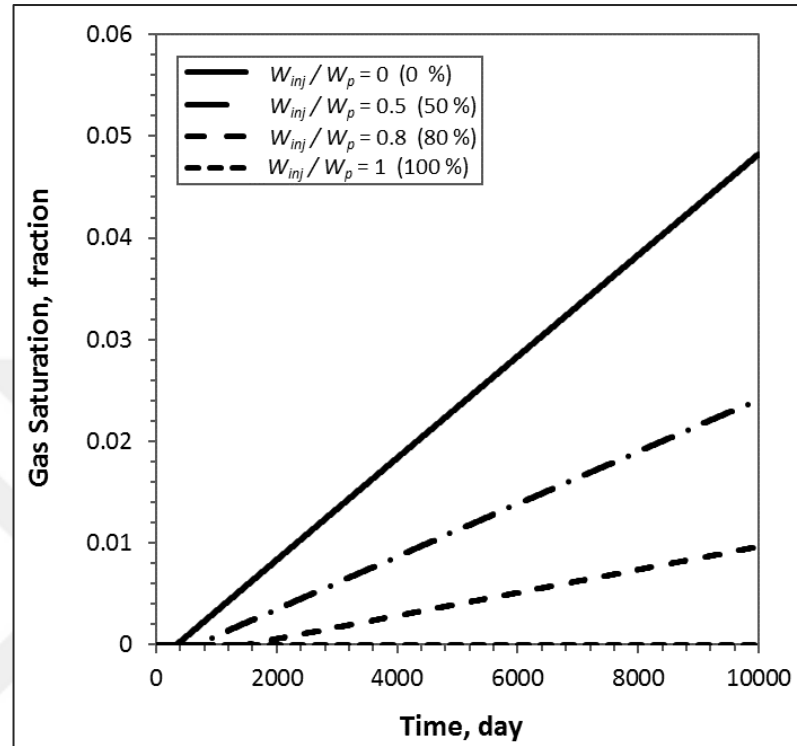


Figure 3.50 : Gas saturation behavior for various percentage of reinjection.

Figure 3.51 illustrates the change of mass fraction of CO_2 dissolved in liquid. The flashing point pressure is reached first in case where no reinjection is applied because pressure decreases faster and there is no reinjected fluid for the pressure support. Without reinjection, mass fraction of CO_2 in water is decreased from 0.01 to 0.0082 whereas mass fraction of dissolved CO_2 is decreased to 0.0096. This difference will be much higher for the higher production rates. In 100 % reinjection case the mass fraction of CO_2 continues to decrease because of the reinjected water does not contain dissolved CO_2 . Figure 3.52 gives the evolution of the mass fraction of CO_2 in the gas phase for various injection percentage. With the pressure decline with production, the flashing point pressure is reached and gas phase that is made up of mostly CO_2 starts to form. With the reinjection this occurrence is reached subsequently. The gas phase forms first in no reinjection case as expected. Dissolved CO_2 in liquid transform to gas phase and 0.87 of gas phase is formed from gaseous CO_2 . This value decreases with

time and the maximum decreases is performed in no reinjection case. In 100 % reinjection case, the system stay in liquid phase so no gaseous CO₂ is formed.

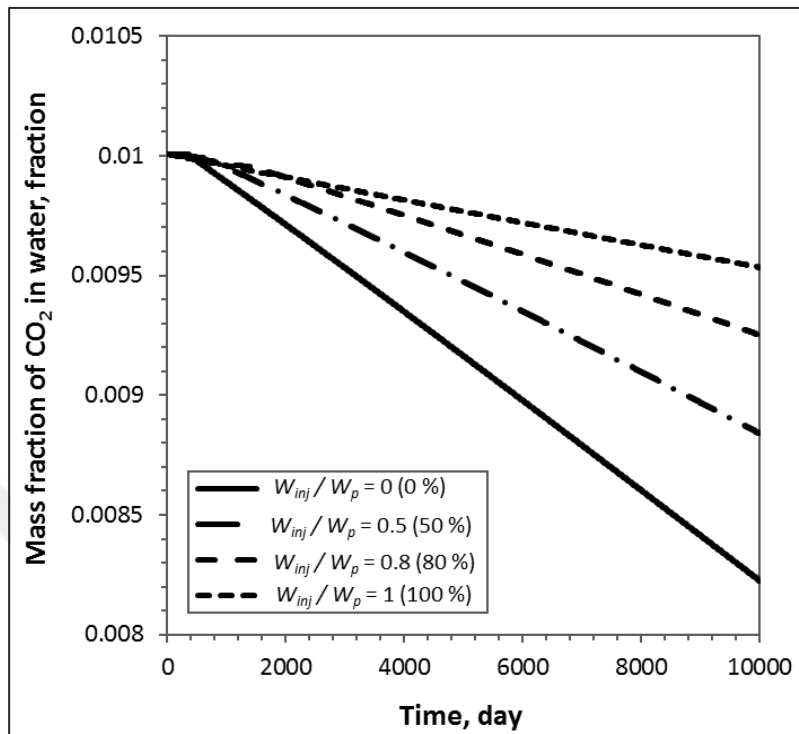


Figure 3.51 : Evolution of the mass fraction of CO₂ in water for various percentage of reinjection.

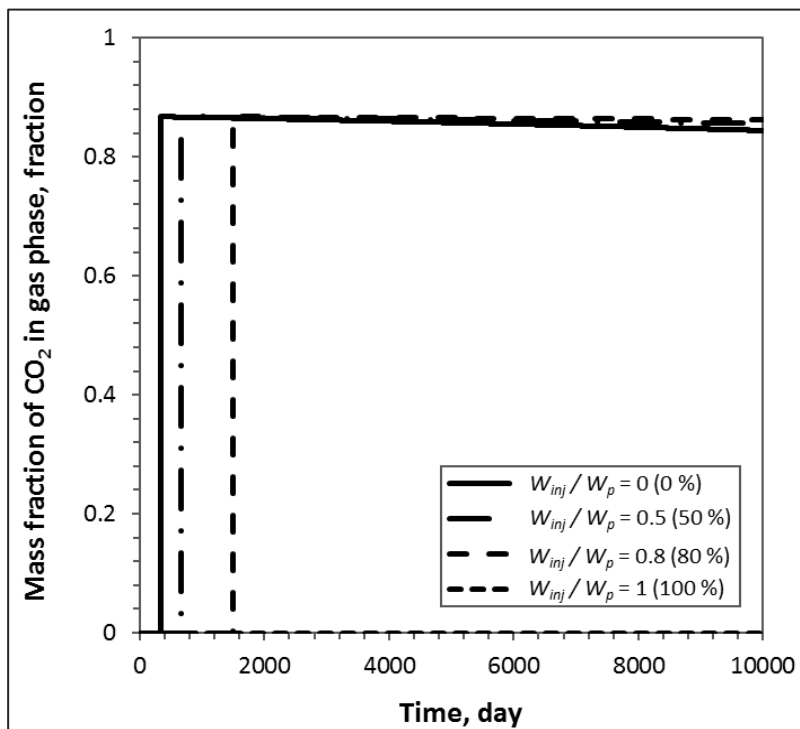


Figure 3.52 : Evolution of the mass fraction of CO₂ in the gas phase for various percentage of reinjection.

3.11.1.4 The effect of physical parameters to tank model

The storage capacity of the reservoir is important and detailed information is given in next chapter. The equation of storage capacity of reservoir can be rewritten by defining total compressibility as the sum of the fluid and rock compressibilities in equation 3.44.

$$\kappa = V_b \rho \phi (c_f + c_r) \quad (3.44)$$

The effects of these physical parameters of the reservoir including porosity, bulk volume and compressibility of rock on reservoir performance are examined in details in this subsection. Reservoir that has properties given in table 3.13 is examined in each case.

Porosity

Porosity is one of the crucial parameter for the reservoir modelling. It has an extremely important role when assessing the reservoir potential of a given rock type. The effect of porosity is examined by keeping bulk volume same. Four different initial porosity values (0.05, 0.1, 0.15, 0.2) are selected and effect of them on pressure, temperature, gas saturation, mass fraction of CO₂ in liquid and gas phases are examined. In the developed tank model, porosity is taken as not a constant value, yet it is changing with pressure and temperature as it was given in equation 3.9. The above mentioned porosities are evaluated at the initial pressure and temperature. From Figure 3.53, it can be seen that pressure is inversely proportional to porosity. Reservoir pressure decreases more in reservoir having smallest porosity because there is less amount of fluid in the reservoir. With the production, there is a sharp pressure decline and saturation pressure is reached quickly. When gas phase is formed the pressure decline slows down but it is higher in reservoir having lower porosity.

On the other hand, temperature is directly proportional to porosity. Temperature decreases more in reservoir having higher porosity because two phase region is reached much later and most of the temperature reduction occurs in single phase region. In the two phase region, similar trend in temperature reduction for each porosity value can be seen as shown in Figure 3.54. Temperature decreases less like pressure in two phase region.

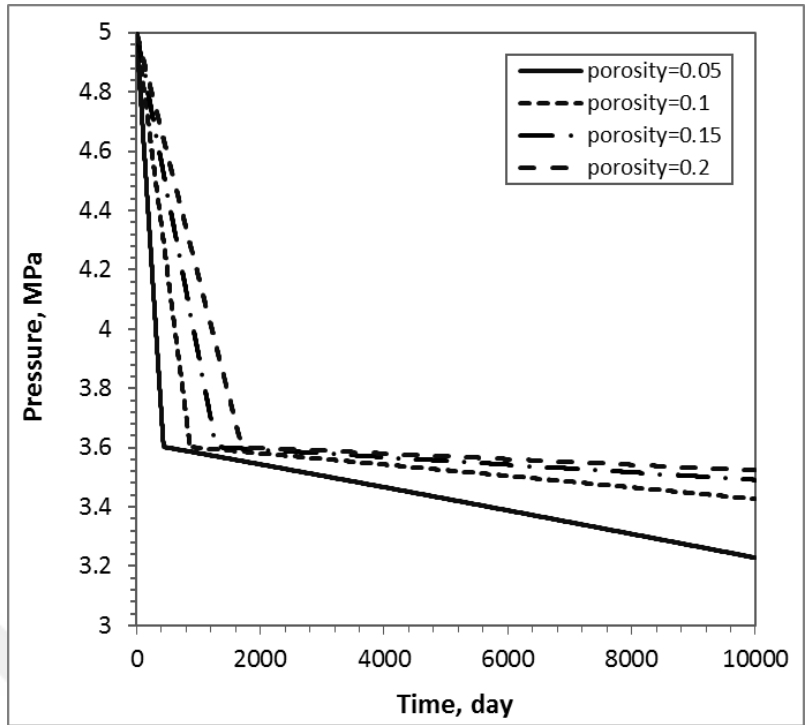


Figure 3.53 : Pressure behavior for various porosity.

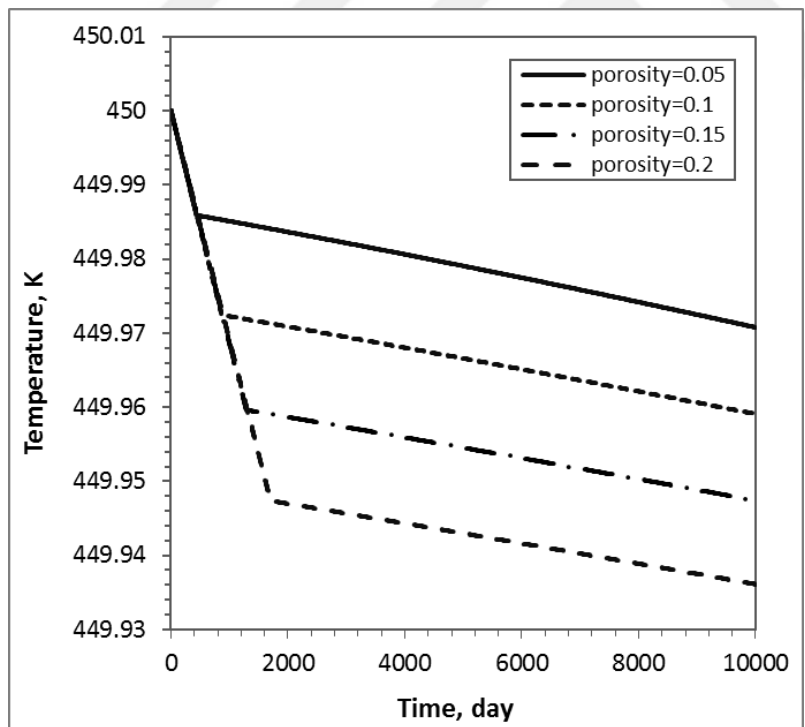


Figure 3.54 : Temperature behavior for various porosity.

Gas saturation behavior of the system is given in Figure 3.55. After the flashing point pressure is reached the gas phase begins to form. The time of the occurrence of the first flashing is extended with the increase in porosity and reservoir having higher

porosity contains less amount of gas. For example, gas saturation in the reservoir having 5 % porosity is 0.038 whereas it is 0.008 in the reservoir having 20 % porosity at the end of 10000 days.

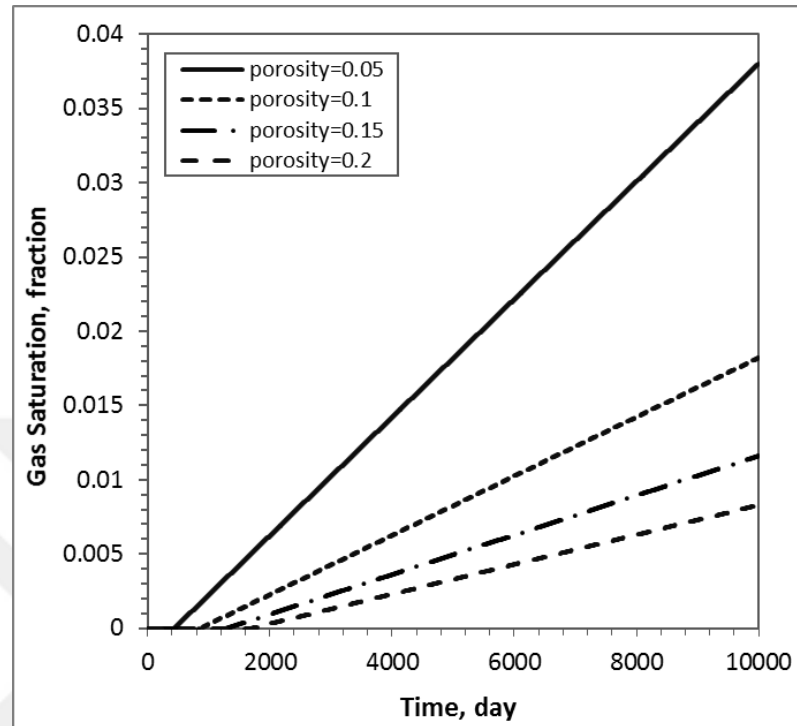


Figure 3.55 : Gas saturation behavior for various porosity.

Figure 3.56 gives the evolution of the mass fraction of the CO₂ dissolved in the water for various porosity. In the compressed liquid region there is no change in the mass fraction of CO₂ as it is still dissolved in the water, after the flashing point is reached the mass fraction starts to decrease. Thus, dissolved CO₂ tends to decrease more as the porosity is decreased. Here, reservoir having porosity of 0.05 has reached to two phase region earlier, the final mass fraction after 10000 days is smaller when it is compared with reservoir having higher porosity.

In Figure 3.57, initially the mass fractions are zero since no gas phase is present. With the production, reservoir having smaller porosity reaches the flashing point pressure earlier and gas phase that is made up of mostly CO₂ starts to form. Transition of liquid CO₂ to gaseous CO₂ occurs very quickly and tends to stabilize. After stabilization, mass fraction of CO₂ in gas phase begins to decrease with the production as it is expected and this reduction is higher in the reservoir having smaller porosity.

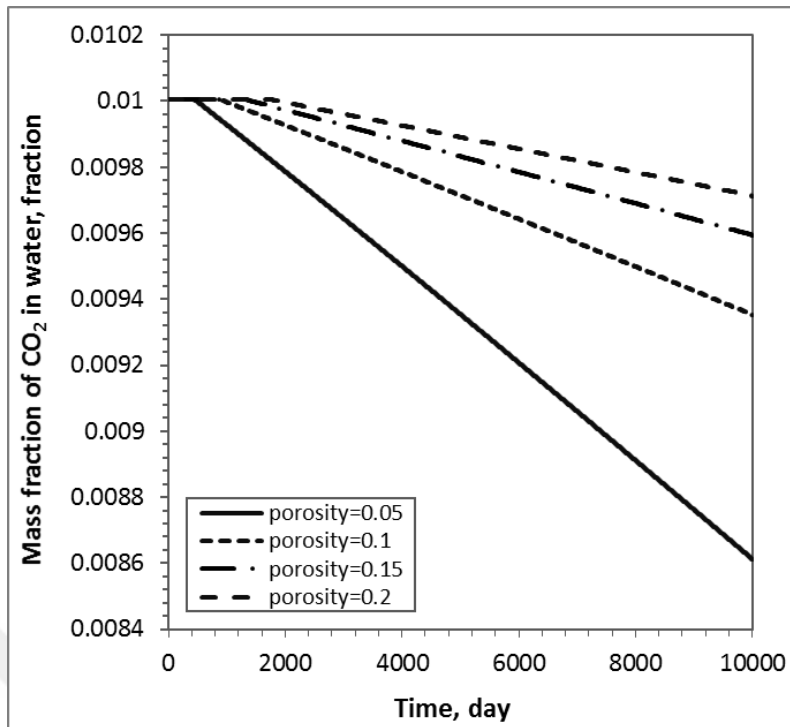


Figure 3.56 : Evolution of the mass fraction of CO₂ in water for various porosity.

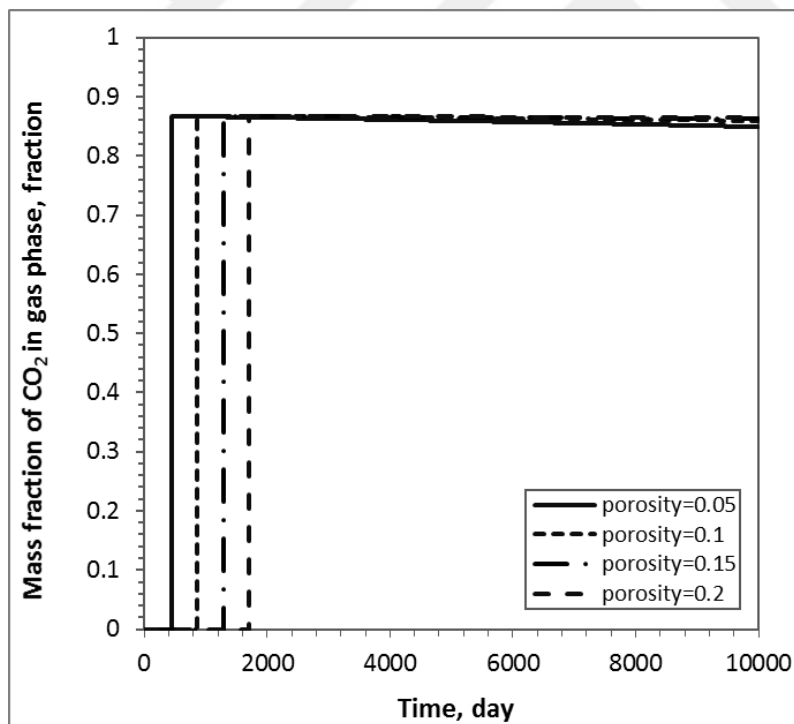


Figure 3.57 : Evolution of the mass fraction of CO₂ in gas phase for various porosity.

Bulk volume

In this case, four different reservoir bulk volume values that varies from $10 \times 10^8 \text{ m}^3$ to $10 \times 10^{11} \text{ m}^3$ having same porosity value of 0.1 are used in the simulation. The pressure behavior of each cases are given in Figure 3.58. In the smallest reservoir volume the pressure decreases quickly and two phase region is reached so pressure decline is higher. It decreases from initial pressure of 5 MPa to 2.5 MPa. But the reservoir having highest bulk volume has lowest pressure drop. The flashing points are not reached so there is no phase change occurred in reservoirs having volumes of 10^{11} m^3 and 10^{10} m^3 . There is not much pressure drop in those ones either. For example, only 0.1 MPa and 0.7 MPa pressure reduction occurred for those reservoirs in 10000 days. Bulk volume is a very important parameter like porosity so it should be calculated or assumed precisely. It can be stated that temperature, saturation, f_{CL} and f_{CG} behaviors dependent on the pressure.

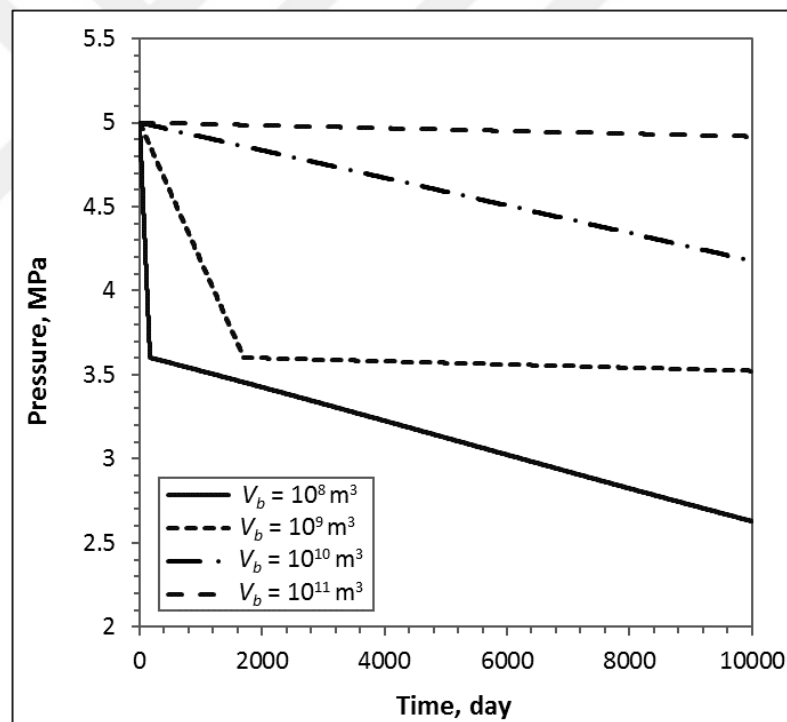


Figure 3.58 : Pressure behavior for various bulk volumes.

Similar trend is valid for temperature drop. There is not much temperature drop occurred relatively in high bulk volumes as given in Figure 3.59. Because pressure reduction is very low in reservoirs having high bulk volume, temperature reduction shows coherent trend with pressure. For the gas saturation behaviour, the smallest reservoir has reached the highest gas saturation value. There is no gas phase occurred

in two reservoirs having highest bulk volume because their pressure does not reach to flashing point pressure as can be seen from Figure 3.60.

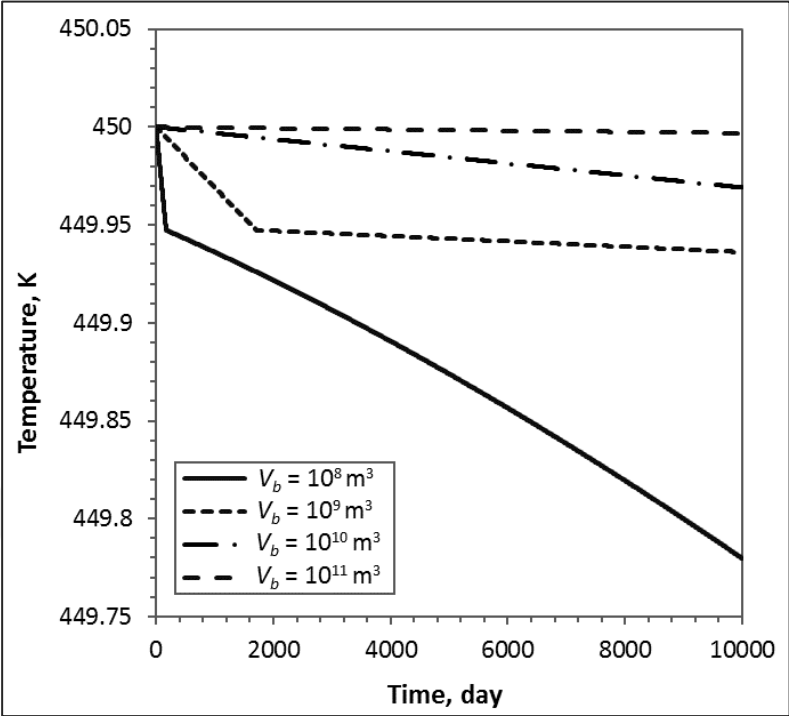


Figure 3.59 : Temperature behavior for various bulk volumes.

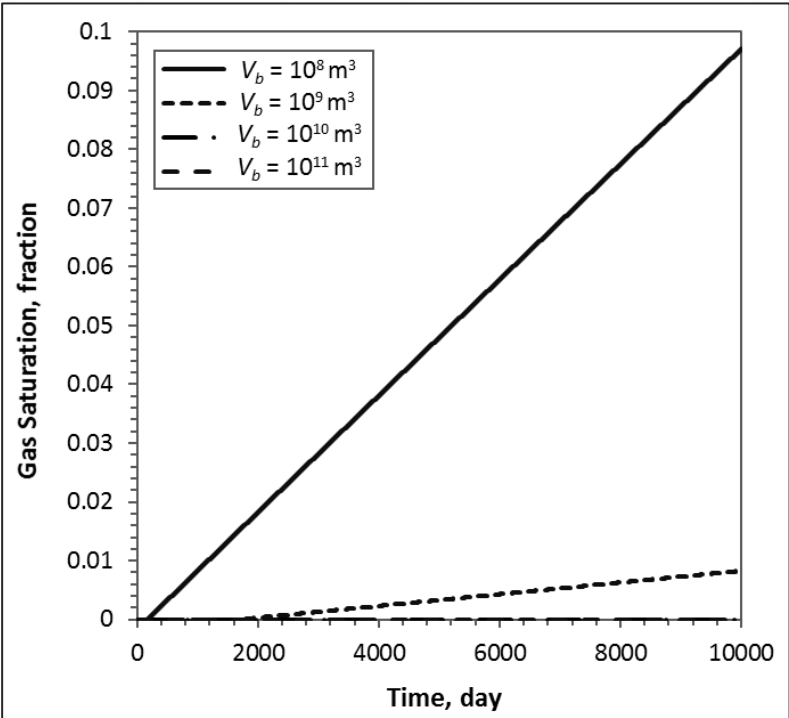


Figure 3.60 : Gas saturation behavior for various bulk volumes.

Depending upon pressure behaviour described above, the amount of dissolved CO₂ in water decreases most in the reservoir having smallest bulk volume as shown in Figure 3.61. The reduction in mass fraction of CO₂ dissolved in water is quite small in single phase liquid region whereas it is high in two phase region because dissolved CO₂ is transformed to the gas phase rapidly. In reservoir having bulk volume of 10x10⁸ m³, the gas phase is formed early and pressure decrease is high so reduction in mass fraction of CO₂ in water is higher. In that case, f_{CL} decreases from 0.01 to 0.0063 in 10000 days period.

Figure 3.62 represents the behaviour of mass fraction of CO₂ in gas phase. In the reservoirs having bulk volumes of 10¹¹ m³ and 10¹⁰ m³, no gas phase has occurred. When the other two reservoirs are compared, the reservoir having smallest bulk volume has reached the flashing point pressure in 154 days and gas phase is occurred. The mass fraction of CO₂ in the gas, f_{CG} , directly becomes 0.87. Then, f_{CG} decreases to 0.8 at the end of 10000 days. On the other hand, gas phase is formed after 1652 days in the reservoir having bulk volumes of 10⁹ m³ and there is not much reduction occurred in f_{CG} because of the smaller pressure drop.

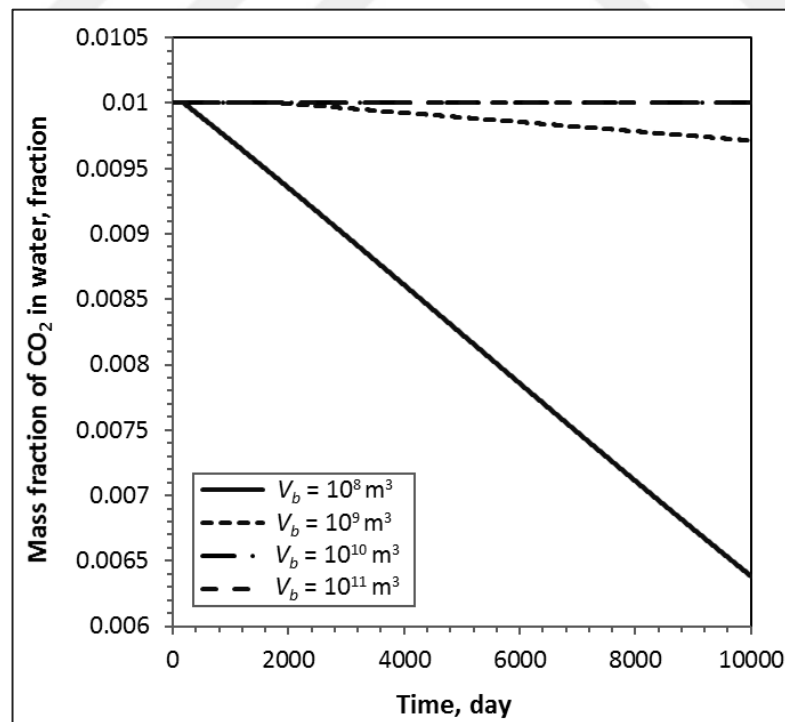


Figure 3.61 : Behaviour of mass fraction of dissolved CO₂ in water for various bulk volumes.

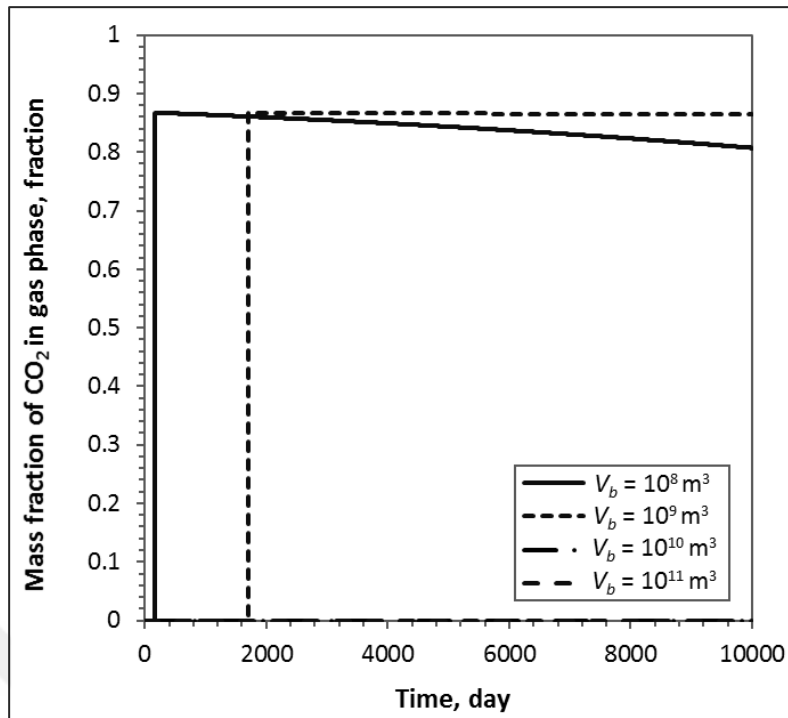


Figure 3.62 : Behaviour of mass fraction of CO₂ in gas phase for various bulk volumes.

Compressibility of rock

The rock compressibility is the fractional change in volume of the rock with a unit change in pressure. Even though the formation is a solid material, it is compressible. In this case, four different rock compressibilities, 5×10^{-10} , 1×10^{-9} , 1.5×10^{-9} and $2 \times 10^{-9} \text{ Pa}^{-1}$, are used to evaluate the effect of rock compressibility on pressure, temperature, gas saturation, mass fraction of CO₂ in liquid water and mass fraction of CO₂ in gas phase, by keeping other parameters same. In the model, compressibility of rock is taken as constant but it also directly effect the change in porosity as given in equation 3.9 in the previous chapter.

Trends of pressure and compressibility are directly proportional. If the rock compressibility is high, pressure drop will be less because rock compressibility supports pressure. In this instance, rate of pressure drop in the reservoir having highest compressibility is lower and this reservoir reaches two phase region much more later. After flashing point pressure is reached, all reservoir display similar pressure drop trend in two phase region as given in Figure 3.63. Because flashing point pressure is reached later in the reservoir having highest compressibility, temperature also drops slowly as can be seen from Figure 3.64. Moreover, because reservoir having smallest

compressibility reaches the two phase region first, more pressure and temperature drops occurred.

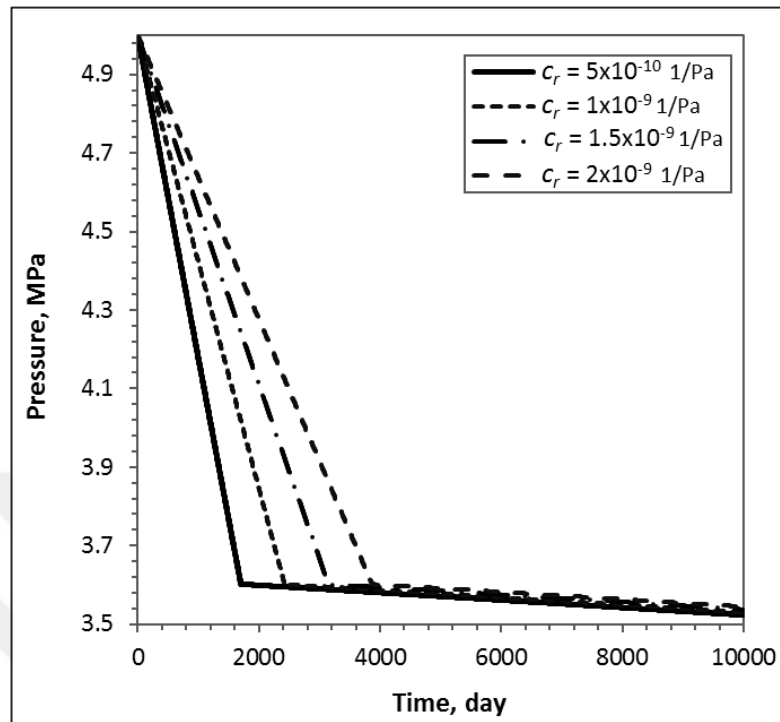


Figure 3.63 : Pressure behavior for various rock compressibility.

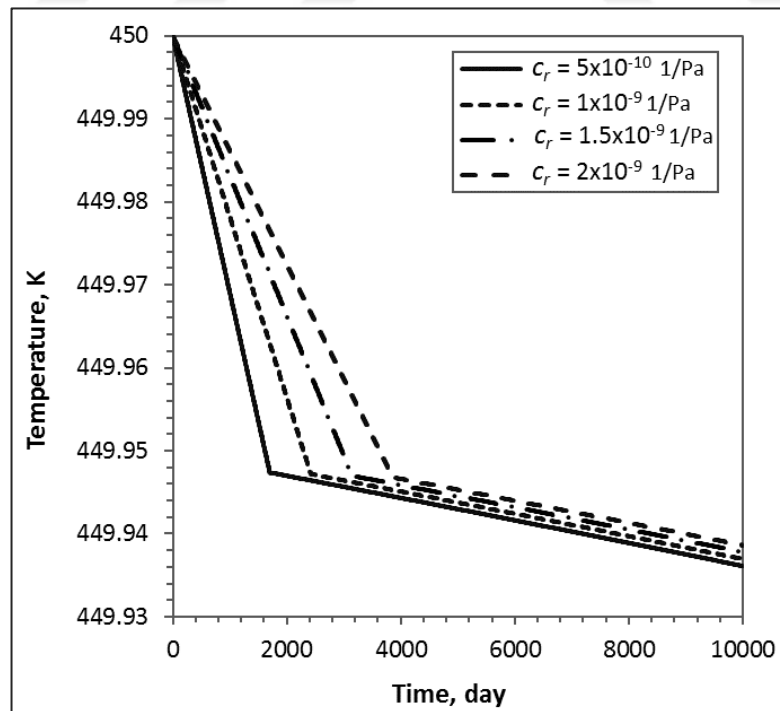


Figure 3.64 : Temperature behavior for various rock compressibility.

The gas saturation behaviour is given in Figure 3.65. The reservoir having smallest rock compressibility of $5 \times 10^{-10} \text{ Pa}^{-1}$ has reached the highest gas saturation value of 0.0084 at the end of 10000 days as it is expected because gas phase has formed earlier and the pressure decline in this reservoir is higher. Whereas, the gas saturation is 0.0055 in the reservoir having compressibility of $2 \times 10^{-9} \text{ Pa}^{-1}$.

The reduction of mass fraction of dissolved CO_2 in water is very small in liquid phase region. When gas phase evolves, CO_2 dissolved in water rapidly migrates to the gas phase. Again the one having higher rock compressibility reaches the flashing point pressure later so dissolved CO_2 mass fraction is kept relatively high as it is given in Figure 3.66.

After two phase region is reached, the mass fraction of CO_2 in gas phase directly increases to 0.86. In Figure 3.67, the dissolved CO_2 starts to change to gas phase after 1722 days in the reservoir having lower rock compressibility because of the rapid pressure drop. But phase transition appears after 3934 days in the reservoir having higher rock compressibility. Then in both cases the mass fraction of CO_2 in gas phase decreases slowly in two phase region.

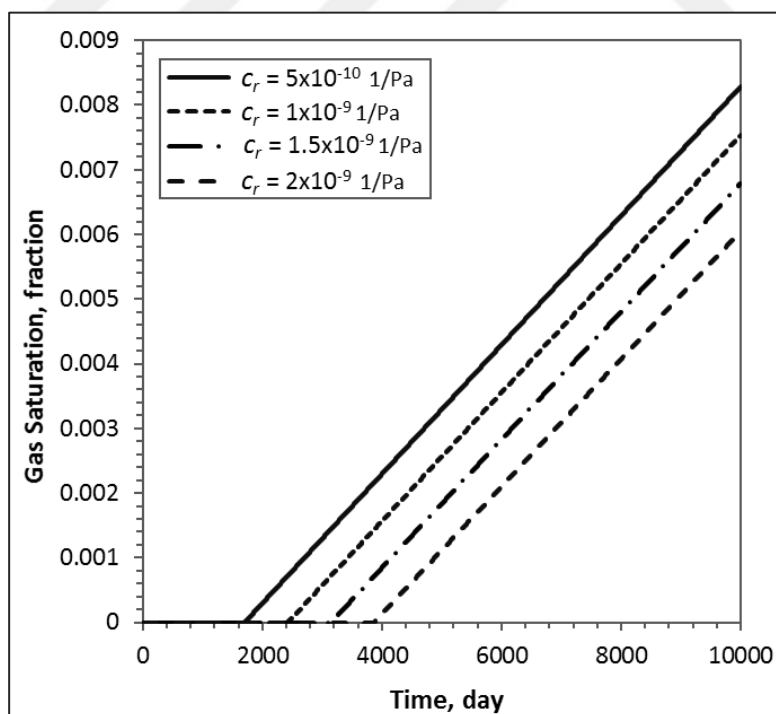


Figure 3.65 : Gas saturation behavior for various rock compressibility.

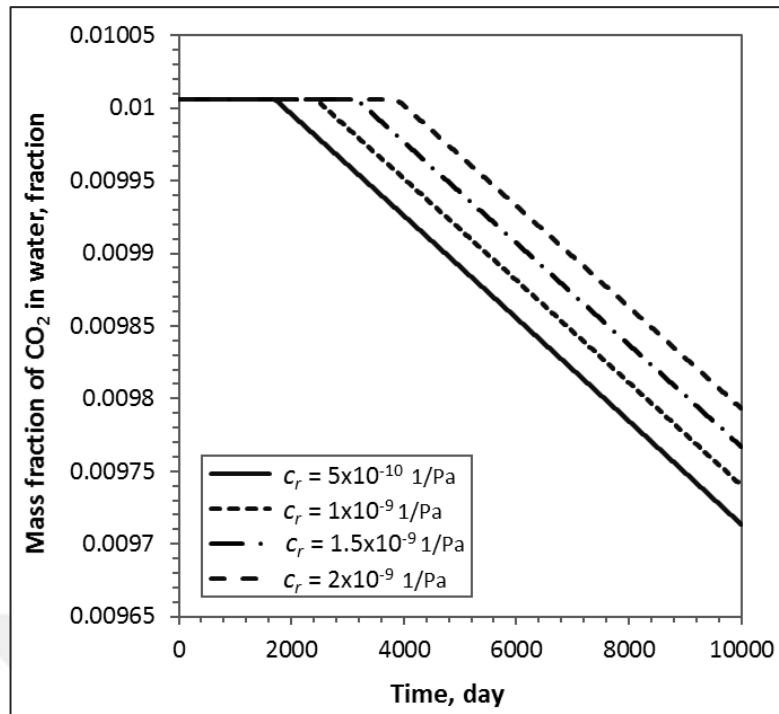


Figure 3.66 : Behaviour of mass fraction of dissolved CO₂ in water for various rock compressibility.

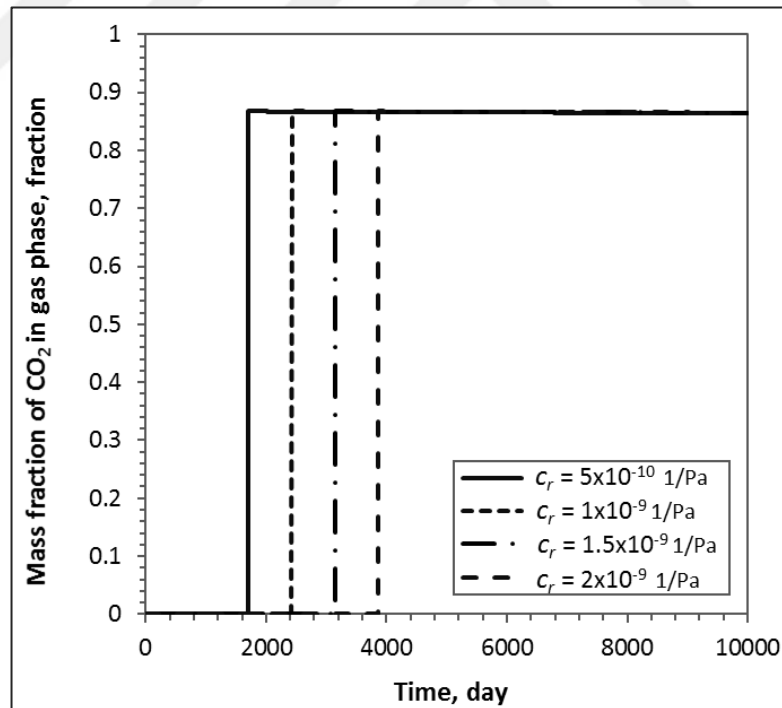


Figure 3.67 : Behaviour of mass fraction of CO₂ in gas phase for various rock compressibility.

3.11.2 One Tank Open Model

In this section, three different cases to illustrate the effects of CO₂ on the performance of geothermal reservoirs are provided. Cases consider one reservoir tank and one recharge source as it is illustrated in Figure 3.68. The effect of initial mass fraction of CO₂ in the reservoir, initial mass fraction of CO₂ in the aquifer water and the recharge constant are examined.

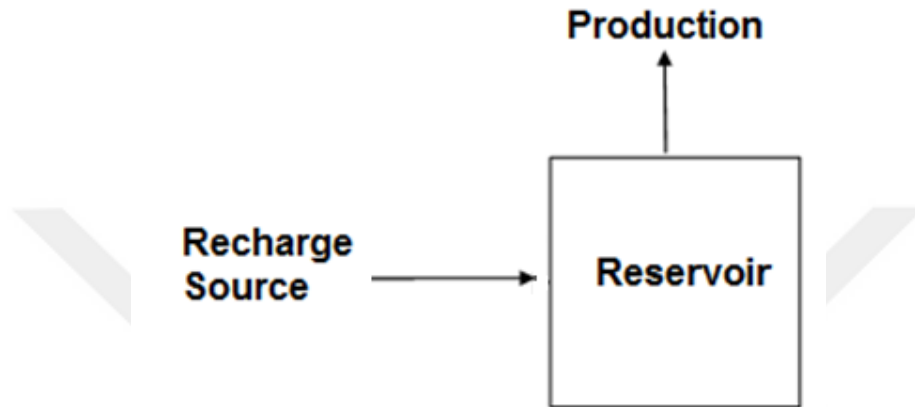


Figure 3.68 : Illustration of one tank open model.

The main properties of the reservoir and the aquifer that are used in the models are given in Table 3.14, other circumstances are explained for each case.

Table 3.14 : Reservoir properties for one tank open model.

Reservoir bulk volume, m ³	1×10 ⁹
Porosity, fraction	0.1
Initial pressure, Pa	50×10 ⁵
Initial Temperature, K	450
Rock compressibility, Pa ⁻¹	1×10 ⁻⁹
Rock thermal expansion coefficient, K ⁻¹	0
Density of rock, kg/m ³	2600
Heat capacity of rock, J/(kg.K)	1000
Rock part of the recharge index, m ³	1×10 ⁻¹¹

3.11.2.1 The effect of mass fraction of CO₂

In this case, the effect of mass fractions of CO₂ on the behavior of the reservoir is examined for five different mass fractions of CO₂ (0%, 0.1%, 0.5%, 1% and 1.5). Constant production at 300 kg/s is assumed for duration of 10000 days. When $f_{CL}=0$ there is no dissolved CO₂ in the liquid phase so the reservoir stays in compressed liquid

state longer so pressure decline is relatively higher. When the CO₂ content is increased the system reaches the flashing point pressure earlier and once the reservoir fluid becomes two-phase, the decline rate of pressure is decreased. This is due to the much higher compressibility of the gas phase that co-exists with the liquid. As a result, increasing the CO₂ content results in pressure maintenance at even earlier times as given in Figure 3.69. For temperature, this is quite the opposite. Because the temperature drop based on phase transition is higher. Increasing the CO₂ content results in more temperature reduction because the system loses heat while dissolved CO₂ in the liquid phase transform to gas phase. For this reason, the final temperature in the reservoir that does not contain CO₂ is 445.5 K, while the temperature in the reservoir with $f_{CL} = 0.015$ is 439.5 K after 10000 days as it is shown in the Figure 3.70.

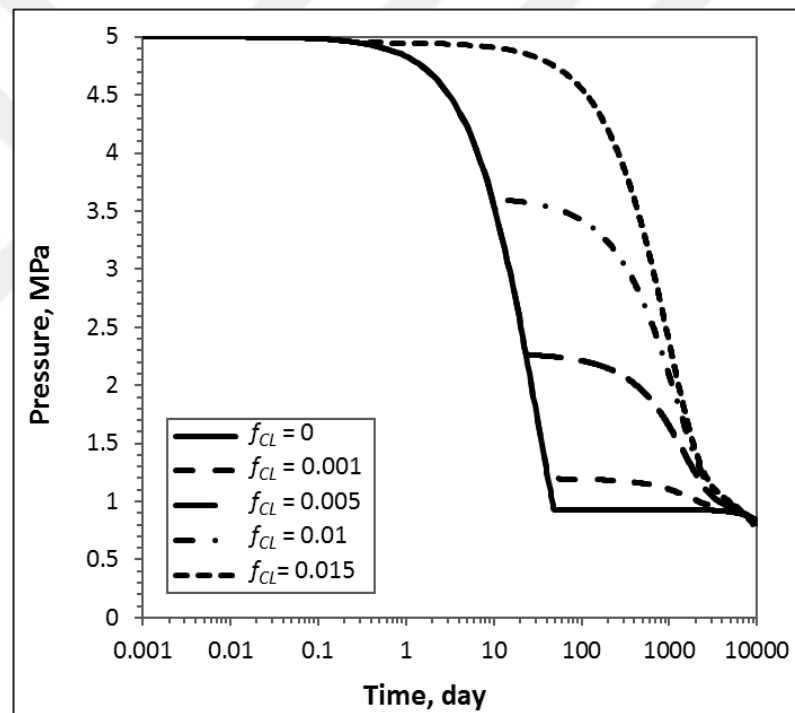


Figure 3.69 : Pressure behavior for various amounts of CO₂ dissolved in water for one tank open model.

Figure 3.71 illustrates the change of gas saturation with time for the various amounts of dissolved CO₂. As expected, the gas saturation starts increasing as soon as the flashing point pressures are reached in the reservoir. The increases associated with the saturations are linear. Gas saturation increases with the increase in CO₂ mass fraction. From Figure 3.71, it can be inferred that around 2500-3000 days the CO₂ effect is dominant, after 3000 days steam dominated region is started which means the gas is

made up of mostly CO₂ up to 3000 days. Once the gas phase becomes steam dominated after 3000 days than a linear trend is observed in the saturation curves.

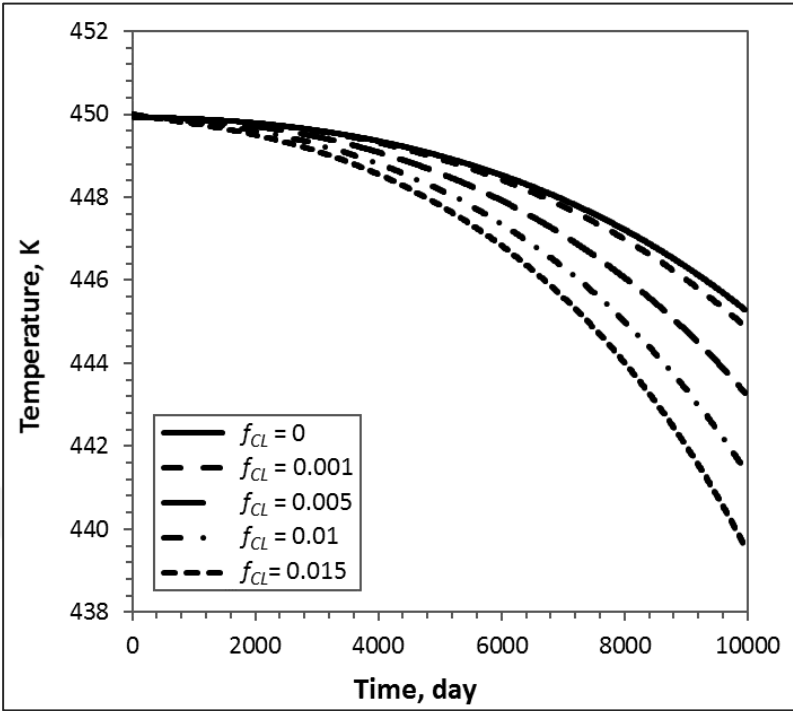


Figure 3.70 : Temperature behavior for various amounts of CO₂ dissolved in water for one tank open model.

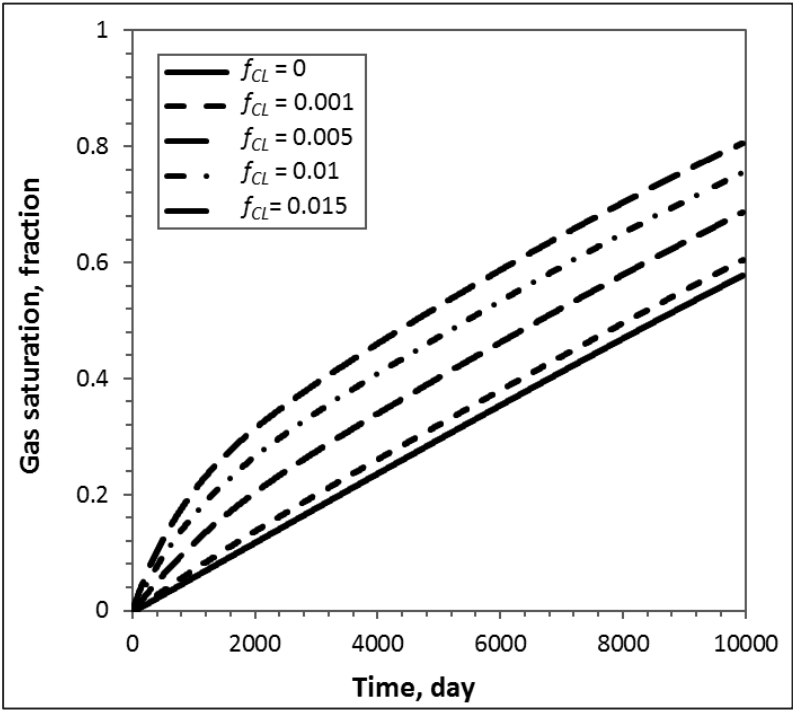


Figure 3.71 : Gas saturation behavior for various amounts of CO₂ dissolved in water for one tank open model.

Figure 3.72 gives the behavior of the mass fraction of the CO₂ dissolved in the water. For each initial mass fraction, the mass fractions of dissolved CO₂ tend to decrease. This decrease is very small in liquid dominated region but it is higher in the two phase region. This decrease is associated with the transfer of carbon dioxide into the gas phase in two phase region. In this example, because the production rate is relatively high, CO₂ tends to be depleted.

Figure 3.73 gives the evolution of the mass fraction of CO₂ in the gas phase. At first the mass fractions are zero since no gas phase is present. Then when the flashing point pressure is reached and gas phase starts to form, it is observed that the gas phase is made up of mostly CO₂. For a mass fraction of 1.5% CO₂ dissolved in water, the gas phase is composed 90% of CO₂ whereas for a mass fraction of 0.1% CO₂ dissolved in water, the gas phase is composed 36% of CO₂. The mass fraction of CO₂ in the gas phase decreases with production as it is expected. But as it is stated before, after around 3000 days, the steam becomes dominant which means the gas phase predominantly forms of water vapour so the reduction rate of CO₂ in water slows down at late times accordingly.

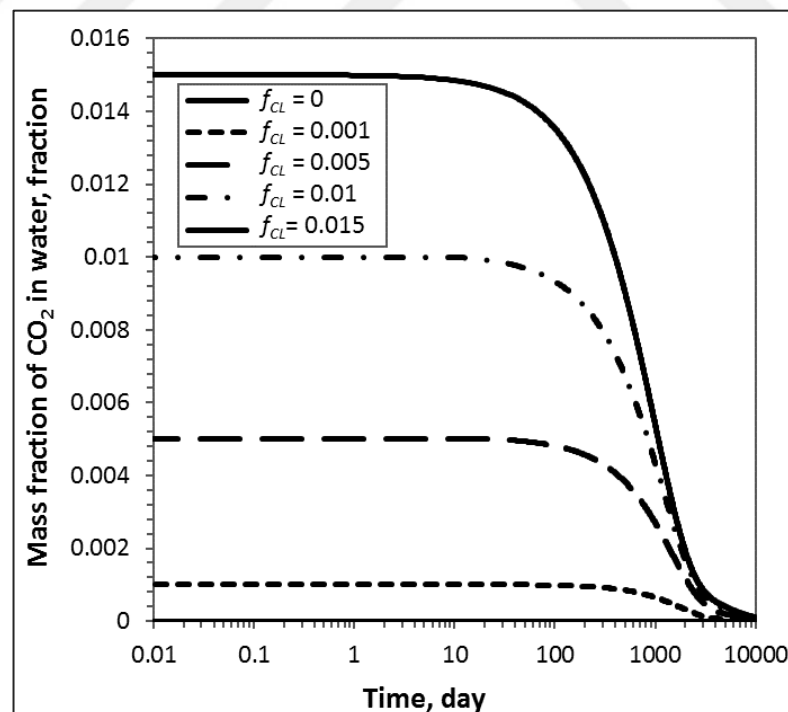


Figure 3.72 : Evolution of the mass fraction of CO₂ in water for various amounts of CO₂ dissolved in water for one tank open model.

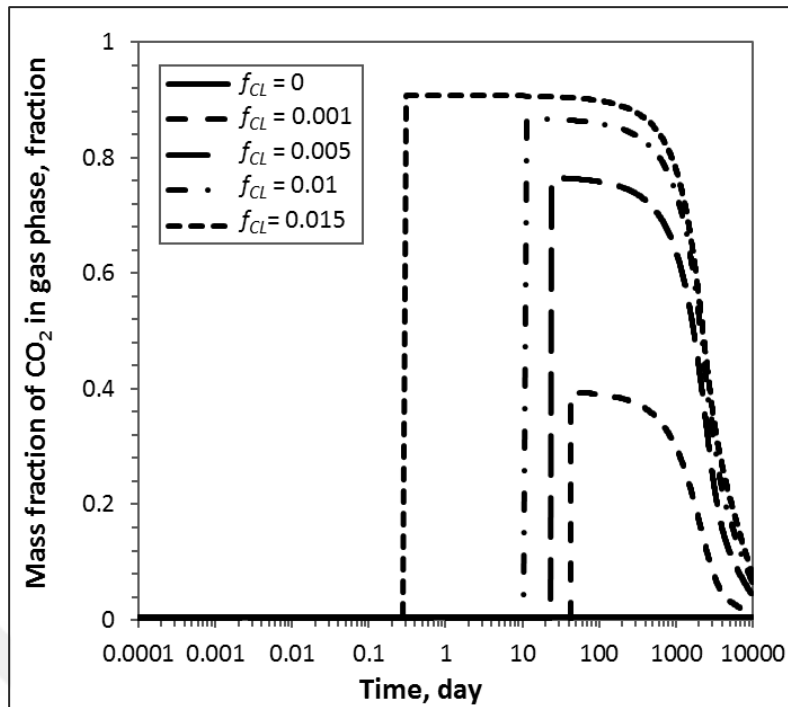


Figure 3.73 : Evolution of the mass fraction of CO₂ in gas phase for various amounts of CO₂ dissolved in water for one tank open model.

3.11.2.2 The effect of recharge constant

In this case, to emphasize the importance of recharge constant a one tank open reservoir model is formed and different recharge constants of rock part ($\psi = 10^{-10} \text{ m}^3$, 10^{-11} m^3 and 10^{-12} m^3) are used for the evaluation. Here, it is important to note that initial mass fraction of CO₂ in liquid is 0.01 and recharge fluid also contains 1 % dissolved CO₂ in the liquid water. The results of this case are given in Figures 3.74 to 3.76.

Pressure behaviour is shown in Figure 3.74. According to this figure, pressure decline increases with reduction in recharge. Because recharge supports pressure. Also recharge source contains CO₂ so decrease in mass fraction of CO₂ is slower as can be seen from Figure 3.74. This affects the pressure drop in two phase region and reduction in pressure is even smaller.

Figure 3.75 illustrates the temperature trend. Because pressure drop is higher in the reservoir that has lower recharge constant, more gas phase is formed as given in Figure 3.76 and temperature reduction is also higher. The gas saturation is 0.25 in the reservoir that has ψ of 10^{-12} m^3 , whereas it is 0.44 in the reservoir that has ψ of 10^{-10} m^3 . Gas saturation profiles increases with less recharge.

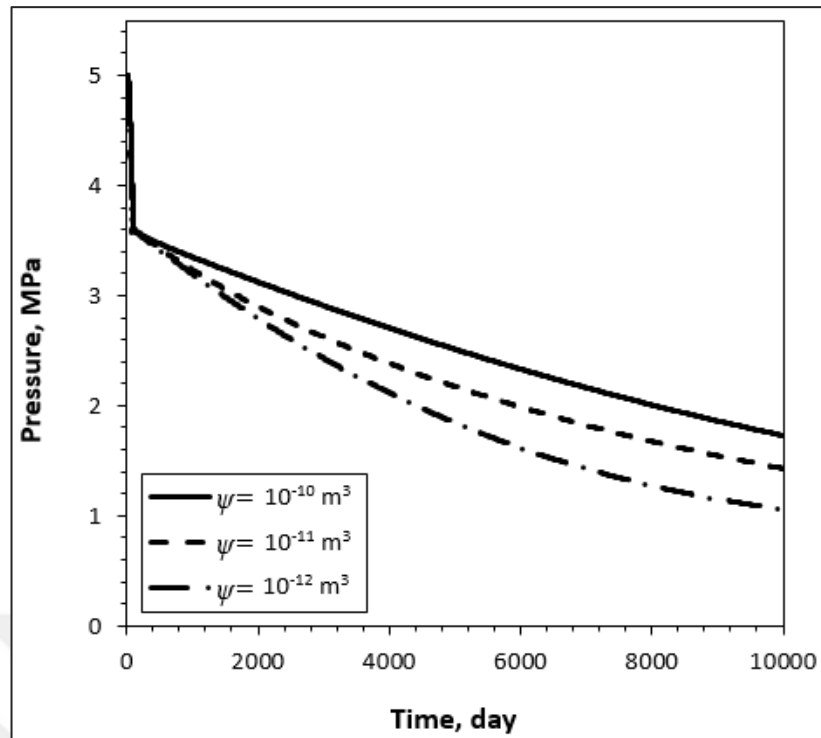


Figure 3.74 : Pressure behavior for different ψ .

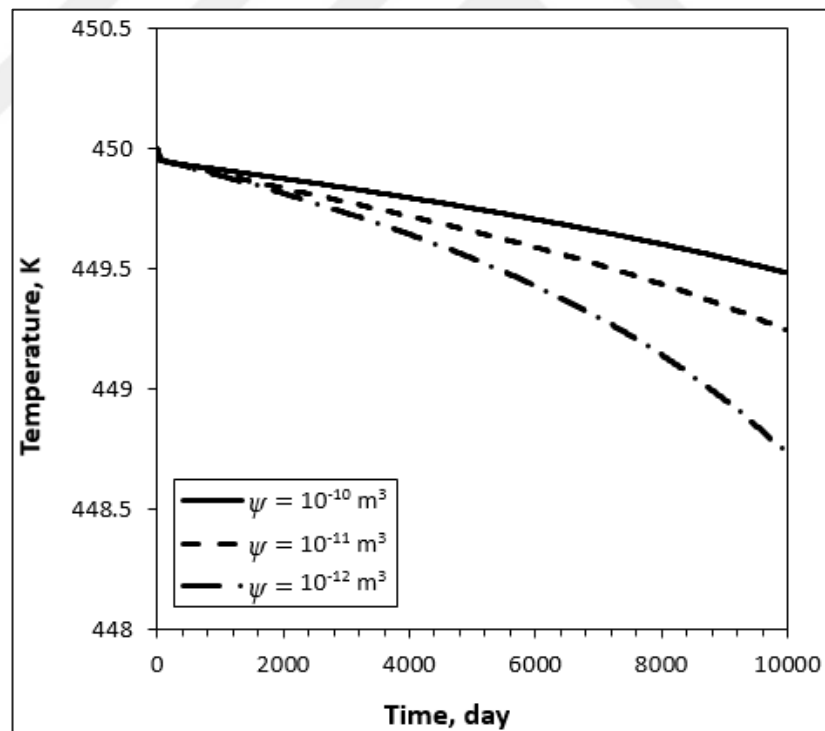


Figure 3.75 : Temperature behavior for different ψ .

Evolution of mass fraction of CO_2 in water is given in Figure 3.77. The recharge liquid contains dissolved CO_2 so it also feeds the amount of dissolved CO_2 in reservoir water.

Thus if the recharge constant is high and contains CO₂ in the liquid phase it shows similar trend with pressure, the reduction in f_{CL} is smaller and slower.

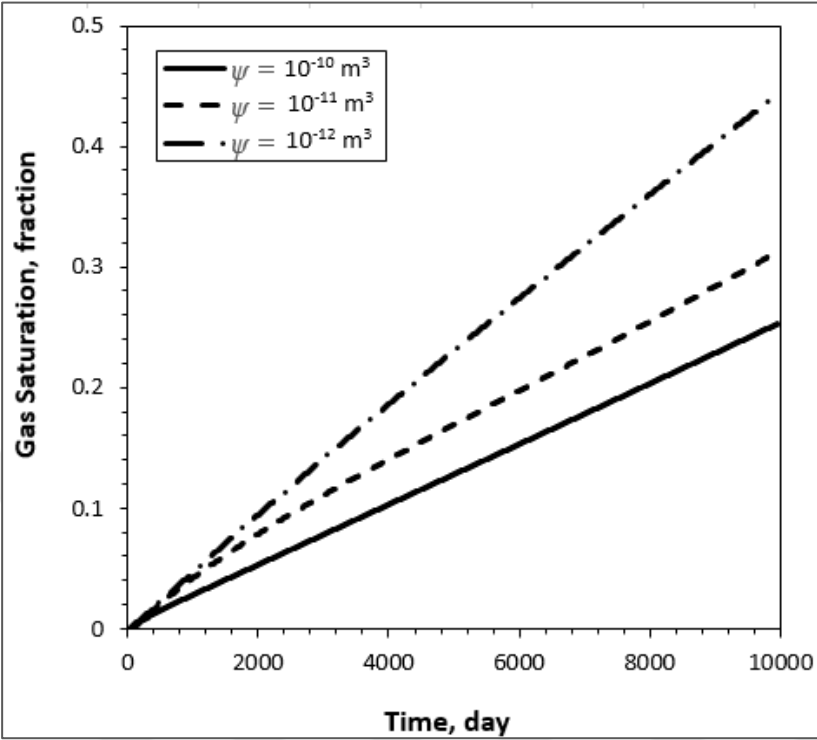


Figure 3.76 : Gas saturation behavior for different ψ .

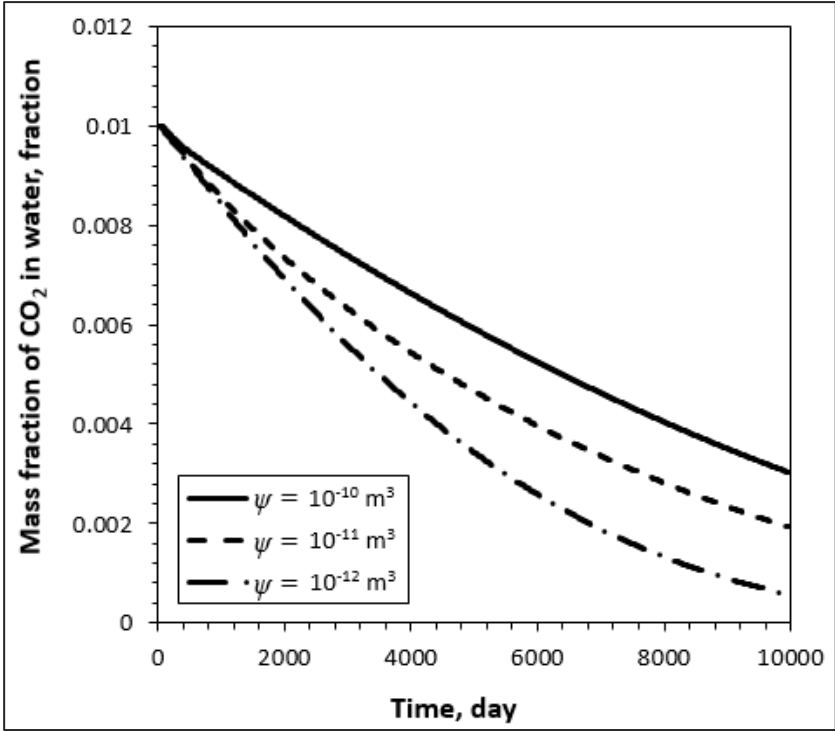


Figure 3.77 : Evolution of the mass fraction of CO₂ in water for different ψ .

When the flashing point pressure is reached and gas phase starts to form, it is observed that the gas phase which is composed of 87 % CO₂ is formed as can be seen in Figure 3.78. Then CO₂ in the gas phase decreases with time. This reduction is small if the recharge is high and pressure drop is less accordingly.

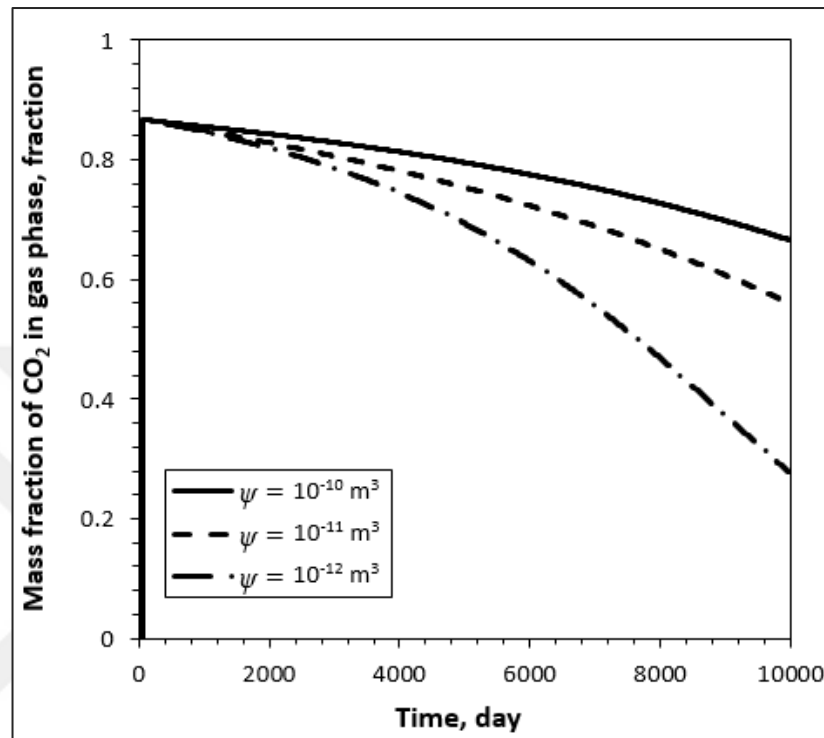


Figure 3.78 : Evolution of the mass fraction of CO₂ in gas phase different ψ .

3.11.2.3 The effect of initial mass fraction of CO₂ in recharge source

In this application, the effect of recharge source and initial mass fraction of CO₂ in the recharge source are examined. In the first case recharge source does not contain dissolved CO₂ but in the second case recharge source water contains 0.015 % CO₂ by mass. The results are given in Figures 3.79 – 3.83. In this scenario, reservoir quickly reaches the flashing point pressure due to relatively high flow rate. If the recharge source contains CO₂ decrease in mass fraction of CO₂ is slower. This causes reduction in the pressure drop in two phase region as can be seen from Figure 3.79. At late times, around 8000 days, the amount of CO₂ in the liquid phase is nearly finished so the pressure trend becomes similar in both cases. After 3500 days the amount of CO₂ is finished in the case where recharge source does not contain dissolved CO₂. But phase changes of CO₂ continues in the second case so temperature decreases little bit more

in second case as shown in Figure 3.80. According to the Figure 3.81, gas saturation is again little bit more in the case where recharge source contains 1.5 % dissolved CO₂.

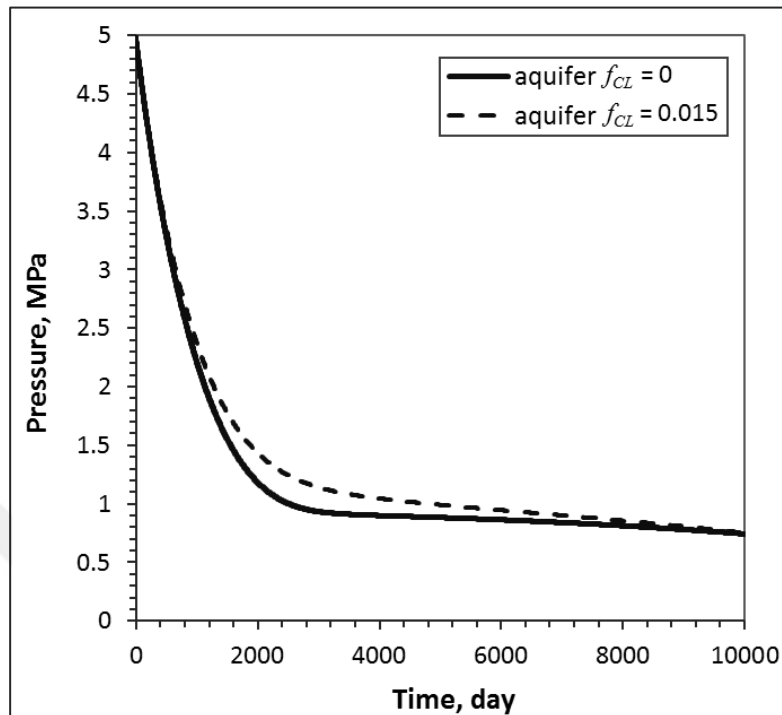


Figure 3.79 : Pressure behavior as per initial mass fraction of CO₂ in recharge source.

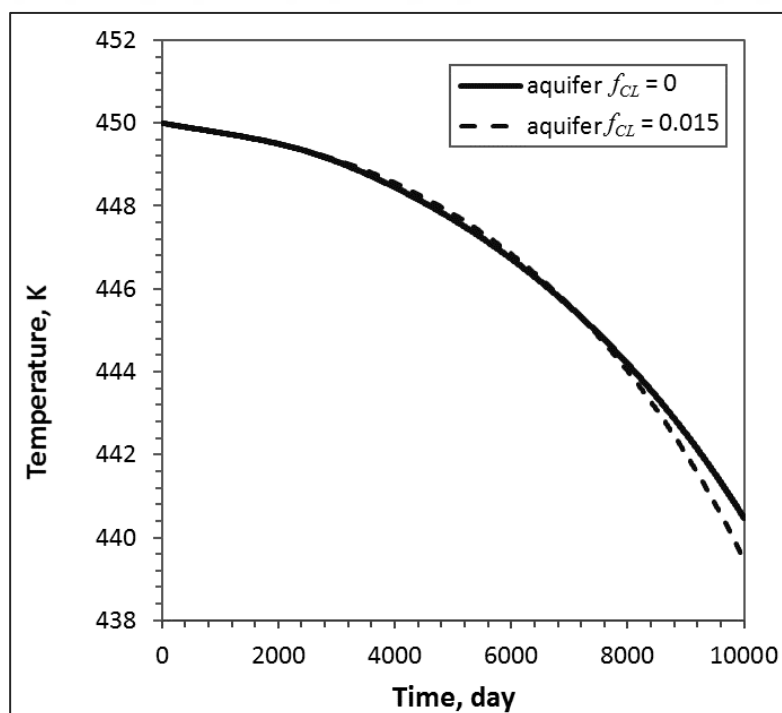


Figure 3.80 : Temperature behavior as per initial mass fraction of CO₂ in recharge source.

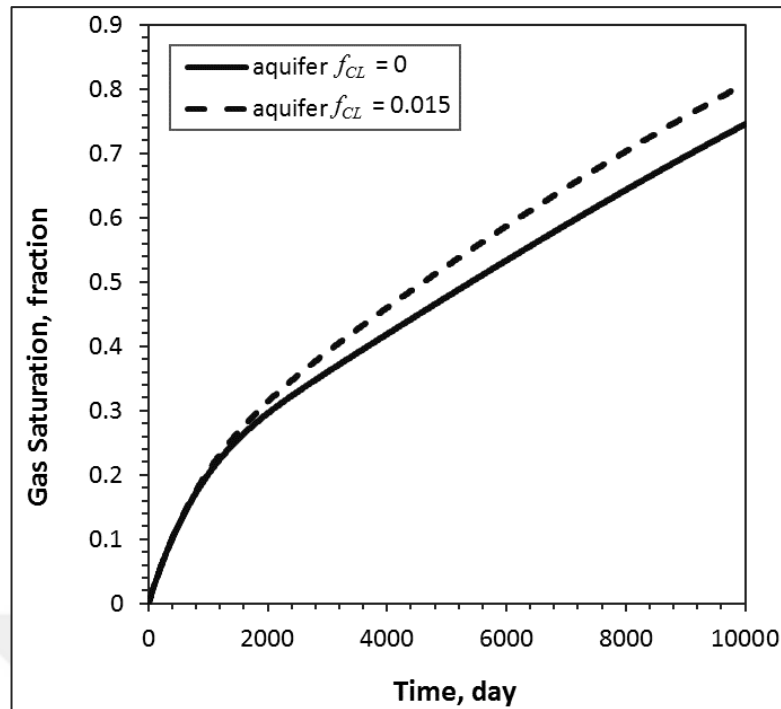


Figure 3.81 : Gas saturation behavior as per initial mass fraction of CO₂ in recharge source.

Two effects can be deduced from Figure 3.82. First one is, after two phase region is reached gas phase begins to form. Thus, the mass fraction of CO₂ in liquid phase decreases. Secondly, when there is no CO₂ in the recharge source, f_{CL} dramatically decreases and becomes zero after 3500 days. This especially influences pressure behavior. After two phase region is reached and gas phase starts to form, it is observed that the gas phase which is composed 91 % of CO₂ is formed as shown in Figure 3.83. Then CO₂ in the gas phase decreases much more quickly in the case where there is no CO₂ in the recharge source. Furthermore, if behavior of mass fraction of CO₂ in gas phase is examined in detailed, it can be seen that f_{CG} also becomes zero after around 4400 days in the case where recharge/ aquifer f_{CL} is zero. Because there is no gaseous CO₂ left in the reservoir, the system becomes fully steam dominated. In the second case, the recharge source contains dissolved CO₂ and continues to support the amount of CO₂ in the liquid phase and so the gaseous CO₂. But around 3500 days the steam becomes dominant this can be forecast from the shape of the f_{CG} versus time line. As a result, the initial mass fraction of CO₂ in recharge source does not have significant effect except for the mass fractions.

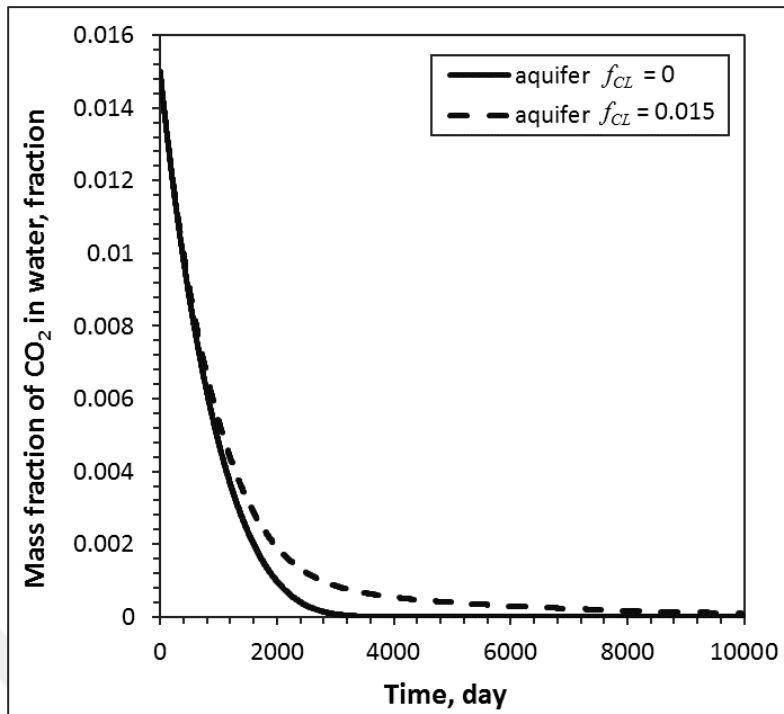


Figure 3.82 : Behavior of mass fraction of CO₂ in water as per initial mass fraction of CO₂ in recharge source.

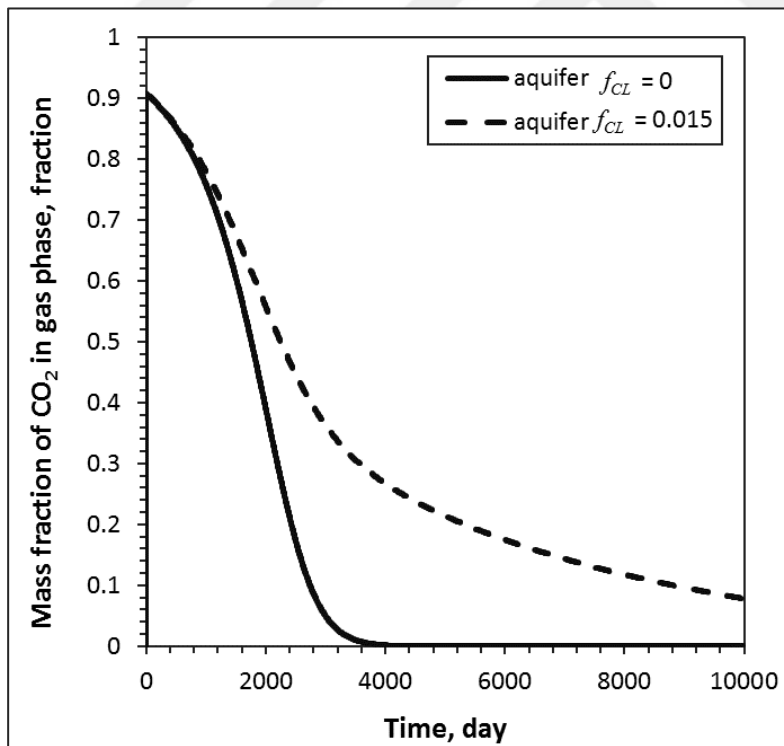


Figure 3.83 : Behavior of mass fraction of CO₂ in gas phase as per initial mass fraction of CO₂ in recharge source.

4. ANALYTICAL MODEL

4.1 Description of the Model

In this thesis, a new analytical model that give the amount of carbon dioxide as a function of time and amounts of production, reinjection and recharge for liquid dominated reservoirs is developed. The details of the analytical equations derived in this study are explained in this section. The analytical equations model the change of carbon dioxide with time for a given specific production/reinjection scheme and it is valid for liquid dominated reservoirs (Hosgor et al., 2016). The basis of the model is application of mass balance on carbon dioxide over any tank volume. Such a tank system is illustrated in Figure 4.1. It is assumed that the tank has a bulk volume V_b , a porosity ϕ and an initial mass fraction of carbon dioxide in the reservoir f_0 . It is also assumed that the tank contains water with a density of ρ . The mass fraction of carbon dioxide is denoted by f . Three sources of carbon dioxide are considered:

- Carbon dioxide extraction due to production.
- Carbon dioxide contribution due to reinjection.
- Carbon dioxide to/from the recharge.

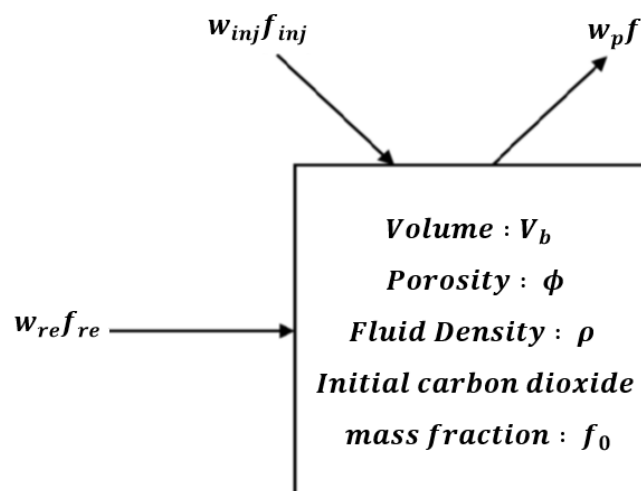


Figure 4.1 : Mass balance on carbon dioxide over any tank volume.

The mass balance on this tank can be stated as shown in equation 4.1.

$$\begin{bmatrix} \text{The rate of} \\ \text{accumulation} \\ \text{carbon dioxide} \end{bmatrix} = \begin{bmatrix} \text{Mass rate of} \\ \text{carbon dioxide} \\ \text{re-injected} \end{bmatrix} + \begin{bmatrix} \text{Mass rate of} \\ \text{carbon dioxide} \\ \text{from recharge} \end{bmatrix} - \begin{bmatrix} \text{Mass rate of} \\ \text{carbon dioxide} \\ \text{extracted due to} \\ \text{production} \end{bmatrix} \quad (4.1)$$

4.1.1 Constant Carbon Dioxide Mass Fraction

The equation representing the relationship given by equation 4.1 for constant production and reinjection rates is given by equation 4.2;

$$\frac{dM_{CO_2}}{dt} = W_{inj} f_{inj} + W_{re}(t) f_{re} - W_p f(t) \quad (4.2)$$

Here m represents the mass (kg), t represents time (s), f represents mass fraction and W represents the mass flow rate (kg/s), the subscripts of inj , re and p refers to injection, recharge and production respectively. At this point, it is important to note that the recharge rate is a function of time. Furthermore, the reinjection and recharge carbon dioxide mass fractions are assumed to be constant. In other words, it is assumed that the amount of carbon dioxide in the recharge water and the injected water is constant. The mass fraction of carbon dioxide on the other hand will also be function of time. Hence, the amount of carbon dioxide extracted by way of production will also change with time.

Equation 4.2 can also be written in terms of the volume, porosity and density as shown by equation 4.3;

$$\frac{d[V_b \phi \rho f(t)]}{dt} = W_{inj} f_{inj} + W_{re}(t) f_{re} - W_p f(t) \quad (4.3)$$

Assuming constant bulk volume, porosity and density leads to equation 4.4:

$$V_b \phi \rho \frac{df(t)}{dt} = W_{inj} f_{inj} + W_{re}(t) f_{re} - W_p f(t) \quad (4.4)$$

Equation 4.4 can also be written in terms of a storage capacity term as given equation 4.5.

$$\frac{\kappa}{c_t} \frac{df(t)}{dt} = W_{inj} f_{inj} + W_{re}(t) f_{re} - W_p f(t) \quad (4.5)$$

Here κ is the storage capacity (kg/bar) and c_t is the total compressibility (which is the sum of the rock compressibility and the water compressibility) of the tank. The storage capacity is given by equation 4.6:

$$\kappa = V_b \rho \phi c_t \quad (4.6)$$

The Schilthuis (1936) approach is used for modeling the water recharge as a function of time as follows (equation 4.7);

$$W_{re} = \alpha (p_0 - p(t)) \quad (4.7)$$

Because P_0 is constant, w_{re} can be written as equation 4.8;

$$W_{re} = \alpha \Delta p(t) \quad (4.8)$$

If equation 4.8 is inserted into equation 4.5, equation 4.9 is formed:

$$\frac{\kappa}{c_t} \frac{df(t)}{dt} = W_{inj} f_{inj} + \alpha \Delta p(t) f_{re} - W_p f(t) \quad (4.9)$$

Here α is the recharge constant (kg/bar/s) and represents the amount of water mass rate per unit pressure drop per unit time, Δp is the pressure drop in the tank (bar). When closed system is modelled is set to 0.

The rate of water accumulation can be illustrated as in Figure 4.2. The equation for accumulation term is given by equation 4.10.

$$V_b \phi \rho c_t \frac{dp}{dt} = W_{re} - W_p + W_{inj} \quad (4.10)$$

The production and injection terms can be defined as ‘net production term’ as given by equation 4.11:

$$W_{net} = W_p - W_{inj} \quad (4.11)$$

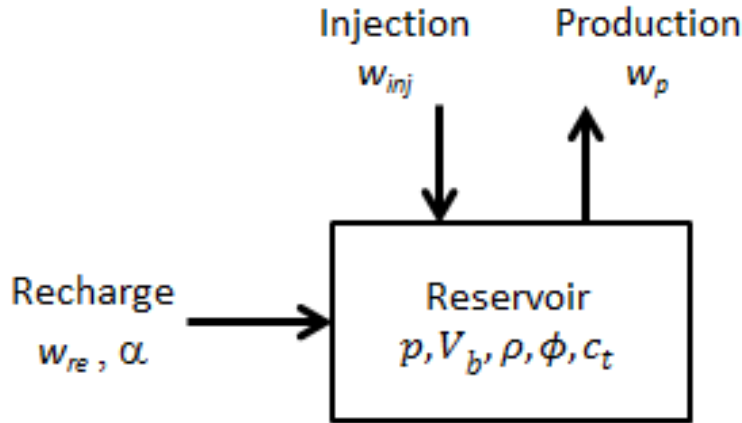


Figure 4.2 : Terms for the rate of water accumulation.

Mass balance of water for a reservoir with recharge source becomes equation 4.12:

$$W_{re} - W_n = \kappa \frac{dp}{dt} \quad (4.12)$$

And with the Schilthuis approach, dp term can be written as in equation 4.13

$$\Delta p = \frac{W_n}{\alpha} \left[1 - e^{-\frac{\alpha t}{\kappa}} \right] \quad (4.13)$$

This equation gives the pressure behaviour of a geothermal system as a function of production time under the conditions of a constant production rate and constant aquifer pressure.

Using equation 4.14 in equation 4.9 and further manipulation results in equation 4.14;

$$\frac{\kappa}{c_t} \frac{df(t)}{dt} + W_p f(t) - (W_{inj} f_{inj} + W_n f_{re}) + W_n f_{re} e^{-\left(\frac{\alpha t}{\kappa}\right)} = 0 \quad (4.14)$$

The initial condition for this equation is given in equation 4.15;

$$f(t=0) = f_0 \quad (4.15)$$

The solution of the ordinary differential equation 4.14 is given in equation 4.16.

$$\begin{aligned}
f(t) = f_0 e^{-\left(\frac{W_p c_t}{\kappa} t\right)} + \frac{W_{inj} f_{inj} + W_n f_{re}}{W_p} + \\
\frac{W_n f_{re}}{W_p - \frac{\alpha}{c_t}} e^{-\left(\frac{W_p c_t}{\kappa} t\right)} - \frac{W_n f_{re}}{W_p - \frac{\alpha}{c_t}} e^{-\left(\frac{\alpha}{\kappa} t\right)} \\
- \frac{W_{inj} f_{inj} + W_n f_{re}}{W_p} e^{-\left(\frac{W_p c_t}{\kappa} t\right)}
\end{aligned} \tag{4.16}$$

The solution of this equation represents the solution for the case where the injected carbon dioxide mass fraction is kept at a constant value.

4.1.2 Variable Carbon Dioxide Mass Fraction

In many cases, the reinjected carbon dioxide mass fraction could be a function of the carbon dioxide mass fraction that is produced. In such a case the injected amount is modeled as shown by equation 4.17:

$$f_{inj} = \beta f(t) \tag{4.17}$$

Here β is a number that varies between 0 and 1. If $\beta=0$, then the injected carbon dioxide mass fraction becomes zero. If $\beta=1$, then the injected carbon dioxide mass fraction becomes equal to the carbon dioxide mass fraction in the tank at any particular time.

Using equation 4.17 in equation 4.9 forms equation 4.18:

$$\frac{\kappa}{c_t} \frac{df(t)}{dt} + (W_p - \beta W_{inj}) f(t) - W_n f_{re} + W_n f_{re} e^{-\left(\frac{\alpha}{\kappa} t\right)} = 0 \tag{4.18}$$

At initial time, the mass fraction of dissolved CO₂ in water can be given as f_0 . With the application of initial condition $f(t=0) = f_0$ and further manipulation, the solution of equation 4.18 can be written as in equation 4.19:

$$f(t) = f_0 e^{-\frac{(W_p - \beta W_{inj})c_t}{\kappa} t} + \frac{(W_p - \beta W_{inj})W_n f_{re} \left(1 - e^{-\frac{(\alpha t)}{\kappa}}\right)}{(W_p - \beta W_{inj}) \left[(W_p - \beta W_{inj}) - \frac{\alpha}{c_t} \right]} - \frac{\frac{\alpha W_n f_{re}}{c_t} \left(1 - e^{-\frac{(W_p - \beta W_{inj})c_t}{\kappa} t}\right)}{(W_p - \beta W_{inj}) \left[(W_p - \beta W_{inj}) - \frac{\alpha}{c_t} \right]} \quad (4.19)$$

4.2 Reduced forms of the equations

In this subsection the equations specific to various conditions are provided. The first condition considered is the case when the reinjection rate is taken equal to the production rate and all the produced carbon dioxide is reinjected back into the reservoir. This corresponds to $\beta=1$ for equation 4.19 and $f_{inj}=f_0$ for equation 4.16. Equations 4.16 and 4.19 reduce to equation 4.20. As expected the mass fraction of carbon dioxide does not change with time and is kept constant at the initial mass fraction of carbon dioxide. This is an expected result since the recharge carbon dioxide will not play any role since the reinjection rate is equal to the production rate. This keeps from any recharge water to move into the reservoir.

$$f(t) = f_0 \quad (4.20)$$

The second case considered is the case where again the reinjection rate is taken to be equal to the production rate, but this time no carbon dioxide is re-injected back into the reservoir, $\beta=0$ for equation 4.19 and $f_{inj}=0$ for equation 4.16. Then these equations reduce to equation 4.21.

$$f(t) = f_0 e^{-\frac{W_p c_t}{\kappa} t} \quad (4.21)$$

In the third case the recharge constant is considered to be zero ($\alpha=0$, $f_{re}=0$) for equations 4.16 and 4.19. These equations reduce to equations 4.22 and 4.23, respectively.

$$f(t) = \frac{W_{inj} f_{inj} - (W_{inj} f_{inj} - W_p f_0) e^{-\frac{W_p c_t}{\kappa} t}}{W_p} \quad (4.22)$$

$$f(t) = f_0 e^{-\frac{c_t (W_p - \beta W_i)}{\kappa} t} \quad (4.23)$$

4.3 Comparison of Analytical Model with Lumped Parameter Model

In this section the verification of the developed analytical model is given. The verification is provided on a synthetic example by way of comparing the analytical solutions presented in this study with that of the model provided in this thesis.

At this point it is important to note that the recharge constant used in the developed model is not the same as the one used in the tank model. The relationship between the two recharge indices is given by equation 4.24:

$$\psi = \alpha \frac{\rho}{\mu} \quad (4.24)$$

The tank model handles the density and viscosity fully implicitly. In other words the change of fluid density and viscosity are treated as a function of pressure and temperature. However when using equation 4.24 to determine α given ψ , the fluid properties at the initial pressure and temperature have been used. The scenario illustrated in Figure 4.3 is studied as an example.

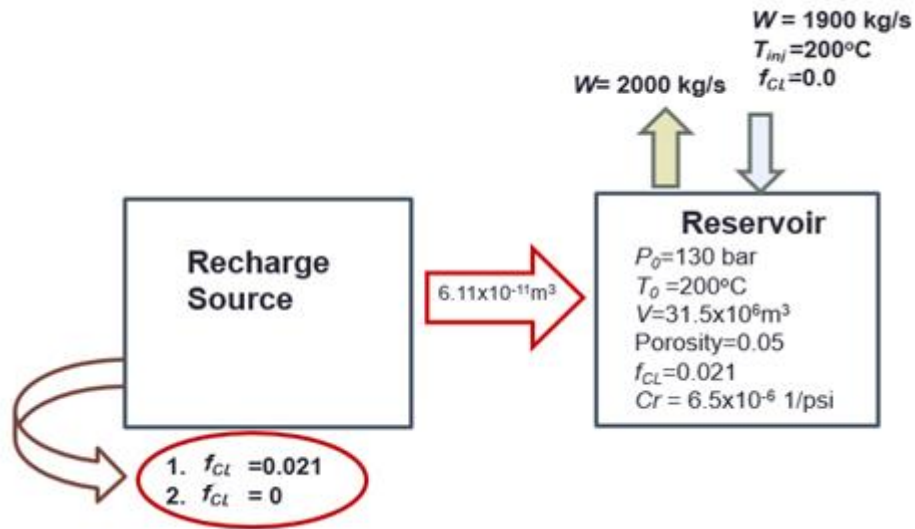


Figure 4.3 : Illustration of the sample scenario.

Two cases are considered. In the first case the mass fraction of carbon dioxide from the recharge source is considered to be zero. In the second case, the mass fraction of carbon dioxide from the recharge source is considered to be equal to the initial mass fraction of carbon dioxide in the reservoir. The behavior of the mass fraction of carbon dioxide from both models are compared. The comparison is given in Figure 4.5. The analytical model parameters and parameters used in the tank model used for this example are given in Tables 4.1 and 4.2, respectively.

Table 4.1 : Parameters used in the analytical model for the verification example.

Bulk volume, m ³	31.5x10 ⁹
Porosity, fraction	0.05
Recharge index, kg/(bar/s)	40
Initial mass fraction of carbon dioxide, fraction	0.021
Reinjection mass fraction of carbon dioxide, fraction	0
Total compressibility, bar ⁻¹	1x10 ⁻⁴
Production rate, kg/s	2000
Reinjection rate, kg/s	1900

Table 4.2 : Model parameters used in the tank model for the verification.

Rock compressibility, bar ⁻¹	9.425x10 ⁻⁵
Density of rock, kg/m ³	2600
Recharge constant, m ³	6.11x10 ⁻¹¹
Bulk volume, m ³	31.5x10 ⁹
Porosity, fraction	0.05
Initial mass fraction of carbon dioxide, fraction	0.021
Reinjection mass fraction of carbon dioxide, fraction	0
Production rate, kg/s	2000
Reinjection rate, kg/s	1900
Initial Pressure, bar	150
Initial Temperature, K	473.15
Reinjection temperature, K	333.15

As it is clear from Figure 4.4 the mass fraction of carbon dioxide in the reservoir decreases for both cases. This is expected since the reinjected water contains no carbon dioxide. Hence the mass fraction of carbon dioxide decreases. The effect of the carbon dioxide from the recharge water for this case seems to be small. This is because 95% of the produced water is reinjected into the reservoir. Hence the contribution of recharge then becomes relatively small. The results of the analytical model developed

in this study fit well to the behavior of those provided from the tank model as given in Figure 4.5.

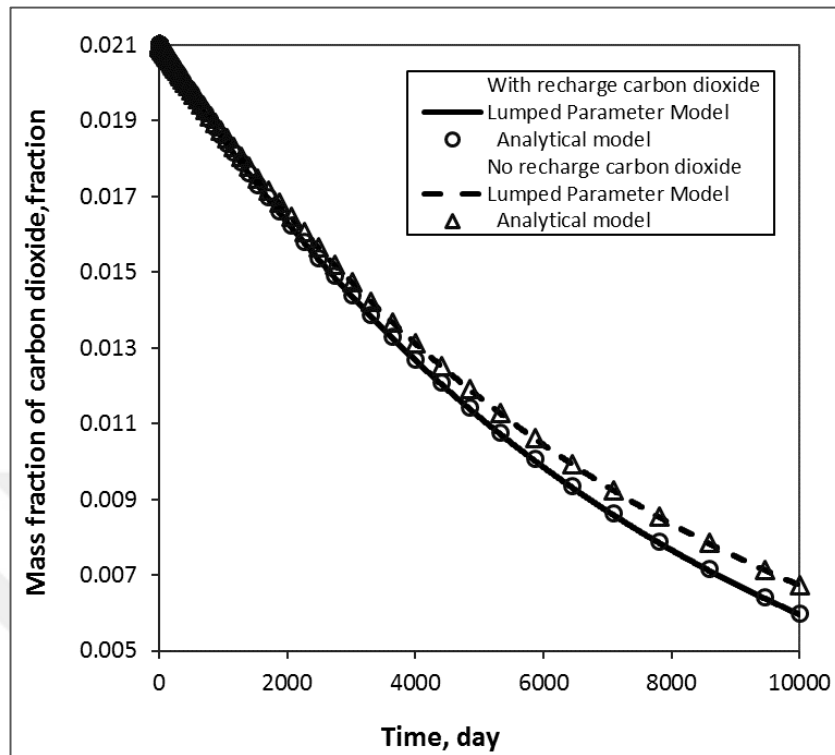


Figure 4.4 : Comparison of mass fraction of CO₂ in gas phase from analytical model and tank model.

4.4 Applications with Analytical Model

In this section an analysis of the model and the effects of various parameters on the change of the mass fraction of carbon dioxide in the reservoir are investigated. First reduced forms of the equations are provided.

4.4.1 Effects of various parameters on the behavior of carbon dioxide content

In this section the effects of the following items are analyzed:

- The ratio of reinjected to produced carbon dioxide mass fraction.
- The recharge and reinjection mass rates.

These effects are demonstrated on a synthetic example. The parameters given in Table 4.3 are used in the example, unless otherwise is stated.

Table 4.3 : Model parameters used in the analytical model.

Bulk volume, m ³	31.5x10 ⁹
Porosity, fraction	0.05
Recharge index, kg/(bar/s)	40
Initial mass fraction of carbon dioxide, fraction	0.021
Reinjection mass fraction of carbon dioxide, fraction	0
Total compressibility, bar ⁻¹	1x10 ⁻⁴
Production rate, kg/s	2000
Reinjection rate, kg/s	1900

4.4.1.1 The ratio of reinjected to produced carbon dioxide mass fraction

First the effect of the reinjection to production ratio (β) of carbon dioxide is considered. Hence when $\beta=1$ this means that all of the produced carbon dioxide is reinjected back into the reservoir. If $\beta=0$, then no carbon dioxide is reinjected back. Results are given in Figure 4.5 and Figure 4.6

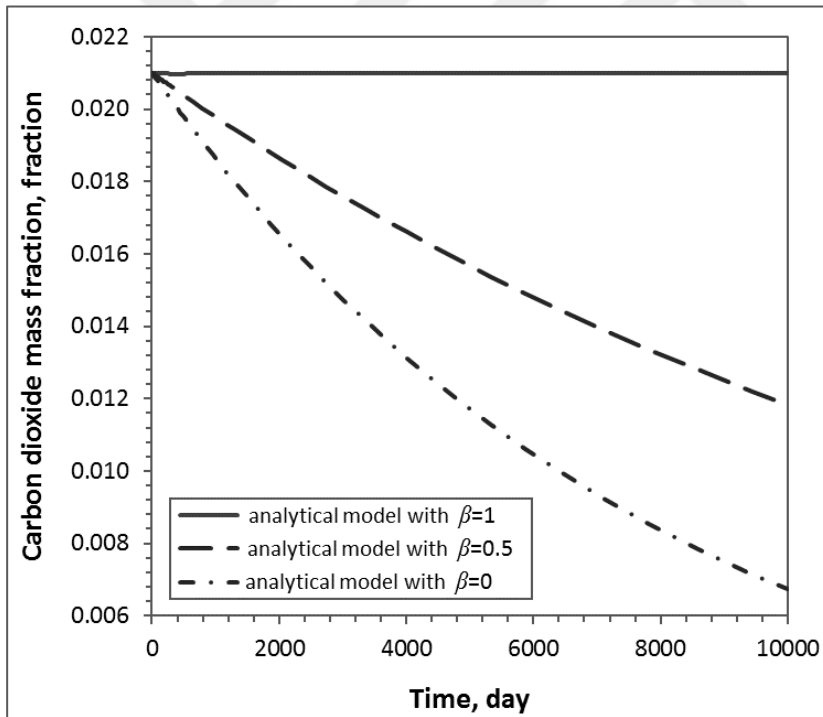


Figure 4.5 : Analytical model results for various β values.

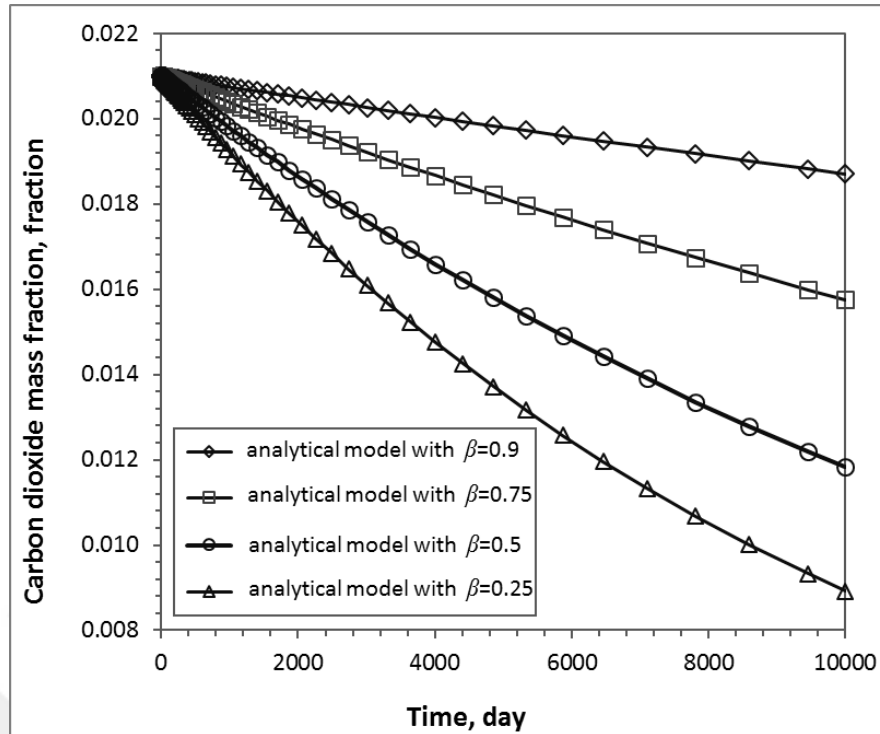


Figure 4.6 : Comparison of mass fraction of CO₂ in liquid phase.

As it is clear from Figures 4.5 and 4.6, if all produced carbon dioxide is reinjected back into the reservoir, the carbon dioxide content does not change with time. Once β is decreased, the carbon dioxide content also starts to decrease for any given time. This is an expected result since not all the produced carbon dioxide is reinjected back. The carbon dioxide mass fraction increases with increase in β as it is expected.

In addition to this, the results of the analytical model and tank model for variable reinjection case are compared in Figure 4.7. Here, comparison results for $\beta= 0.5$ is given. As it can be seen from this figure analytical model developed in this study also fit well to the behavior of the one provided from the tank model.

4.4.1.2 The recharge and reinjection mass rates

Two cases are considered to demonstrate the effect of recharge carbon dioxide. In the first case a 95% reinjection ($W_{inj}=1900$ kg/s) is performed. In the second case a 60% reinjection ($W_{inj}=1200$ kg/s) is considered. For both cases the reinjection mass fraction of carbon dioxide is assumed to be zero.

The results are given in Figure 4.9. The circles and the crosses represent the 95% reinjection and the 65% reinjection cases, respectively. The lines on the other hand

represent the differences in the mass fraction of carbon dioxide in the recharge water. The solid line represents a mass fraction of 0, and the dashed line represents a mass fraction of 0.021. For the 95% reinjection case, not much difference is observed in the behavior of the carbon dioxide content in the reservoir. This is because the recharge rate is low due to the high reinjection rates. If steady state (for pressure) conditions have been reached (steady state conditions could be reached relatively quickly compared to the overall project life) if we have a 95% reinjection rate, the contribution will be 5 % of the production rate.

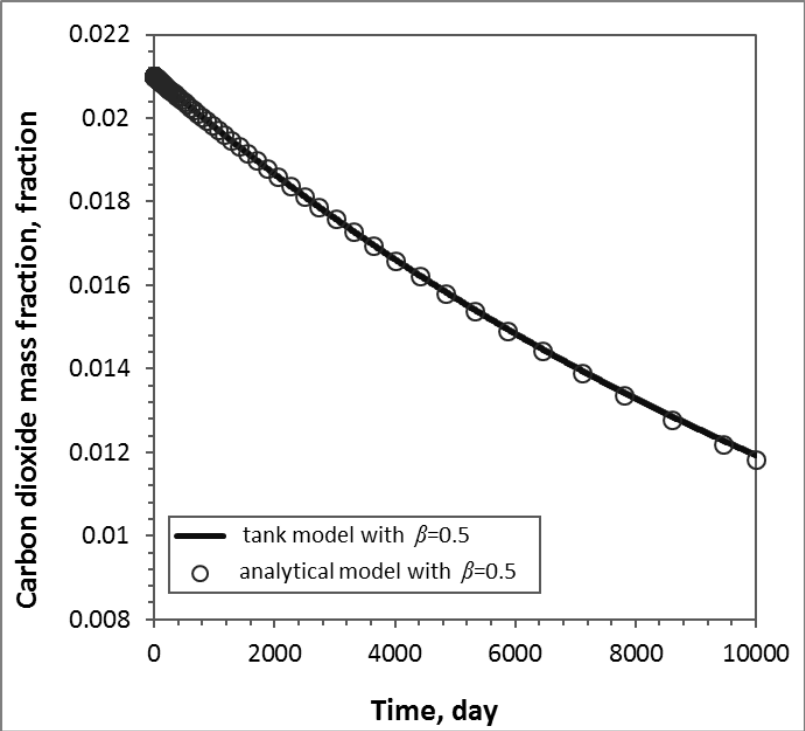


Figure 4.7: Comparison of tank model and analytical model with CO₂ reinjection.

For this specific example, once steady state is reached the contribution of recharge is 100 kg/s. Once the reinjection rate is decreased, the recharge rate increases. Hence the carbon dioxide content of the recharge water starts having a considerable impact. This is clearly observed in Figure 4.8. When we compare the 60% reinjection case, we see a clear difference between the recharge water having no carbon dioxide and having a fraction of 0.021. In conclusion, it can be stated that the impact of recharge can become profound only when reinjection rates become smaller. For high reinjection rates the contribution of recharge decreases.

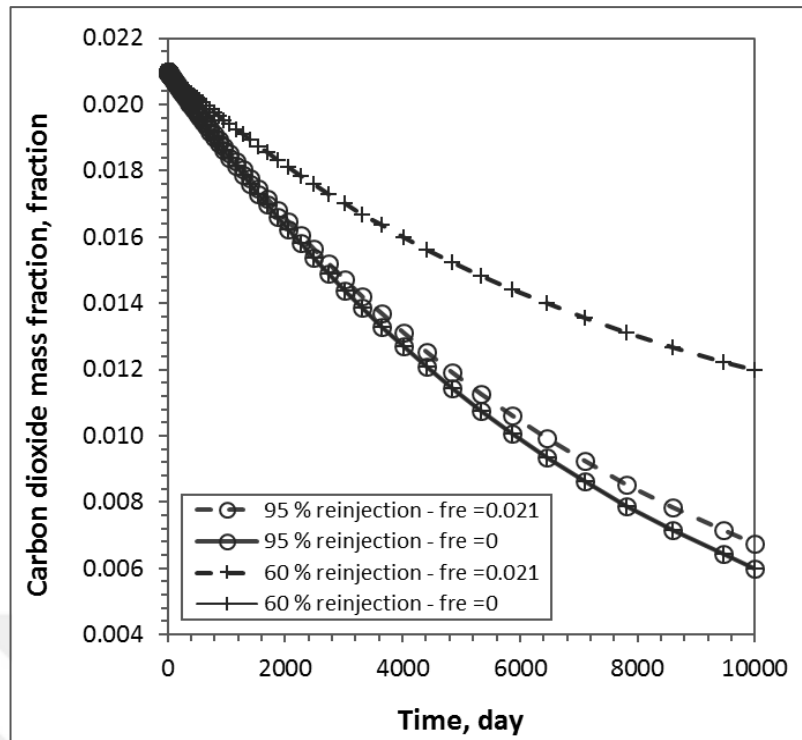


Figure 4.8 : Comparison of mass fraction of CO₂ in liquid phase with various CO₂ reinjection.

Finally the $\beta=1$ curve given in Figure 4.6 is considered again. This curve alone is given in Figure 4.9.

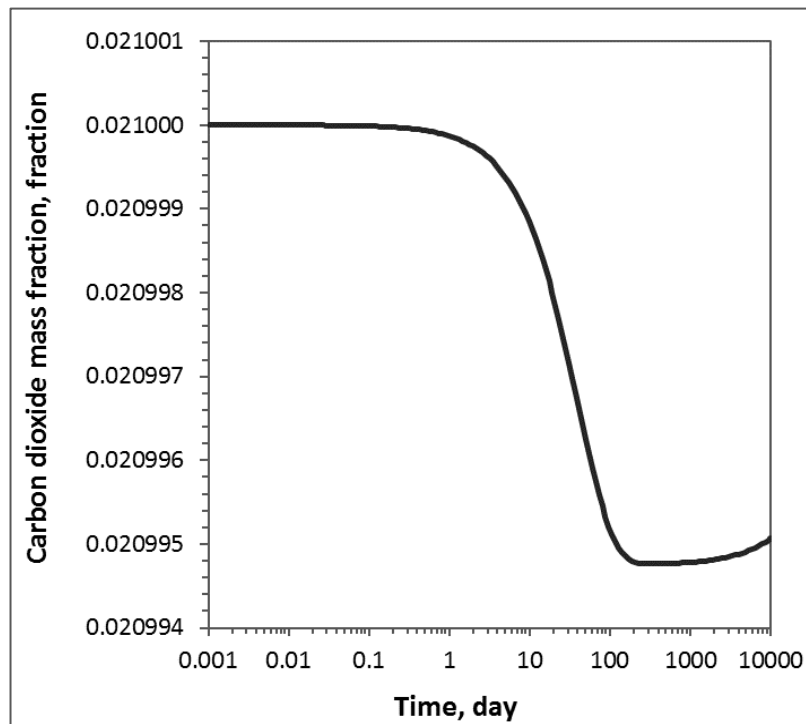


Figure 4.9 : Behaviour of mass fraction of CO₂ in liquid phase at early times.

As it is clear, although the magnitudes are small, an initial decrease in the carbon dioxide mass fraction is observed. Then it starts increasing again. This is because of the transient behavior of pressure in the tank. Initially once production is started, the recharge water mass rate is negligible. Hence due to production the carbon dioxide mass fraction decreases. As the recharge mass rate increases (it becomes equal to the production rate once steady state pressure is reached) the carbon dioxide mass fraction also starts increasing due to the carbon dioxide mass fraction in the recharge water.



5. APPLICATION TO GERMENCİK FIELD

5.1 Germencik Field

In this section, the application of the developed model to the Germencik geothermal field is given. In the western part of the Büyük Menderes Graben about 40 km from Aegean Sea and within Ömerbeyli residential area in the Aydın province in western Turkey, the Germencik geothermal field is situated and considered to be one of the most important geothermal fields of Turkey (Tureyen et al, 2014b). The location map of Aydın-Germencik geothermal field is given in Figure 5.1.

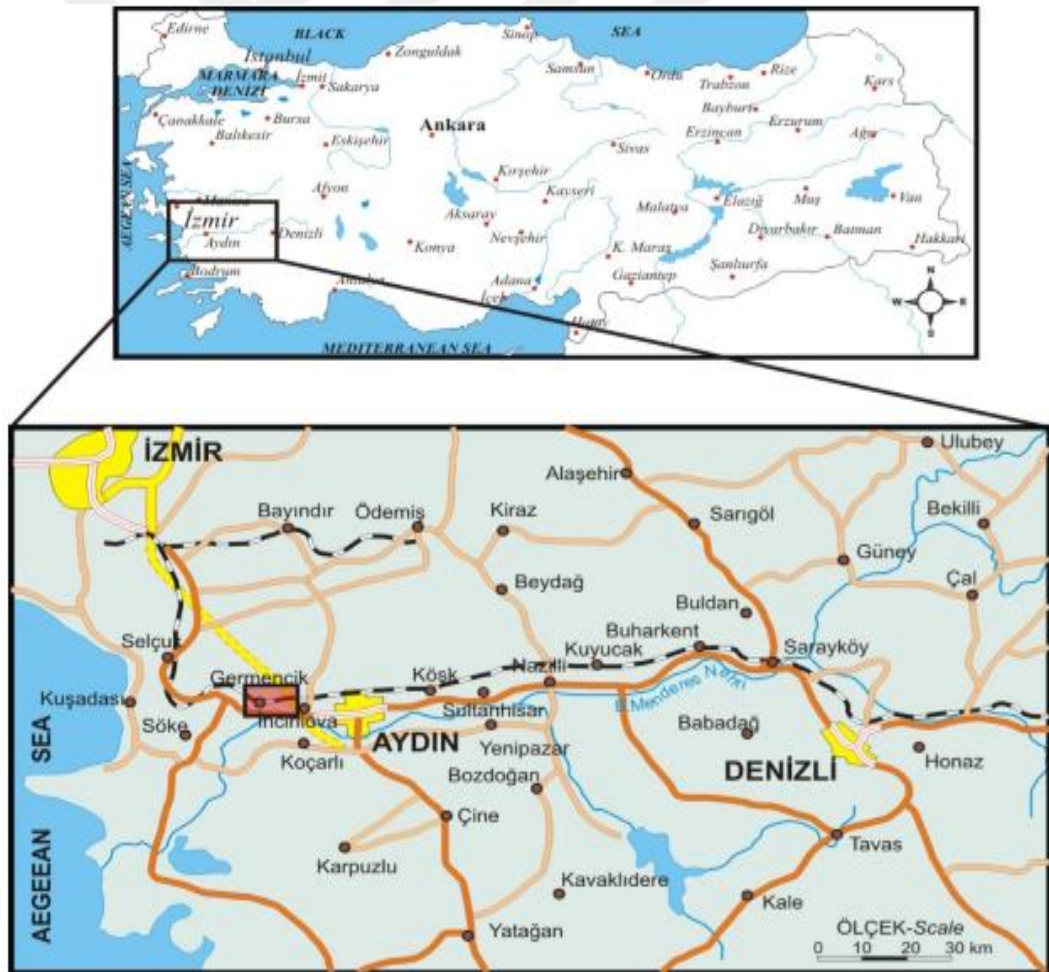


Figure 5.1 : The location map of Aydın-Germencik gothermal field (Karaduman, 2016).

5.2 Field Development

In Aydın-Germencik area the preliminary studies were carried out in 1967. The Germencik field was discovered by MTA (General Directorate of Mineral Research and Exploration) in 1968. Nine exploration wells (OB-1 to OB-9) given in Table 5.1 were drilled by MTA between 1982 and 1986 and a water dominated hydrothermal system was discovered. After initial exploration studies, MTA carried over the field license to two different operators; GÜRİŞ Construction and Engineering Co. Inc. and Maren Energy. After GÜRİŞ Construction and Engineering Co. Inc. has become one of the operator of the field, more wells were drilled between 2007 and 2008 as tabulated in Table 5.2.

Table 5.1 : Wells drilled in Germencik geothermal field by MTA (Filiz et al, 2000)
(A: Artesian)

Well No	Drilling Date	Depth, m	Temp, °C	Discharge (l/s)	Production Type (Wellhead Pressure)
OB-1	1982	1002	203	Geyser	Geyser
OB-2	1982	975	231	25	A (4-7 bar)
OB-3	1983	1197	230	65	A (13-15 bar)
OB-4	1984	285	213	180-100	A (15 bar)
OB-5	1984	1270	221	65	A (6 bar)
OB-6	1984	1048	221	140	A (15 bar)
OB-7	1985	2398	203	65	A (2.7 bar)
OB-8	1986	1970	220	120	A (5.4 bar)
OB-9	1986	1460	224	145	A (6.8 bar)

Table 5.2 : Wells drilled in Germencik Omerbeyli geothermal field by GÜRİŞ (Tekin and Akın, 2011)

Well No	Drilling Date	Depth, m	Temp, °C
OB-10	2007	1524	224
OB-11	2007	965	210
OB-14	2007	1205	228
OB-17	2008	1706	228
OB-19	2008	1651	227
AG-22	2008	2260	205
AG-24	2008	1252	199
AG-25	2008	1838	191
AG-26	2008	2432	195

Later on, detailed geological mapping, hydrogeological, geophysical and geochemical studies and drilling tests were implemented and more than 70 wells were drilled up to date. The locations of the wells in the field are shown in Figure 5.2 (Tureyen et al, 2016).

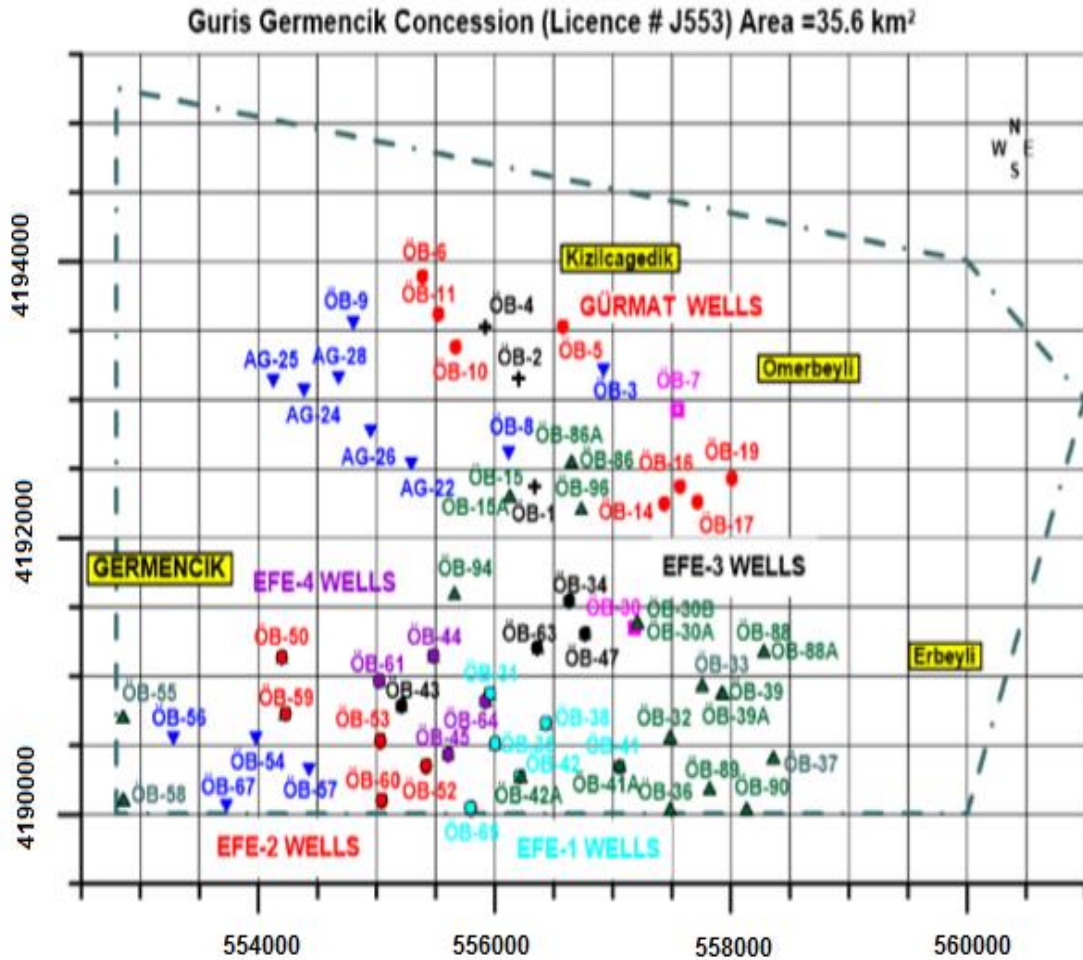


Figure 5.2 : The locations of the wells drilled in the field (Tureyen et al, 2016).

Germencik field is a liquid dominated reservoir that contains noncondensable gas which is mainly CO₂, about 2.5% by weight. Temperatures up to 240°C have been recorded in the field. The basement of the Germencik field is comprised by the Paleozoic metamorphic rocks of the Menderes Massif . The metamorphic rocks consist of gneisses and schists, as well as marbles, quartzites and calcschists. Figure 5.3 (Şimşek, 1984) represents the geological map of the Germencik geothermal field.

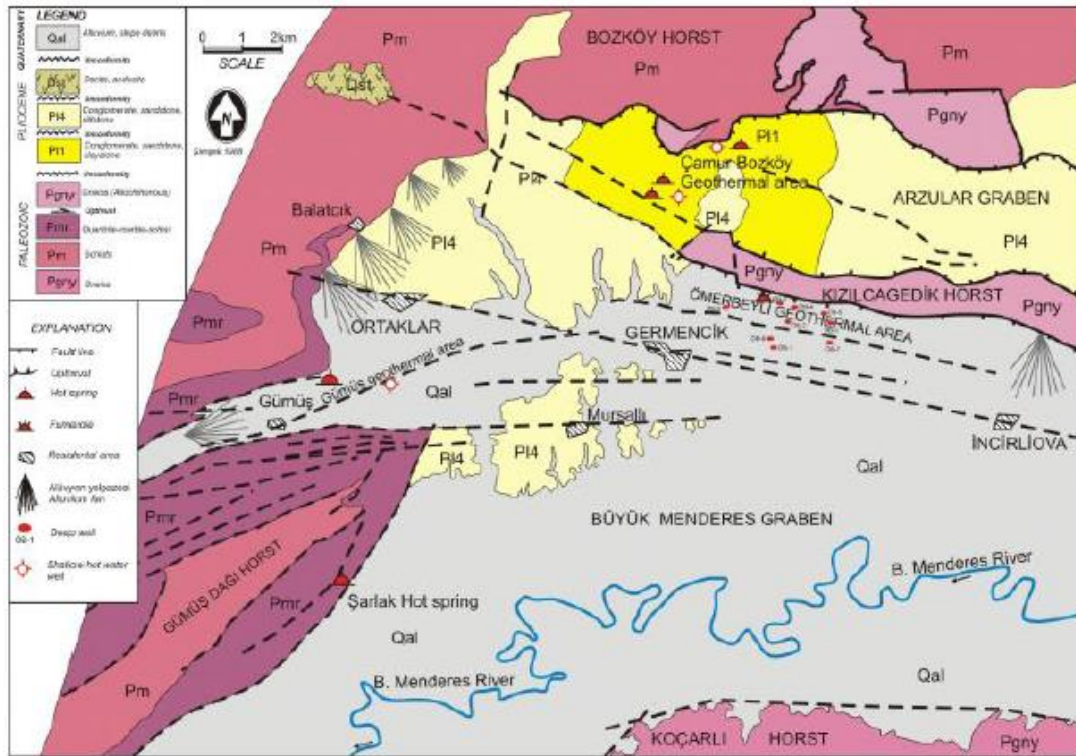


Figure 5.3 : The Geological map of the Germencik Ömerbeyli geothermal field (Şimşek, 1984).

The Germencik geothermal system is a convective hydrothermal system. It is considered to be consisted of two different types of rock. The shallow one is comprised of Neogene conglomerates and sandstones while the deep one is comprised of fractured karstic marble, schist, quartzite and gneiss. (Şimşek, 1984; Correia et al., 1990; Tekin and Akin, 2011). The heat source is considered to be near surface magma intrusion and deep circulation of meteoric waters. Aquifer water is heated at depth and move along faults and fracture zones to recharge the reservoir.

The reservoir is considered to be the primary target for power generation and has a potential of up to 200 MWe approximately (Satman et al., 2013). One of the operator of the field, GÜRİŞ initially constructed a 47.4 MWe double flash power plant and has been producing electricity since 2009.

5.3 Modelling Study

A production/reservoir performance study (Tureyen et al, 2014b) was conducted at the Germencik geothermal field. The objective of that study was to assess the energy production potential of Germencik field. The storage capacity and recharge constant

of the field was determined by applying one tank lumped parameter isothermal model developed by Sarak et al (2005). Their modeling approach is based on history matching of the pressure data in the observation well, OB-7, between February 2009 and November 2011. In this period, only the power plant operated by GÜRIŞ was in operation so the reservoir response is only affected by the production and reinjection in the GÜRIŞ field. In the modelling total rate is used which is the difference between the production and the reinjection rate. The obtained match from the modelling study is given in Figure 5.4. Modelling study indicated that there is a fairly strong natural recharge into the system. Once the best model that simulates pressure data from a geothermal system is found, it can be used to predict future pressure and temperature changes, which can consequently be used to estimate the production capacity of the given system.

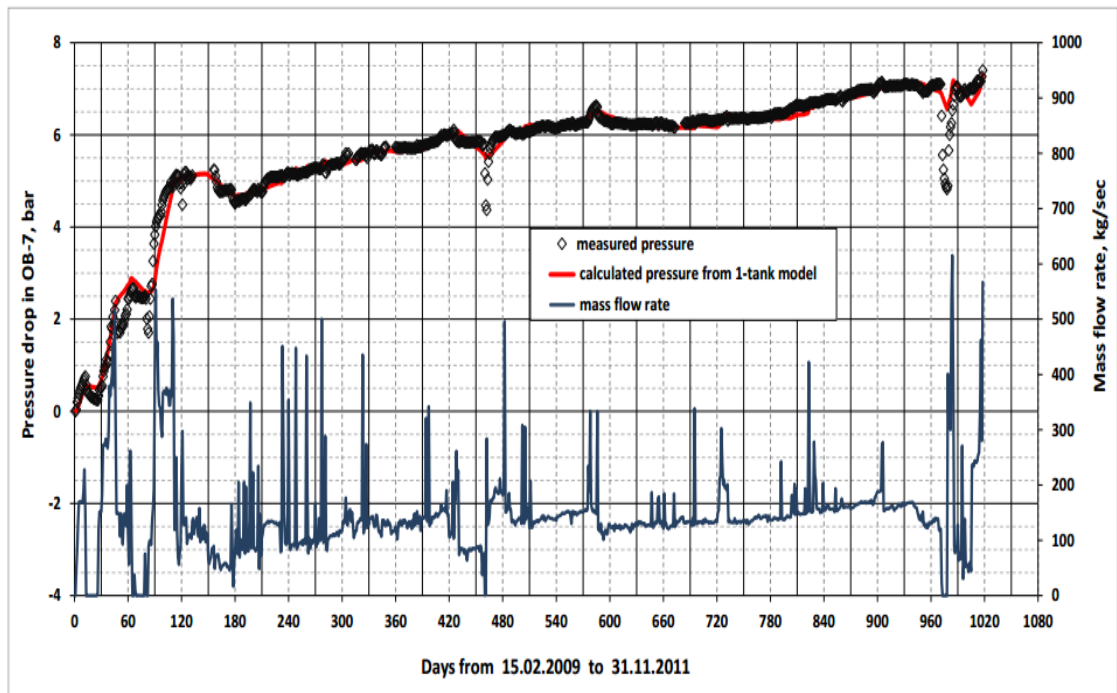


Figure 5.4 : Matching of pressure drop response at Well OB-7 (Tureyen et al., 2014b).

The model and parameters of Tureyen et al. (2014b) are the basis of this study. In our study, new production data are incorporated into the developed tank model and the pressure response of OB-7 covering the period from 15 February 2009 to May 2015 as shown in Figure 5.5 are used in history matching. Especially, the variation in amount of CO₂ with time is determined.

Rock part of the recharge index, ψ , is computed from to recharge index that is given in Tureyen et. al (2014b). By using recharge index and the fluid density and viscosity at the initial reservoir pressure and temperature, ψ is calculated. Reservoir bulk volume, porosity and rock compressibility is calculated according to storage constant given in Tureyen et al. (2014b) and related maps and well data provided by GÜRIŞ Construction and Engineering Co. Inc. The results for temperature and mass fraction of dissolved CO₂ are presented and discussed here.

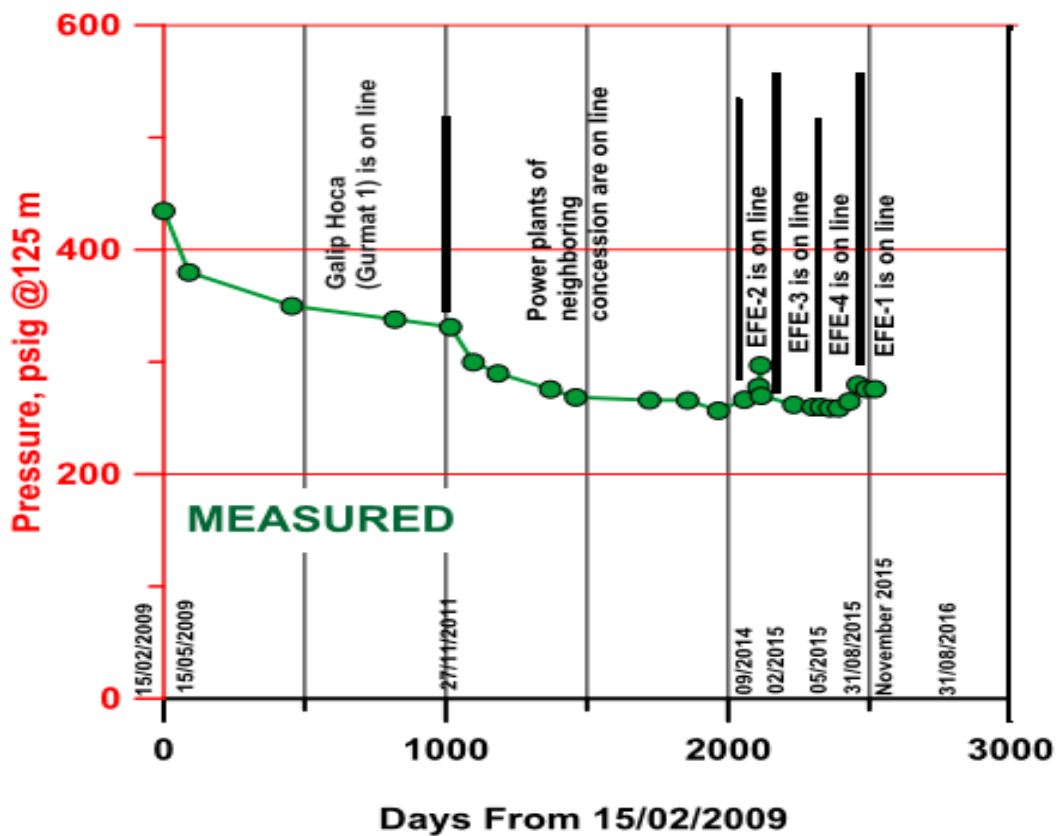


Figure 5.5 : Measured pressure behavior response at Well OB-7 (Tureyen et al., 2016).

5.3.1 Case study: one tank open system

In the first scenario, one tank open system as illustrated in Figure 5.6 is used to model the Germencik field. The parameters that are used in the tank model are listed in Table 5.3. The history matching process is carried out manually with trial and error effort without using any tool or simulator. The match for the first 1000 days (Figure 5.4) are from the study of Tureyen et al. (2014b). In this match the GÜRIŞ company was the only producer. Thus, the recharge index and storage constant obtained from the match

represent the whole geothermal field. After 1000 days, pressure drop is increased due to the production from the other operator.

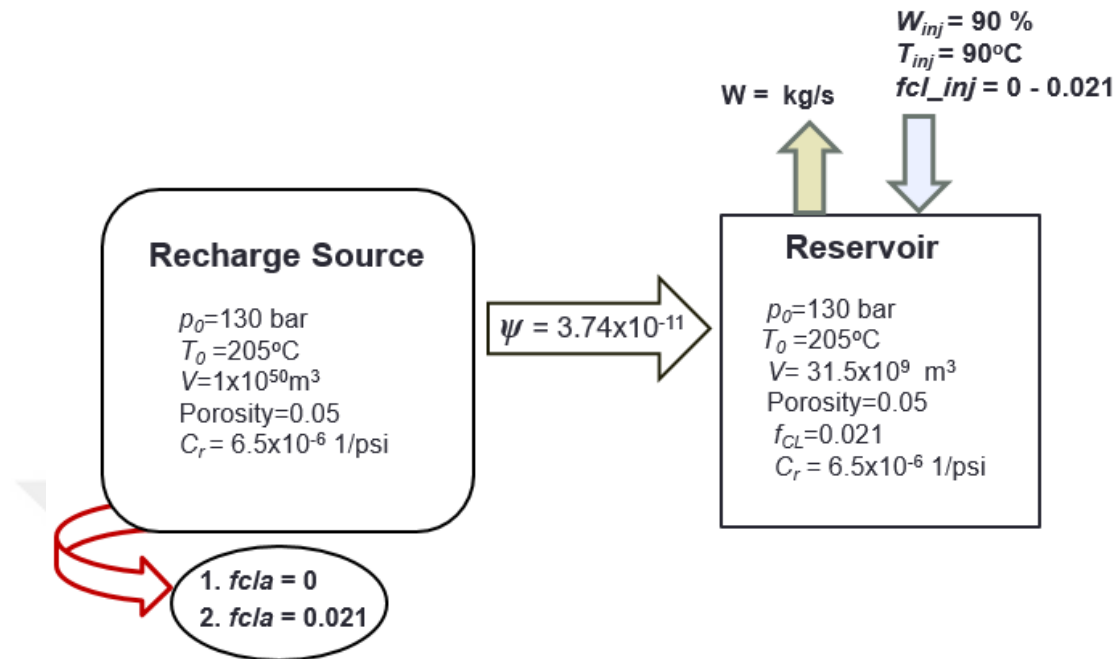


Figure 5.6 : Illustration of one tank open system for Germencik Field.

Table 5.3 : Data used in one tank open model.

Bulk volume, m ³	31.5×10 ⁹
Porosity, fraction	0.05
Initial pressure, Pa (bar)	130×10 ⁵ (130)
Initial temperature, K	478.15
Rock compressibility, Pa ⁻¹	9.427×10 ⁻¹⁰
Rock thermal expansion coefficient, K ⁻¹	0
Density of rock, kg/m ³	2600
Heat capacity of rock, J/(kg.K)	1000
Rock part of the recharge index, m ²	3.72×10 ⁻¹¹
Injection temperature, K	300
Injection rate, %	90
Initial CO ₂ fraction, fraction	0.021

History matching process is used as a tool to obtain a model that provides best match to the pressure data. After the appropriate history match is obtained, the model is used to simulate future reservoir behavior. After this point, different scenarios can be considered. In our case, it is assumed that reservoir produces with a constant production and injection rates of 3787 kg/s and 3408 kg/s for 10 years and pressure,

temperature and CO₂ mass fraction projections are performed. Temperature and CO₂ mass fraction projections are given as follows.

The projection for the temperature is given in Figure 5.7. According to this figure, temperature decreases from 478 K to 470 K in 10 years. The main reason for the temperature drop is the reinjection temperature. The temperature of reinjection water is assumed as 300 K that is fairly colder than reservoir temperature. So it cools the reservoir.

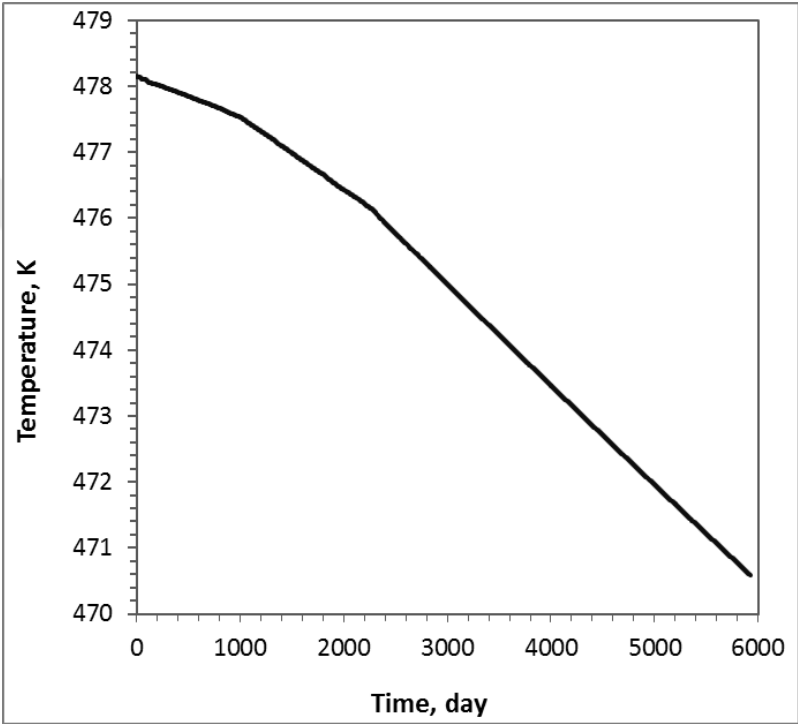


Figure 5.7 : Temperature drop projection for Germencik field.

At the final pressure and temperature, the reservoir water still remains in liquid phase. As a result no gas phase will be formed in the reservoir after 10 years. The projection for the mass fraction of CO₂ that is dissolved in reservoir water is given in Figure 5.8. Two scenarios are considered for this case. In first scenario, it is assumed that recharge water is pure water so it does not contain any dissolved CO₂. In the second one, it is assumed that recharge water contains 2.1 % CO₂ by mass ($f_{cla}=0.021$). This value equals to the initial CO₂ mass percentage of the reservoir. The reinjection water is considered as pure water in both cases. According to Figure 5.8, for $f_{cla}=0.021$, the dissolved CO₂ mass fraction (f_{CL}) in reservoir water decreases to 0.008 and for $f_{cla}=0$ it decreases to 0.0064. There is a slight difference in two values. For this model based

on the assumption of reinjection rate at 90 % of production, recharge water dissolved CO₂ fraction has minor effect on reservoir performance projection. The effect of carbon dioxide content of the aquifer on the reservoir CO₂ content behavior is not appreciable when reinjection mass flow rates are high. The important point is, there will be a significant reduction in CO₂ amount of reservoir fluid in both cases.

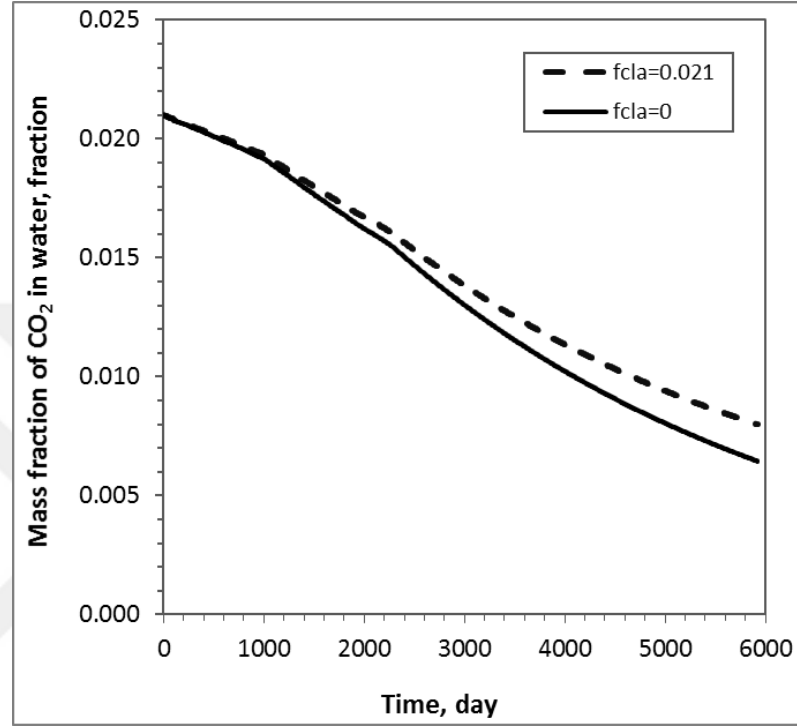


Figure 5.8 : The projection for the mass fraction of CO₂ in Germencik field.

For the case discussed above, the reinjection water is assumed as pure water without any CO₂ content. For another scenario, it is assumed that 90 % of produced water containing CO₂ is directly reinjected into the reservoir. In that case, mass fraction of injected CO₂ varies with time and it is equal to mass fraction of CO₂ in reservoir water produced ($f_{CL}=f_{cl_inj}$). This time, mass fraction of CO₂ decreases to 0.019. Carbon dioxide level in the reservoir can be maintained better when the amount of injected carbon dioxide is increased. The comparison of this case and pure water injection case without CO₂ content is given in Figure 5.9. Constant CO₂ reinjection scenario is also considered. If the amount of CO₂ in reinjection water is kept constant at a value of 1.5 %, it is expected that the mass fraction of CO₂ decreases to 0.018. The projection of mass fraction of CO₂ in liquid water where constant amount of CO₂ is reinjected into the reservoir is given in Figure 5.10.

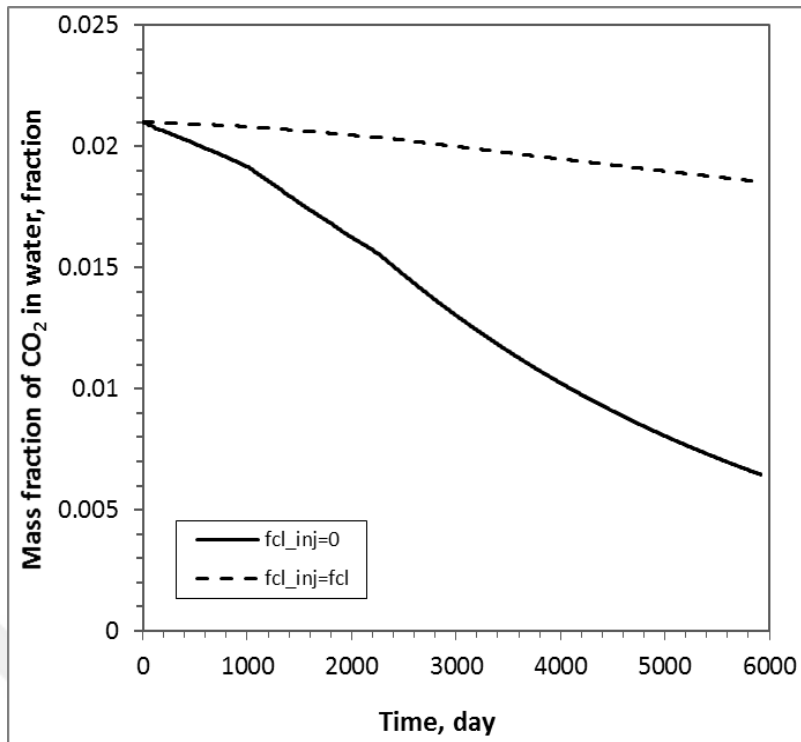


Figure 5.9 : Projection of mass fraction of CO₂ in water with and without CO₂ reinjection.

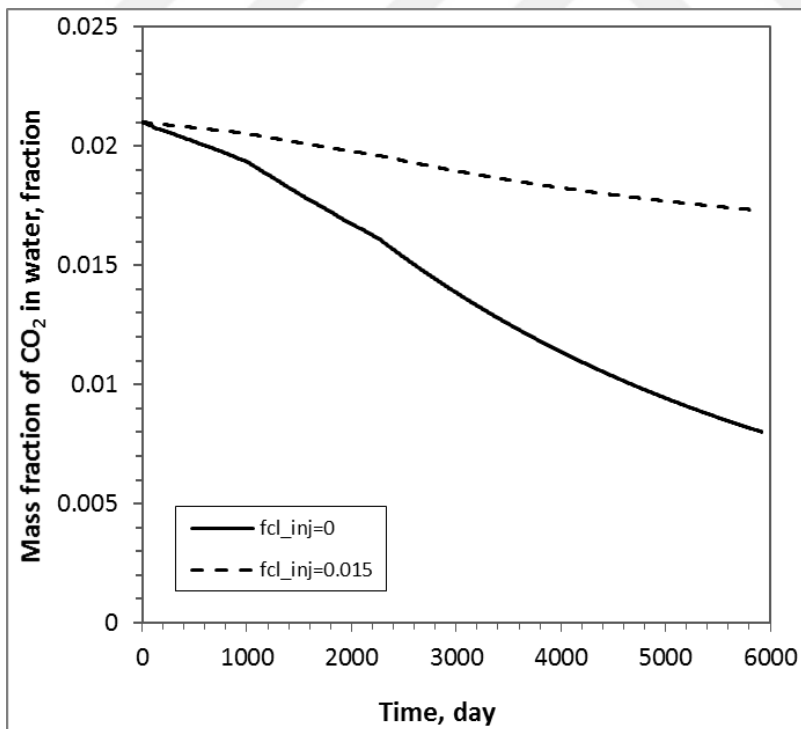


Figure 5.10 : Projection of mass fraction of CO₂ in water with constant amount of CO₂ reinjection.

6. CONCLUSIONS AND RECOMMENDATIONS

The conclusions obtained from this thesis study and recommendations for future works are given here.

6.1 Conclusions

In this thesis, a lumped parameter model capable of modelling the pressure and temperature behaviour of the geothermal systems that contain carbon dioxide is developed. The model is similar to the lumped parameter model found in the literature but it can reflect the effect of carbon dioxide on reservoir performance. The model is compared with the pure water model and the effect of carbon dioxide on thermodynamic and transport properties of geothermal fluids are examined.

The behavior of liquid dominated geothermal reservoirs are influenced by the presence of carbon dioxide significantly. Even small amounts of carbon dioxide can have significant effect on the flashing point and other physical properties of water. Hence it becomes very important to know the amount of carbon dioxide present in the reservoir at any given time. The amount of carbon dioxide as well as average reservoir pressure and temperature can be monitored with the addition of mass balance on carbon dioxide in the tank model.

The effect of carbon dioxide are most profound on the flashing point pressure. A small amount of CO₂ dissolved in the liquid water phase can significantly increase the flashing point pressure for any given temperature. Due to the increase in flashing point pressure, two phases can form in the reservoir at relatively higher pressures. With the formation of the gas phase in the reservoir, the pressure decline rate is slowed down. This is because of the much higher compressibility of the gas phase compared to water and rock compressibilities. Gas expands more and supports reservoir pressure.

The amount of CO₂ dissolved in reservoir water decreases with production. If a gas phase is formed, dissolved CO₂ in the water will begin to migrate to the gas phase with

production. Reinjection can also cause reduction of CO₂ if water reinjected to the reservoir contains less CO₂ than the produced water. The recharge source can also be a factor if the recharge water contains less CO₂ than the reservoir water initially existed in the reservoir.

When gas phase is formed in the reservoir, two components exist in the gas phase; carbon dioxide and steam. Initially, gas composition mainly consist of CO₂. With production, as the gas saturation increases, the fraction of CO₂ in the gas phase decreases and steam in gas phase increases.

Our lumped parameter developed in this study can handle a wide variety of geothermal systems. Reservoir can be modelled with one tank or multiple tank for constant or variable production rate with the consideration of recharge and injection. The model is able to work for pure water or H₂O-CO₂ injection with the constant or variable CO₂ amounts and rates.

The lumped parameter model is verified and validated using a newly developed analytical model and the commercial simulator PETRASIM. The results are consistent and highly satisfactory. Then various synthetic cases that demonstrate the effects of parameters such as production and injection rate, recharge constant, porosity, rock density, bulk volume, compressibility of rock, on the change of carbon dioxide in the reservoir are presented.

New analytical expressions that give the amount of carbon dioxide as a function of time and amounts of production, reinjection and recharge for liquid dominated reservoirs are developed. This new analytical approach is an original contribution to the literature. The expressions for the CO₂ content in liquid dominated reservoirs are developed for two different carbon dioxide reinjection scenarios;

- a-) reinjection of carbon dioxide at a fixed mass fraction,
- b-) reinjection of carbon dioxide at a variable mass fraction.

Finally, the model is applied to the Germencik field that initially contains approximately 2.1 % carbon dioxide by mass. The early production rate-reservoir pressure history are used and an almost perfect match is obtained. The best model that fits the Germencik field is formed and production performance of this field is

evaluated. The modelling study based on production/reinjection scenarios yielded significant results and observations. There is a substantial recharge to the geothermal system. The amount of carbon dioxide in the reservoir is expected to decrease in time. The parameters that effect reduction of carbon dioxide are amount of CO₂ that enters the reservoir with the natural recharge and reinjection. Low reservoir pressure drop is aimed for the sustainability of the reservoir. The pressure decline rate is slowed down with the formation of the gas phase in the reservoir and well head pressure is directly proportional to the amount of CO₂. Thus, the CO₂ reinjection is essential for the sustainable management of the field. Temperature drop of 8 K is expected.

The sustainability issues concerning the liquid dominated geothermal reservoirs containing dissolved carbon dioxide are better described when the model presented in this study is considered for pressure behavior. Keeping the track of CO₂ in the reservoir is crucial since CO₂ plays an extremely important role in the pressure behaviour either in the reservoir (if two phase forms) and in the well. It is important to note that a change in CO₂ significantly affects well head pressures.

6.2 Recommendations for Future Works

Based on this thesis study, the following recommendations can be given for further improvements and for future works that can be performed related to the subject of this study.

6.2.1 Effects of brine salinity

The effects of salt content on the thermodynamic properties of geothermal fluids can be added to thermodynamic package. With the implementation of equations for the dissolved salt content to the thermodynamic package salty water reservoirs can be modelled. The dependency of density, viscosity, enthalpy, vapor pressure of brine on salt concentration and effects of salinity on CO₂ and vapour solubility can be examined in detailed. H₂O, H₂O-CO₂ and H₂O-CO₂-NaCl systems can be compared.

6.2.2 Gravity effect

Gravity effect is ignored in this study. Gravitational forces can be a major factor in production especially in the case of layered reservoirs and deep reservoir/recharge source. Velocity terms can be modified to include the gravity.

6.2.3 Time stepping

Fluctuations occurs especially during phase transition periods, therefore, length of time steps is crucial in these periods. With the relatively small time steps, fluctuation problem can be overcome. Current model can be improved by modification of time step selection during phase transition zones.



REFERENCES

- Aksoy, N.** (2013). Germencik Aydın sahası Germencik jeotermal sahası–jeotermal kaynaklı elektrik üretimi. *11th National HVAC&Sanitary Congress and Teskon+SODEX Exhibition*, Izmir, Turkey, 17-20 April.
- Alkan, H. and Satman, A.** (1990). A new lumped parameter model for geothermal reservoirs in the presence of carbon dioxide. *Geothermics*, 19, 469-479.
- Alkan, H., Baadagli T. and Satman, A.** (1995). The prediction of the PVT/phase behaviour of the geothermal fluid mixtures. *World Geothermal Congress*, Florence, Italy, May 19-31.
- Arps, J.J.** (1945). Analysis of Decline Curves. *Trans. AIME*, vol. 160, pp. 228-247.
- Atkinson, P. G., Celati, R., Corsi, R. and Kucuk, F.** (1980). Behavior of the Bagnore steam/CO₂ geothermal reservoir, Italy. *Society of Petroleum Engineers Journal*, 20, 228-238.
- Axelsson, G.** (1985). *Hydrology and thermomechanics of liquid-dominated hydrothermal systems in Iceland*. (PhD. Thesis). Oregon State University, Corvallis, Oregon.
- Axelsson, G.** (1989). Simulation of pressure response data from geothermal reservoir by lumped parameter models. *Proceedings of the 14th Workshop on Geothermal Reservoir Engineering*, 257-263, Stanford University, California.
- Axelsson, G. and Gunnlaugsson, E.** (2000). Long-term monitoring of high-and low-enthalpy fields under exploitation. *International Geothermal Association, WGC2000 Short Courses*, Kokonoe, Kyushu District, Japan, 28-30 May.
- Axelsson, G., Björnsson, G., and Quijano, J.,** (2005). Reliability of lumped parameter modelling of pressure changes in geothermal reservoirs. *Proceedings of the World Geothermal Congress 2005*, Antalya, Turkey, CD, 8 pp.
- Battistelli, A., Calore, C. and Prues, K.** (1993). A fluid property module for the Tough2 simulator for saline brines with non-condensable gas. *Proceedings, Eighteenth Workshop on Geothermal Reservoir Engineering Stanford University*, Stanford, California, January 26-28.
- Battistelli, A., Calore, C. and Pruess, K.** (1997). The simulator TOUGH2/EWASG for modelling geothermal reservoirs with brines and non-condensable gas, *Geothermics*, 26, 437-464.
- Bodvarsson, G.** (1966). Direct interpretation methods in applied geophysics. *Geoexploration*, 4, 113-138.

- Bodvarsson, G. S., Benson, S. M. and Witherspoon, P. A.** (1982). Theory of the development of geothermal systems charged by vertical faults. *J. Geophys. Res.*, 87 (B11), 9317–9328.
- Bodvarsson, G.S., K Pruess and MJ. Lippmaan,** (1986). Modeling of geothermal systems, *Journal of Petroleum Technology*, 1007-1021.
- Brigham, W., E. and Morrow, B.,** (1977). P/Z Behavior of geothermal steam reservoirs. *Society of Petroleum Engineers Journal*, Vol. 17, pp.407-412.
- Budd, C. F. Jr.** (1972). Producing geothermal steam at the geysers field. *SPE Paper 4178 presented at Bekersfield, California*, Htg. Hov. 8-10.
- Castanier, L. M.** (1979). Lumped parameter model of a two-phase geothermal reservoir. *Geothermal Resources Council Annual Meeting*, Reno.
- Castanier, L. M., Sanyal, S. K., and Brigham, W. E.** (1980). A practical analytical model for geothermal reservoir simulation. *Proceedings of the 50th Annual California Regional Meeting of SPE*. SPE 8887, 1-6, Los Angeles, CA, USA April 9-11.
- Castanier, L.M. and Brigham, W.E.** (1983). Use of lumped parameter modeling for geothermal engineering. *Proceedings of SPE California Regional Meeting*, Ventura, SPE 11730, 593-601, CA, USA, March 23-25.
- Chierici, A.** (1964). Planning of a geothermoelectric power plant: technical and economic principles. *Proc. U.N. Conf. New Sources Energy, Sol. Energy, Wind Power, Geotherm. Energy*, 1961 Vol. 4, Pap. 9162, pp. 299-313.
- Coats, K. H., George, W. D., Chu, Chieh, and Marcum, B. E.** (1974). Three-dimensional simulation of steamflooding. *Society of Petroleum Engineers Journal*, Vol. 257, Trans., AIME, 573-592.
- Coats, K.H.** (1977). Geothermal reservoir modeling. Paper SPE-6892, *SPE-AIME 52nd Annual Fall Technical Conference*, Denver, Colorado, Oct. 9-12.
- Correia, H., Escobar, C., Gauthier, B. and Ozten, M.** (1990). *Germencik Geothermal Field Feasibility Report*, Technical Report, T.C. Ministry of Energy and Natural Resources Turkey, Ankara.
- Cramer, S.D.** (1982). *The Solubility of Methane, Carbon Dioxide and Oxygen in Brines From 0° to 300°C*, US Bureau of Mines, Report No. 8706, U.S.A., 16 pp.
- Donaldson, I.G., Grant, M.A., and Bixley, P.F.** (1983). Nonstatic reservoirs: the natural state of the geothermal reservoir. *Journal of Petroleum Technology*, 189-194.
- Dağistan, H.** (2012). Türkiye Jeotermal Kaynak Aramaları, Kullanımı Ve Sürdürülebilirliğinin Sağlanması. *MTA Ekonomi Bülteni*. Maden Tetkik ve Arama Genel Müdürlüğü, Ankara.
- Ellis, A.J. and Golding, R.M.** (1963). The solubility of CO₂ above 100°C in pure water and in sodium chloride solutions. *American Journal of Science*, 261, 47-60.

- Faust, C.R. and Mercer, J. W.** (1976). Comparison of finite-difference and finite-element techniques applied to geothermal reservoir simulation. *SPE 5742 presented at the SPE-AIME Fourth Symposium on Numerical Simulation of Reservoir Performance*, Los Angeles, Feb. 19-20.
- Filiz, S., Tarcan, G., Gemici, U.** (2000). Geochemistry of the Germencik geothermal fields, Turkey. *Proceedings World Geothermal Congress*, Japan.
- Grant, M.A.**, (1977a). Broadlands - a gas dominated geothermal field. *Geothermics*, 6, no.p. 9-29.
- Grant, M.A.**, (1977b). Approximate calculations based on a simple one phase model of a geothermal reservoir. *New Zealand Journal of Science*, 20, 19.
- Gringarten, A.C. and Sauty, J.P.** (1975). A theoretical study of heat extraction from aquifers with uniform regional flow. *Journal of Geophysical Research*, 80, No. 35, 4956-4962, December 10.
- Hoşgör, F. B., Çınar, M., Hakkıdır, F., Tureyen, O.I. and Satman, A.** (2013). A new lumped parameter (tank) model for reservoirs containing carbon dioxide. *Proceedings 38th Workshop on Geothermal Reservoir Engineering*, Stanford University, USA.
- Hoşgör, F. B., Tureyen, O.I., Satman, A. and Çınar, M.** (2015). Effects of carbon dioxide dissolved in geothermal water on reservoir performance. *Proceedings of the World Geothermal Congress 2015*, Melbourne, Australia, 19-25 April.
- Hoşgör, F. B., Tureyen, O.I., Satman, A.**, (2016). Keeping inventory of carbon dioxide in liquid dominated geothermal reservoirs. *Geothermics*, 64, 55-60.
- IAPWS** (2007). *Revised Release on the IAPWS Industrial Formulation 1997 for the Thermodynamic Properties of Water and Steam*, Lucerne, Switzerland.
- Karaduman, A.** (2016). Gürmat Germencik jeotermal enerji santral projeleri. *Geothermal Resources*, Ankara, Turkey, 15 April.
- Karamanderesi, İ. H.** (2013). Characteristics of geothermal reservoirs in Turkey. IGA Academy Report 0102-2013.
- Kaya, E., Onur, M. and Satman, A.** (2005) Effects of CO₂ on reservoir and production performance of geothermal systems, *TPDD*, 11, 27-36.
- Lasseter, T.J., Witherspoon, P.A. and Lippmann, M.J.** (1975). Multiphase, multidimensional simulations of geothermal reservoirs. *2. United Nations Symposium for the Development and use of Geothermal Resources*, San Francisco, California, pp.1715, 23 May.
- Malinin, S.D.** (1959). The System H₂O-CO₂ at high temperatures and pressures. *Geochemistry*, No:3, pp. 2021-2032.
- Mercer, J. W.** (1973). *Finite element approach to the modelling of hydrothermal systems* (Ph. D. Thesis). University of Illinois at Urbana-Champaign.
- Mercer, J. W. and Faust, C. R.** (1975). Simulation of water and vapor-dominated hydrothermal reservoirs. *SPE 5520 presented at the SPE-AIME 50th Annual Fall Technical Conference and Exhibition*, Dallas, Sept. 28-Ott.1.

- Meyer, C. A., McClintock, R. B., Silvestri, G. J. and Spencer, R. C.** (1977). ASME SteamTables. *The American Society of Mechanical Engineers*, New York, 329 pp.
- Michels, D.E.** (1979). Reaction mechanisms associated with CaCO₃ scale and release of CO₂ East Mesa. *Geothermal Reservoir Council, Transactions*, 3, 457-460.
- Morris, C.W. and Campbell, D.A.** (1979). Geothermal reservoir energy recovery: a three dimensional simulation study of the East Mesa Field. SPE 8229, *Annual Fall Meeting of the SPE*, Las Vegas, NV.
- Moya, S. L. and Iglesias, E. R.** (1995). Numerical simulation of carbon dioxide effects in geothermal reservoirs. *Proceedings, TOUGH Workshop '95*, LBL-37200, 119-130.
- Nayfeh, A.H., Brownell, D.H. and Garg, S.K.** (1975). Heat exchange in fluid perclating through poroud media. *Proceedings Society of Engineering Science Meeting*, Austin, Texas. Oct. 20-22.
- Olsen, G.,** (1984). Depletion Modeling of Liquid Dominated Geothermal Reservoir. Technical Report, *SGP-TR-80, Stanford Geothermal Program*, Stanford University, Palo Alto, California.
- Onur, M., Sarak, H., Tureyen, O.I., Cinar, M. and Satman, A.** (2008). A new non-isothermal lumped parameter model for low temperature, liquid dominated geothermal reservoirs and its applications. *Proceedings 33rd Workshop on Geothermal Reservoir Engineering*, Stanford University, USA.
- O'Sullivan, M. J., Bodvarsson, G. S., Pruess, K. and Blakeley, M. R.** (1985). Fluid and heat flow in gas-rich geothermal reservoirs. *Society of Petroleum Engineers Journal*, 25, 215-226.
- Parlaktuna, M., Mertoglu, O., Simsek, S., Paksoy, H. and Basarir, N.** (2013). Geothermal Country Update Report of Turkey (2010-2013). *European Geothermal Congress 2013*, Pisa, Italy.
- Pollitzer, F. and Strebel, E.** (1924). The influence of an indifferent gas on the saturation vapor concentration of a liquid. *Zeit, Physik. Chem.*, 110, p.768-785.
- Potter, R. W. and Brown, D. L.** (1977). The volumetric properties of aqueous sodium chloride solutions from 0 ° to 500°C at pressures up to 2000 bars based on a regression of available data in the literature. *USGS Bulletin 1421-C*, Washington, D.C., 36 pp.
- Press, W.H., Teukolsky, S.A., Vetterling, W.T. and Flannery, B.P.** (2007). *Numerical Recipes: The Art of Scientific Computing* (3rd ed.). New York: Cambridge University Press. ISBN 978-0-521-88068-8.
- Pritchett, J.W., Rice M.H. and Riney, T.D.** (1981). Equation-of-state for water-carbon dioxide mixtures: implications for Baca reservoir. Report DOE/ET/27163-8, *Systems, Science and Software*, La Jolla, CA.
- Pruess, K.** (1983). Heat Transfer in Fractured Geothermal Reservoirs with Boiling. *Water Resources Research*, 19 (1), 201-208.

- Pruess, K.** (1988). SHAFT, MULKOM, TOUGH: a set of numerical simulators for multiphase fluid and heat flow, *Geothermia, Rev. Mex. Geoenergia*, 4 (1), 185–202.
- Pruess, K.** (1991). TOUGH2 - A general purpose numerical simulator for multiphase fluid and heat flow. *Lawrence Berkeley Laboratory Report*, LBL-29400, Berkeley, CA.
- Pruess, K., Oldenburg, C. and Moridis, G.** (1998). An overview of TOUGH2, version 2.0. *Proceedings of the TOUGH Workshop '98*, Berkeley, California, pp. 307–314.
- Pruess, K., Schroeder R.C. and Witherspoon, P.A.** (1979). Description of the three-dimensional two-phase simulator shaft78 for use in geothermal reservoir studies. *SPE Reservoir Simulation Symposium*.
- Pruess, K. and Wu, Y.S.** (1989). A New semianalytical method for numerical simulation of fluid and heat flow in fractured reservoirs. *SPE 18426 presented at Tenth SPE Symposium on Reservoir Simulation*, Houston, TX.
- Rezvani-Khalilabad, M., and Axelsson, G.** (2008). Assessment of the Hofstadir geothermal system in W-Iceland. *Proceedings of the 33th Workshop on Geothermal Reservoir Engineering*, Stanford, Ca.
- Sanyal, S.K., Sengul, M. and Mediav, H. T.** (1976). A Semi-analytical approach to geothermal reservoir performance prediction. *2nd Workshop on Geothermal Reservoir Engineering Stanford University*, Palo Alto, California, December, 1-3.
- Sarak, H., Onur, M., and Satman, A.** (2005). Lumped-parameter models for low temperature geothermal reservoirs and their application. *Geothermics*, 34, 728-755.
- Satman, A.**, (2006). Geothermal energy course notes, Istanbul Technical University, Istanbul.
- Satman, A., Onur, M., Serpen, U. and Aksoy, N.** (2007). A Study on production and reservoir performance of Ömer-Gecek/Afyon geothermal field. *Proceedings, Thirty-Second Workshop on Geothermal Reservoir Engineering Stanford University*, Stanford, California.
- Satman, A., Sarak, H., Onur, M. and Korkmaz, E.P.** (2005). Modeling of production/reinjection behavior of the Kizildere geothermal field by a 2-Layer Geothermal Reservoir Lumped Parameter Model. *Proceedings, World Geothermal Congress*, Antalya, Turkey.
- Satman, A. and Ugur, Z.** (2002). Flashing point compressibility of geothermal fluids with low CO₂ content and its use in estimating reservoir volume. *Geothermics*, 31, 29-44.
- Schilthuis, R. J.** (1936). Active oil and energy. *Trans. AIME*, 118, 33-52.
- Serpen, U., Aksoy, N., Öngür, T., Korkmaz, E.D.,** (2009). Geothermal energy in turkey: 2008 update, *Geothermics*, 38, Issue 2, 227-237.

- Serpen, U., Aksoy, N. and Öngür, T.** (2010). 2010 Present status of geothermal energy in Turkey. *Thirty-Fifth Workshop on Geothermal Reservoir Engineering Stanford University*, Stanford, California, February 1-3.
- Şimşek, Ş.** (1984). Aydın-Germencik-Ömerbeyli geothermal field of Turkey. *Seminar on Utilization of Geothermal Energy for Electric Power Production and Space Heating EP/SEM.9IR.37*, Florence, Italy, 14-17 May.
- Smith, T.** (2007). A Bright future for geothermal energy. energy resources. *Geo Expro*, October.
- Span, R. and Wagner, W.** (1996). A new equation of state for carbon dioxide covering the fluid region from the triple point temperature to 1100 K at pressures up to 800 Mpa. *J. Phys. Chem. Ref. Data*, 25 (6):1509-1596.
- Stanford Geothermal Program** (1980). Proceedings of the Special Panel on Geothermal Model Intercomparison Study. Report *SGP-TR-42*, Stanford University, Stanford, CA, USA, 120 pp.
- Stockton, A.D., Thomas, R.P. and Chapman, R.H.** (1984). A reservoir assessment of the Geysers geothermal field. *Journal of Petroleum Technology*, 36, 12, pp.2.137 - 2.159.
- Sutton, F.M.** (1976). Pressure-temperature curves for a two-phase mixture of water and carbon dioxide. *New Zealand Journal of Science*, 19, 297-301.
- Sutton F.M. and McNabb, A.** (1977). Boiling curves at Broadlands field. *New Zealand Journal of Science*, 20, 333-337.
- Takenouchi, S. and Kennedy G.C.** (1964). The binary system H₂O-CO₂ at high temperatures and pressures. *American Journal of Science*, 262, p.1055-1074.
- Tekin, S. and Akin, S.** (2011). Estimation of the formation temperature from the inlet and outlet mud temperatures while drilling geothermal formations. *Proceedings, Thirty-Sixth Workshop on Geothermal Reservoir Engineering*, Stanford University, Stanford, California, Jan. 31-Febr. 2.
- TGA,** (2013). Geothermal Energy Development Report, *Turkish Geothermal Association (TJD)*, Ankara.
- Thomas, K.L. and Pierson, R.G.** (1978). Three-Dimensional geothermal reservoir simulation. *SPEJ*, 151461.
- Toronyi, R. M. and Farouq Ali, S. M.** (1975). Two phase, two-dimensional simulation of a geothermal reservoir and the wellbore system. *Paper SPE 5521 presented at the 50th annual fall meeting of the SPE*, AIME, Dallas.
- Tureyen, O. I. and Akyapi, E.** (2011). a generalized non-isothermal tank model for liquid dominated geothermal reservoirs. *Geothermics*, 40, 50-57.
- Tureyen, O.I., Gulgor, A., Erkan. B. and Satman, A.** (2016). Recent expansions of power plants in gürüş concession in the Germencik geothermal field, Turkey, *Proceedings, Forty-First Workshop on Geothermal Reservoir Engineering*, Stanford University, Stanford, CA.

- Tureyen, O. I., Kirmaci, A. and Onur, M.** (2014a). Assessment of uncertainty in future performance predictions by lumped-parameter models for single-phase liquid geothermal systems. *Geothermics*, 51, 300-311.
- Tureyen, O.I., Onur, M. and Sarak, H.** (2009). A Generalized non-isothermal lumped parameter model for liquid dominated geothermal reservoirs. *Proceedings 34th Workshop on Geothermal Reservoir Engineering*, Stanford University, USA.
- Tureyen, O.I., Sarak, H., Gulgor, A., Erkan. B. and Satman, A.** (2014b). A study on the production performance of the Germencik geothermal field, *Proceedings, Thirty-Ninth Workshop on Geothermal Reservoir Engineering*, Stanford University, Stanford, CA.
- Upton, P. S. and Santoyo, E.** (2002). A comprehensive evaluation of empirical correlations for computing the solubility of CO₂ in water. *Proceedings of the 24th NZ Geothermal Workshop*, New Zealand.
- Url-1** <<http://www.thinkgeoenergy.com/geothermal/>>, date retrieved 29.05.2016
- Url-2** <<http://www.enerjiatlas.com/jeotermal/>>, date retrieved 29.05.2016
- Vargaftik, N. B., Vinogradov, Y. K., and Yargin, V. S.** (1996). *Handbook of Physical Properties of Liquids and Gases*. Begell House, New York, third edition.
- Wagner, W., and Pruess, A.** (2002), “The IAPW formulation 1995 for the thermodynamic properties of ordinary water substance for general scientific use,” *Jour. Phys. Ref. Data*, 31, 387–535.
- Wahl, E. F.** (1977). *Geothermal Energy Utilization*. New York, Wiley.
- Whiting, R. L. and Ramey, H. J.** (1969). Application of material and energy balances to geothermal steam production. *Journal of Petroleum Technology*, 21, 893-900.
- Zyvoloski, G. A. and O'Sullivan, M. J.** (1978). Simulation of the Broadlands geothermal fields. *Proceedings Workshop on Geothermal Reservoir Engineering*, Stanford University, USA.
- Zyvolosky, G. A. and O'Sullivan, M. J.** (1980). Simulation of a gas-dominated, two-phase geothermal reservoir. *Society of Petroleum Engineers Journal*, 20, 52-58.



CURRICULUM VITAE



Name Surname : Fatma Bahar Hoşgör

Place and Date of Birth : Istanbul, 1981

E-Mail : ozturun@itu.edu.tr

EDUCATION :

- **B.Sc.** : 2003, Istanbul Technical University, Mining Faculty, Petroleum and Natural Gas Engineering Department
- **M.Sc.** : 2006, Istanbul Technical University, Mining Faculty, Petroleum and Natural Gas Engineering Department

PROFESSIONAL EXPERIENCE AND REWARDS:

SPE (Society of Petroleum Engineers) Turkey Section, Student Paper Contest, Graduate Division, 2nd Place, June 24, 2016.

SPE (Society of Petroleum Engineers) Turkey Section, Student Paper Contest, Graduate Division, 2nd Place, June 9, 2007.

PUBLICATIONS AND PRESENTATIONS ON THE THESIS:

- **Hoşgör, F. B.**, Tureyen, O.I., Satman, A., (2016). Keeping inventory of carbon dioxide in liquid dominated geothermal reservoirs. *Geothermics*, 64, 55-60.
- **Hoşgör, F. B.**, Türeyen, Ö. İ., Satman, A., Çınar, M., (2015). Effects of carbon dioxide on production performance of geothermal reservoir, *Engineer and Machinery*, ISSN 1300-3402, 664, 54-64, May.
- **Hoşgör, F. B.**, Tureyen, O.I. and Satman, A., (2015). Karbondioksit içeren jeotermal rezervuarların modellenmesi. *25th ITU Petroleum and Natural Gas Seminar and Exhibition*, Istanbul, Turkey, 26 June.
- **Hoşgör, F. B.**, Tureyen, O.I., Satman, A. (2013). Modeling of Geothermal Reservoirs Containing Carbon dioxide with a New Lumped Parameter Model. *19th International Petroleum and Natural Gas Congress and Exhibition of Turkey*, Ankara,

Turkey, 15-17 May.

- **Hoşgör, F. B.**, Tureyen, O.I., Satman, A. and Cinar, M., (2015). Karbondioksitin jeotermal rezervuarın üretim performansı üzerindeki etkisi. *The 12th National HVAC&Sanitary Congress and Teskon+SODEX Exhibition*, Izmir, Turkey, April.
- **Hoşgör, F. B.**, Tureyen, O.I., Satman, A. and Cinar, M. (2015). Effects of carbon dioxide dissolved in geothermal water on reservoir production performance. *Proceedings World Geothermal Congress*, Melbourne, Australia, 19-25 April.
- **Hoşgör, F. B.**, Tureyen, O.I., Satman, A. (2013). Modelling of geothermal systems that contain carbon dioxide. *The 11th National HVAC&Sanitary Congress and Teskon+SODEX Exhibition*, Izmir, Turkey, 17-20 April.
- **Hoşgör, F. B.**, Cinar, M., Haklıdır, F. T., Tureyen, O. I., and Satman, A. (2013). A new lumped parameter (tank) model for reservoirs containing carbon dioxide. *Stanford Geothermal Workshop*, Stanford, CA, USA, 11 -13 February.

